Crustal Structure of the Western United States

GEOLOGICAL SURVEY PROFESSIONAL PAPER 1034

Crustal Structure of the Western United States

By CLAUS PRODEHL

GEOLOGICAL SURVEY PROFESSIONAL PAPER 1034

A reinterpretation of seismic-refraction measurements made from 1961 to 1963 and a comparison with the crustal structure of central Europe

UNITED STATES GOVERNMENT PRINTING OFFICE, WASHINGTON: 1979

UNITED STATES DEPARTMENT OF THE INTERIOR

CECIL D. ANDRUS, *Secretary*

GEOLOGICAL SURVEY

H. William Menard, *Director*

Library of Congress Cataloging in Publication Data

Prodehl, C. 1936-
Crustal structure of the Western United States.

(Geological Survey professional paper ; 1034)
Includes bibliographical references.
Supt. of Docs. no.: I 19.16:1034
1. Geology–The West. 2. Earth–Crust. 3. Seismic refraction method.
4. Geology–Central Europe. I. Title. II. Series: United States.
Geological Survey. Professional paper ; 1034.
QE79.P76 551.1'3'0978 79-607072

For sale by the Superintendent of Documents, U.S. Government Printing Office
Washington, D.C. 20402

Stock Number 024-001-03214-7

CONTENTS

ILLUSTRATIONS

[Plates are in pocket]

TABLES

CRUSTAL STRUCTURE OF THE WESTERN UNITED STATES

BY CLAUS PRODEHL

ABSTRACT

A network of 64 seismic-refraction profiles recorded by the U.S. Geological Survey in Nevada and California and adjacent areas in Idaho, Wyoming, Utah, and Arizona from 1961 to 1963 was reinterpreted. The investigation was concentrated on the Basin and Range province and the Sierra Nevada. Two recording lines extended into the western Snake River Plain of Idaho and the southern Cascade Range in California. Other profiles were recorded in the Coast Ranges of California, in the Colorado Plateau, and in the Middle Rocky Mountains.

A basic traveltime diagram for P waves can be derived from record sections compiled for the profiles. The first arrivals generally aline on two traveltime curves. The first one (curve a) can be traced to distances of 100–150 km, yields velocities of 5.9–6.3 km/s, and is correlated with the basement. The second one (curve d) is observed mainly at distances greater than 150–200 km, yields velocities of 7.6–8.2 km/s, and is correlated with the top of the upper mantle. One or two dominant phases can be correlated in secondary arrivals by traveltime curves over distances of 50–200 km; their velocity decreases with increasing distance. The most significant one (curve c) is observed between distances of 80 and 200 km from the shotpoint and is correlated with the crust-mantle boundary zone.

An approximation method was used for the depth calculations. The method does not require sharp discontinuities and takes into account steady velocity gradients. A test for the existence of low-velocity zones within the crust was made on each profile. A velocity-depth function was calculated for each profile, and the results of profiles along lines were combined to form crustal cross sections represented by contour lines of equal velocity.

Basement velocities between 5.9 and 6.2 km/s were recorded on the profiles in the Basin and Range province, whereas velocities of 6.6–7.0 km/s result from the first arrivals at relatively small distances on the profiles in the adjacent Snake River Plain. A velocity inversion within the upper crust is present on many profiles; the velocity in this inversion zone decreases from about 6.2 to 6.1 or 6.0 km/s, most markedly in the profiles terminating at Lake Mead. Two dominant phases characterized by large amplitudes can be correlated in secondary arrivals on the profiles in the north and east parts of the Basin and Range province. These phases are interpreted as reflected phases from transition zones in which the velocity gradients are very steep. One of these phases is reflected from an intermediate boundary zone between the upper and lower crust and the other from the transition zone between the crust and upper mantle. On the profiles in the southern part of the Basin and Range province, however, the phase correlated with an intermediate boundary zone disappears, and only one phase remains, indicating that a lower crust there is not distinct but rather is part of a thick transition zone between a crust with a low mean velocity of 6.2 km/s and the upper mantle. Upper-mantle velocities based on first arrivals at distances greater than 130 km generally do not exceed 7.8–7.9 km/s, except on profiles recorded in the Mojave Desert. No first arrivals representing upper-mantle velocities were recorded in the Snake River Plain from chemical explosions.

Traveltime curves for the southern part of the Basin and Range province are similar to the ones recorded in the Sierra Nevada. However, the secondary arrivals were less prominent, and P_n arrivals were not recorded on some of the profiles. A low-velocity zone is not present under the central Sierra Nevada but was found at depths 6–10 km under the nearby Lassen Peak National Park area. The mean crustal velocity is higher in the Sierra Nevada than in the Basin and Range province. The velocity in the Sierra increases gradually from 6.2 to 6.6 km/s between depths of 5 and 35 km. The transition zone between crust and mantle is as much as 10 km thick in the Sierra Nevada, and its base rises from 42 to 33 km in depth toward the south.

A fairly sharp crust-mantle boundary was found under the Coast Ranges of California west of the San Andreas fault. The average crustal velocity between 10 and 24 km depth there is 6.3–6.4 km/s, and the total crustal thickness is about 26 km beneath the central Coast Ranges but is greater under the Transverse Ranges.

An intermediate boundary zone within the crust as well as the crust-mantle transition zone can be clearly distinguished from secondary arrivals on the profiles in the Colorado Plateau and in the Middle Rocky Mountains. A low-velocity zone within the crust is apparently present under the Middle Rocky Mountains at a depth of approximately 17 km. The velocity in this zone decreases from 6.4 to 5.8 km/s.

Some basic parameters can be measured on the traveltime curves that may yield objective information on general crustal structure. These parameters were plotted on contour maps. The distance Δ_d at which the P_n traveltime curve d crosses the distance axis and the "critical" distance Δ_c at which the refracted P_n traveltime curve d is tangent to the reflected curve c, which is correlated with the crust-mantle transition zone, represent to a first approximation the variation of the total crustal thickness. High values of the reduced traveltime $\overline{T}_c$ at the distance of critical reflection at the crust-mantle boundary indicate that the crust contains material with relatively low P-wave velocities. The upper-mantle velocity does not exceed 8.0 km/s under the Great Basin and Range province, the Sierra Nevada, or the Colorado Plateau. The lowest upper mantle velocity (7.6 km/s) was found under central and southern Utah. The upper mantle velocity was found to be 8.0 km/s or slightly higher only under the Coast Ranges of California, the Mojave Desert, and the Middle Rocky Mountains.

A fence diagram constructed from the seismic-refraction lines represents the 15 crustal cross sections by contour lines of equal velocity. The contour map of the depth of strongest velocity gradient represents a map of the total crustal thickness. The crust is generally thinner under the Basin and Range province, which has an average thickness of 32–34 km, than under the surrounding

Sierra Nevada, Snake River Plain, Middle Rocky Mountains, and Colorado Plateau, where crustal thicknesses exceed 40 km. Minimums of crustal thickness were found south of the line from Kingman, Ariz., to Barstow, Calif., (28 km) and under the Coast Ranges of central California (24–26 km).

With a few exceptions, the results reported by other authors who studied the same data were confirmed in this study. In some areas, however, velocity inversions in the upper crust were found that have not been reported by previous authors. There is a general correspondence between crustal structure as derived from explosion seismology and Bouguer gravity anomalies, except in the Basin and Range province, in which only regional gravity differences can be explained by differences in crustal structure, whereas the general low gravity there must be attributed to an anomalous upper mantle.

The present results support a previous interpretation for the upper 20 km of the Sierra Nevada crust but differ for the lower part of the Sierra crust, which seems to have lower velocities than previously reported. Upper crustal silicic material is probably absent under the southern Cascade Mountains and the western Snake River Plain. The average composition of the crust in the Basin and Range province must be fairly silicic to account for the seismic velocities, but in the northern part of the province an increasing proportion of mafic mantle material within the lower crust is indicated by the higher crustal velocities. This is true also for the western Snake River Plain. The velocity inversions within the upper crust may be explained by an increase of temperature with depth, which may have stronger influence on velocity than the increase of pressure or grade of metamorphism with depth.

The reinterpretation presented in this report is based on the principles that were used by other seismologists in the Alps and southern Germany. The principal results for central Europe are presented for a comparison of crustal structure of the Western United States and central Europe. The basic traveltime graph in central Europe is generally the same as that found for the Western United States. Contour maps of the parameters Δ_d, Δ_c, and $\overline{T}_c$ represent approximately the general configuration of the crust of the Alps, all three parameters increasing toward the main Alpine axis. The total crust and crust-mantle transition zone are thickest under the main axis of the Alps. A 10-km-thick low-velocity zone exists in the crust between depths of 10 and 30 km, where the velocity decreases from 6.0–6.2 to 5.5–5.6 km/s. The velocity inversion is less marked outside of the Alps.

INTRODUCTION

During the past 10 years, many studies have used explosion seismology to examine the structure of the Earth's crust. Summaries of most of the results in Europe and North America have been published, for example by Steinhart and Meyer (1961), Kosminskaya and Riznichenko (1964), Pakiser and Steinhart (1964), James and Steinhart (1966), Morelli, Bellemo, Finetti, and de Visintini (1967), Closs (1969), Healy and Warren (1969), Kosminskaya, Belyaevsky, and Volvosky (1969), and Sollogub (1969). Detailed experiments have resulted in a huge amount of seismic data, and the methods used and the results obtained by many different authors are heterogeneous; nevertheless, these experiments have also shown that crustal structure does vary from area to area. The U.S. Geological Survey began a detailed study of crustal and upper mantle structure in the Western United States by explosion seismology in April 1960 (Stuart and others, 1964). From 1961 to 1963, 64 profiles were recorded, mainly in California and Nevada, but also in adjacent areas of Idaho, Wyoming, Utah, and Arizona. From 31 shotpoints, 255 chemical explosions, varying in size from less than 1,000 to 20,000 lb, and several underground explosions of nuclear devices at the Nevada Test Site (NTS) served as seismic energy sources. Most profiles were reversed; the average profile length was 300–400 km. Recordings were made at approximately 2,700 individual sites along the profiles. Results concerning the structure of crust and upper mantle in the Western United States have been previously summarized by Pakiser (1963, 1965), Stuart, Roller, Jackson, and Mangan (1964), and Pakiser and Robinson (1966a, b).

This report presents a model of the crustal structure under the Western United States as derived from seismic-refraction measurements and compares this model with one of the crustal structure under the Alps and central Europe (see also Prodehl, 1970a, b). Detailed comparison of the crust of the Western United States and the Alps requires a comparable model for both regions. For this reason, I have reinterpreted many of the seismograms that were recorded in the Western United States by the U.S. Geological Survey from 1961 to 1963 using the same interpretive principles that were used for the construction of the Alpine model by Choudhury, Giese, and de Visintini (1971).

ACKNOWLEDGMENTS

This study was made possible by a grant from the Deutsche Forschungsgemeinschaft (German Research Association) and my succeeding appointment as a Visiting Scientist at the U.S. Geological Survey in Menlo Park, Calif., while on leave from Geophysikalisches Institut der Universität, Karlsruhe, Germany. Fieldwork was supported by the Advanced Research Projects Agency, Department of Defense, as part of VELA UNIFORM, under ARPA Order No. 193. I am indebted to the staff of the U.S. Geological Survey for discussion, advice, and help, especially to L.C. Pakiser, J.H. Healy, S.W. Stewart, and W. Hamilton for review and detailed discussion; J.P. Eaton, W.H. Jackson, J.C. Roller, D.J. Stuart, and S.W. Stewart for unpublished reports, record sections, and computer programs; and Ray Eis for drafting the many drawings.

I am also indebted to Prof. Peter Giese, Freie Universität, Berlin, Germany for detailed discussions

and for figures 91–96. Prof. Stephan Mueller, Universität Karlsruhe, Germany (now at ETH Zürich, Switzerland), and Prof. Mark Landisman, University of Texas, Dallas, made available record sections they compiled of the Mojave-Ludlow profile from the U.S. Geological Survey.

GEOPHYSICAL FIELDWORK

The network of shotpoints and recording stations at which seismograms analyzed in this report were recorded extends from eastern Utah to the Pacific coast and from southern California to central Idaho (fig. 1; pl. 1; table 1).

Except for the nuclear tests, seismic energy was generated by chemical explosions fired in the Pacific Ocean, in lakes, or in drill holes. Ocean shots ranged from 2,000 to 6,000 lb and were placed on the seafloor. The charges in lakes ranged from 2,000 to 10,000 lb and were placed on the lake bottoms. At all the other shotpoints, the charges were fired in drill holes and ranged in size from 250 to 20,000 lb (Roller and Gibbs, 1964). Details of the shot procedure were discussed by Jackson, Stewart, and Pakiser (1963). Usually 10 recording units were used in the field programs. Each unit recorded with an array of six vertical- and two horizontal-component seismometers having natural frequencies of 1 or 2 Hz. Where terrain permitted, the vertical-component seismometers are placed at one-half-km-intervals to form a 2½-km spread that was oriented as far as possible in line with the direction to the shotpoint. The output of the six vertical-component seismometers was recorded on a frequency-modulated magnetic tape system at two levels of amplification separated by 30 dB. In addition, output of the vertical- and horizontal-component seismometers was recorded by an oscillograph on photographic paper at two levels of amplification separated by 15 dB. The paper speed of the recording units was usually 2½ inches per second, but in some instances, especially for the recording of some nuclear tests, the speed was changed to 1¼ inches per second. On a typical record (fig. 3), traces 1–6 and 9–14 show the low-gain and high-gain traces of the six vertical-component seismometers, and traces 7–8 and 15–16 show the low-gain and high-gain traces of the two horizontal-component seismometers. The profile was timed by recording the output of broadcast station WWV (trace 19), a calibrated chronometer (trace 20), and when possible, the shot instant transmitted by radio from the shotpoint (trace 17). A detailed description of the instrumentation used and the procedure of recordings is given by Warrick, Hoover, Jackson, Pakiser, and Roller (1961) and Jackson, Stewart, and Pakiser (1963). The average spacing of the recording units on profiles recorded from chemical explosions was about 10 km, but in a few instances the units were closer together.

The westernmost profiles were recorded in the Coast Ranges of California, partly parallel to and partly across the geologic structures. In the Sierra Nevada, which is separated from the Coast Ranges by the Great Valley of central California, several profiles were recorded parallel to and across the geologic structures. One of these profiles extends into the southern Cascade Range north of the Sierra Nevada. The main part of the investigation was concentrated in the Basin and Range province of Nevada and adjacent areas in southern California, northwestern Arizona, and western Utah. One profile extends into the western Snake River Plain of southern Idaho. In the Middle Rocky Mountains, which border the Snake River Plain and the Great Basin of the Basin and Range province to the east, one profile system was recorded. From the profiles observed in the Colorado Plateau, only one line recorded in 1963 is included in this report. Figure 4 is a simplified geologic map of the area covered by seismic profiles. More details of this fieldwork can be obtained from unpublished reports such as those by Cooper, Strozier, and Martina (1962), Frankovitch, Cooper, and Forbes (1962), Healy and others (1962), Roller and Gibbs (1964), Roller, Jackson, Cooper, and Martina (1963), and Roller, Strozier, Jackson, and Healy (1963), from which many of the data such as distances and coordinates were taken for the present investigation.

PROCEDURE OF INTERPRETATION

RECORD SECTIONS

One of the most difficult tasks in interpreting seismic-refraction measurements is the correlation of the different wave groups from seismogram to seismogram along the profile. The correlation of later arrivals is especially delicate. To facilitate this correlation, all seismograms along a profile were arranged into a record section according to their distance from shotpoint and reduced traveltimes. Because the present study is confined to the investigation of compressional (P) waves propagating in the crust and uppermost mantle, 6 km/s is a suitable reduction velocity. The reduced traveltime ($\overline{T}$) is defined as the observed traveltime (T) minus distance (Δ) divided by reduction velocity (V_r): $\overline{T} = T - \Delta/V_r = T - \Delta/6$. Record sections were drawn by hand for 52 profiles (see, for example, fig. 10 and table 55). Because of the array length of 2.0–2.5 km at nearly every recording site, it was possible to draw more than one seismic

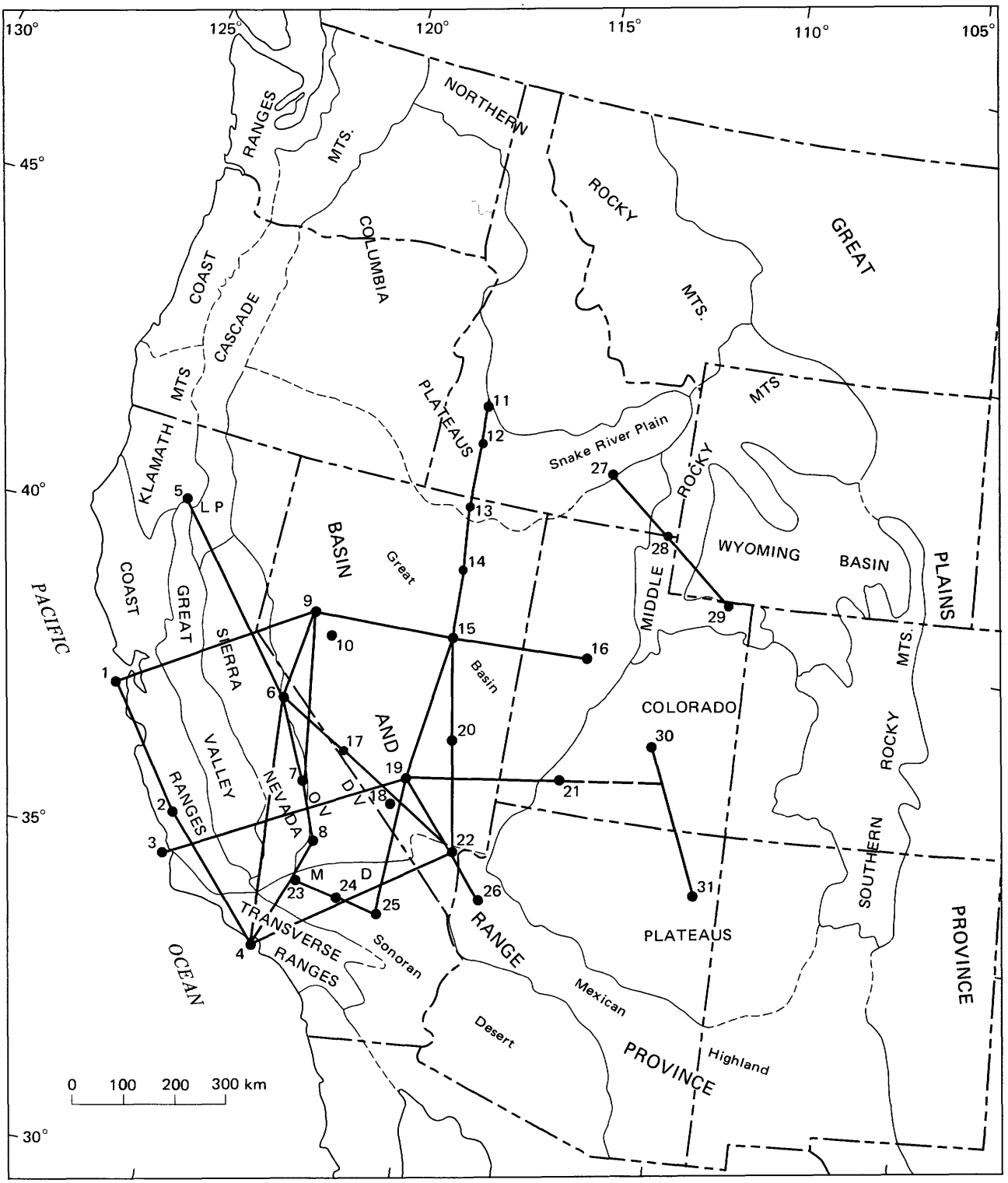

FIGURE 1.—Physical divisions of the Western United States and location of seismic profiles. After the map of the physical divisions of the United States by Fenneman and Johnson (1946). M. D., Mojave Desert; O. V., Owens Valley; D. V., Death Valley; L. P., Lassen Peak National Park. Shotpoints are listed in table 1.

trace per seismogram. In most instances the traces recorded nearest to and most distant from the shotpoint at each station were used (traces 1, 6, 9, and 14, fig. 3). The high-gain traces (9 and 14) were used if the peak-to-peak amplitude of the most prominent phase on the original record did not exceed 4 cm. For

TABLE 1.—*Location of shotpoints*

No.	Shotpoint	Coordinates N. lat	Coordinates W. long	Altitude (m)
1	San Francisco	37°36.08′	122°41.55′	Sea level
2	Camp Roberts	35°47.38′	120°49.98′	208
3	San Luis Obispo	35°07.60′	120°47.10′	Sea level
4	Santa Monica Bay	34°00.06′	118°33.28′	Sea level
5	Shasta Lake	40°46.17′	122°13.92′	314
6	Mono Lake	37°59.00′	119°07.60′	1,950
7	Independence	36°44.79′	118°15.72′	1,655
8	China Lake	35°47.00′	117°44.96′	677
9	Fallon	39°31.43′	118°52.48′	1,220
10	SHOAL	39°12.02′	118°22.82′	1,740
11	Boise	43°34.70′	115°58.95′	931
12	Strike Reservoir	42°55.29′	115°53.70′	748
13	Mountain City	41°50.24′	115°53.70′	1,683
14	Elko	40°46.23′	115°40.97′	1,625
15	Eureka	39°30.82′	115°39.00′	1,806
16	Delta	39°40.55′	112°35.55′	1,150
17	Lida Junction	37°20.96′	117°29.54′	1,658
18	Lathrop Wells	36°37.18′	116°13.76′	951
19	Nevada Test Site (NTS)[1]	37°07′	116°02′	1,400
20	Hiko	37°54.20′	115°13.80′	1,538
21	Navajo Lake	37°32.53′	112°47.55′	2,912
22	Lake Mead	36°05.28′	114°47.96′	369
23	Mojave	35°03.02′	118°00.33′	786
24	Barstow	34°58.34′	117°04.23′	755
25	Ludlow	34°49.36′	116°11.02′	396
26	Kingman	35°19.36′	114°03.92′	1,180
27	American Falls Reservoir	42°50.14′	112°48.66′	1,360
28	Bear Lake	41°56.35′	111°17.10′	1,820
29	Flaming Gorge Reservoir	40°56.77′	109°38.43′	1,730
30	Hanksville	38°21.99′	110°55.64′	1,430
31	Chinle	35°55.64′	109°34.44′	1,830

[1]Approximate center of location of the NTS shots used in this report.

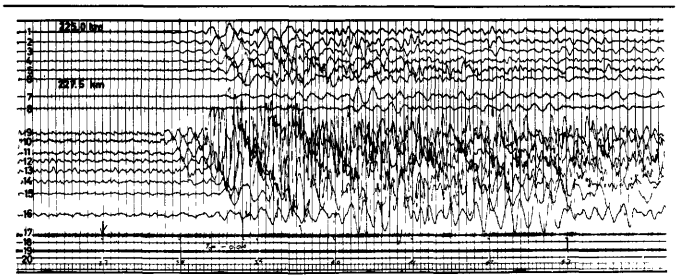

FIGURE 3.—Typical seismic record. Seismic signals: Nos. 1-6 and 9-14: low- and high-gain traces of six vertical-component seismometers; Nos. 7-8 and 15-16: low- and high-gain traces of two horizontal-component seismometers. The two levels are separated by 15 dB. Timing signals: No. 19: broadcast station WWV; No. 20: calibrated chronometer; No. 17: shot instant if possible.

seismograms with weak first arrivals and secondary phases with extremely high amplitudes, the low-gain traces (1 and 6) were used together with a high-gain trace from near the middle of the record. The last column of the tables 55-107 shows which traces of each record were used for the corresponding record section. No corrections were made to eliminate the influence on a recording site of near-surface low-velocity sediments, because little is known about the thickness and seismic velocities of these sediments.

For one profile (Delta-SHOAL) an unpublished record section prepared by S.W. Stewart and P.R. Stevenson was available. The analog records for this profile were digitized and the digitized records plotted by computer into a record section. The record section for the profile NTS-Kingman was compiled by Diment, Stewart, and Roller (1961).

PRINCIPLES OF THE OBSERVED TRAVELTIME DIAGRAMS

Most previous interpretations of the profiles studied were based on the assumption that the Earth's crust consists of layers that are characterized by constant velocities and are separated from each other by sharp discontinuities. As Stuart, Roller, Jackson, and Mangan (1964) pointed out, first-arrival times for most profiles were approximated by a two- or three-segment straight-line traveltime curve. These segments represent the arrival times of compressional waves that have been refracted at velocity interfaces in the upper crust (P_g), in the lower crust (P), and beneath the Mohorovičić discontinuity (M-discontinuity) (P_n). Large-amplitude reflected phases that arrived at times appropriate for reflections from the top of the upper mantle (P_MP) and from the top of a lower crustal layer (P_lP) (Healy and Warren, 1969) were also found. No attempt was made in these studies to determine whether or not low-velocity layers exist within the crust.

In the present investigation, no assumption was made concerning the character of correlated phases (refraction, reflection, or other). The method of depth calculation used does not require sharp discontinuities, but takes into account steady velocity gradients. Also, the possibility of low-velocity crustal zones was investigated. Careful study of the record sections showed that within the Western United States, similar phases can be found that fit into a basic traveltime diagram. On any profile, one or more traveltime branches may be missing, but a generalized traveltime diagram can be drawn (fig. 5). In this report only the structure of the Earth's crust is investigated systematically. Phases concerning local sedimentary sequences or upper mantle structure are not investigated in detail. Phases that are present only sporadically on a few profiles are not considered here.

At distances of up to 100-150 km from the shotpoint, a traveltime curve, *a*, can be observed in the first arrivals. This phase can be correlated with the basement rocks. Usually the first arrivals aline on a continuous convex-upward curve that starts at the origin of the traveltime diagram. However, delays often occur, especially in the Basin and Range province, owing to sediments that cover the basement and whose thickness varies from station to station. With increasing distance the amplitudes of wave group *a* get smaller and gradually die out, usually between 100 and 150 km. A prominent phase, *c*, characterized by large amplitudes, was recorded in the later arrivals on all profiles between 70 and 240 km from the shotpoint (fig. 9). Traveltime curve *c* is concave upward with respect to the distance axis. Most authors who have worked on seismic-refraction profiles in the Western United States denote these arrivals by P_MP and interpret them as P waves reflected from the Mohorovičić discontinuity. On the assumption of a monotonic velocity

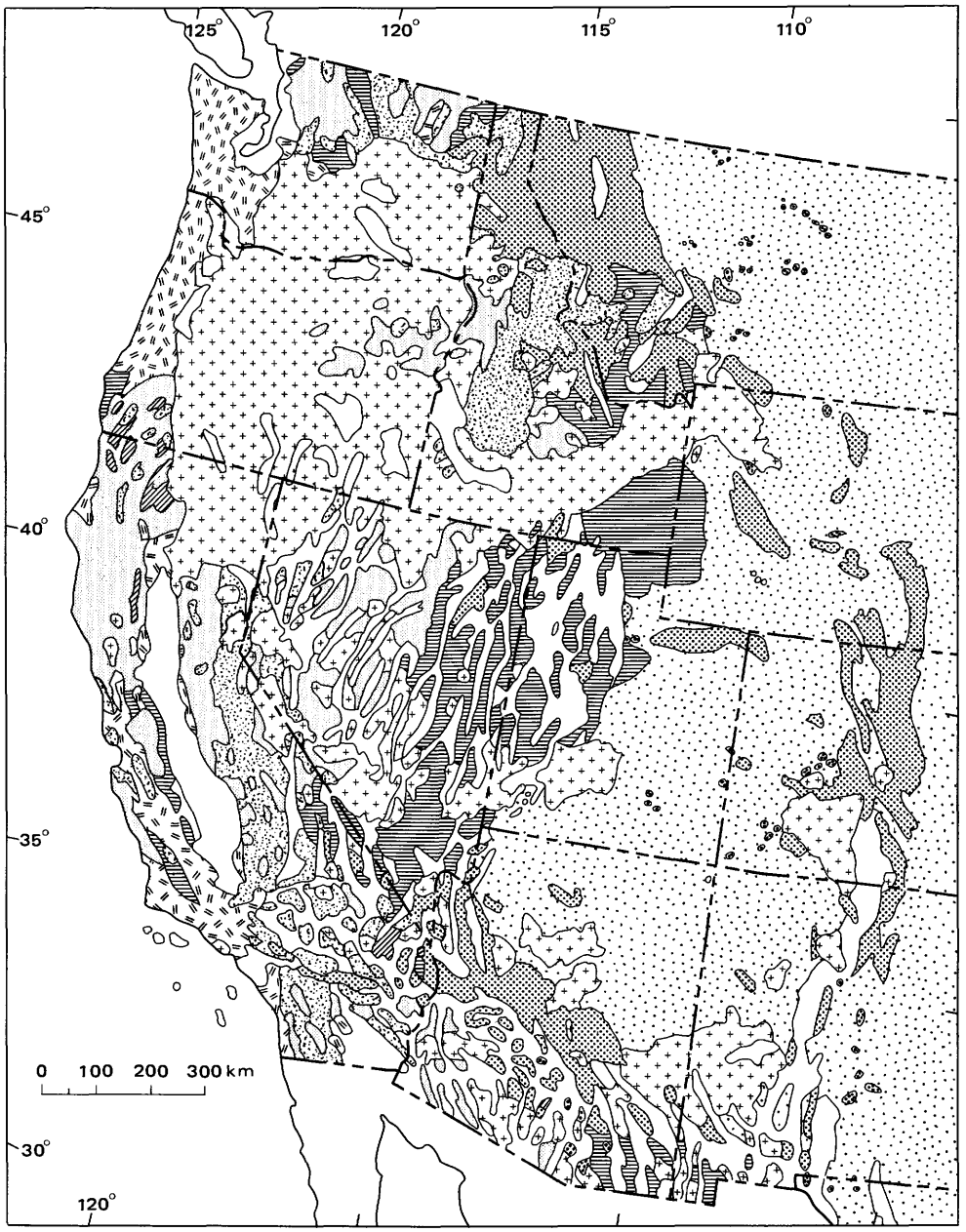

EXPLANATION

- Terrestrial basin fill of Tertiary and Quaternary age
- Marine deposits of Tertiary age
- Miogeosynclinal deposits and shelf deposits of Paleozoic and Mesozoic age
- Eugeosynclinal deposits of Paleozoic and Mesozoic age
- Terrestrial volcanic rocks of Tertiary and Quaternary age
- Granitic and other intrusive rocks of Mesozoic and Tertiary age
- Ultramafic rocks
- Precambrian rocks
- Platform deposits overlying basement rocks of Precambrian age

FIGURE 4.—Simplified geologic map of the Western United States. After King (1967).

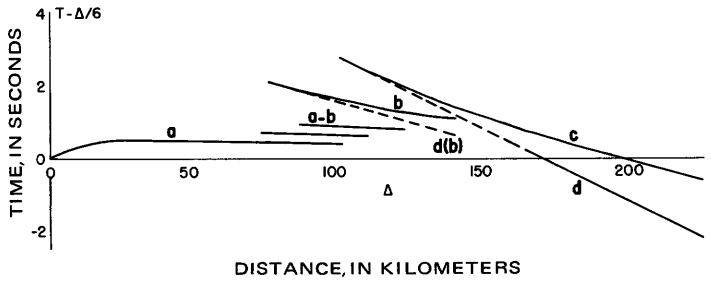

FIGURE 5.—Basic traveltime diagram. The numbers on both axes indicate approximate values. The curves can be shifted as much as 30-50 km and up to ±2-3 seconds.

increase with increasing depth, Bullen (1963), Officer (1958), Giese (1966), and others have shown that the corresponding traveltime curve becomes retrograde where the velocity increases very quickly within a certain depth range, forming the type of traveltime curve that is observed as c or P_MP on the seismic-refraction profiles. The velocity measured by the reciprocal slope of such a traveltime curve decreases with increasing distance from about 7.2-8.0 km/s to 6.2-6.6 km/s. Traveltime curve c therefore is explained as a strong increase in velocity at the base of the crust.

Phase d is observed in first arrivals at distances greater than about 130-200 km, depending on crustal thickness and velocity (for example, fig. 9). The extension of traveltime curve d as a secondary arrival toward smaller distances ends where it becomes tangent to curve c. The measured velocities at that point are 7.4 km/s or more. Phase d can usually be recognized only where it occurs as a first arrival, however. The waves represented by d penetrate the upper mantle. This phase is usally called P_n if its velocity is greater than 7.6 km/s.

Another phase, represented by traveltime curve b, is present on many profiles (for example, fig. 9). On some seismograms it is as prominent as phase c. This traveltime curve is also concave upward with regard to the distance axis, and it is interpreted as a retrograde curve reflecting a fairly strong increase in the velocity between the upper and lower crust. However, although very well observed in some areas, this phase is very weak (for example, fig. 11) or does not seem to exist in others. In some areas where the phase b is very well expressed, a forerunning phase, $d(b)$, can be observed (for example, figs. 9, 17). The traveltime curve $d(b)$ is tangent to curve b in a manner analogous to the curves c and d.

All of these phases can usually be correlated over 10 km in distance or more. On some profiles, additional phases between traveltime curves a and b can be correlated. These curves have nearly the same velocity as the most distant end of curve a and also of curve b. These curves were named a–b by Giese (1966) (for example, fig. 10).

If the velocity is assumed to increase monotonically with depth but with variable velocity gradients, the corresponding traveltime diagram should be a continuous system with cusps (triplications) corresponding to depths where the velocity gradients are very strong. However, many traveltime curves cannot be combined to form a closed system, even under the assumption that some phases are missing, owing to a lack of energy or too wide spacing of the recording units. Rather, the extension of the curves a and b or $d(b)$ and c toward greater distances sometimes results in parallel segments that cannot be combined to form continuous cusps, because b or c is delayed for fractions of a second or more with respect to a or $d(b)$. One explanation for this delay is the existence of a velocity-inversion zone with increasing depth.

The arrangement of traveltime curves described above was first described in detail by Giese (1966) in a systematic investigation of 12 profiles in southern Germany and the Alps. These seismic-refraction profiles in central Europe as interpreted by Giese (1966) and by Choudhury, Giese, and de Visintini (1971) are compared in this report with the seismic-refraction profiles in the Western United States.

CALCULATION OF THE VELOCITY-DEPTH FUNCTION FROM THE TRAVELTIME DIAGRAM

As shown above, a consistent arrangement of the different traveltime segments, $T(\Delta)$, exists for all profiles. For the determination of the corresponding velocity-depth function, $V(z)$, several methods can be applied. The simplest case is that the correlated traveltime curves are straight line segments. Under the assumption that the Earth's crust consists of layers with constant velocities separated by discontinuities at which

the velocity increases discontinuously from V_i to V_{i+1}, formulas have been developed to calculate depth and dip of the corresponding layers (for example, Bullen, 1963; Officer, 1958; Perrier, 1973; Steinhart and Meyer, 1961). However, as has been shown, usually the arrivals correlated do not aline along straight line segments.

Curved segments can occur in first as well as in later arrivals. When later arrivals are fitted by concave traveltime curves, they can be interpreted as reflection from first-order discontinuities (T^2, Δ^2 method). All these methods assume constant-velocity layers with first order discontinuities.

A more general method for inversion of traveltime data into depth values is offered by the Wiechert-Herglotz method (Giese, 1963). This method can be applied for the determination of the complete velocity-depth function when the traveltime curve, $T(\Delta)$, starts at the origin ($T=0$, $\Delta=0$) and forms a continuous function including cusps and when the derivative, $d\Delta/dT$, increases continuously along the traveltime curve. Then the depth, z, at which the velocity reaches the value $V(\Delta_1)$ is obtained by the following equation:

$$z = \frac{1}{\pi}\int_0^{\Delta_1} \cosh^{-1} \frac{V(\Delta_1)}{V(\Delta)}\, d\Delta, \quad \Delta < \Delta_1 \qquad (1)$$

However, an exact solution is not possible if the traveltime curves cannot be combined into a continuous function, because then the conditions of integration are no longer fulfilled. This is the case for many profiles discussed herein. Instead of a continuous system, interruptions occur within the traveltime diagram. Such an interruption can have several causes (fig. 6*A*):

a. A discontinuity of first order exists. The distance of point B is infinite (neglecting the curvature of the Earth). In this case the traveltime curve BC is a true reflection hyperbola.

b. The profile is too short; one part of the cusp is located beyond the maximum recording distance.

c. A velocity inversion exists within the crust.

d. The connection of the different traveltime segments is open, because only short segments of traveltime curves can be correlated clearly. This may be the case, for instance, when two cusps are interfering.

In each case, the determination of $V(z)$ is no longer unique. In order to get information on crustal structure, some simplification must be introduced. Assuming first-order discontinuities, for example, different methods have been proposed. For instance, the T^2, Δ^2 method can be applied on the "reversed" segments — "reversed" meaning those parts of the traveltime-curve system where the velocity, $V(\Delta)$, decreases with increasing Δ (for example, reflection hyperbolas). The application of this method, however, is satisfactory for $T(\Delta)$ values in the critical and subcritical range only but not in the supercritical range (Stewart, 1968b).

Because the seismic-refraction profiles recorded for crustal studies show mainly the supercritical part, a more general method should be applied. Fuchs and Landisman (1966) and Mueller and Landisman (1966) use an indirect method to calculate the velocity-depth function for the case of interrupted traveltime curves. Starting from a rough model, they try to correct this model by trial and error until the best fit is reached between observed and theoretical traveltimes. Any model that fulfills the conditions of flat-layering is possible. Usually discontinuous velocity increases are assumed.

Giese (1966) has proposed an approximation method to calculate rapidly the velocity-depth distribution directly from any given traveltime-curve system. The method assumes also homogeneity in the horizontal direction but takes especially into account the existence of finite velocity gradients, meaning that the velocity is not constant but may increase continuously with increasing depth. Also, the possible existence of velocity inversions is recognized in this method.

The crustal models in this paper for the different parts of the Western United States are based on Giese's method exclusively (fig. 6). This method was used for the reinterpretation of the data shown below for several reasons. Firstly, the method allows a quick determination of deep structure from traveltime data.

FIGURE 6.—Diagrams illustrating principles of observations and their inversion into velocity-depth functions based on a method after Giese (1966). *A*, Examples of disconnected traveltime curves and the corresponding velocity-depth functions: (*a*) First-order discontinuity. The corresponding traveltime curve is a hyperbola BC, but the distance of point B is infinite. (*b*) Second-order discontinuity. The distance range of observations is insufficient. (*c*) Velocity inversion. (*d*) Interference of two cusps causing uncertainties in the correlation of phases. *B*, Ray path in a homogeneous (full lines) and an inhomogeneous layer (dashed lines) and the corresponding velocity-depth functions. *C*, Presentation of $V(z_{max})$ (full lines) for (*a*) $dV/dz_{max} = 0$, (*b*), $dV/dz_{max} < 0$ and (*c*) $dV/dz_{max} > 0$ and the corresponding velocity-depth functions $V(z)$ (dashed lines). *D*, The possible solutions of velocity-depth functions from a given traveltime diagram are located between the curves $V(z_{max})$ and $V(z_{min})$. *E*, Sketch demonstrating the position of points A and B of a traveltime diagram necessary for the direct determination of the maximum thickness δz_{max} and the average velocity $\overline{V}_i$ of a low-velocity zone, that is, the range between the depths corresponding to the rays emerging at $\Delta(A)$ and $\Delta(B)$. *F*, Sketch for the estimation of the average velocity $\overline{V}_i$ within a depth range δz for which $V(z)$ cannot be calculated directly.

Secondly, the ability to account for the existence of velocity-gradient zones and of zones with velocity inversions within the crust is of great importance for the reinterpretation. The inclination of reversed traveltime curves usually differs considerably from the inclination of a traveltime curve interpreted as a reflection from a sharp discontinuity within the crust. Finally, because the comparison of the crustal structure of the Western United States with that of central Europe is one of the aims of the reinterpretation presented here,

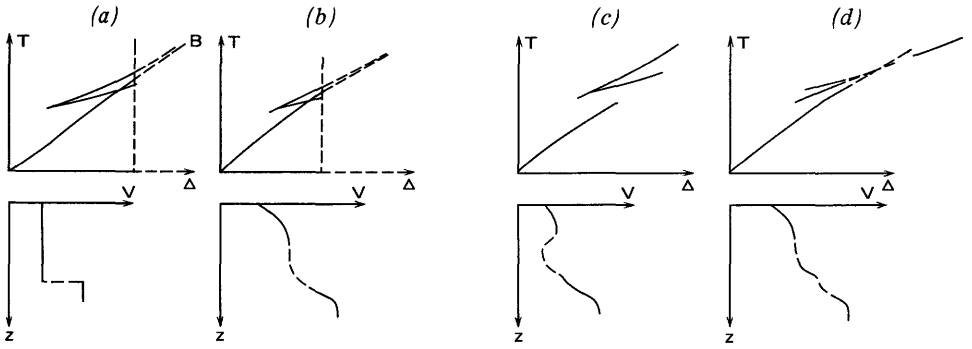

A

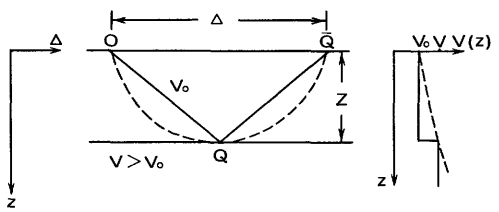

B

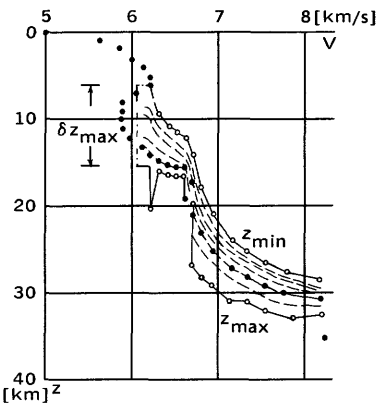

D

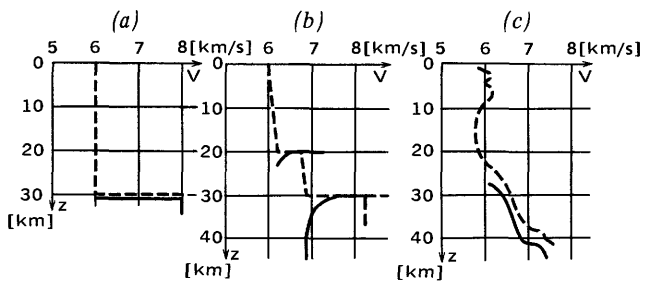

C

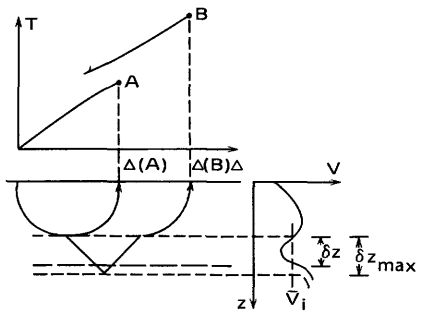

E

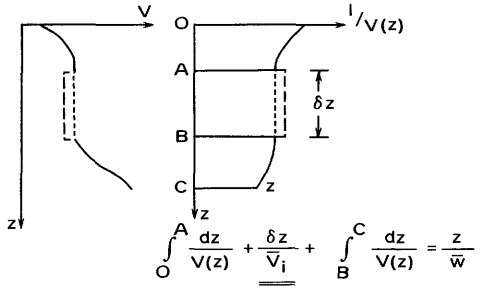

F

the same methods should be used for the interpretation of seismic-refraction measurements in both areas. In Europe, Giese's method was applied in many seismic-refraction investigations carried out in western Germany, the Alps, Italy, and elsewhere, as will be discussed in some detail in the last section. Therefore it is essential to apply the same method to as many profiles in the Western United States as possible, if a valid comparison of structures is to be realized.

Cross sections are compiled on the basis of velocity-depth functions calculated for each profile (for example, fig. 12). Though the depth calculations are made under the assumption that no horizontal changes occur, the resulting velocity-contour lines actually dip and rise. Dips less than 5° can be neglected, however, because the uncertainty in arrival times in the records is greater than errors in depth calculation caused by dips less than 5° (Peter Giese, written commun., 1975).

For some examples presented here, velocity-depth calculations have been made by the author using other methods, including the computation of synthetic seismograms, in order to prove the reliability of the models obtained by Giese's method. The resulting models do not differ in essential parts; rather, slight deviations in models occur at depths where the velocity gradient is weak or where the error of velocity distribution is rather large owing to uncertainties in the correlation of the corresponding phases. The greatest relative difference occurred in profiles whose corresponding velocity-depth functions contain zones with marked velocity reversals. It turned out that the approximate determination of the velocity within such low-velocity zones leads to slightly different values from those obtained with other methods. However, in the following section only the models are presented that were obtained with the method of Giese, even if there are some discrepancies with the depth determinations using other methods.

The approximation method by Giese will be described in detail below, following description and discussions published by Giese (1966), Bram and Giese (1968), and Perrier (1973). For all following discussions, the term "normal" traveltime curves or segments will be used for the cases in which the recording distance increases with increasing depth of penetration of the corresponding wave, approximated by a curved ray path. The term "reversed" traveltime curve or segment will be used when the recording distance decreases with decreasing angle of incidence.

Assuming a two-layered model consisting of homogeneous upper and lower layers characterized by the respective velocities V_o and V, for the wave reflected from the discontinuity between upper and lower layer, the following equations are valid:

$$\left(\frac{\Delta}{2}\right)^2 + z^2 = \left(V_o \cdot \frac{T}{2}\right)^2 \tag{2}$$

and

$$V = \frac{d\Delta}{dT} \cdot \tag{3}$$

From these equations the following relation can be deduced:

$$z = \frac{\Delta}{2}\sqrt{\frac{T\,d\Delta}{\Delta\,dT} - 1}\,, \tag{4}$$

which allows us to determine exactly the depth of the reflecting horizon. This depth determination can be used also when the overburden is inhomogeneous, in which V_o corresponds to an average velocity equal to the average velocity, $\bar{u}$, of a ray that traverses the upper medium perpendicular to the layers of the upper medium:

$$\bar{u} = \int_0^z dz / \left(\int_0^z dz/V(z)\right). \tag{5}$$

Continuously refracted waves (called by some authors diving waves or "Tauchwellen") can be regarded as the critical case of reflected waves, their angle of apparent reflection being 90° (curved ray path O-Q-$\bar{Q}$ in fig. 6*B*). The principle of Fermat requires that the calculated depth value be greater than the real depth (Dix, 1955), and for each value of $d\Delta/dT = V$ (velocity at the point of maximum penetration of the corresponding ray) the following relation is valid:

$$z(V) \leqslant z_{max} = \frac{\Delta}{2}\sqrt{\frac{Td\,\Delta}{\Delta\,dT}} \cdot \tag{4a}$$

Jobert and Perrier (1974) demonstrated with the aid of the "Schwarz'sche Ungleichung" that z_{max} is really the maximum depth to which the corresponding ray can penetrate. By equation 4a, z_{max} can easily be calculated for all points of normal and reversed traveltime curves.

For normal traveltime curves, the quantity dV/dz_{max} derived from the curve $V = V(z_{max})$ is always positive.

For reverse segments three cases are possible (fig. 6*C*):

(a) $dV/dz_{max} = 0$: The mean velocity is independent of the angle of incidence. The overburden is homogeneous. The T^2, Δ^2 method can be used.

(b) $dV/dz_{max} < 0$: The overburden is not homogeneous, and the velocity increases sharply within the corresponding depth range.

(c) $dV/dz_{max} > 0$: The velocity gradient, dV/dz, is also positive; a transition zone exists.

By this very simple method it is possible to tell if the corresponding boundary zone is a discontinuity or a broader transition zone.

For the case of correlated traveltime segments separated from each other, a minimum depth can also be determined using the integral of Wiechert-Herglotz for the traveltime segments known:

$$z_{min} = \frac{1}{\pi}\left(\int_0^{\Delta_1} \cosh^{-1} \frac{V(\Delta_n)}{V(\Delta)}\, d\Delta + \right.$$

$$\Delta_2\int^{\Delta_3} \cosh^{-1} \frac{V(\Delta_n)}{V(\Delta)}\, d\Delta$$

$$\left. + \ldots + \Delta\int_{n-1}^{\Delta_n} \cosh^{-1} \frac{V(\Delta_n)}{V(\Delta)}\, d\Delta \right) , \; z_{min} < z(V). \quad (6)$$

z_{min} can be calculated for all points of the normal and reversed traveltime segments.

After the correlation of traveltime curves is fixed, the unknown velocity-depth function, $V(z)$, must be located between the two limiting functions of z_{max} and z_{min}. It must be asumed that the velocity gradient, dV/dz, changes linearly between z_{min} and z_{max}. Figure 6*D* shows an example of a velocity-depth function that was calculated after the method described below.

For the selection of the most probable velocity-depth relation, the solutions that show a negative gradient must be rejected. Furthermore, one can reduce the number of possible solutions by taking other data into account. As mentioned above, the velocity gradient, dV/dz, has an important influence on the determination of the velocity-depth function, $V(z)$. Having this in mind, Giese (1966) assumed several velocity-depth distributions that characterize reasonable crustal models, V ranging from 5 to 8.2 km/s. From these models he calculated the corresponding traveltime curves and plotted the values z/Δ versus $V(T/\Delta)$ (fig. 7). As can be seen in figure 7, all points belonging to the same velocity gradient can be approximately represented by a curve in which the scatter of points is much greater for small velocity gradients than for large ones. With increasing velocity gradient, the curves approach the limiting curve, which is valid for an infinite velocity gradient ($dV/dz \rightarrow \infty$) and is identical with z_{max}.

In order to approach the real solution it is sufficient to start with the determination of z_{max} by equation 4a, where T, Δ, and $\frac{d\Delta}{dT} = V$ are read from the traveltime diagram, and to deduce for each point of the curve $V(z_{max})$ thus obtained the corresponding velocity gradient dV/dz_{max}. Using this gradient as the new

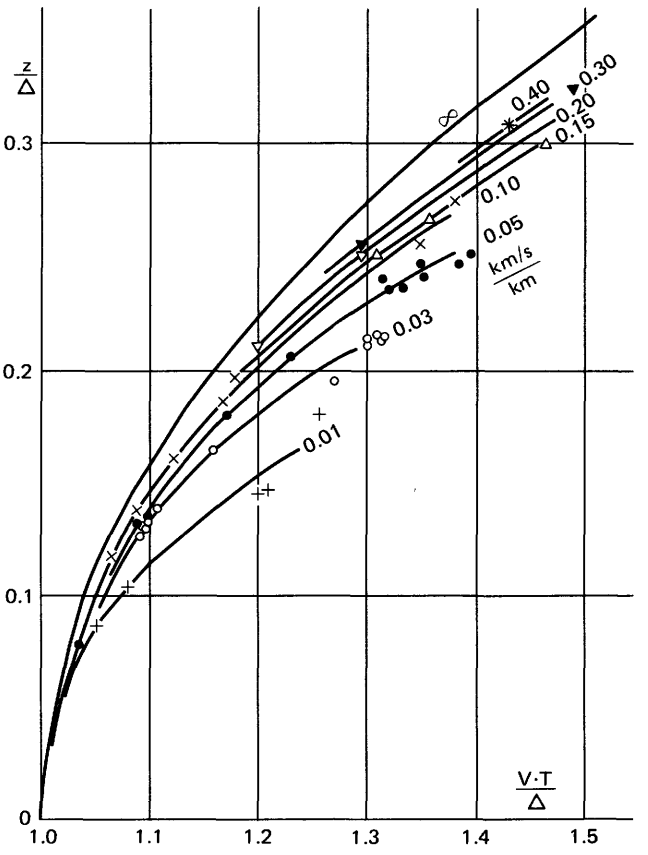

FIGURE 7.—Diagram showing z/Δ versus $V(T/\Delta)$ with velocity gradient, dV/dz, being parameter. After Giese (1966).

parameter, the diagram of figure 7 gives now a new depth, z, for each point (T, Δ, V). From the resulting new function, $V(z)$, again the velocity gradient can be determined for each point (T, Δ, V) and the corresponding depth obtained. This procedure is repeated three or four times until the curve $V(z)$ does not change significantly. A specific solution results from this procedure because the diagram of figure 6 is constructed on the base of velocities that are probable within the Earth's crust. Figure 8 shows examples of three profiles in the Western United States demonstrating the three possible cases of reversed traveltime curves as discussed above. The open circles show the calculated values of z_{max} using equation 4a, and the full circles show the corrected values using the iteration process described above.

Giese has also empirically deduced the following equation, which allows us to approach the solution:

$$z = p \cdot \frac{\Delta}{2}\sqrt{\left(\frac{T}{\Delta} \cdot V\right) - 1}\,, \quad (7)$$

where

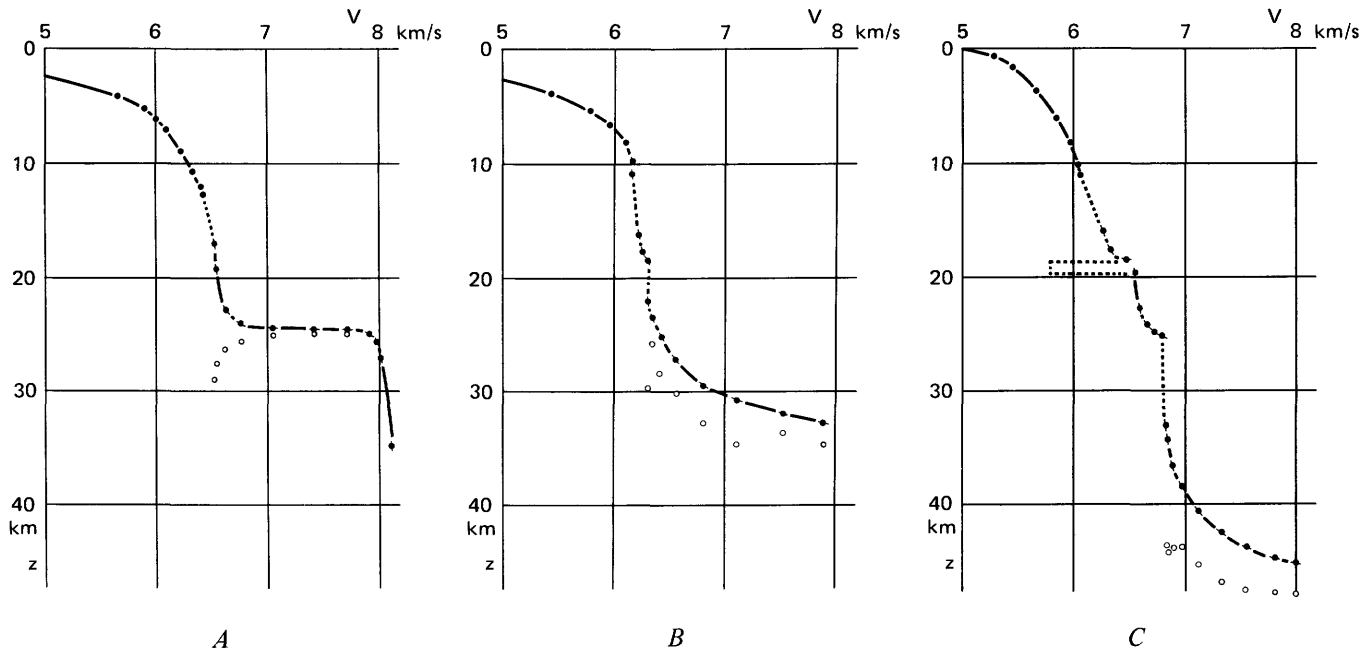

FIGURE 8.—Velocity-depth functions calculated by the approximation method after Giese (1966). Open circles represent the calculation of z_{max}, the first approximation. Full circles show the result after the last approximation step; the slope of the short lines through points is equal to the velocity gradient, dV/dz. *A*, Calculated from the traveltime diagram of the profile San Luis Obispo—NTS (fig. 73; table 47): $dV/dz_{max} < 0$, $dV/dz \rightarrow \infty$. *B*, Calculated from the traveltime diagram of the profile Fallon—China Lake (fig. 58; table 38): $dV/dz_{max} < 0$ and > 0. *C*, Calculated from the traveltime diagram of the profile American Falls—Flaming Gorge (fig. 77; table 50): $dV/dz_{max} > 0$, $dV/dz > 0$. The values for z_{max} are only presented for the part concerning curve *c*. All velocity-depth functions are cut off for velocities less than 5 km/s.

$$p = \frac{1}{4\sqrt{1 + \frac{\alpha}{\beta}}}$$

where $\alpha = (V - V_1)$ is the mean gradient (V_1 — velocity at the surface) and $\beta = dV/dz$ is the local velocity gradient at the depth z.

Giese (1966) has estimated the error on the depth determination when using equation (7):

(a) The error in the determination of Δ can be neglected.

(b) The error in dV is

$$\frac{dz}{z} = \frac{TdV}{2\Delta\left(\frac{T}{\Delta} \cdot V - 1\right)},$$

where $\Delta/T = 6$ km/s, $VT/\Delta = 1.2$, and $dV = 0.1$ km/s. It results in

$$\frac{dz}{z} = \frac{0.1}{2.4} = 0.04 = 4\% .$$

(c) The error in dT is

$$\frac{dz}{z} = \frac{VdT}{2\Delta\left(\frac{T}{\Delta} \cdot V - 1\right)},$$

where $V = 7$ km/s, $\Delta = 140$ km, $dT = 0.05$ s (accuracy of traveltime determination from a record section), and $VT/\Delta = 1.2$;

$$\frac{dz}{z} = 0.006 = 0.6\% .$$

(d) The error in $d\left(\frac{\alpha}{\beta}\right)$ is

$$\frac{dz}{z} = \frac{1}{4\left(1 + \frac{\alpha}{\beta}\right)} d\left(\frac{\alpha}{\beta}\right),$$

where $\frac{\alpha}{\beta} = 1$ and $d\left(\frac{\alpha}{\beta}\right) 0.2$;

$$\frac{dz}{z} = \frac{0.2}{8} = 0.025 = 2.5\%.$$

Given the inaccuracy of the values chosen above, an average error of 5 percent may result. The error determination shown here requires that the correlation be

certain. The total error in the determination of the depth, z, depends on the gradient, dV/dz, at the point of maximum penetration of the corresponding ray. If the gradient is strong (>0.1 km/s/km), the error is about 3 percent. It increases to 5-10 percent for smaller gradients (between 0.01 and 0.1 km/s/km).

When the segments of the traveltime diagram are interrupted, only parts of the complete function $V(z)$ can be determined, whereas between these determinable parts of $V(z)$, velocity inversions may be present. It is possible to determine the maximum thickness, z_{max}, and the mean velocity, $\overline{V}_i$ (see fig. 6*E*) for those depth ranges not determinable from the traveltime diagram if the coordinates of points A and B, as well as the apparent velocity, $V_{A,B}$, at these points, can be determined. Then the following equations can be applied:

$$\delta z_{max} = \frac{\delta\Delta}{2} \sqrt{\left(\frac{\delta T}{\delta\Delta} \cdot V_{A,B}\right)^{-1}}, \tag{8}$$

$$\overline{V}_i = \sqrt{\frac{\delta\Delta}{\delta T} \cdot V_{A,B}}, \tag{9}$$

with

$$\delta\Delta = \Delta(B) - \Delta(A),$$

$$\delta T = T(B) - T(A), \text{ and}$$

$$V_{A,B} = \frac{d\Delta(B)}{dT} = \frac{d\Delta(A)}{dT}.$$

With these equations a homogeneous low-velocity zone is assumed. δz_{max} is the upper limit for the thickness of the low-velocity zones; its lower limit is equal to zero.

In most cases, however, the points A and B cannot be defined precisely. Nevertheless it is possible to estimate the average velocity, $\overline{W}$, with such a depth range, for which $V(z)$ is not determined, by the following expression (fig. 6*F*):

$$\frac{\delta z}{\overline{V}_i} = \frac{z}{\overline{W}} - \int_0^A \frac{dz}{V(z)} - \int_B^C \frac{dz}{V(z)}, \tag{10}$$

where

$$\overline{W} = \frac{2}{T} \sqrt{z^2 \quad (\Delta/2)^2}. \tag{11}$$

Giese has proposed the following procedure to estimate the average velocity for the undetermined depth ranges: Having calculated for a point (Δ, T, V) the corresponding depth, z, by equation (5) one can determine the mean velocity, $\overline{u}_\perp$, for a ray traversing the Earth's crust perpendicularly, that is, travelling perpendicular to the lines of equal velocity. Assuming that the path for other rays that do not travel perpendicularly is a straight line, that is, neglecting Snellius' law, the average velocity, $\overline{W}$, along this way is the same as that for $\overline{u}_\perp$. $\overline{W}$ can be determined by equation 11. In reality according to the principle of Fermat, the traveltime along the straight line is greater than the traveltime along the actual curved ray path (see ray paths O-Q-$\overline{Q}$ in fig. 6*B*). In consequence (according to equation 11) the calculated average velocity, $\overline{W}$, based on the observed traveltime, T, is greater than $\overline{u}_\perp$:

$$\overline{W} \geq \overline{u}_\perp, \tag{12}$$

the equal sign being valid for rays travelling perpendicular to the lines V = constant, or for a homogeneous overburden.

As described above, for a point (Δ, T, V), the depth, z, and the average velocity, $\overline{W}$, can be determined. The determination of the average velocity, $\overline{u}_\perp$, however, is not immediately possible if the function $V(z)$ can only be determined piecewise, as is true for most cases. Therefore, in a first step, a linear interpolation across the missing parts of $V(z)$ is made and the integral

$$\overline{u}_\perp = z/\left(\int_0^z dz/V(z)\right) \tag{5a}$$

is calculated (for instance, graphically, as indicated in figure 6*F* by the dotted part of $V(z)$ and $1/V(z)$). Commonly, the resulting values for $\overline{u}_\perp$ are greater than $\overline{W}$, in contradiction to equation 12. This contradiction can be avoided by introducing velocity inversions, $\overline{V}_i$, within the indeterminate parts δz of $V(z)$ and recalculating the integral 5a until the relation in equation 12 is fulfilled. Of course, only an average value can be estimated for the corresponding depth ranges. For the determination of $\overline{W}$ (equation 11) it is recommended to use a ray characterized by the relation

$$\Delta/z < 4/1. \tag{13}$$

The condition is fulfilled mostly by critical rays.

ANALYSIS OF SEISMIC-REFRACTION PROFILES

The profiles recorded from each shotpoint in the different azimuths were analyzed in detail. A record section is presented for each profile. With two exceptions (Delta-SHOAL and NTS-Kingman), tables present the following data for each section: the distance of the least and most distant seismometers from the shotpoint (traces 1 and 6, and 9 and 14, respectively, of fig. 3) at each recording site, coordinates and elevation of one of the seismometers along each spread, and the numbers of the traces (according to fig. 3) included in

the corresponding record section. The velocity-depth functions calculated for each profile and listed in tables are shown in figures that summarize the results of all profiles along a recording line (for example, fig. 12). The numbers given in parentheses after the shotpoint names refer to the shotpoint numbers listed in table 1. The discussion that follows is arranged according to the geologic setting of the profiles. The three profiles recorded in the Snake River Plain between Boise, Idaho, and Mountain City, Nev., are included in the description of the profiles in the Basin and Range province. The profiles from Shasta Lake, Mono Lake, and China Lake, Calif., and the profiles from Fallon, Nev., to the south and southwest are combined in the discussion of the Sierra Nevada. The different traveltime curves are named *a*, *a–b*, *b*, *d(b)*, *c*, and *d* following the notation of figure 5. The respective depth ranges calculated for each segment are named by the same letters.

BASIN AND RANGE PROVINCE

The following brief summary of the main geologic features of the Basin and Range province is based on Eardley (1962), Gilluly (1963), Hamilton and Myers (1966), Nolan (1943), Osmond (1960), Roberts (1968), and Thompson (1959).

The broad Great Basin of the Basin and Range province in Nevada and western Utah is bordered on the west by the Sierra Nevada and on the east by the Wasatch Mountains. The north-trending ranges stand 500–1,200 m above the alluvial floors of flanking basins. Ranges and basins cover about equal areas in most of the province north of the 35th parallel. The blocks are typically between 10 and 20 km wide and are bounded on one or both sides by normal faults. The mountains are composed principally of sedimentary rocks of Paleozoic age, volcanic rocks of Tertiary age, and continental deposits and volcanic rocks of Pliocene and Pleistocene age. The individual ranges have complex internal structures, including folds (some overturned), overthrusts, granitic intrusions, and high-angle faults with vertical and horizontal components of movement. Basin-and-range faulting began during Miocene time and still continues. The basin-and-range faults are not alined with the earlier Precambrian and Laramide structures. According to Hamilton and Myers (1966) and Thompson and Talwani (1964), the geometry of the tilted normal-fault blocks requires regional extension as the basic cause of faulting. Hamilton and Myers (1966) estimated the total Cenozoic crustal extension indicated by the faults to be at least 100 km, and possible as much as 300 km in the north, the larger value representing nearly half the present width of the province.

DELTA, UTAH, TO FALLON, NEV.

The recording line extending from Delta, Utah (16), through Eureka, Nev. (15), to Fallon, Nev. (9), crosses the central part of the Great Basin transverse to the structure of the basins and ranges. The line was continued west from Fallon to San Francisco (1) across the Sierra Nevada, the Great Valley, and the Coast Ranges (discussed in the next sections). Reversed observations were carried out between Fallon and Eureka; both profiles were recorded in 1961. The distance between the two shotpoints is 275.3 km. Eaton (1963) has reported on the entire line from Eureka to San Francisco. In 1963, records were made along a 400-km-long line from Delta, Utah, to the nuclear shotpoint SHOAL (10) 55 km southeast of Fallon, passing Eureka 263.2 km from Delta. Only two stations were occupied beyond 280 km from Delta. This line was not reversed from Eureka, but it was possible to record with nine stations spread over the entire line between 150 and 550 km east of SHOAL. However, the stations on this profile are about 50 km apart, a separation too great to allow a detailed crustal study. Both profiles, Delta-SHOAL and SHOAL-Delta, were discussed by Eaton, Healy, Jackson, and Pakiser (1964). The record section of the profile Delta-SHOAL (S.W. Stewart and P.R. Stevenson, written commun., 1967) is shown in figure 9, and the record sections and corresponding tables for the profiles Eureka-Fallon and Fallon-Eureka are presented in figures 10 and 11 (pl. 2) and tables 55 and 56.

The record section of the profile Delta-SHOAL figure 5. First arrivals between 30 and 90 km from the shotpoint form the traveltime curve *a*. A gentle curve seems to be a better representation of *a* than a straight line. The first arrivals at 30 km and between 70 and 80 km from Delta probably are delayed by sedimentary basin fills. According to laboratory measurements on granite (Birch, 1958) and seismic-refraction results of profiles made in the Bohemian massif in southern Germany (Giese, 1963, 1966), it is reasonable to expect a velocity gradient within approximately the upper 5 km of the basement in which the velocity increases from 5.0 km/s or less to about 5.85 km/s, resulting in a curvature of the traveltime curve *a* at short distances. Where sediments cover the basement, however, the curvature due to the gradient in the upper part of the basement is hidden and commonly cannot be recognized.

Between 50 and 80 km from the shotpoint, a second strong phase can be recognized in later arrivals after the first wave group *a*; this phase is identified as curve *b*. It is interpreted as a retrograde curve, and it can be traced in secondary arrivals as far as 125 km from the

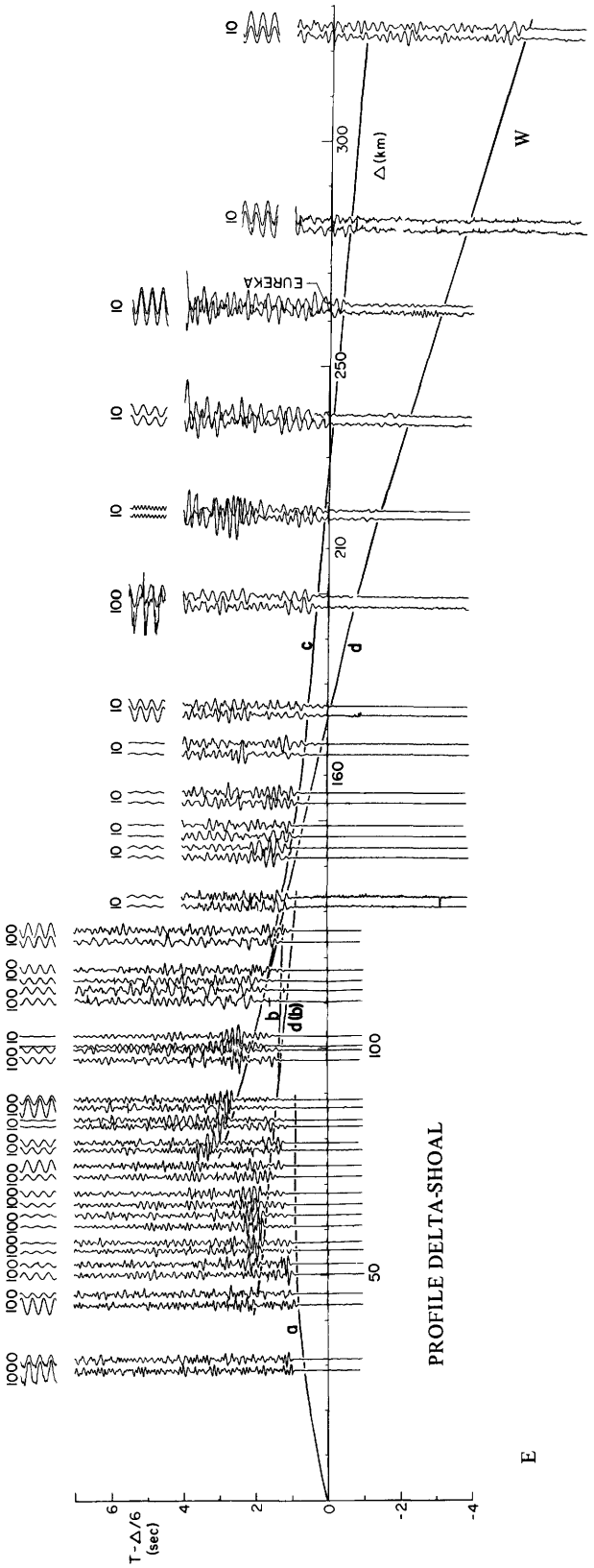

FIGURE 9.—Record section of the profile from Delta (16) to SHOAL (10). The numbers behind the shotpoints refer to figure 1, plate 1A, and table 1. Two traces of each seismogram are plotted. The corresponding calibration at the top of each trace is marked in microvolts. Section produced by S.W. Stewart and P.R. Stevenson, U.S. Geological Survey.

shotpoint. Another phase, $d(b)$, can be seen tangent to this curve in the first arrivals between 100 and 133 km. Curve b is correlated between 90 and 125 km with a strong velocity gradient at the bottom of the upper crust where the velocity increases relatively rapidly over a depth range of several kilometers. The first part of b between 50 and 80 km, however, must be regarded as a true reflection from the top of the lower crust at a depth of 19 km below the crustal transition zone. The wave corresponding to $d(b)$ penetrates the lower crust, its traveltime curve indicating the velocity within the lower crust.

The first arrivals beyond a distance of 140 km form the traveltime curve d, the velocity of which increases from 7.3 km/s at 150 km to 7.8 km/s at 325 km. This curve is correlated with the uppermost upper mantle. Its extension toward smaller distances is tangent to the curve c at about 100 km. Curve c can be traced between 75 and 325 km. The corresponding secondary arrivals are accentuated by significant changes of wave form and amplitude, the amplitudes decreasing with increasing distance. Similar to the traveltime curve b, the curve c consists of two parts: The part between 75 and 100 km is interpreted as a reflected phase from the base of the crust at 29 km depth; the part beyond 100 km distance is correlated with continuously refracted waves that reach the transition zone between lower crust and upper mantle. Table 2 shows the values that were used to calculate the corresponding velocity-depth function in figure 12 (pl. 3). Depth calculations for points of the reflected parts of the traveltime curves b and c yield equal depths for increasing apparent velocity, supporting the interpretation of the curves as reflections. They are not included in table 2 because they do not represent true velocities. Because the profile was not reversed, it was not possible to decide if the velocity of 7.3 km/s for the curves c and d at the point of critical reflection is a true or an apparent velocity. Therefore, the values calculated from curve d are not included in table 2. On the assumption that no significant horizontal changes occur, the depth calculation for the curve d shows a slow increase of the velocity from 7.3 km/s at a depth of 30 km to 7.8 km/s at about 50 km depth.

To find the velocity distribution for the parts of the velocity-depth function for which the observed traveltime curves do not give information, a comparison of the velocities $\overline{W}$ and $\overline{u}$ from equations 5 and 11 must be made. Using straight interpolation for the unknown parts of the velocity-depth function, the condition 12a, $\overline{u} \cdot 1.005 \leqslant \overline{W}$, is not fulfilled, but the assumption of a basement with low P-wave velocity of 5.86 km/s from 6.4 to 10.0 km depth gives equality of $\overline{u} \cdot 1.005 = \overline{W} =$ 6.16 km/s. The depth range of a low-velocity zone and the velocity within it can only be approximated.

TABLE 2.—*Velocity-depth function of the profile from Delta(16) to SHOAL(10)*

Curve	Distance, Δ (km)	Traveltime, T (s)	Velocity, V (km/s)	Depth, z (km)	Gradient, dV/dz (km/s/km)
a	0	0	4.60	0	
	32	6.03	5.59	3.1	
	44	8.16	5.64	3.7	
	52	9.57	5.78	5.5	
	60	10.94	5.85	6.4	
b	68	12.93	6.40	15.4	0.40
	76	14.19	6.32	15.1	.15
	84	15.46	6.24	14.4	.075
	92	16.74	6.18	13.6	.03
	108	19.34	6.12	12.0	.01
$d(b)$	130	22.60	6.405	15.6	.01
c	100	18.83	7.24	29.3	1.00
	116	21.07	7.02	28.8	.30
	132	23.36	6.84	28.1	.175
	148	25.66	6.70	27.2	.110
	160	27.43	6.60	26.1	.080
	200	33.60	6.44	22.2	.020
	264	43.57	6.41	18.5	.005

$z = 29.3$ km: $\overline{u} = 6.16$ km/s, $\overline{w} = 6.16$ km/s, $V = 5.86$ km/s for $z = 6.4$–10.0 km, $V = 6.06$ km/s at $z = 10.1$ km.

The profile Eureka-Fallon (fig. 10; table 55) shows traveltime curves similar to those of the profile Delta-SHOAL. Curve a shows increasing velocity from 4.7 km/s at the shotpoint to 6.2 km/s at 100 km distance. Some records between 40 and 60 km show delays of the first arrivals caused by thick sediments in Antelope Valley west of Eureka. First arrivals between 100 and 130 km cannot be correlated with curve a but form a separate curve, a–b_1. In the same distance range, further secondary arrivals may be correlated into a second short traveltime curve, a–b_2, preceding curve b.

The retrograde traveltime curve b is well recorded between 80 and 140 km. It is delayed for about 0.9 s at 140 km with respect to the linear extension of curve a.

Curve c is well defined between 80 and 215 km and can be traced to a distance of 280 km with some uncertainty. The velocity of the phase corresponding to curve c increases from 6.43 km/s at 220 km to 7.86 km/s at the point of critical reflection at about 80 km. P_n arrivals are weak on this profile; curve d, which is based on the first arrivals between 140 and 170 km, 250 km, and 315 km, shows an average velocity of 7.9 km/s between 140 km and the end of the profile 40 km west of Fallon. Table 3 and figure 12 show the details and results of the depth calculation. The velocity derived from curve a increases from 4.7 km/s at the surface to 6.2 km/s at a depth of 10 km. A transition zone between the upper and lower crust derived from curve b is indicated, the velocity of which reaches 6.41 km/s at a depth of about 19 km. With depth increasing to 32 km, the velocity increases gradually from 6.41 to 6.8 km/s. The velocity increases sharply at the base of

TABLE 3.—*Velocity-depth function of the profile from Eureka(15) to Fallon(9)*

Curve	Distance, Δ (km)	Traveltime, T (s)	Velocity, V (km/s)	Depth, z (km)	Gradient, dV/dz (km/s/km)
a	0	0	4.50	0	
	20	3.99	5.34	2.4	
	40	7.51	5.85	5.3	
	60	10.80	6.06	7.5	
	90	15.69	6.13	9.6	
b	90	16.92	6.41	18.8	0.150
	110	20.04	6.37	18.3	.030
	130	23.20	6.34	16.5	.010
c	90	18.40	7.86	34.6	2.00
	100	19.69	7.62	34.5	2.00
	120	22.41	7.29	34.3	.45
	140	25.15	7.02	33.5	.20
	160	28.01	6.79	31.8	.06
	180	31.03	6.60	28.4	.04
	200	34.09	6.48	25.2	.02
	220	37.21	6.43	22.4	.01

z = 34.5 km: $\bar{u}$ = 6.17 km/s, $\bar{w}$ = 6.17 km/s, V = 6.1 km/s for z = 10.0–16.4 km.

the crust to 7.9 km/s at a depth of 34.8 km.

To find the average velocity for the undefined parts of the velocity-depth function, the values of 100 km distance were used to calculate $\overline{W}$ with equation 11 using the following values (table 3): Δ = 100 km, T = 19.69 s, z = 34.5 km. The resulting velocity $\overline{W}$ is 6.17 km/s. Using straight interpolation from the calculated velocity-depth function, we get an average velocity $\bar{u}$ of 6.17 km/s, which corrects to 6.20 km/s. Because of condition $\bar{u} \cdot 1.005 \leqslant \overline{W}$ is not fulfilled, a velocity is required in the undefined parts of the velocity-depth function that is lower than the velocity obtained by straight interpolation. A velocity decrease of 0.1 km/s between 10.0 and 14.4 km depth fulfills the condition. Alternatively, either a low-velocity zone could be introduced between 19 and 22 km depth, the second undefined part of the velocity-depth function, or a decrease of velocity could be distributed between the two undefined parts. However, a low-velocity zone at a depth of about 21 km below Eureka would cause a delay in curve *c* relative to curve *b* of figure 10. Because such a delay is not observed, there is no reason to insert the low-velocity zone at 21 km. The unknown part in the velocity-depth function between *b* and *c* is due to the uncertainty of the calculation of depths for which the velocity gradient is very small. This is true for the depth calculations based on points of curve *c* at distances greater than 200 km. Therefore, it seems reasonable to place the low-velocity zone between areas *a* and *b*, as is indicated qualitatively by the offset of curve *b* relative to *a* (fig. 10).

Traveltime curve *b* is not very strong. Between 50 and 95 km it is correlated with continuously refracted waves originating in a zone at a depth of 13-14 km where the velocity gradient increases from 0.01 to 0.05 km/s/km. The phases 30 km from the shotpoint that lie on the backward extension of curve *b* are probably reflections from that depth. Curve *c* can be traced clearly between 65 and 235 km from the shotpoint. Curve *d*, which is tangent to *c* at about 80 km distance, is well defined. The delays of *d* at several stations can be qualitatively correlated with sedimentary fillings in basins.

Table 4 shows the calculated depths for the corresponding velocity-depth function in figure 12 (pl. 3). The velocity comparison of $\overline{W}$ = 6.07 km/s and $\bar{u} \cdot 1.005$ = 6.03 km/s shows no evidence for a low-velocity zone east of Fallon. The base of the crust is at about 29 km depth with a *P*-wave velocity of 7.68 km/s, which is also the average velocity found for the curve *d* between 100 and 260 km distance.

Figure 12 summarizes the results of the profiles between Delta, Utah, and San Francisco, Calif. The results of the profiles west of Fallon are discussed below. Within the upper 5–10 km of the crust (lower half of fig. 12), the velocity increases from less than 5 km/s to about 6.2 km/s between Eureka and Fallon, whereas the *P*-wave velocity is less than 6 km/s beneath Delta to a depth of 10 km. This result corresponds to the result for the eastern part of the Basin and Range province of Berg, Cook, Narans, and Dolan (1960), who found a layer 9 km thick with a velocity of 5.73 km/s in the area southwest of the Great Salt Lake. On the profile Eureka-Fallon a low-velocity zone was found at greater depth, between 10 and 17 km, in which the velocity decreases from 6.2 to 6.1 km/s, whereas on the profile Fallon-Eureka no velocity decrease was observed. All the profiles show the existence of an intermediate transition zone within the crust. This transition zone is well expressed beneath Delta but poorly expressed beneath Fallon. The intermediate boundary and the base of the crust are deeper near Eureka than near Fallon and Delta. The transi-

TABLE 4.—*Velocity-depth function of the profile from Fallon(9) to Eureka(15)*

Curve	Distance, Δ (km)	Traveltime, T (s)	Velocity, V (km/s)	Depth, z (km)	Gradient, dV/dz (km/s/km)
a	0	0	3.36	0	
	20	4.51	5.47	4.2	
	40	7.94	5.98	6.7	
	60	11.26	6.11	8.4	
	80	14.50	6.26	10.9	
b	60	12.29	6.33	13.8	0.05
	80	15.47	6.29	12.8	.01
c	80	16.23	7.68	28.8	1.00
	90	17.53	7.40	28.5	.60
	100	18.91	7.14	27.9	.40
	120	21.79	6.77	26.5	.15
	140	24.80	6.55	24.5	.05
	160	27.88	6.45	21.8	.025
	180	30.99	6.42	20.7	.01

z = 29.3 km: $\bar{u}$ = 6.00 km/s, $\bar{w}$ = 6.07 km/s.

tion zone between crust and mantle is less than 5 km thick; the upper mantle velocity immediately beneath the crust is about 7.8 km/s between Eureka and Fallon, as was also reported by Eaton (1963). West of Delta the apparent velocity was found to be less than 7.5 km/s at the top of the mantle. Eaton, Healy, Jackson, and Pakiser (1964) reported that the apparent velocity of the P_n arrivals on the profile SHOAL-Delta is about 7.6 km/s between 410 and 547 km distance from SHOAL. However, they interpreted this as an apparent downdip velocity corresponding to a true upper mantle velocity of about 7.8 km/s. Berg, Cook, Narans, and Dolan (1960) reported a similar low velocity of 7.59 km/s for the east part of the Basin and Range province. The thickening of the crust in the middle of the line beneath Eureka supports the results of Eaton (1963) and Eaton, Healy, Jackson, and Pakiser (1964) and the reported total crustal thickness for Delta and Eureka. For Fallon, however, a crustal thickness of 28–29 km was found on the basis of curve *c*, whereas Eaton (1963) reported 24 km as the crustal thickness there.

The upper half of figure 12 shows the crustal cross section along this line based on the velocity-depth functions. The velocity values were plotted at an interval of 0.2 km/s at the vertex of the corresponding ray. Further points for the lines of equal velocity result from intersections with other seismic-refraction lines. Velocity lines less than 5.0 km/s are not plotted because they do not represent the basement but rather sedimentary fillings of basins for which detailed distributions cannot be derived from these measurements. (For a low-velocity zone only an average velocity can be given.) Because of the wide spacing of the shotpoints, the resulting cross section cannot reveal detailed changes in the horizontal direction but only an approximate picture of changes in crustal structure.

BOISE, IDAHO, TO LAKE MEAD, NEV.

The line extending from Delta to Fallon is crossed at Eureka by a north-trending line that also has a central shotpoint at Eureka. This recording line extends from Boise, Idaho (11), to Lake Mead, Nev. (22), and crosses the western Snake River Plain and the Basin and Range province (fig. 1).

The Snake River Plain, just north of the Basin and Range province, is considered by some authorities to be part of the Columbia Plateaus. The Columbia Plateaus extend west to the Cascade Range. They are covered by little-deformed middle Tertiary basaltic flow rocks that form plateaus in northeastern Oregon and southeastern Washington. In southeastern Oregon and adjacent parts of Idaho and Nevada the volcanic rocks are younger. To the south they are part of the block-faulted rocks of the Basin and Range province. Eastward the younger basaltic flows fill the great transverse depression of the Snake River Plain. This complex structural depression is bounded by faults with large vertical displacements. Subsidence of crustal blocks within the depression was accompanied by voluminous eruptions of basaltic lava that accumulated to great thicknesses in local troughs (Hill, 1963). On the southwest the Snake River Plain is bordered by the Basin and Range province and on the northeast by granitic rocks of the Idaho batholith. Hamilton and Myers (1966) interpreted the Snake River Plain as a lava-filled tension rift formed in the lee of the northwestward-drifting plate of the Idaho batholith.

The line from Boise to Eureka is the best line recorded during the 1961 and 1962 seasons in terms of quality and completeness of data. Several reports on this line and the recordings along the line extending south to Nevada Test Site (19) have been published (Pakiser and Hill, 1963; Hill and Pakiser, 1966, 1967). Five shotpoints were located along this line over a distance of 450 km: Boise (11) and C.J. Strike Reservoir (12) in Idaho, and Mountain City (13), Elko (14), and Eureka (15) in Nevada. Distances between the shotpoints were: Boise to Strike, 73.3 km; Strike to Mountain City, 120.4 km; Mountain City to Elko, 119.8 km; and Elko to Eureka, 139.6 km. Between Eureka and Mountain City, the profiles are parallel to the structural grain of the Basin and Range province. The line passes into the western Snake River Plain of southwestern Idaho just north of Mountain City. Shotpoints Strike and Boise are located in reservoirs, Boise lying just south of the outcropping granitic rocks of the Idaho batholith. Along the southernmost part of the recording line, between Eureka and Lake Mead, only unpublished results were available (Roller, Jackson, Cooper, and Martina, 1963). Two shotpoints were located south of Eureka: Hiko (20), 182.4 km, and Lake Mead (22), 387.5 km, from Eureka. The shots south of Eureka and north of Lake Mead were recorded only to distances of 290 km. Three shots from Hiko were recorded only to distances of 100 km toward the north and the south. Record sections and tables for the profiles of the line from Boise to Lake Mead are presented in figures 13–24 (pl. 2) and tables 57–68. Although the profiles Boise-Elko and Strike-Elko are located partly in the Basin and Range province, the interpretation presented here concerns only the Snake River Plain, because the depth points of the corresponding rays are under the Snake River Plain. Similarly, the interpretation of the profile Elko-Boise concerns only the Basin and Range province. The profiles between Boise and

Eureka, with intermediate shotpoints at Strike, Mountain City, and Elko, are reversed. The profiles between Eureka and Lake Mead, with the intermediate shotpoint at Hiko, however, are not reversed along the subsurface refraction path.

The profile Boise-Elko (fig. 13; table 57) was recorded to a distance of 315 km. The first arrivals between 50 km and 180 km from Boise show a velocity of 6.6–6.7 km/s and can be combined with the first arrivals between 0 and 50 km by a cusp (curve *a*). The velocity of the first arrivals is constant beyond 90 km. The retrograde curve *b* and curve *d*(*b*), tangent to it at 120 km, can be traced very clearly in secondary arrivals and, at distances greater than 200 km, as first arrivals. Curve *c* is a very clear event in secondary arrivals at distances greater than 120 km. No indications of P_n arrivals (curve *d*) were found on this profile. The comparison of $\bar{u} = 6.40$ km/s and $\bar{W} = 6.46$ km/s indicates that the condition $\bar{u} \cdot 1.005 \leqslant \bar{W}$ is fulfilled, and so along this profile no velocity inversion exists within the crust (table 5).

The profile Boise-Elko is partly reversed by the short 70-km-long profile Strike-Boise (fig. 14; table 58). The first arrivals on this profile confirm the result of the profile Boise-Elko, indicating that in this area material with velocities higher than 6.0–6.2 km/s must be located at relatively shallow depths. The depth calculations for this profile yield a velocity of 7.0 km/s at depths of less than 10 km; on the profile to the south, velocities of 6.8–7.0 km/s are found at 16–17 km depth. The extraordinary delay of the first arrivals noted on this profile is the result of a thick sedimentary basin beneath the Strike Reservoir, as was pointed out by Hill and Pakiser (1966, 1967), who assumed a 2-km-thick near-surface layer with a velocity of 2.0 km/s on both sides of the shotpoint in Strike Reservoir.

TABLE 5.—*Velocity-depth function of the profile from Boise(11) to Elko(14)*

Curve	Distance, Δ (km)	Traveltime, *T* (s)	Velocity, *V* (km/s)	Depth, *z* (km)	Gradient, *dV/dz* (km/s/km)
a	0	0	4.49	0	
	30	5.84	5.63	3.9	
	60	10.83	6.32	9.1	
	90	15.52	6.44	11.4	
	120	20.14	6.50	13.5	
	60	11.03	6.60	13.7	
	90	15.54	6.69	14.5	
b	140	23.44	6.74	22.4	0.06
	160	26.42	6.71	21.9	.03
	180	29.42	6.69	20.7	.015
	210	33.88	6.68	18.3	.005
d(*b*)	140	23.39	6.80	23.2	.08
c	130	23.36	7.55	38.4	5.00
	140	24.69	7.46	38.4	2.00
	160	27.45	7.30	38.3	.40
	180	30.21	7.17	38.0	.18
	200	33.04	7.07	37.4	.12
	220	35.90	6.99	36.6	.06
	250	40.22	6.90	35.0	.03
	270	43.14	6.85	33.6	.025
	300	47.53	6.80	30.6	.01

$z = 38.4$ km: $\bar{u} = 6.40$ km/s, $\bar{w} = 6.46$ km/s.

The profiles Strike-Elko (fig. 15; table 59) and Mountain City-Boise (fig. 16; Table 60) show the same features. The 190-km-long profile Mountain City-Boise reverses the profiles Boise-Elko and Strike-Elko in the Snake River Plain.

At distances of 70-90 km, the first arrivals form curve *a*, the extension of which can be connected with the retrograde curve *b* at a distance of about 160 km. Owing to the low-velocity sediments near Strike, the first arrivals of the profile Strike-Elko are delayed more than on the profile Mountain City-Boise. From 90 to 105 km, the first arrivals form traveltime curve *d*(*b*) that is tangent to *b* at a distance of about 50 km on both profiles. The traveltime curves *a*, *b*, and *d*(*b*) form a complete cusp that can be analyzed by the Herglotz-Wiechert method. (The calculated depths are given in tables 6 and 7.) Beyond 120 km, curve *c* can be traced through very clear secondary arrivals similar to those on the profile Boise-Elko. No P_n arrivals are found on either of the profiles. The slope of curve *c* is steeper on the profile Mountain City-Boise than on Strike-Elko. Because of the lack of P_n arrivals, the location of the point of critical reflection is not clear. Therefore it cannot be determined if the steep slope of curve *c* on the profile Mountain City-Boise at 120 km reflects the true velocity at the base of the crust or if this point is part of the reflection hyperbola.

The velocity comparison of $\bar{u}$ and $\bar{W}$ yields the following: Strike-Elko, $\bar{u} = 6.31$ km/s, $\bar{W} = 6.39$ km/s; Mountain City-Boise, $\bar{u} = 6.56$ km/s, $\bar{W} = 6.57$ km/s. Although the condition $\bar{u} \cdot 1.005 \leqslant \bar{W}$ is fulfilled for the profile Strike-Elko, indicating that no velocity inversion is evident within the crust, a slight velocity decrease from 7.1 to 7.0 km/s between depths of 24.7 and 28.4 km seems to be indicated for the profile Mountain City-Boise.

The profiles Mountain City-Eureka (fig. 17; table 61), Elko-Boise (fig. 18; table 62), and Elko-Eureka (fig. 19; table 63) in the northernmost part of the Basin and Range province have traveltime curves that are very similar to that of the profile Delta-SHOAL. Curve *a* is formed by first arrivals up to 40–60 km distance; the delays of the first arrivals at the stations 60–70 km from Mountain City and 50–60 km from Elko may be the result of a local change in the thickness of the sedimentary cover in the basin east of the Independence Mountains. However, for distances greater than 70 km the delays cannot be explained by sediments alone; they more likely result from the fact that velocity does not increase with depth below 6–8 km but remains con-

TABLE 6.—*Velocity-depth function of the profile from Strike Reservoir(12) to Elko(14)*

Curve	Distance, Δ (km)	Traveltime, T (s)	Velocity, V (km/s)	Depth, z (km)	Gradient, dV/dz (km/s/km)
a	0	0	3.03	0	
	30	6.32	5.71	5.3	
	60	11.42	6.04	8.6	
	90	16.21	6.38	13.0	
b	130	22.41	6.49	16.0	
	50	10.31	6.69	16.4	
d(b)	70	13.28	6.79	16.6	
	90	16.19	6.93	18.1	
c	130	24.06	7.77	41.0	0.60
	140	25.34	7.65	40.8	.40
	160	28.00	7.44	40.2	.175
	180	30.68	7.29	39.5	.09
	200	33.37	7.16	37.5	.045
	220	34.17	7.05	35.0	.025
	240	39.03	6.94	30.2	.01

z = 41.0 km: $\bar{u}$ = 6.31 km/s, $\bar{w}$ = 6.39 km/s.

TABLE 7.—*Velocity-depth function of the profile from Mountain City(13) to Boise(11)*

Curve	Distance, Δ (km)	Traveltime, T (s)	Velocity, V (km/s)	Depth, z (km)	Gradient, dV/dz (km/s/km)
a	0	0	4.95	0	
	30	5.82	5.52	3.3	
	60	10.94	6.02	7.5	
	90	15.86	6.14	9.7	
	120	20.72	6.20	11.7	
	150	25.54	6.24	13.9	
b	170	28.74	6.27	15.3	
	150	25.56	6.32	16.9	
	60	11.67	6.70	17.1	
d(b)	80	14.55	6.90	17.4	
	140	23.20	6.99	20.3	
	180	28.86	7.11	24.7	
c	(140)	(25.09)	(8.10)	(43.5)	(0.28)
	150	26.31	7.91	43.0	.23
	160	27.57	7.73	42.0	.175
	170	28.87	7.57	40.4	.10
	180	30.20	7.40	37.8	.05
	190	31.57	7.25	34.6	.03
	200	32.97	7.11	28.4	.01

z = 43.0 km: $\bar{u}$ = 6.56 km/s, $\bar{w}$ = 6.57 km/s, V = 7.0 km/s for z = 24.7–28.4 km.

TABLE 8.—*Velocity-depth function of the profile from Mountain City(13) to Eureka(15)*

Curve	Distance, Δ (km)	Traveltime, T (s)	Velocity, V (km/s)	Depth, z (km)	Gradient, dV/dz (km/s/km)
a	0	0	4.20	0	
	20	4.11	5.41	2.9	
	40	7.62	6.08	6.5	
	43	8.13	6.22	7.4	
b	80	15.35	6.60	19.1	0.175
	100	18.40	6.50	17.9	.03
	120	21.48	6.44	16.2	.01
d(b)	80	15.31	6.76	19.8	.175
	100	18.27	6.84	20.7	.04
	130	22.60	6.90	22.8	.025
c	120	21.86	7.48	33.7	.30
	130	23.22	7.35	33.3	.18
	140	24.60	7.24	32.6	.10
	160	27.33	7.07	30.4	.04
	180	30.12	6.96	26.4	.015
d	140	24.51	7.65	34.8	.075
	160	27.10	7.79	37.0	.045
	180	29.65	7.90	39.5	.04

z = 33.7 km: $\bar{u}$ = 6.32 km/s, $\bar{w}$ = 6.30 km/s, V = 6.25 km/s for z = 8.0–16.1 km.

TABLE 9.—*Velocity-depth function of the profile from Elko(14) to Boise(11)*

Curve	Distance, Δ (km)	Traveltime, T (s)	Velocity, V (km/s)	Depth, z (km)	Gradient, dV/dz (km/s/km)
a	0	0	4.90	0	
	20	3.83	5.68	2.4	
	40	7.18	6.02	4.2	
a–b1	40	7.48	6.07	5.2	0.01
a–b2	100	17.64	6.12	(10.4)	(.01)
b	90	16.84	6.88	23.2	.40
	110	19.80	6.63	22.0	.10
	130	22.87	6.38	17.5	.02
d(b)	120	21.11	6.96	23.6	.04
	180	29.76	6.98	24.3	.01
c	110	20.74	7.75	36.0	1.00
	120	22.08	7.54	35.8	1.00
	140	24.76	7.26	35.4	.30
	160	27.60	7.11	34.8	.15
	180	30.42	7.04	34.2	.06
	220	36.18	7.00	33.2	.03
	260	41.89	6.98	32.2	.01

z = 36.0 km: $\bar{u}$ = 6.37 km/s, $\bar{w}$ = 6.34 km/s, V = 6.1 km/s for z = 6.0–17.4 km.

stant or decreases slightly with increasing depth. On the profile Elko-Eureka, the very well defined phase *a–b* was found in later arrivals between 60 and 120 km distance; this phase is also evident on the profile Elko-Boise but not on the profile Mountain City-Eureka. On all three profiles, phases *b* and *c* are revealed clearly in later arrivals, *b* between 70 and 140 km and *c* beyond 100 km. Tangent to *b*, the phase *d(b)* can be seen clearly between Mountain City and Elko but not on the profile Elko-Eureka. Curve *d* is clearly expressed by first arrivals beyond 200 km distance only on the profile Mountain City-Eureka. Tables 8–10 show the corresponding depth calculations.

In contrast to the profiles described above, the profiles Eureka-Mountain City (fig. 20; table 64) and Eureka-Lake Mead (fig. 21; table 65) do not show well-developed phases *b* or *d(b)*. Curve *b* can be traced through some emergent arrivals between 60 and 120 km north and 75 and 135 km south of Eureka. However, phases *c* and *d* are both well developed, *d* showing an average velocity of 7.9 km/s on the profile Eureka-Mountain City and 7.9–8.0 km/s on the profile Eureka-Lake Mead. On the latter profile, curve *d* can be correlated only to a distance of 220 km. First arrivals beyond 230 km form a traveltime curve with the same slope as curve *d* but are delayed for 0.4 second. This delay cannot be explained by near-surface features. Phase *c* can be recognized on both profiles. It disappears at about 220 km distance on the profile Eureka–Lake Mead, where it has velocity of 6.64 km/s at 200 km distance. Clear arrivals with large

TABLE 10.—*Velocity-depth function of the profile from Elko(14) to Eureka(15)*

Curve	Distance, Δ (km)	Traveltime, T (s)	Velocity, V (km/s)	Depth, z (km)	Gradient, dV/dz (km/s/km)
a	0	0	3.97	0	
	20	4.16	5.58	3.4	
	40	7.49	6.19	6.4	
	56	10.13	6.31	7.7	
a–b	90	16.37	6.38	13.7	0.02
	100	17.97	6.36	13.1	.01
b	70	13.98	6.77	20.4	2.00
	80	15.45	6.69	20.2	.20
	100	18.47	6.60	19.5	.04
	120	21.47	6.51	17.5	.01
c	90	18.07	7.74	33.1	1.50
	100	19.34	7.58	33.0	1.00
	120	22.03	7.33	32.1	.175
	130	23.41	7.26	31.5	.08

z = 33.1 km: $\bar{u}$ = 6.29 km/s, $\bar{w}$ = 6.18 km/s, V = 6.1 km/s for z = 7.8–13.0 km and 13.8–17.4 km.

TABLE 11.—*Velocity-depth function of the profile from Eureka(15) to Mountain City(13)*

Curve	Distance, Δ (km)	Traveltime, T (s)	Velocity, V (km/s)	Depth, z (km)	Gradient, dV/dz (km/s/km)
a	0	0	5.21	0	
	20	3.67	5.58	1.4	
	40	7.24	5.68	2.8	
	60	10.73	5.76	4.2	
	80	14.16	5.88	6.8	
	100	17.54	6.00	9.7	
b	80	15.54	6.44	18.8	0.20
	90	17.10	6.39	18.5	.075
	100	18.67	6.36	18.0	.04
c	90	18.13	7.90	33.8	1.00
	100	19.40	7.73	33.7	.60
	110	20.71	7.49	33.4	.60
	130	23.45	7.17	32.6	.20
	150	26.28	6.98	31.0	.075
	170	29.18	6.82	26.6	.02
d	150	25.61	7.92	34.0	.03

z = 33.8 km: $\bar{u}$ = 6.28 km/s, $\bar{w}$ = 6.21 km/s, V = 6.1 km/s for z = 12.0–17.9 km.

amplitudes beyond 240 km on the profile Eureka-Mountain City may belong to *c*; the slope of *c* at 200 km distance yields a velocity of 6.8 km/s. The delay of phases *c* and *d* on the profile Eureka-Lake Mead between 160 and 180 km distance is very likely the result of a thick sedimentary cover with low *P*-wave velocities below the dry lake north and west of Hiko.

The comparison of the velocities $\bar{u}$ and $\bar{W}$ indicates, in contrast to the profiles north of Mountain City, that the average velocity within the upper crust is constant or decreases below 6–8 km depth. For the profile Mountain City-Eureka (table 8), the condition $\bar{u} \cdot 1.005 \leqslant \bar{W}$ is fulfilled by the assumption that the velocity of 6.25 km/s remains constant at depths between 8 and 16 km. To the south, the average velocity within the upper crust decreases to 6.1 km/s, as shown on the profiles Elko-Boise, Elko-Eureka, Eureka-Mountain City, and Eureka-Lake Mead (figs. 18-21; tables 9–12).

However, as sporadic arrivals and some short traveltime curves between curves *a* and *b* indicate, local lenses of material with high *P*-wave velocities seem to exist, especially as expressed by the curve *a–b* on the profile Elko-Eureka. This curve is explained by a thin layer of 6.3–6.4 km/s velocity at a depth of 13–15 km within material with lower *P*-wave velocity. The condition $\bar{u} \cdot 1.005 \leqslant \bar{W}$ can be fulfilled for the profile Elko-Eureka by assuming an average velocity of 5.8 km/s at depths of 7.7 to 13.1 km and a gradual increase of the velocity with depth from 6.38 to 6.51 km/s between 13.8 and 17.5 km. However, this solution seems to be unlikely. On similar profiles, material having a 6.1 km/s average velocity is found to a depth of 18 km.

The profiles from Hiko (figs. 22, 23; tables 66, 67) are too short for a detailed interpretation of arrivals at

TABLE 12.—*Velocity-depth function of the profile from Eureka(15) to Lake Mead(22)*

Curve	Distance, Δ (km)	Traveltime, T (s)	Velocity, V (km/s)	Depth, z (km)	Gradient, dV/dz (km/s/km)
a	0	0	4.33	0	
	20	3.84	5.86	3.1	
	40	7.17	6.13	4.9	
	65	11.34	6.30	7.2	
b	110	20.39	6.59	17.6	0.01
c	110	21.37	7.80	37.6	.50
	120	22.70	7.58	37.2	.40
	140	25.40	7.30	36.4	.175
	160	28.22	7.03	34.5	.08
	180	31.09	6.80	31.4	.04
	200	34.07	6.64	25.4	.01
d	120	22.64	7.90	38.0	.20

z = 37.6 km: $\bar{u}$ = 6.36 km/s, $\bar{w}$ = 6.25 km/s, V = 6.1 km/s for z = 7.3–17.5 km.

distances beyond curve *a*. However, the existence of a phase *c* can be assumed in later arrivals at distances of 80–100 km.

The profile Lake Mead-Eureka (fig. 24; table 68) is at the southernmost part of the line Boise-Lake Mead. Curve *a* can be traced to a distance of 80 km, yielding a velocity of 6.2 km/s at a depth of about 6 km. The dominant event in later arrivals is phase *c*, which has a velocity of 7.5 km/s at a distance of 100 km; the velocity decreases to 6.4 km/s at a distance of 260 km. Tangent to *c* at distances of 100–110 km, curve *d* defines the first arrivals beyond 170 km distance; the apparent velocity of phase *d* increases gradually to 8.1 km/s at 300 km distance. Between curves *a* and *c*, two different phases can be traced, $a–b_1$ and $a–b_2$, for which layers with velocities of 6.20 km/s and 6.23–6.37 km/s at depths of 10.8 km and 17.4–18.9 km were calculated. Indications of phase *b* may be seen at 75–80 km distance, but no corresponding traveltime curve can be

traced over several tens of kilometers distance. The velocity comparison of $\bar{u}$ (6.22 km/s) and $\bar{W}$ (6.10 km/s) (table 13) indicates that velocity decreases downward within the crust. Two solutions were reasonable: (1) an average velocity of 6.0 km/s between 6 and 25 km depth, enclosing local lenses with higher *P*-wave velocity at depths of about 11 and 18 km, and (2) a low-velocity zone with an average velocity of 5.8 km/s, with a local lens of higher *P*-wave velocity at 11 km depth. The first solution seems more likely and is used for the crustal cross section in figure 25 (pl. 3).).

The velocity-depth functions of all profiles between Boise and Lake Mead are plotted in the lower part of figure 25. The top part of figure 25 shows the corresponding crustal cross section. As pointed out above, the character of the traveltime curves changes from the Snake River Plain to the Basin and Range province and also from the northern to the southern part of the Basin and Range province. On the profiles in the Snake River Plain the curves *a*, *b*, and *d*(*b*) can be combined to form a complete cusp. Curve *c* can be traced as a second dominant event in later arrivals, but no P_n arrivals (curve *d*) were found. In the northern Basin and Range province, curves *b* and *d*(*b*) are not connected with curve *a*. However, *b* is based on an easily correlated phase in later arrivals at distances between 50 and 150 km. Phase *c* is the second dominant event in later arrivals and can be correlated from about 80–100 km to the end of the profile. Curve *d* can be traced on most record sections. Further south, between Elko and Eureka, the character of curve *b* changes completely. Here phase *c* is the only dominant event in later arrivals, and phase *b* is expressed only by weak arrivals on the profiles from Eureka. The slope of curve *c* becomes smaller at large distances, and curve *c* does not cross the distance axis on the southernmost profile, Lake Mead-Eureka, in contrast to the profiles Mountain City-Eureka and Elko-Boise. The velocity at 260 km is about 6.4 km/s on the profile Lake Mead-Eureka, whereas it is 7.0 km/s on the profile Elko-Boise at the same distance.

TABLE 13.—*Velocity-depth function of the profile from Lake Mead(22) to Eureka(15)*

Curve	Distance, Δ (km)	Traveltime, *T* (s)	Velocity, *V* (km/s)	Depth, *z* (km)	Gradient, *dV/dz* (km/s/km)
a	0	0	5.04	0	
	20	3.63	5.90	2.3	
	40	6.94	6.07	3.6	
	60	10.19	6.22	5.7	
a-b1	120	20.51	6.22	10.8	0.01
a-b2	100	19.69	6.37	18.9	.20
	140	24.43	6.24	18.2	.05
	190	32.44	6.22	17.4	.01
c	110	19.67	7.50	33.2	.80
	110	21.02	7.31	33.0	.60
	120	22.39	7.16	32.8	.35
	140	25.25	6.90	31.8	.16
	160	28.20	6.67	30.3	.10
	180	31.24	6.51	28.4	.05
	200	34.31	6.45	27.4	.03
	240	40.57	6.40	25.2	.01
d	120	22.26	7.74	34.4	.10
	160	27.42	7.91	37.6	.04

z = 33.0 km: $\bar{u}$ = 6.22 km/s, $\bar{w}$ = 6.10 km/s, V = 6.0 km/s for z = 5.8–10.7 km, 10.9–17.3 km, 19.0–25.1 km.

The nature of the traveltime-curve system *a*, *b*, and *d*(*b*) on the profiles in the Snake River Plain and the resulting velocity-depth relations suggest the possibility that upper crustal silicic material is absent there, as can be inferred from surface geology (Hamilton and Myers, 1966). The separation of curves *a* and *b*/*d*(*b*) on the profiles in the adjacent Basin and Range province shows that here crustal material with *P*-wave velocities of about 6 km/s is present, also as indicated by surface geology. The calculated velocity-depth functions and the corresponding crustal cross section reflect the change in the arrangement of the traveltime curves that show the change of crustal structure from north to south in three steps. Under the Snake River Plain, between 11 and 17 km depth, the velocity increases from 6.3–6.5 km/s to about 6.7–6.9 km/s. Within the lower crust, having an average velocity of 6.8 km/s, a local zone with slightly higher velocity was found north of Mountain City. At a depth below about 35 km, the velocity increases from 6.8–7.2 km/s to 7.6–8.0 km/s, indicating a transition zone between crust and mantle the base of which ranges in depth from 38 to 43 km. The upper crust between Mountain City and Eureka ranges in thickness from 18 to 22 km and is separated from the lower crust by a well-defined transition zone 3–5 km deep within which the velocity increases from 6.4 to 6.6–7.0 km/s. The average velocity within the upper crust decreases southward from 6.25 km/s near Mountain City to 6.1 km/s near Eureka. This low-velocity upper crust extends to a depth of approximately 18 km. There are indications that some local, possibly lens-shaped zones with higher *P*-wave velocity than in the surrounding material are enclosed within the upper crust. The lower crust is about 10 km thick between Mountain City and Eureka, and its wave velocity averages 6.8–7.0 km/s. The total crustal thickness between Mountain City and Eureka is about 33–36 km.

In the vicinity of Eureka, crustal structure changes. The thickness of the upper crust increases toward the south from 18 km at Eureka to 25 km north of Lake Mead, and the intermediate transition zone between upper and lower crust disappears southward. North of Lake Mead no distinct lower crust was found, and the transition zone between crust and upper mantle seems

to be located directly beneath material of the upper crust. The velocity of the transition zone increases gradually from 6.4 to 7.8 km/s at depths between 26 and 33 km. As the lower crust thins, the average crustal velocity decreases, and just north of Lake Mead it averages 6.0 km/s. Several local lenses with higher *P*-wave velocity, however, seem to be enclosed within the upper crustal material. The average total crustal thickness of 33–37 km between Eureka and Lake Mead is the same as that between Eureka and Mountain City.

The crustal cross section published by Hill and Pakiser (1966, 1967) generally corresponds well to the cross section in figure 25, and the average velocities chosen by Hill and Pakiser are close to those found here except that average velocities in the upper and lower crust under the Snake River Plain were found to be higher. From traveltime delays of P_n arrivals from NTS (Nevada Test Site) in the vicinity of Eureka, Hill and Pakiser suggested the possibility of a zone with low-velocity material within the upper 20 km of the crust. This suggestion was confirmed; however, the low-velocity material probably extends farther north than is suggested by P_n delays. On the other hand, it has been shown in this paper that the boundary between upper and lower crust disappears between Elko and Eureka, indicating that the lower crust thins rapidly to the south. This fact may partly explain why the low-velocity material of the crust causes a delay of P_n arrivals near Eureka but not farther north, where a distinct lower crust is well established. This low-velocity material seems to pinch out toward NTS. As indicated by the profile Mountain City–Eureka, the average velocity in the upper crust increases between Elko and Mountain City to the north, which is in agreement with Hill and Pakiser's high-velocity material inferred from forerunners of P_n between 300 and 450 km north of NTS.

PROFILES IN THE SOUTHERN BASIN AND RANGE PROVINCE

The profiles recorded from NTS, Lake Mead, Kingman, Ariz., Ludlow, Calif., Barstow, Calif., and Mojave, Calif., cover much of the southern part of the Basin and Range province of southern Nevada, southern California, and northwestern Arizona. This area includes the southernmost part of the Great Basin but extends into the northernmost part of the Sonoran Desert, the Mojave Desert, and the northwestern edge of the Mexican Highland (Fenneman and Johnson, 1946) (fig. 1).

In addition to the profile toward Eureka, two other profiles were recorded from Lake Mead toward the northwest and the southwest. The profile toward the northwest lies entirely within the Basin and Range province and was reversed from Mono Lake (6), a shotpoint located immediately east of the Sierra Nevada, 438.7 km from Lake Mead. From both shotpoints seismic energy was recorded up to distances of about 360 km. Drill-hole shots from two intermediate shotpoints, Lida Junction (17) and Lathrop Wells (18), were not efficient, and therefore the data from these shotpoints are not included in this report. The entire line was first studied by Johnson (1965).

The profile toward the southwest crosses the Mojave Desert and the Transverse Ranges of southern California and was reversed from Santa Monica Bay (4) at a distance of 413.4 km from Lake Mead. From both shotpoints records of usable quality were obtained to distances of about 300 km. Both profiles were interpreted by Roller and Healy (1963). Because the distances between Lake Mead and Mono Lake and Lake Mead and Santa Monica are more than 400 km, the subsurface paths of the seismic observations are not really reversed.

The most prominent shotpoint in the southern Basin and Range province is at the Nevada Test Site, about 160 km northwest of Las Vegas, Nev. Many recordings were obtained from nuclear tests at NTS. In this report, observations along five profiles from NTS are included: to Ludlow, Calif., to Kingman, Ariz., to Navajo Lake, Utah, to Eureka, Nev., and to San Luis Obispo, Calif. The profile NTS-Ludlow crosses the profiles from Lake Mead to Mono Lake and from Lake Mead to Santa Monica Bay about 140 km west of Lake Mead. The profile was reversed from Ludlow about 250 km south of NTS.

Records were obtained from NTS up to a distance of about 500 km, near the Mexican border, but only the observations up to 320 km are included in this report. Gibbs and Roller (1966) reported earlier on this line. The line NTS-Kingman passes through Lake Mead 108 km from Kingman, but no observations are available from Lake Mead toward NTS or Kingman. The profile from NTS to Kingman was recorded in 1957 and 1958, and the results were published by Diment, Stewart, and Roller (1961). This profile was reversed from Kingman in 1962 (Roller, 1964). The line Lake Mead-Santa Monica Bay intersects a line from Mojave to Ludlow near Barstow. This line was recorded from shotpoints at Ludlow, Barstow, and Mojave with shotpoint separations of 85.8 km (Ludlow to Barstow) and 82.7 km (Barstow to Mojave). The recording instruments were installed up to 60 km east of Ludlow and 70 km west of Mojave. This line crosses the Mojave Desert from east to west. The traveltime diagrams

shown in figures 32-34 are based on unpublished record sections of the U.S. Geological Survey recordings prepared by Stephan Mueller and Mark Landisman (written commun., 1969). The profiles from Lake Mead to Mono Lake and Lake Mead to Santa Monica Bay (figs. 26, 27; pl. 2) and the profiles from NTS to Kingman, including their reversed observations (figs. 28-31; pl. 2), show features that are very similar to those found on the profile Lake Mead-Eureka (fig. 24). Details concerning the record sections are given in tables 69-73 except for the profile NTS-Kingman, the details of which were reported by Diment, Stewart, and Roller (1961).

Curve *a* can be traced in the first arrivals on these profiles to distances of 100-110 km. The average velocity of this phase is 6.1-6.2 km/s. On most of the profiles, one or two curves *a-b* can be correlated. Curve *b*, which would give evidence for a separate lower crust of higher velocity, does not seem to exist. Only one phase is dominant in later arrivals. This is correlated as phase *c* between 60 and 200 km distance or more, and it is characterized by very large amplitudes. The corresponding velocity is 6.3-6.5 km/s at a distance of 190 km. With decreasing distance, the velocity of this phase increases to 7.3-7.9 km/s at the point of critical reflection where curve *d* is tangent to curve *c*. The measured average apparent velocities of curve *d* are as follows:

Lake Mead-Mono Lake	7.7-7.9 km/s
Lake Mead-Santa Monica Bay	8.0-8.1 km/s
NTS-Kingman	8.0 km/s
Kingman-NTS	7.6-7.9 km/s
NTS-Ludlow	8.2 km/s
Ludlow-NTS	7.9 km/s

Although the true P_n velocity corresponding to curve *d* does not reach 8.0 km/s on the profiles within the Great Basin, the velocity in the uppermost mantle seems to exceed 8.0 km/s in the area south of NTS.

The traveltime curves of the profiles along the line extending through Ludlow, Barstow, and Mojave (figs. 32-34; fig. 35, pl. 2) are similar to those of other profiles within the southern Basin and Range province. As for the profile Ludlow-NTS, phases with the properties of *a-b* are suggested. However, a correlation of these phases is difficult and arbitrary. Phase *c* was prominently recorded on all profiles and can be traced from distances of about 60-70 km to the end of each profile. The corresponding traveltime curves for phase *c* approach the distance axis at distances of 220 km from the shotpoints. P_n arrivals (curve *d*) cannot be recognized beyond 180 km from Ludlow and 140 km from Mojave. The measured P_n velocities are: Ludlow-Mojave, 8.20 km/s; Barstow-Ludlow, 8.25 km/s; Barstow-Mojave, 7.85 km/s; and Mojave-Ludlow, 8.05 km/s. The velocity in the uppermost part of the mantle

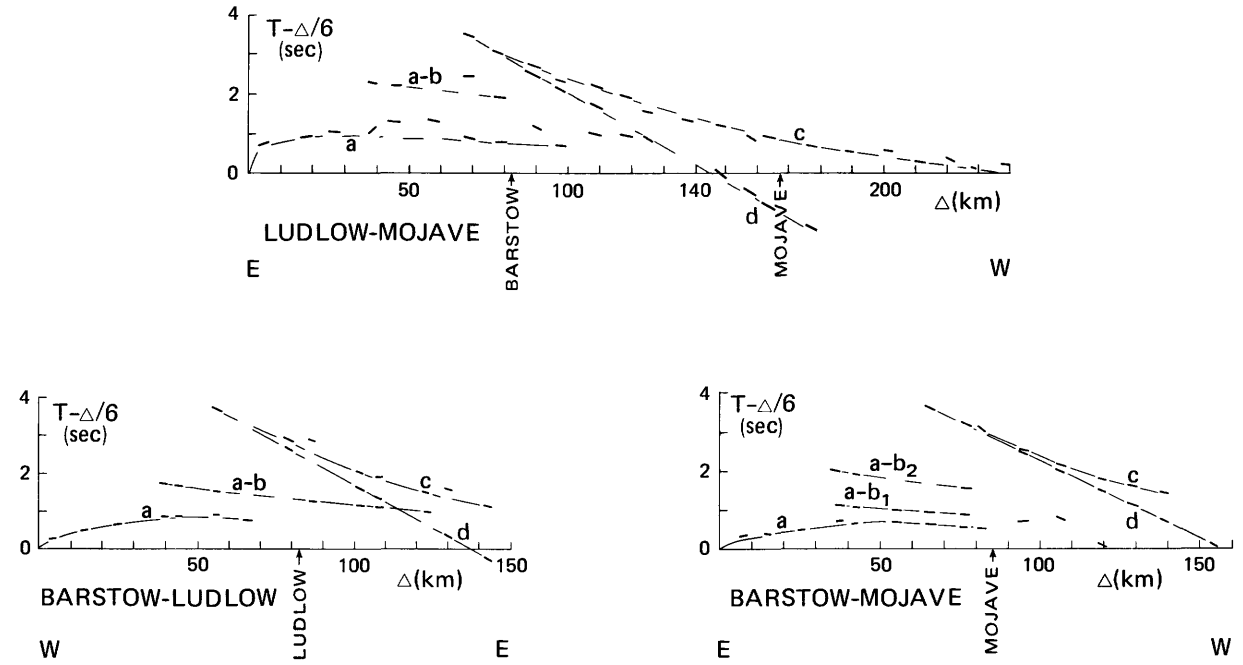

FIGURES 32-34.—Reduced traveltime graphs of the profiles from Ludlow (25) to Mojave (23), Barstow (24) to Ludlow (25), and Barstow (24) to Mojave (23).

beneath the Mojave Desert seems therefore to be equal to or greater than 8.0 km/s, confirming the result obtained on the profiles between Ludlow and NTS. The upper mantle velocity is consistently less than 8.0 km/s elsewhere in the Basin and Range province.

The details of the depth calculations for the profiles described in this section are given in tables 14-23, and the corresponding velocity-depth functions are shown in figures 36-40 (pl. 3). The crustal cross sections were obtained in the same way as were those for the line Delta-Fallon (see fig. 12). Intersections with other seismic refraction lines yielded additional information for the lines of equal velocity.

The total crustal thickness decreases along the lines

TABLE 14.—*Velocity-depth function of the profile from Lake Mead(22) to Mono Lake(6)*

Curve	Distance, Δ (km)	Traveltime, T (s)	Velocity, V (km/s)	Depth, z (km)	Gradient, dV/dz (km/s/km)
a	0	0	4.43	0	
	20	3.79	5.94	3.1	
	40	7.09	6.07	4.1	
	70	12.03	6.10	5.0	
a-b	60	12.06	6.30	14.4	0.20
	100	18.46	6.23	13.4	.01
c	90	18.36	7.61	33.5	>2.00
	100	19.68	7.41	33.4	2.00
	110	21.04	7.25	33.3	.75
	130	23.79	7.01	32.8	.30
	150	26.65	6.80	31.9	.175
	170	29.62	6.65	30.9	.10
	190	32.68	6.51	29.2	.075
	220	37.31	6.40	27.4	.04
	240	40.44	6.35	26.2	.03
	290	48.27	6.30	24.4	.01
d	150	26.20	7.72	35.0	.04
	190	31.37	7.80	37.0	.02
	230	36.45	7.85	40.0	.015

z = 33.5 km: $\bar{u}$ = 6.17 km/s, $\bar{w}$ = 6.11 km/s, V = 6.0 km/s for z = 5.1-13.3 km and 14.5-24.3 km.

TABLE 15.—*Velocity-depth function of the profile from Lake Mead(22) to Santa Monica Bay(4)*

Curve	Distance, Δ (km)	Traveltime, T (s)	Velocity, V (km/s)	Depth, z (km)	Gradient, dV/dz (km/s/km)
a	0	0	4.40	0	
	20	3.88	5.81	3.1	
	40	7.19	6.09	4.8	
	60	10.47	6.11	5.3	
	90	15.38	6.12	6.0	
a-b1	40	7.94	6.13	8.0	0.05
	70	12.84	6.12	7.3	.005
a-b2	70	13.47	6.19	14.0	.125
	110	19.96	6.15	13.2	.01
c	70	15.03	7.90	28.9	5.00
	80	16.30	7.60	28.8	1.00
	100	19.00	7.10	28.3	.50
	120	21.95	6.80	27.6	.20
	140	24.96	6.55	26.3	.125
	160	28.07	6.38	24.5	.06
	180	31.21	6.30	22.8	.03
	200	34.41	6.26	20.4	.01

z = 28.9 km: $\bar{u}$ = 6.07 km/s, $\bar{w}$ = 6.04 km/s, V = 6.0 km/s for z = 6.1-7.2 km, 8.1-13.1 km, 14.1-20.3 km.

TABLE 16.—*Velocity-depth function of the profile from NTS(19) to Kingman(26)*

Curve	Distance, Δ (km)	Traveltime, T (s)	Velocity, V (km/s)	Depth, z (km)	Gradient, dV/dz (km/s/km)
a	0	0	5.16	0	
	20	3.60	5.91	2.1	
	40	6.90	6.10	3.6	
	60	10.16	6.17	5.0	
	80	13.38	6.21	6.1	
	100	16.60	6.22	6.4	
a-b	150	25.22	6.38	18.0	0.075
	210	34.64	6.34	17.0	.01
c	90	17.80	7.57	30.7	.80
	100	19.09	7.33	30.4	.70
	120	21.90	6.98	29.8	.30
	140	24.86	6.74	28.7	.15
	160	27.87	6.60	27.6	.075
	180	30.87	6.50	26.2	.04
	210	35.50	6.42	24.0	.02
	230	38.62	6.40	23.0	.01
d	90	17.68	7.93	31.6	.35
	180	28.80	8.06	33.7	.015

z = 30.7 km: $\bar{u}$ = 6.30 km/s, $\bar{w}$ = 6.12 km/s, V = 6.0 km/s for z = 6.5-16.9 km and 18.1-22.9 km.

TABLE 17.—*Velocity-depth function of the profile from Kingman(26) to NTS(19)*

Curve	Distance, Δ (km)	Traveltime, T (s)	Velocity, V (km/s)	Depth, z (km)	Gradient, dV/dz (km/s/km)
a	0	0	5.58	0	
	30	5.37	5.68	1.5	
	60	10.38	6.13	6.0	
	90	15.27	6.14	6.6	
	120	20.15	6.15	7.1	
a-b1	130	21.97	6.20	9.9	0.01
a-b2	160	27.23	6.34	16.5	.01
c	90	17.40	7.34	27.7	.50
	100	18.76	7.08	27.2	.40
	120	21.69	6.70	26.0	.22
	140	24.72	6.53	25.0	.10
	180	30.91	6.42	23.4	.025
	220	37.13	6.38	21.0	.008
d	100	18.62	7.71	29.0	.125
	120	21.19	7.80	30.2	.05
	140	23.74	7.86	31.4	.035
	160	26.30	7.90	32.8	.025

z = 27.7 km: $\bar{u}$ = 6.27 km/s, $\bar{w}$ = 6.07 km/s, V = 6.0 km/s for z = 7.2-9.8 km, 10.0-16.4 km, 16.6-20.9 km.

TABLE 18.—*Velocity-depth function of the profile from NTS(19) to Ludlow(25)*

Curve	Distance, Δ (km)	Traveltime, T (s)	Velocity, V (km/s)	Depth, z (km)	Gradient, dV/dz (km/s/km)
a	0	0	5.00	0	
	60	10.36	6.01	4.4	
	80	13.67	6.06	5.9	
	100	16.96	6.10	7.2	
a-b	80	14.53	6.13	11.5	0.035
	90	16.17	6.10	10.0	.01
c	100	19.83	7.80	35.5	1.00
	110	21.12	7.58	35.2	.40
	130	23.84	7.20	34.2	.25
	150	26.66	6.88	32.2	.125
	170	29.58	6.62	29.5	0.75
	190	32.69	6.40	25.9	.04
	220	37.40	6.20	20.7	.03
	260	43.89	6.13	18.0	.01

z = 35.5 km: $\bar{u}$ = 6.23 km/s, $\bar{w}$ = 6.18 km/s, V = 6.0 km/s for z = 7.3-9.9 km and 11.6-17.9 km.

TABLE 19.—*Velocity-depth function of the profile from Ludlow(25) to NTS(19)*

Curve	Distance, Δ (km)	Traveltime, T (s)	Velocity, V (km/s)	Depth, z (km)	Gradient, dV/dz (km/s/km)
a	0	0	3.97	0	
	30	5.82	5.99	5.0	
	60	10.80	6.05	6.1	
	90	15.73	6.10	7.8	
	110	19.00	6.11	8.2	
a-b_1	80	14.29	6.15	9.7	0.02
a-b_2	70	13.50	6.31	14.6	.10
	110	19.86	6.25	13.7	.01
c	80	15.86	7.85	28.3	.50
	90	17.18	7.45	27.6	.45
	100	18.51	7.18	27.0	.36
	120	21.35	6.80	25.6	.175
	140	24.41	6.53	23.4	.075
	160	27.56	6.37	20.7	.03
	190	32.29	6.33	19.2	.01

$z = 27.5$ km: $\bar{u} = 6.03$ km/s, $\bar{w} = 6.14$ km/s.

TABLE 20.—*Velocity-depth function of the profile from Ludlow(25) to Mojave(23)*

Curve	Distance, Δ (km)	Traveltime, T (s)	Velocity, V (km/s)	Depth, z (km)	Gradient, dV/dz (km/s/km)
a	0	0	3.60	0	
	20	4.22	5.71	4.0	
	40	7.59	6.11	6.3	
	60	10.85	6.16	7.1	
	80	14.09	6.18	7.8	
	100	17.33	6.19	8.6	
a-b	80	14.17	6.32	12.7	0.10
	120	20.56	6.27	11.9	.01
c	80	16.30	7.80	30.8	∞
	100	18.98	7.40	30.7	1.00
	120	21.74	7.12	30.4	.30
	140	24.54	6.92	29.6	.14
	160	27.44	6.70	28.0	.085
	180	30.47	6.54	26.2	.06
	200	33.56	6.42	23.6	.04
	230	38.27	6.34	20.2	.01
d	90	17.53	8.11	31.0	.20
	140	23.60	8.21	32.0	.025

$z = 30.3$ km: $\bar{u} = 6.04$ km/s, $\bar{w} = 6.13$ km/s.

TABLE 21.—*Velocity-depth function of the profile from Barstow(24) to Ludlow(25)*

Curve	Distance, Δ (km)	Traveltime, T (s)	Velocity, V (km/s)	Depth, z (km)	Gradient, dV/dz (km/s/km)
a	0	0	4.66	0	
	20	3.89	5.51	2.3	
	40	7.46	5.74	4.4	
	60	10.78	6.21	8.5	
a-b	70	13.05	6.41	14.7	0.21
	80	14.61	6.33	14.1	.075
	100	17.81	6.25	11.9	.01
c	70	14.81	8.00	28.6	2.00
	80	16.09	7.63	28.4	1.00
	100	18.77	7.27	28.2	.30
	120	21.58	6.91	25.9	.075
	140	24.54	6.58	20.5	.05
d	80	15.94	8.21	29.0	.20
	140	23.21	8.25	29.6	.02

$z = 28.6$ km: $\bar{u} = 6.18$ km/s, $\bar{w} = 6.10$ km/s, $V \leq 6.1$ km/s for $z = 8.7$-11.8 km and 14.8-17.9 km, and $V = 6.48$ km/s at $z = 18.0$ km.

TABLE 22.—*Velocity-depth function of the profile from Barstow(24) to Mojave(23)*

Curve	Distance, Δ (km)	Traveltime, T (s)	Velocity, V (km/s)	Depth, z (km)	Gradient, dV/dz (km/s/km)
a	0	0	4.93	0	
	20	3.73	5.60	1.9	
	40	7.30	5.71	3.3	
	60	10.66	6.17	7.9	
	80	13.87	6.23	9.1	
a-b_1	60	10.97	6.25	9.4	0.03
a-b_2	50	10.14	6.48	13.0	.20
	60	11.71	6.33	11.5	.03
c	80	16.41	7.80	30.0	2.00
	90	17.71	7.51	29.8	.70
	100	19.04	7.29	29.4	.40
	120	21.81	6.92	28.0	.15
	140	24.74	6.64	25.3	.05

$z = 30.0$ km: $\bar{u} = 6.22$ km/s, $\bar{w} = 6.09$ km/s, $V = 6.1$ km/s for $z = 9.5$-11.4 km and 13.1-23.9 km, and $V = 6.58$ km/s at $z = 24.0$ km.

TABLE 23.—*Velocity-depth function of the profile from Mojave(23) to Ludlow(25)*

Curve	Distance, Δ (km)	Traveltime, T (s)	Velocity, V (km/s)	Depth, z (km)	Gradient, dV/dz (km/s/km)
a	0	0	4.19	0	
	20	3.93	5.79	3.3	
	40	7.29	6.12	5.4	
	60	10.50	6.25	7.0	
	80	13.69	6.27	7.6	
a-b	80	14.17	6.32	12.7	0.10
	120	20.56	6.27	11.9	.01
c	80	16.30	7.80	30.8	∞
	100	18.98	7.40	30.7	1.00
	120	21.74	7.12	30.4	.30
	140	24.54	6.92	29.6	.14
	160	27.44	6.70	28.0	.085
	180	30.47	6.54	26.2	.06
	200	33.56	6.42	23.6	.04
	230	38.27	6.34	20.2	.01
d	90	17.46	8.00	31.1	.30
	130	22.43	8.05	31.8	.04

$z = 30.8$ km: $\bar{u} = 6.16$ km/s, $\bar{w} = 6.19$ km/s.

from NTS to Kingman from 31 to 28 km and from NTS to Ludlow from 35 to 28 km. On the profiles Lake Mead-Mono Lake and Lake Mead-Santa Monica Bay, the crustal thickness at Lake Mead changes from 33 km for the northern profile to 29 km for the southern one. Comparison of $\bar{u}$ and $\bar{W}$ (tables 14-19) shows that except for the profile Ludlow-NTS (table 19), velocity inversions are evident within the upper crust. The condition $\bar{u} \cdot 1.005 \leqslant \bar{W}$ can be fulfilled for all profiles by assuming an average velocity of 6.0 km/s for the depth range between the depth points calculated from the most distant end of curve a and curve c, and by assuming that within this low-velocity material there are extended areas with higher P-wave velocity as indicated by curves a-b between a and c. With this assumption the upper crust is 18-24 km thick, and a distinct lower crust does not exist; rather, the lower crust is a transition zone between crustal and upper mantle material.

Another solution could be obtained by assuming that a low-velocity zone exists only between the depth ranges corresponding to a and $a-b$. The lower limit of the low-velocity zone is the greatest depth range $a-b$ if more than one $a-b$ curve exists. In this solution, the velocity inversion above $a-b$ should be strong, and an average velocity of 5.8 km/s would be required. Several scattered arrivals between curves a and c suggest several additional short $a-b$ branches for which no depth calculations were made. These short branches weaken the assumption of an extensive low-velocity zone, and so the first solution seems more probable.

The velocity-depth functions for the line between Ludlow and Mojave are presented in figure 40 and tables 20–23. Whereas the curves a from the shotpoint at Ludlow indicate a basin filled with about 2 km of sediments, the curves a of the profiles from Barstow and Mojave indicate an increase of the velocity with depth from less than 5 km/s to 6.20–6.25 km/s. This increase is due mainly to a gradual increase in the velocity of the basement rocks. On the basis of phase c, the total crustal thickness between Ludlow and Mojave ranges from 29 to 31 km. As the comparison of $\bar{u}$ and $\overline{W}$ shows, the P-wave velocity seems to decrease to 6.1 km/s at a depth range between 9 and 18 or 24 km in the vicinity of Barstow. Within this zone there may be material with higher velocity (up to 6.4–6.5 km/s), but the correlation of the corresponding phases in the record sections is ambiguous.

Comparison with the results published by Diment, Stewart, and Roller (1961) and Roller (1964) for the line NTS-Kingman and by Gibbs and Roller (1966) for the line NTS-Ludlow shows total crustal thicknesses close to those obtained here; the base of the crust rises from 3–34 km south of NTS to 27 km at Kingman and Ludlow. The average velocity in the crust, according to Diment, Stewart, and Roller (1961) and Roller (1964), corresponds to the velocity distribution found here. The average velocity reported by Gibbs and Roller (1966) is higher than that obtained here; no traveltime curve corresponding to 6.8 km/s could be found in the present study. Rather, the first arrivals between 120 and 145 km are interpreted here as P_n arrivals that can be correlated up to a distance of 150 km, whereas the first arrivals beyond 150 km are delayed for 0.3 second to form a traveltime curve approximately parallel to curve d. A similar feature is found on the profile Kingman-NTS at 175 km, as reported by Roller (1964). Johnson (1965) and Roller and Healy (1963) presented evidence for traveltime curves with a velocity of 7.0 km/s for the profiles Lake Mead-Mono Lake and Lake Mead-Santa Monica Bay. However, these traveltime curves are based on weak secondary arrivals and could not be confirmed in the present reinterpretation. Although the average velocity distribution in the crust determined by the above authors is somewhat higher than that obtained in this paper, their resulting total crustal thicknesses agree fairly well with those reported here.

OTHER PROFILES FROM NTS

In addition to the profiles discussed above, three other profiles from NTS are included in this paper: NTS to Navajo Lake, Utah; NTS to Elko, Nev.; and NTS to San Luis Obispo, Calif. The profile to Navajo Lake was extended to a distance of about 1,000 km into the Great Plains of Colorado. Initial results for this profile were published by Ryall and Stuart (1963). In this report, only the recordings up to a distance of 400 km were reinterpreted (fig. 41, pl. 2; table 75). On this line, the shotpoint at Navajo Lake is located approximately at the border between the Basin and Range province and the Colorado Plateau, 290 km from NTS. Three drill-hole shots were recorded to a distance of 250 km from Navajo Lake toward NTS (fig. 42, pl. 2; table 76). The profile from NTS to Eureka and Elko was also extended to a distance of 1,000 km into northern Idaho, crossing the Basin and Range province, the western Snake River Plain, and the Idaho batholith. It was interpreted by Pakiser and Hill (1963) and Hill and Pakiser (1966, 1967). In this report, only the recordings up to a distance of 440 km from NTS are included (fig. 43, pl. 2; table 77). The first part of this profile, to Eureka at a distance of 270 km from NTS, was not reversed. North of Eureka, some of the same recording sites were used from the shotpoints of the line from Boise to Eureka.

The profile from NTS to San Luis Obispo crosses the Basin and Range province, the Sierra Nevada, the Great Valley of California, and the Coast Ranges of California. It was "reversed" from San Luis Obispo by offshore shots in the Pacific Ocean at a distance of 480 km from NTS. Similar to the "reversed" profiles between Lake Mead and Mono Lake or Lake Mead and Santa Monica Bay, the observations from the shotpoints at both NTS and San Luis Obispo were not really reversed because the interval distance is too large to provide a common reversed subsurface path along the M-discontinuity. In this report, the profile from NTS (fig. 44, pl. 2; table 78) is analyzed only with regard to the crustal structure under the Basin and Range province. The profile enters the Sierra Nevada at a distance of 190 km from NTS. The first four shots recorded along this profile were chemical explosions; the other recordings were obtained from underground explosions of nuclear devices.

On the profiles from NTS to Navajo Lake and NTS

to Elko, no stations were recorded between the respective 0–55 and 0–70 km distance, and so the determination of curve *a* is based on only a few records at distances less than 120 or 130 km from NTS. The delay at the first two stations on the profile between NTS and San Luis Obispo at distances of 5 km and 25 km from the shotpoint northeast of NTS is the result of sedimentary covers in Emigrant Valley and Yucca Flat. It is generally assumed that the velocity increases gradually within the uppermost few kilometers of the basement. If the nearby stations are not located on basement rocks, the convex-upward curvature of curve *a* within the first 30 km cannot be recognized in the first arrivals.

Because of wider spacing of recording stations on these profiles and gaps of several tens of kilometers, the correlation of phases between *a* and *c* is more doubtful than on other profiles. Only on the profile NTS-San Luis Obispo and on the reverse profile Navajo Lake-NTS are there enough indications to permit the correlation of wave group *b*. On all profiles, however, phase *c* can be correlated confidently. Phase *d* is strong only on the profiles NTS-Elko and NTS-Navajo Lake. It is recognizable on the profile NTS-San Luis Obispo only at distances beyond 250 km, which may result partly from the energy released at NTS. On the profile Navajo Lake-NTS there are only weak indications for phase *d*. Tables 24–27 show the computed results.

The trend of curve *c* at distances beyond 200 km on the profiles NTS-Elko, NTS-Navajo Lake, and NTS-Ludlow is similar to that found on the line Boise-Lake Mead. From north to south, the velocity corresponding to the slope of curve *c* at 250 km decreases from 6.30 to 6.15 km/s. Whereas curve *c* crosses the distance axis on the profile NTS-Elko at 250 km, this distance increases to 320 km on the profile NTS-Navajo Lake. Curve *c* does not cross the distance axis on the profile NTS-Ludlow. Figure 39 (pl. 3) shows the combined crustal cross sections of the lines Ludlow-NTS and NTS-Elko. In addition, the results of interpretation of the profile Eureka-Lake Mead were projected on the line Eureka-NTS. As is indicated by the

TABLE 24.—*Velocity-depth function of the profile from NTS(19) to Navajo Lake(21)*

Curve	Distance, Δ (km)	Traveltime, T (s)	Velocity, V (km/s)	Depth, z (km)	Gradient, dV/dz (km/s/km)
a	0	0	4.52	0	
	50	9.43	5.92	6.9	
	80	14.47	5.98	8.3	
	100	17.81	6.02	9.8	
	130	22.76	6.09	12.2	
c	90	18.09	7.70	32.1	0.80
	100	19.41	7.40	31.7	.50
	120	22.14	7.04	31.0	.30
	140	25.01	6.76	29.8	.18
	160	28.06	6.56	28.7	.15
	180	31.18	6.43	27.8	.15
	200	34.31	6.35	27.2	.10
	240	40 62	6.30	26.4	.04
	300	50.16	6.28	25.2	.01

z = 32.1 km: $\bar{u}$ = 5.99 km/s, $\bar{w}$ = 6.11 km/s.

TABLE 25.—*Velocity-depth function of the profile from Navajo Lake(21) to NTS(19)*

Curve	Distance, Δ (km)	Traveltime, T (s)	Velocity, V (km/s)	Depth, z (km)	Gradient, dV/dz (km/s/km)
a	0	0	3.19	0	
	20	4.51	5.71	4.6	
	40	7.88	6.04	6.4	
	70	12.78	6.17	8.5	
b	60	12.55	6.37	15.2	0.10
	90	17.28	6.30	14.0	.01
c	100	20.23	7.80	36.6	1.00
	110	21.55	7.62	36.4	.42
	120	22.85	7.44	36.0	.30
	140	25.53	7.07	34.1	.15
	160	28.41	6.75	31.5	.075
	180	31.46	6.52	28.2	.035
	210	36.16	6.40	24.0	.01

z = 36.4 km: $\bar{u}$ = 6.07 km/s, $\bar{w}$ = 6.12 km/s.

TABLE 26.—*Velocity-depth function of the profile from NTS(19) to Elko(14)*

Curve	Distance, Δ (km)	Traveltime, T (s)	Velocity, V (km/s)	Depth, z (km)	Gradient, dV/dz (km/s/km)
a	0	0	5.04	0	
	80	13.86	6.01	6.5	
	100	17.19	6.03	7.4	
	120	20.50	6.05	8.3	
c	100	18.90	7.60	31.4	0.50
	120	21.62	7.15	30.1	.25
	140	24.48	6.80	28.0	.15
	160	27.51	6.55	25.4	.075
	180	30.57	6.38	22.3	.04
	220	36.90	6.30	19.6	.01

z = 31.4 km: $\bar{u}$ = 6.19 km/s, $\bar{w}$ = 6.25 km/s.

TABLE 27.—*Velocity-depth function of the profile from NTS(19) to San Luis Obispo(3)*

Curve	Distance, Δ (km)	Traveltime, T (s)	Velocity, V (km/s)	Depth, z (km)	Gradient, dV/dz (km/s/km)
a	0	0	3.57	0	
	30	6.20	5.72	5.2	
	60	11.33	5.87	6.8	
	90	16.42	5.96	9.3	
	120	21.43	6.02	11.6	
	155	27.45	6.11	15.1	
b	90	17.12	6.23	18.2	0.15
	120	21.95	6.18	17.3	.025
c	100	20.20	7.65	36.1	5.00
	120	22.91	7.24	36.0	1.00
	140	25.71	7.03	35.7	.30
	160	28.60	6.84	35.0	.175
	180	31.56	6.67	34.0	.12
	200	34.59	6.55	32.8	.08
	220	37.67	6.46	31.4	.05
	240	40.77	6.38	29.3	.03
	270	45.47	6.30	25.6	.015

z = 36.1 km: $\bar{u}$ = 5.92 km/s, $\bar{w}$ = 6.11 km/s.

crustal cross section of the line Navajo Lake-San Luis Obispo in figure 45 (pl. 3), the velocity decrease in the upper crust from 6.15 to 6.0 km/s south of NTS is not evident beneath NTS. The average velocity at depths of 18 km is about 6.1 km/s south of Eureka but may be somewhat higher north of NTS. The average crustal velocity increases also from NTS to the east. West of Navajo Lake, at the border of the Colorado Plateau, the velocity increases to nearly 6.4 km/s at a depth of 15 km and is about constant to a depth of 24 km.

The total crustal thickness reported by Pakiser and Hill (1963) for the profile NTS-Elko is 28 km without and 31 km with an intermediate layer in the lower crust (velocity 6.7 km/s). In later publications, Hill and Pakiser (1966, 1967) reported a 29-km crustal thickness 100 km north of NTS under the assumption that an intermediate layer exists with a velocity of 6.7 km/s at a depth of 20 km beneath an upper crustal layer with a velocity of 6.0 km/s. The average velocity obtained in this paper corresponds roughly to the average velocity of Hill and Pakiser, although the velocity distribution differs significantly between depths of 8 and 26 km. No evidence was found for an intermediate layer separated from the upper crust by a discontinuity but rather for a continuous increase of velocity from 6.0 km/s at 7 km to 7.6 km/s at the base of the crust at 31 km depth. The velocity gradient also increases gradually at depths greater than 20 km. The increasing thickness of the crust from NTS toward Eureka reported by Hill and Pakiser is confirmed here. The total crustal thickness of 25–26 km reported by Ryall and Stuart (1963) under NTS is significantly less than that reported here (32 km east of NTS). However, the increasing thickness to 42 km to the east reported by Ryall and Stuart under the western part of the Colorado Plateau is confirmed here by the results of the profile from Navajo Lake to NTS, with 36 km crustal thickness, and by the line from Hanksville (30) to Chinle (31), with 42–43 km crustal thickness. The apparent P_n velocities reported by the above authors for the profile NTS-Elko as well as the NTS-Navajo Lake correspond to the values reported in this paper.

THE SIERRA NEVADA

The Sierra Nevada (figs. 1, 4) is bounded by the Great Basin of the Basin and Range province on the east, the Great Valley of central California on the west, and the Cascade Range on the north. The general features of Sierra Nevada geology that follow are based mainly on Bateman and Wahrhaftig (1966), Bateman and Eaton (1967), Bateman (1968), and Pakiser, Kane, and Jackson (1964). The Sierra Nevada is a strongly asymmetrical mountain range with a gentle western slope and a high and steep eastern escarpment, a huge block formed by westward tilting and profound late Cenozoic faulting on the east. Most of the southern and the northeastern parts of the Sierra Nevada are composed of plutonic rocks of the Sierra Nevada batholith of Mesozoic age. In the north half of the range, the batholith is flanked on the west by the western metamorphic belt composed of strongly deformed and metamorphosed sedimentary and volcanic rocks of Paleozoic and Mesozoic ages. Farther south, scattered remnants of metamorphic rock are found in the western foothills and also along the crest in the east-central Sierra Nevada (Kistler and Bateman, 1966; Rinehart and Ross, 1964). These rocks are overlapped on the west by sedimentary rocks of the Great Valley and discontinuously overlain on the north by Cenozoic volcanic sheets that extend southward from the Cascade Range. The great eastern escarpment was created in Pliocene and Pleistocene times. The main faulting may represent collapse of the Owens Valley block in the crest of a broad arch (Bateman, 1968). The Sierra Nevada constitutes the west flank of this arch, and the desert ranges as far east as Death Valley constitute the faulted east flank. The Cascade Range, in which one line was partly recorded, is a volcanic mountain range that extends north through Oregon and Washington from the Sierra Nevada in northeastern California (fig. 1). According to Macdonald (1966) and Macdonald and Gay (1968), the older part of the range (the Western Cascades) consists of early and middle Tertiary basalt, andesite, and dacite. The High Cascades to the east were built by eruptions of basaltic to rhyolitic lava during Pliocene and Quaternary time. Andesites are the predominant rocks of the High Cascades. The most recently active volcano, Lassen Peak, erupted last in 1915.

SHASTA LAKE TO CHINA LAKE

The line extending from Shasta Lake (5) through Mono Lake to China Lake (8) yielded the most reliable data on the crustal structure under the Sierra Nevada. The northernmost 100-km segment of the profile, between Shasta Lake and Mono Lake, is located in the southern Cascade Mountains near Lassen Volcanic National Park. South of Mono Lake (409.0 km south of Shasta Lake and 273.3 km north of China Lake) the recording sites were located immediately east of the eastern escarpment of the Sierra Nevada (fig. 1). Previous investigations of Mono Basin and Owens Valley (for example, Pakiser and

others, 1964) make possible estimation of the influence that sediments and near-surface structures have on the broader seismic observations. This influence seems to be relatively small. The Mono Lake shotpoint was located in the western part of the lake just outside the deepest part of the Mono Basin structure (Pakiser, 1970). A depth to basement of 1.1 km was calculated for this shotpoint. Most of the recording sites up to 212 km south of Mono Lake were located directly on the granitic basement rocks or at places where the thickness of overlying sediments seems to be rather small.

Between Mono Lake and China Lake, an intermediate shotpoint was located at Independence, 157.2 km south of Mono Lake and 116.4 km north of China Lake. Figures 46–49 (pl. 2) and tables 79–82 present the record sections and corresponding data for the profiles from Shasta Lake, Mono Lake, and China Lake. Although the line between Mono Lake and China Lake was recorded east of the crest of the Sierra Nevada, the Bouguer gravity anomaly and geologic evidence suggest that the Sierra Nevada block is tilted toward the west and that the recording line follows closely the deep crustal axis of the Sierra Nevada. The profiles were observed in 1962 and first interpreted by Eaton (1966).

Because the northernmost part of the profile from Shasta Lake to Mono Lake was located in the southern Cascade Mountains, the first part of the record section (fig. 46) differs significantly from the other record sections of this line. Traveltime curve a shows a relatively steep slope that defines a velocity of 6.5–6.6 km/s at distances beyond 50 km. Curve a crosses the distance axis about 75 km from the Shasta Lake shotpoint. Secondary arrivals between 110 and 150 km define a traveltime curve a' parallel to curve a. This curve can be traced farther in weak first arrivals up to a distance of 175 km. Whereas this first part of the profile Shasta Lake-Mono Lake yields information on the crustal structure under the southernmost Cascade Mountains, the phases recorded at greater distances yield information on the Sierra Nevada. This explains the fact that the velocity indicated by curves a–b and b is slightly lower than that recorded at distances to 175 km. Phases b and c are not very clear but nevertheless can be traced with fair reliability between about 210 and 300 km. P_n arrivals were well recorded beyond 210 km, yielding an apparent upper mantle velocity of about 7.9 km/s. However, the point of critical distance can only be estimated because of the absence of corresponding arrivals in the appropriate distance range. This zone of weak arrivals is probably due to the change of crustal structure along the geologic boundary between the Sierra Nevada and Cascade Mountains. The resulting velocity-depth function (table 28; fig. 50, pl. 3) consequently must be considered as reflecting two geologic units: The upper part (to a depth of 17–18 km) is related to the Cascade Mountains, and the lower part is related to the Sierra Nevada. Comparison of the average velocities $\bar{u}$ and $\bar{W}$ suggests a velocity inversion from 6.55 to 6.0 km/s at depths below 7.5 km. However, the curve a' suggests that zones with higher velocity material probably exist within the low-velocity zone.

On the other profiles of the line from Shasta Lake to China Lake (figs. 47–49), the reciprocal slope of the traveltime curve a yields velocities corresponding to typical values for granitic rocks and to the location of the recording sites on or near rocks of the Sierra Nevada batholith. On the profile from Mono Lake to Shasta Lake, curve a can be traced to distances as great as 170 km, suggesting a gradual increase of velocity within the crust to 6.38 km/s at a depth of 17 km. This increase in velocity with depth was not found between Mono Lake and China Lake, along which line the resulting velocity at 160–170 km distance is about 6.1 km/s. A rather easily correlated curve a–b can be seen in secondary arrivals, and the record sections also support the existence of curve b, indicating a slight increase in velocity to 6.4–6.5 km/s at a depth of 21–24 km within the crust.

Curve c can be traced between 80 and 300 km on all profiles. However, the arrivals defining curve c are not as dominant as they are on most profiles in the Basin and Range province. P_n arrivals are generally very weak on the profile from Mono Lake to Shasta Lake; at many stations the first part of the P_n phase is either delayed or cannot be detected. The determination of the apparent upper mantle velocity is therefore uncertain. No P_n arrivals could be found on the profile from Mono Lake to China Lake. The first arrivals at 160–170 km distance from China Lake are probably P_n arrivals having an apparent velocity of 7.8 km/s when these arrivals are connected by a straight line with curve c at 80 km distance.

The comparison of the average velocities $\bar{u}$ and $\bar{W}$ shows that the condition $\bar{u} \cdot 1.005 \leqslant \bar{W}$ is fulfilled for the profiles from Mono Lake and that no decrease of velocity within the crust is evident (tables 29, 30). However, the profile from China Lake to Mono Lake indicates that the velocity in the upper crust does not exceed 6.1 km/s at depths above approximately 20 km (table 31).

Figure 50 shows the computed velocity-depth functions (tables 28–31) and a crustal cross section along

TABLE 28.—*Velocity-depth function of the profile from Shasta Lake(5) to Mono Lake(6)*

Curve	Distance, Δ (km)	Traveltime, T (s)	Velocity, V (km/s)	Depth, z (km)	Gradient, dV/dz (km/s/km)
a	0	0	4.98	0	
	20	3.89	5.59	2.3	
	40	7.14	6.45	6.3	
	60	10.20	6.55	7.7	
a	140	22.81	6.55	10.8	0.005
a-b	210	34.26	6.48	18.7	.02
b	180	30.37	6.55	26.4	.05
	220	36.47	6.52	25.0	.02
	280	45.69	6.50	22.4	.005
c	140	25.73	7.54	40.8	.35
	160	28.46	7.22	39.8	.225
	180	31.25	7.03	38.9	.15
	200	34.13	6.87	37.6	.10
	220	37.07	6.73	35.9	.065
	240	41.10	6.64	34.2	.045
	260	43.16	6.59	33.0	.03
	280	46.23	6.57	32.4	.02
	320	52.33	6.55	31.4	.01
d	140	25.70	7.60	41.0	.30
	160	28.26	7.75	41.9	.085
	210	34.71	7.84	43.8	.03
	340	51.20	7.90	48.0	.008

z = 40.8 km: $\bar{u}$ = 6.43 km/s, $\bar{w}$ = 6.29 km/s, V = 6.0 km/s for z = 7.8–10.6 km and 11.0–18.6 km.

TABLE 29.—*Velocity-depth function of the profile from Mono Lake(6) to Shasta Lake(5)*

Curve	Distance, Δ (km)	Traveltime, T (s)	Velocity, V (km/s)	Depth, z (km)	Gradient, dV/dz (km/s/km)
a	0	0	3.57	0	
	30	6.19	5.76	5.4	
	60	11.27	6.14	9.1	
	90	16.11	6.22	10.7	
	120	20.92	6.26	12.1	
	150	25.68	6.34	15.6	
	170	28.82	6.40	17.9	
a-b	130	22.75	6.44	20.7	0.06
	180	30.54	6.40	19.2	.01
b	140	24.89	6.55	25.2	.075
	170	29.47	6.51	24.4	.025
	190	32.54	6.49	22.6	.01
c	130	24.67	7.65	41.6	.50
	140	25.97	7.44	41.1	.50
	160	28.78	7.14	40.5	.30
	180	31.65	6.96	39.9	.20
	200	34.52	6.84	39.2	.125
	240	40.42	6.68	37.2	.05
	280	46.43	6.59	34.8	.028
	340	55.53	6.55	33.0	.01

z = 41.6 km: $\bar{u}$ = 6.15 km/s, $\bar{w}$ = 6.26 km/s.

TABLE 30.—*Velocity-depth function of the profile from Mono Lake(6) to China Lake(8)*

Curve	Distance, Δ (km)	Traveltime, T (s)	Velocity, V (km/s)	Depth, z (km)	Gradient, dV/dz (km/s/km)
a	0	0	3.45	0	
	20	4.34	5.66	4.1	
	40	7.79	5.86	5.5	
	60	11.17	5.96	7.1	
	90	16.11	6.11	10.5	
a-b	90	16.58	6.30	17.0	0.15
	170	30.91	6.26	15.6	.005
b	120	21.79	6.44	23.8	.20
	140	24.89	6.40	23.4	.075
	170	29.59	6.36	22.8	.025
	200	34.31	6.32	21.0	.01
c	110	22.03	7.86	40.1	1.00
	120	23.30	7.70	39.9	.40
	140	25.92	7.38	39.2	.25
	160	28.62	7.10	38.0	.15
	180	31.50	6.85	36.3	.10
	200	34.47	6.66	34.2	.075
	220	37.56	6.54	31.9	.035
	240	40.65	6.47	30.0	.025
	280	46.87	6.42	28.0	.01

z = 40.1 km: $\bar{u}$ = 6.09 km/s, $\bar{w}$ = 6.18 km/s.

TABLE 31.—*Velocity-depth function of the profile from China Lake(8) to Mono Lake(6)*

Curve	Distance, Δ (km)	Traveltime, T (s)	Velocity, V (km/s)	Depth, z (km)	Gradient, dV/dz (km/s/km)
a	0	0	4.48	0	
	20	4.04	5.33	2.4	
	40	7.65	5.71	5.0	
	60	11.08	5.94	7.6	
	80	14.41	6.04	9.2	
	110	19.36	6.06	9.9	
a-b	80	14.60	6.08	10.6	0.02
b	100	18.55	6.43	21.2	.30
	130	23.26	6.40	20.8	.035
	170	29.50	6.38	19.9	.01
c	90	18.53	7.60	33.5	2.00
	110	21.25	7.20	33.3	.75
	120	22.63	7.06	33.0	.50
	140	25.52	6.85	32.2	.175
	160	28.49	6.71	31.2	.075
	180	31.47	6.61	29.2	.03
	200	34.51	6.54	25.2	.01

z = 33.5 km: $\bar{u}$ = 6.08 km/s, $\bar{w}$ = 6.06 km/s, V = 6.1 km/s for z = 11.5–19.8 km.

the line from Shasta Lake through Mono Lake to China Lake. As discussed above, at a depth of 7.5 km a low-velocity zone was found in the area southeast of Shasta Lake in which the velocity decreases from 6.55 km/s to 6.0 km/s. This part of the profile is located on volcanic material that consists mainly of pyroxene andesites and basaltic andesites (Pakiser, 1964) having the observed high velocity of 6.5–6.6 km/s near the surface (see also Eaton, 1966). A similar velocity was found beneath the Snake River Plain at relatively shallow depth in an area of high regional Bouguer gravity, suggesting that upper crustal material may be absent there. The more recent eruptions of Lassen Peak and the observed local gravity low in that area (Pakiser, 1964) suggest a low-velocity zone below 7 km there.

Whether the seismic low-velocity zone is confined to the area of Lassen Volcanic National Park only or is a general feature of the Cascade Mountains cannot be decided on the basis of the available seismic-refraction data. The average velocity within the upper 20 km decreases under the Sierra Nevada from the northwest toward the southeast, as is suggested by the 6.2- and 6.4-km/s contour lines. The average velocity below 20 km depth is 6.4–6.6 km/s to a depth of approximately 33–35 km under Mono Lake and 30

km northwest of China Lake. At this depth, the velocity begins to increase to 7.6-7.8 km/s at the base of the crust. The total computed crustal thickness is 41-43 km in the middle part of the line and decreases to 33 km toward the southeast. On the basis of the velocity estimated from curve *c* at distances beyond 200 km, there does not seem to be a thick layer with 6.9 km/s average velocity under the Sierra Nevada, as interpreted by Eaton (1966); rather, the average velocity does not seem to exceed 6.6 km/s to a depth of 30-35 km. Consequently, the crustal thickness obtained herein is less than that reported by Eaton in 1966 but agrees well with that reported by Eaton in 1963. Mikumo (1965) also reported a crustal thickness of 43 km under the central Sierra Nevada, assuming an average crustal velocity of 6.3 km/s.

OTHER PROFILES IN THE SIERRA NEVADA

In addition to the line extending from Shasta Lake through Mono Lake to China Lake, several other profiles were recorded from shots at Mono Lake and China Lake. Three profiles were recorded from Fallon toward the west and south. Eaton (1963) reported on the profiles recorded from Fallon, and Johnson (1965) reported on the profile from Mono Lake to Lake Mead. The other profiles interpreted herein have not been previously published.

Figures 51-59 (pl. 2) and tables 83-91 present the record sections and corresponding data for all profiles discussed in this section. Figure 60 (pl. 2) and table 92 present a record section and data for fan observations that were recorded approximately 230 km from Mono Lake between the profiles from Mono Lake to China Lake and Mono Lake to Lake Mead (azimuths 119° to 152°). A corresponding record of the profile from Mono Lake to Santa Monica Bay (azimuth 166°) is also included.

Recording sites for shots from China Lake were irregularly distributed in a pattern that can be approximated by three profiles. Only seven recordings were obtained along the profile from China Lake (fig. 51; table 83) to a distance of 175 km to the northwest. Although the spacing along this profile is very large, the four most distant stations show clearly the phase *c* in later arrivals. No P_n arrivals were recorded because the profile was too short. The velocity-depth function calculated from curves *a* and *c* is shown in table 32 and figure 61 (pl. 3), together with an approximate crustal cross section based on this profile only. Like the profile from China Lake to Mono Lake, the total crustal thickness beneath this profile is 33 km, and a low-velocity zone is interpreted to exist between depth of 13 and 23 km in which the velocity decreases from 6.26 to 6.0 km/s.

The record section for the profile from China Lake to the west is shown in figure 52 (see also table 84). Only four usable stations between 140 and 245 km distance were recorded toward San Luis Obispo. These stations were west of the Sierra Nevada in the Great Valley and the Coast Ranges of California. On the basis of data in Hackel (1966), the stations in the Great Valley at distances of 140 and 165 km were located over 3 km and 6 km, respectively, of sedimentary rocks, and on the basis of data in Payne (1967), one station in the Carrizo Plain area of the Coast Ranges (distance 205 km) was located over sediments more than 2 km thick. Correcting the reduced traveltime ($T - \Delta/6$) by 1.0 s for 3-km- and 1.5 s for 6-km-thick sediments on the basis of data from Eaton (1963) causes later arrivals to aline on a curve yielding an apparent velocity of 6.5 km/s at 140 km and 6.1 km/s at 245 km distance. However, because available observations are insufficient, no depth calculations were made.

The profile from China Lake to Santa Monica Bay (fig. 53; table 85) was recorded along the southeastern edge of the Sierra Nevada. To the south it crosses the western Mojave Desert near Mojave. The first arrivals at distances of 14 and 23 km were delayed for more than one-half second, probably owing to a thick sedimentary cover in the basin at China Lake. At the end of the profile near Santa Monica Bay, good P_n arrivals can be recognized, and fairly well correlated secondary arrivals permit the tracing of phases *b* and *c*. The total crustal thickness calculated for this profile (table 33; fig. 62, pl. 3) is 31 km, and the comparison of the average velocities $\bar{u}$ and $\bar{W}$ indicates that low-velocity material with a velocity of 6.1 km/s extends to a depth of about 12 km south of China Lake.

The 444.9-km-long profile from Mono Lake to Santa Monica Bay (fig. 54; table 86) crosses the Sierra Nevada, but it was recorded in adequate detail only

TABLE 32.—*Velocity-depth function of the profile from China Lake(8) to northwest*

Curve	Distance, Δ (km)	Traveltime, *T* (s)	Velocity, *V* (km/s)	Depth, *z* (km)	Gradient, *dV/dz* (km/s/km)
a	0	0	4.15	0	
	30	5.78	5.95	4.7	
	70	12.41	6.05	6.3	
	100	17.36	6.13	9.2	
	110	18.97	6.21	11.1	
	120	20.58	6.26	12.7	
c	110	21.28	7.35	33.2	0.30
	120	22.67	7.04	32.1	.25
	140	25.59	6.75	30.4	.10
	160	28.58	6.55	28.0	.04
	180	31.65	6.40	23.5	.015

z = 33.2 km: $\bar{u}$ = 6.13 km/s, $\bar{w}$ = 6.04 km/s, V = 6.0 km/s for z = 12.8-23.4 km.

TABLE 33.—*Velocity-depth function of the profile from China Lake(8) to Santa Monica Bay(4)*

Curve	Distance, Δ (km)	Traveltime, T (s)	Velocity, V (km/s)	Depth, z (km)	Gradient, dV/dz (km/s/km)
a	0	0	3.84	0	
	20	4.09	5.83	3.8	
	40	7.42	6.05	5.2	
	60	10.71	6.08	5.9	
	80	13.99	6.10	6.6	
	100	17.27	6.11	7.2	
b	60	11.77	6.26	13.7	0.30
	80	14.97	6.21	13.2	.03
	100	18.21	6.19	12.6	.01
c	80	16.76	7.84	31.1	2.00
	90	18.06	7.54	30.8	.65
	100	19.40	7.29	30.4	.45
	120	22.13	6.85	29.3	.30
	140	25.25	6.58	27.9	.125
	160	28.34	6.41	26.1	.075
	180	31.46	6.32	24.5	.03
	210	36.25	6.26	21.4	.01

z = 31.1 km: $\bar{u}$ = 6.03 km/s, $\bar{w}$ = 6.05 km/s, V = 6.1 km/s for z = 7.3–12.5 km.

TABLE 34.—*Velocity-depth function of the profile from Mono Lake(6) to Santa Monica Bay(4)*

Curve	Distance, Δ (km)	Traveltime, T (s)	Velocity, V (km/s)	Depth, z (km)	Gradient, dV/dz (km/s/km)
a	0	0	4.23	0	
	20	4.10	5.51	3.1	
	40	7.54	5.90	5.3	
	90	15.84	6.12	9.2	
	140	23.95	6.22	13.4	
c	190	32.39	6.98	37.0	0.08
	200	33.85	6.81	34.8	.075
	220	36.87	6.59	31.2	.05
	240	39.95	6.46	28.9	.05
	280	46.16	6.35	25.5	.02
	320	52.49	6.30	21.8	.01

z = 37.0 km: $\bar{u}$ = 6.17 km/s, $\bar{w}$ = 6.30 km/s.

beyond 190 km from Mono Lake. Only two records were available between 50 and 190 km. Because of the lack of observations up to 190 km, only curves *a* and *c* can be determined. Curve *c* is well defined between 190 and 300 km from Mono Lake; however, the continuation of curve *c* toward smaller distances is doubtful. P_n arrivals could not be identified. The calculated velocity-depth function (table 34; fig. 63, pl. 3) shows a gradual velocity increase with depth from 6.3 km/s at 22 km to about 7.0 km/s at 37 km, assuming a velocity gradient of 0.08 km/s/km at that depth as determined from other similar profiles. A low-velocity zone within the crust is not evident.

The profile from Fallon to San Francisco (fig. 55; table 87) crosses the Sierra Nevada between Lake Tahoe and Sacramento at distances between 90 and 220 km from Fallon. The stations east of Lake Tahoe were located in the Basin and Range province, and the stations beyond 220 km were located in the Great Valley of California. In addition to curve *a*, curve *b* can be traced between 80 and 125 km and indicates a velocity increase from 6.2 to 6.4 km/s between depths of 14 and 18 km. Curve *c* was reliably determined between 80 and 230 km. Curve *d* is tangent to *c* at 110 km and can be traced to 230 km. The apparent velocity defined by curve *d* is 7.7–7.8 km/s.

From curve *c*, a velocity increasing with depth from 6.45 km/s at 21 km to 7.90 km/s at 35 km was derived. The center part of figure 12 shows the velocity-depth function of this profile (table 35) and the resulting crustal cross section from Fallon to the west. Additional velocity-depth data are available at the intersection with the line from Shasta Lake to Mono Lake. From east to west, the cross section shows a gradual thickening of the crust from the Basin and Range province near Fallon into the Sierra Nevada, which corresponds with Eaton's (1963) interpretation. The decrease of crustal thickness west of the intersection with the line from Shasta Lake to Mono Lake is not based on seismic observations. According to the considerations of Eaton (1963), however, it is assumed that the crustal thickness under the Great Valley of California is close to that found under the Coast Ranges.

The profiles from Fallon and Mono Lake extend into the Basin and Range province immediately east of the Sierra Nevada, where the crust seems to be similar to that in the Sierra Nevada.

The most distant stations of the profile from Fallon to Mono Lake (fig. 56, pl. 2; table 88) are located beyond a distance of 180 km south of Mono Lake in the Sierra Nevada. Because of lack of observations between 90 and 145 km, only the phases *a* (0–90 km), *c* (90–295 km), and *d* (290–350 km) can be correlated. Phase *d* at a distance of 90 km seems to mark approximately the critical distance because it fits the extrapolated curves *c* and *d* at their point of tan-

TABLE 35.—*Velocity-depth function of the profile from Fallon(9) to San Francisco(1)*

Curve	Distance, Δ (km)	Traveltime, T (s)	Velocity, V (km/s)	Depth, z (km)	Gradient, dV/dz (km/s/km)
a	0	0	3.39	0	
	20	4.40	5.73	4.3	
	40	7.73	6.04	5.9	
	60	11.04	6.06	6.5	
	90	15.97	6.10	7.9	
b	90	16.60	6.44	18.5	0.20
	100	18.17	6.35	17.9	.10
	120	21.35	6.21	13.8	.01
c	100	19.39	7.90	34.7	.40
	110	20.64	7.64	34.1	.42
	120	21.99	7.40	33.5	.30
	140	24.81	7.06	32.0	.15
	160	27.67	6.80	30.2	.09
	180	30.67	6.60	27.2	.04
	200	33.72	6.46	20.8	.01

z = 34.1 km: $\bar{u}$ = 6.05 km/s, $\bar{w}$ = 6.27 km/s.

gency. P_n arrivals that could be confidently identified were not recorded at distances less than 290 km; the apparent P_n velocity beyond 290 km is 7.5–7.6 km/s.

The reverse profile from Mono Lake to Fallon (fig. 57; table 89) was recorded at only eight stations. Curve *a* suggests a gradual velocity increase with depth. However, because there are no stations between 0 and 45 km and only a few stations beyond that distance, the possibility cannot be excluded that the first arrivals were delayed by sediments in such a way that a velocity gradient is erroneously suggested. Therefore, the slope based on the two stations between 15 and 55 km may not yield a true velocity. The position of curve *c* on the profile from Fallon to Mono Lake contains some arrivals of phase *c* that also seem to be delayed on this profile. The results of the depth calculations for the profiles between Fallon and Mono Lake are presented in tables 36 and 37 and shown in figure 63 with the results from the line from Mono Lake to Santa Monica Bay. Crustal thickness increases from 31 km south of Fallon to 33 km west of Walker Lake to 41 km at Mono Lake. Eaton (1963) reported a similar increase in thickness along this line. The thickness obtained on the line from Shasta Lake to China Lake is supported by the profile from Mono Lake to Santa Monica Bay, where a velocity of 7.0 km/s was found at a depth of 37 km. Farther south, the profile extending northwest from China Lake contains some information that can be used to construct the crustal cross section in figure 63. This profile shows that the crust thins under the southern part of the Sierra Nevada. The dotted lines in the cross section of figure 63 for distances greater than 150 km south of Mono Lake show the suggested trend of the lines of equal velocity for the area where no seismic information was available.

The first part of the profile from Fallon to China Lake (fig. 58; table 90) is largely composed of the same stations as the profile from Fallon to Mono Lake. Phase *a* can be traced up to distances of 90–100 km, but the first arrivals beyond 100 km seem to correlate well with later arrivals at shorter distances (curve *a–b*). For only a short distance range, but clearly correlatable, phase *b* indicates a velocity increase from 6.2 to 6.3 km/s at depths of 16–18 km (table 38). Curve *c* is expressed by very strong secondary arrivals between 135 and 220 km, and it can be correlated over the entire distance range from 85 to 355 km. P_n arrivals seem to be delayed between 180 and 220 km. An 8-km-thick transition zone from lower crust to upper mantle between depths of 24 and 32 km was calculated (fig. 62). Results of the two recording lines from Fallon through China Lake to Santa Monica Bay were combined to form a crustal cross section (fig. 62). The reversed part of the line from Fallon to China Lake is based on the results of the profiles from Independence and China Lake along the line from Shasta Lake to China Lake (fig. 50).

TABLE 36.—*Velocity-depth function of the profile from Fallon(9) to Mono Lake(6)*

Curve	Distance, Δ (km)	Traveltime, T (s)	Velocity, V (km/s)	Depth, z (km)	Gradient, dV/dz (km/s/km)
a	0	0	3.43	0	
	20	4.45	5.43	3.9	
	40	7.91	5.97	6.6	
	60	11.20	6.14	8.6	
	90	16.04	6.24	10.6	
c	100	19.37	7.60	32.3	0.40
	110	20.72	7.27	31.5	.40
	120	22.12	7.04	30.8	.28
	140	25.00	6.76	29.8	.18
	160	28.03	6.59	28.6	.10
	180	31.10	6.44	26.4	.05
	200	34.23	6.33	22.6	.02

z = 32.3 km: $\bar{u}$ = 6.00 km/s, $\bar{w}$ = 6.15 km/s.

TABLE 37.—*Velocity-depth function of the profile from Mono Lake(6) to Fallon(9)*

Curve	Distance, Δ (km)	Traveltime, T (s)	Velocity, V (km/s)	Depth, z (km)	Gradient, dV/dz (km/s/km)
a	0	0	5.09	0	
	20	3.81	5.39	1.4	
	40	7.48	5.49	2.6	
	60	11.10	5.63	5.1	
	80	14.55	5.95	9.8	
	110	19.49	6.13	13.2	
c	90	18.25	7.90	33.7	1.00
	100	19.54	7.65	33.5	.50
	120	22.22	7.24	32.2	.20
	140	24.98	6.86	29.7	.10
	160	27.98	6.52	26.1	.05
	180	31.11	6.30	20.9	.02

z = 33.7 km: $\bar{u}$ = 6.13 km/s, $\bar{w}$ = 6.16 km/s.

TABLE 38.—*Velocity-depth function of the profile from Fallon(9) to China Lake(8)*

Curve	Distance, Δ (km)	Traveltime, T (s)	Velocity, V (km/s)	Depth, z (km)	Gradient, dV/dz (km/s/km)
a	0	0	3.56	0	
	20	4.45	5.42	3.9	
	40	7.91	5.96	6.6	
	60	11.21	6.09	8.1	
	90	16.11	6.15	9.8	
a–b	110	19.72	6.15	10.8	0.005
b	100	18.49	6.30	18.5	.10
	120	21.66	6.25	17.7	.03
	140	24.85	6.22	16.1	.01
c	90	18.04	7.90	32.7	.60
	100	19.34	7.52	31.9	.50
	120	22.04	7.10	30.7	.30
	140	24.90	6.79	29.4	.14
	160	27.89	6.55	27.2	.085
	180	31.00	6.40	25.2	.05
	200	34.16	6.33	23.5	.025
	230	38.92	6.30	22.1	.01

z = 32.7 km: $\bar{u}$ = 5.98 km/s, $\bar{w}$ = 6.17 km/s.

The final profile east of the Sierra Nevada was recorded from Mono Lake to Lake Mead, 439 km to the southeast. On this profile (fig. 59; table 91), correlation of phase *b* is uncertain. Phase *c* can be recognized up to a distance of 320 km, but the point of critical reflection at a distance of 110 km was not as confidently determined as on other profiles. The P_n arrivals form two parallel branches; weak first arrivals were followed by strong arrivals one-half second later. The general delay of P_n between 270 and 310 km seems to be explainable by a section of thick sediments overlying the basement rocks, whereas at distances greater than 310 km the energy was too weak to produce good P_n arrivals. The measured apparent velocity of P_n is 8.0 km/s.

The calculated velocity-depth function (table 39; fig. 36) for the profile from Mono Lake to Lake Mead includes a velocity increase from 6.15 km/s to 6.4 km/s at a depth of 12–17 km. The average crustal velocity is 6.4 km/s below 17 km. Velocity increases gradually between 28 km and the base of the crust at a depth of 37 km. Crustal thickness decreases from 41 km under Mono Lake to 37 km under the Inyo Mountains (fig. 36) and is uniform toward the southeast to the intersection with the line from Ludlow to NTS (see also fig. 39). The average velocity in the upper 25 km of the crust decreases east of the Inyo Mountains, in agreement with the other profiles from NTS and Lake Mead. Johnson (1965) found a layer with a velocity of 7.1 km/s, which is reinterpreted here as a 7–8-km-thick transition zone in which the velocity increases gradually from 6.5 to 7.8 km/s. The characteristics of the arrivals correlated by curves *c* and *d* change from the Sierra Nevada to the Basin and Range province, as revealed by observations approximately 230 km from Mono Lake (fig. 60; table 92). The amplitudes of the P_n phase decrease with increasing crustal thickness westward toward the Sierra Nevada, and the arrivals gradually disappear at an azimuth of 146°. The early arrival of phase *c* at 166° shows that this phase approaches the distance axis at 225 km. The slope of curve *c* decreases with decreasing azimuth to define a velocity at a distance of 220–240 km and azimuth of 166° at 6.6 km/s decreasing to 6.4 km/s at 119°.

TABLE 39.—*Velocity-depth function of the profile from Mono Lake(6) to Lake Mead(22)*

Curve	Distance, Δ (km)	Traveltime, T (s)	Velocity, V (km/s)	Depth, z (km)	Gradient, dV/dz (km/s/km)
a	0	0	4.02	0	
	30	6.05	5.68	4.7	
	60	11.09	6.06	7.9	
	90	16.01	6.11	9.1	
	110	19.28	6.13	9.9	
	130	22.54	6.15	11.0	
	150	25.79	6.16	11.6	
b	70	13.91	6.38	16.9	0.20
	110	20.19	6.33	16.5	.02
c	120	22.71	7.70	37.3	.25
	130	24.03	7.30	35.4	.20
	140	25.45	6.98	33.6	.18
	160	28.42	6.62	31.2	.15
	180	31.49	6.50	30.0	.08
	210	36.13	6.41	28.1	.03
	230	39.27	6.38	24.9	.01

z = 37.3 km: $\bar{u}$ = 6.14 km/s, $\bar{w}$ = 6.22 km/s.

COAST RANGES OF CALIFORNIA

The Sierra Nevada is bordered on the west by the Great Valley of central California, a nearly flat alluvial plain 750 km long and about 80 km wide on the average. In structure it is a large, elongate, northwest-trending, asymmetric trough with a wide and stable eastern shelf underlain by the buried west-dipping Sierran slope and a narrow western flank formed by the steeply upturned edges of the basin sediments (Hackel, 1966). Hamilton (1969) regards the Great Valley sedimentary rocks as continental shelf deposits and partly, in their westernmost parts, as continental slope deposits of Mesozoic age.

The Coast Ranges, farther west, are a series of ridges and valleys that generally trend northwest near and subparallel to the Pacific Coast. The Coast Ranges are still undergoing folding and warping, and several fault zones are seismically active (Crowell, 1968; Page, 1966). According to Eaton (1967, 1968), earthquakes occur along the San Andreas fault only at depths no greater than 15 km. Two entirely different core complexes, one the Jurassic and Cretaceous eugeosynclinal assemblage called the Franciscan Formation (Bailey and others, 1964) and the other the block consisting of Cretaceous granitic intrusions and older metamorphic rocks, lie side by side and are separated from each other by the San Andreas fault system in central California. Hamilton (1969, p. 2419) suggested that "the undated platform-facies meta-sedimentary rocks, intruded by Cretaceous batholiths and exposed in small areas of the central Coast Ranges west of the San Andreas fault (Compton, 1966), perhaps lay near the southeastern California (Pre-cambrian basement) complexes in Cretaceous time***" and were displaced about 500 km north-northwestward by the right-lateral San Andreas and other faults.

SAN FRANCISCO TO SANTA MONICA BAY

The profiles recorded in 1961 from San Francisco through Camp Roberts to Santa Monica Bay trend parallel to the geologic features of the Coast Ranges of California. The recording sites were located near

the coastline west of the San Andreas fault zone on granitic intrusions, metamorphic rocks, or covering sediments. The line is about 550 km long with the following distances between shotpoints: San Francisco-Camp Roberts, 260.8 km, and Camp Roberts-Santa Monica Bay, 287.6 km. The maximum recording distance was 320 km. Figures 64-67 (pl.2) and tables 93-96 present the record sections and corresponding tables for the profiles. Near San Francisco and Santa Monica Bay, offshore shots were detonated; near Camp Roberts, the shots were fired in drill holes. The line was first interpreted by Healy (1963). In 1967, the U.S. Geological Survey carried out a detailed seismic investigation of the crust between San Francisco and San Luis Obispo. Two lines, each about 200 km long, were recorded from several shotpoints alined parallel to and on both sides of the San Andreas fault zone (see fig. 82 for locations of shotpoints). A preliminary interpretation of these observations was published by Stewart (1968a). In this report, only the profiles recorded in 1961 are included, but main phases on the record sections of these profiles were correlated by visually comparing them with the data of 1967.

In agreement with the results of Healy (1963) and Stewart (1968a), traveltime curves for phase *a* of all four profiles along the line from San Francisco to Santa Monica Bay show a velocity slightly higher than 6.0 km/s beyond distances of 60 km. In contrast, Eaton (1963) and Stewart (1968a) found the velocity within the Franciscan basement rocks east of San Andreas fault zone to range from 3.3 km/s near the surface of 5.7 km/s at depths of several kilometers.

Secondary arrivals were weak on the profile from San Francisco to Camp Roberts (fig. 64), and so curve *c* can be traced only between 65 and 130 km. However, clear P_n arrivals were recorded beyond 190 km, yielding an apparent velocity of 8.0 km/s. The correlation of phase *b* on the profiles from Camp Roberts (figs. 65, 66) and the resulting depth calculation are uncertain. Secondary arrivals corresponding to curve *c* were stronger from the Camp Roberts shots. P_n arrivals can be identified and correlated, yielding average velocities of 7.9-8.1 km/s to the northwest and 7.9 km/s to the southeast. The weakness of the phases of curve *c* from the San Francisco shotpoint is in agreement with the profiles recorded in 1967 west of the San Andreas fault, whereas on some profiles recorded on Franciscan basement east of the San Andreas fault a very clear phase can be recognized as curve *c*. On the profile from Santa Monica Bay to Camp Roberts (fig. 67), secondary arrivals can be correlated relatively well between 50 and 110 km. The corresponding velocity-depth calculation for these arrivals indicates a velocity increase from 6.32 to 6.45 km/s at depths of 15-17 km. The record section of this profile shows prominent phases that can be correlated to form curves *c* and *d*. Curve *d* defines an apparent velocity of 8.3 km/s.

The resulting velocity-depth functions and the crustal cross section (fig. 68, pl. 3; tables 40-43) show that there is a sharp, nearly discontinuous boundary between crust and mantle under the Coast Ranges of central California at which the velocity increases within a depth range of 2 km from 6.6-6.8 to 7.8-8.0 km/s. The crust there is about 26 km thick. Toward the south, under the Transverse Ranges between Santa Barbara and Los Angeles, the crust thickens to 36 km, and the transition zone between crust and mantle thickens to about 6 km. A distinct intermediate boundary does not seem to be present within the crust; the average velocity between depths of 10 and 24 km is 6.3-6.4 km/s. The velocity-depth model proposed by Healy (1963) has an average crustal velocity of 6.1 km/s. This value is approximately that proposed in this report. The total crustal thickness presented by Healy and in this paper is about the same.

OTHER PROFILES FROM SANTA MONICA BAY

In addition to the profile from Santa Monica Bay to Camp Roberts, three other profiles were recorded from Santa Monica Bay: to the north toward Mono Lake (fig. 69, pl. 2; table 97), to the north-northeast toward China Lake (fig. 70, pl. 2; table 98), and to the northeast toward Lake Mead (fig. 71, pl. 2; table 99). Results for the profile from Santa Monica Bay to Lake Mead were published by Roller and Healy (1963). The two profiles from Santa Monica Bay to Mono Lake and China Lake actually constitute a single profile because the recording locations of which

TABLE 40.—*Velocity-depth function of the profile from San Francisco(1) to Camp Roberts(2)*

Curve	Distance, Δ (km)	Traveltime, T (s)	Velocity, V (km/s)	Depth, z (km)	Gradient, dV/dz (km/s/km)
a	0	0	3.79	0	
	20	4.46	5.11	3.2	
	40	8.19	5.60	6.2	
	60	11.60	6.04	9.9	
	80	14.85	6.24	12.5	
c	70	14.50	7.78	26.2	1.00
	80	15.79	7.28	25.5	.75
	100	18.60	6.90	24.7	.20
	120	21.56	6.62	22.0	.04
d	80	15.68	7.96	27.0	.20
	100	18.22	8.00	27.4	.05

z = 26.2 km: $\bar{u}$ = 5.93 km/s, $\bar{w}$ = 6.03 km/s.

TABLE 41.—*Velocity-depth function of the profile from Camp Roberts(2) to San Francisco(1)*

Curve	Distance, Δ (km)	Traveltime, T (s)	Velocity, V (km/s)	Depth, z (km)	Gradient, dV/dz (km/s/km)
a	0	0	2.85	0	
	20	4.80	5.64	5.0	
	40	8.16	6.07	7.2	
	60	11.38	6.34	9.8	
	80	14.51	6.38	10.7	
b	70	13.65	6.89	11.7	.01
c	70	14.48	7.80	26.5	1.00
	80	15.80	7.41	26.1	.70
	100	18.52	6.90	25.3	.40
	120	21.51	6.60	24.4	.20
	140	24.56	6.50	23.9	.10
	160	27.66	6.44	23.1	.04
	180	30.77	6.42	22.5	.025
	210	35.44	6.40	21.4	.01
d	100	18.24	7.98	27.5	.06
	160	25.76	8.05	30.2	.015
	210	31.81	8.10	34.0	.01

z = 26.5 km: $\bar{u}$ = 5.82 km/s, $\bar{w}$ = 6.06 km/s.

TABLE 42.—*Velocity-depth function of the profile from Camp Roberts(2) to Santa Monica Bay(4)*

Curve	Distance, Δ (km)	Traveltime, T (s)	Velocity, V (km/s)	Depth, z (km)	Gradient, dV/dz (km/s/km)
a	0	0	3.49	0	
	20	4.30	5.66	4.1	
	40	7.76	5.89	5.7	
	60	11.09	6.15	8.5	
	80	14.28	6.26	10.2	
b	150	25.86	6.27	15.5	0.01
c	70	14.46	7.70	25.7	.70
	80	15.80	7.20	25.0	.70
	100	18.71	6.70	24.1	.35
	120	21.75	6.47	23.3	.15
	140	24.89	6.37	22.4	.05
	160	28.04	6.34	21.6	.025
	200	34.32	6.33	21.4	.01
d	100	18.33	7.80	26.5	.05
	140	23.52	7.85	28.0	.02
	230	34.93	7.90	31.0	.007

z = 25.7 km: $\bar{u}$ = 5.90 km/s, $\bar{w}$ = 6.01 km/s.

TABLE 43.—*Velocity-depth function of the profile from Santa Monica Bay(4) to Camp Roberts(2)*

Curve	Distance, Δ (km)	Traveltime, T (s)	Velocity, V (km/s)	Depth, z (km)	Gradient, dV/dz (km/s/km)
a	0	0	3.97	0	
	30	6.45	5.51	5.3	
	60	11.44	6.21	9.8	
	90	16.25	6.26	11.2	
	120	21.02	6.30	12.7	
b	60	12.69	6.45	17.3	0.50
	80	15.79	6.35	16.6	.04
	100	18.95	6.32	15.2	.01
c	100	19.86	8.00	36.1	.40
	110	21.14	7.67	35.2	.30
	120	22.43	7.40	34.3	.25
	140	25.10	6.99	32.1	.15
	160	27.98	6.69	29.9	.10
	180	31.07	6.55	28.4	.05
	200	34.16	6.50	27.2	.028
	240	40.33	6.47	25.6	.01
d	110	21.00	8.10	36.6	.18
	140	24.64	8.19	38.0	.06
	200	31.90	8.25	40.0	.02

z = 36.1 km: $\bar{u}$ = 6.07 km/s, $\bar{w}$ = 6.21 km/s.

they are formed are almost identical up to a distance of 200 km. Many stations up to 110 km were located so that their records have been plotted in both record sections (figs. 69, 70). Therefore, the traveltime curves for the profile to Mono Lake do not differ from those on the profile to China Lake. Furthermore, the curve parallel to curve *d* beyond 240 km has the same position on both record sections. The velocity-depth calculations are therefore identical (table 44; figs. 62, 63). However, the arrivals between 40 and 130 km that form a cusp with curve *a* seem to be restricted to the profile to Mono Lake, which crosses the central Sierra Nevada, whereas only curve *a* can be correlated on the profile to China Lake, which crosses the western Mojave Desert.

The traveltime diagram for the profile from Santa Monica Bay to Lake Mead (fig. 71) is very similar to those of the other profiles from Santa Monica Bay. The large delay of curve *a* on all three profiles results from the thick accumulation of sedimentary rocks in the Los Angeles basin. These rocks may be 2 km thick or more under the area crossed by the profiles from the basement map by Yerkes, McCulloch, Schoellhamer, and Vedder (1965). The velocity determined from the curves *a* for the basement rocks exceeds 6 km/s. On the basis of curve *b*, the velocity increases at depths between 17 and 20 km from 6.3–6.4 to about 6.5 km/s. The total crustal thickness is 34–34 km under the Transverse Ranges north of Los Angeles. The velocity gradient increases below depths of about 30 km (table 45; left part of fig. 37). There are no seismic data available that yield direct information about the boundary zone between the Transverse Ranges and the Mojave

TABLE 44.—*Velocity-depth function of the profile from Santa Monica Bay(4) to Mono Lake(6)/China Lake(8)*

Curve	Distance, Δ (km)	Traveltime, T (s)	Velocity, V (km/s)	Depth, z (km)	Gradient, dV/dz (km/s/km)
a	0	0	2.78	0	
	30	6.71	5.71	6.1	
	60	11.81	5.95	8.5	
	90	16.75	6.12	11.5	
	100	18.39	6.15	12.3	
Santa Monica Bay to Mono Lake only:					
	40	8.71	6.29	12.8	
	80	14.96	6.41	13.8	
	120	21.20	6.42	14.3	
b	70	14.75	6.54	19.9	0.25
	90	17.83	6.43	18.5	.03
c	90	18.75	8.00	36.6	>5.00
	100	20.07	7.72	36.5	2.00
	120	22.71	7.46	36.2	.40
	140	25.37	7.26	35.6	.15
	160	28.15	7.08	33.9	.05
	180	31.00	6.92	29.9	.02
d	100	19.95	8.04	36.7	.25
	180	29.88	8.06	37.0	.02

z = 36.6 km: $\bar{u}$ = 5.99 km/s, $\bar{w}$ = 6.19 km/s.

TABLE 45.—*Velocity-depth function of the profile from Santa Monica Bay(4) to Lake Mead(22)*

Curve	Distance, Δ (km)	Traveltime, T (s)	Velocity, V (km/s)	Depth, z (km)	Gradient, dV/dz (km/s/km)
a	0	0	2.74	0	
	30	6.35	6.14	6.1	
	60	11.21	6.18	7.0	
	90	16.06	6.185	7.4	
	110	19.29	6.19	7.6	
b	60	13.08	6.44	18.0	0.40
	80	16.18	6.36	17.4	.04
	100	19.35	6.30	16.0	.01
c	90	18.78	7.84	34.4	.85
	100	20.09	7.49	33.9	.70
	120	22.83	7.07	33.0	.30
	140	25.71	6.84	31.7	.10
	160	28.68	6.70	30.0	.04
	200	34.70	6.59	26.4	.01
d	200	32.56	7.93	35.4	.01

z = 34.4 km: $\bar{u}$ = 5.97 km/s, $\bar{w}$ = 6.03 km/s.

Desert. However, the two areas are separated by the San Andreas fault zone (Dibblee, 1967), so it seems likely that the crust thins to the north and northeast within a small distance as shown in the crustal cross sections and as also suggested by Roller and Healy (1963).

TRANSVERSE PROFILES FROM SAN FRANCISCO AND SAN LUIS OBISPO

The two profiles from San Francisco to Fallon and San Luis Obispo to NTS cross the Coast Ranges, the Great Valley, and the Sierra Nevada transverse to their trends. Only a few recording stations from these shotpoints were located east of the Sierra Nevada. These profiles were especially difficult to interpret because of the poorly known influence of the thick sediments in the Great Valley and because of the structural complexity of the features that the profiles cross. If the thickness and velocity of the sediments were known, the traveltimes of the arrivals at stations in the Great Valley could be corrected. By using the map of central California showing thickness of sedimentary rocks in the Great Valley after C. A. Repenning (Hackel, 1966) and a graph for traveltime delays in sediments published by Eaton (1963, fig. 4), the records of the stations in the Great Valley were shifted in the record sections with respect to the time axis to make approximate corrections. Both the uncorrected (a) and the corrected (b) record sections are shown in figures 72 and 73 (pl. 2). Tables 100 and 101 present the corresponding data, and table 108 lists the corrections made. The uncertainties involved in such a correction were discussed in detail by Eaton (1963). On the west side of the Great Valley, where the sediments reach a thickness of 10 km or even more, the station corrections may be large. The interpretation is further complicated because the profiles cross the granitic basement west of and the Franciscan basement east of the San Andreas fault zone. Therefore it is not possible confidently to define basement velocities from these profiles.

Nevertheless, the transition zone between crust and mantle seems to be fairly well defined by curve *c*. Curve *d* can be well correlated up to 220 km on the profile from San Luis Obispo to NTS, but it is not clearly established in the first part of the profile from San Francisco to Fallon. P_n arrivals can be correlated at distances beyond 270 km where they are delayed 1.2 and 2.7 seconds with respect to curve *d* on the first part of these profiles. This suggests a sharply thickening crust under the foothills of the Sierra Nevada.

The velocity-depth functions (tables 46, 47; figs. 12 and 45, pl. 3) give average crustal models for the Coast Ranges in central California that agree with that obtained for the line from San Francisco to Santa Monica Bay. These results also agree with the model obtained by Eaton (1963, 1966) for the profile from San Francisco to Fallon. Eaton also made a preliminary analysis of the profile from San Luis Obispo to NTS and proposed a slightly thicker crust under San Luis Obispo than under San Francisco.

COLORADO PLATEAU

The network of profiles recorded in 1961–63 in the Basin and Range province, Sierra Nevada, and Coast Ranges of California is fairly dense, but only a few profiles were recorded in the Colorado Plateau and the Middle Rocky Mountains. The Colorado Plateau is bounded by the Basin and Range province on the south and west, the Middle Rocky Mountains on the north, and the Southern Rocky Mountains on the east. It is a region of large plateaus, escarpments, and canyons; the plateaus reach heights of 3,000–3,600 m. The characteristic structures are broad uplifts and intervening basins. Wide areas of nearly flat-lying rocks are separated by abrupt monoclinal flexures. Several clusters of laccolithic intrusions form mountain ranges in Utah. Volcanic fields are present around the periphery of the Colorado Plateau. The Colorado Plateau can be regarded as stable compared with the complex deformational features of the adjacent provinces, but it has been tectonically active compared with the great stable shield areas (Eardley, 1962; King, 1959).

A reversed seismic-refraction profile was recorded in the central part of the Colorado Plateau between Hanksville, Utah, and Chinle, Ariz. The distance between the shotpoints is 296.2 km. No recording site was occupied south of Chinle, but six sites were installed north of Hanksville to distances of 50 km from

TABLE 46.—*Velocity-depth function of the profile from San Francisco(1) to Fallon(9)*

Curve	Distance, Δ (km)	Traveltime, T (s)	Velocity, V (km/s)	Depth, z (km)	Gradient, dV/dz (km/s/km)
a	0	0	4.98	0	
	30	5.50	5.73	2.8	
	60	10.55	6.19	7.5	
	90	15.39	6.22	8.5	
	110	18.59	6.31	11.3	
	90	15.48	6.55	14.2	
	50	9.51	6.80	14.3	
	90	15.35	6.90	15.5	
	120	19.68	6.97	17.4	
	150	23.96	7.05	19.8	
c	170	26.78	7.12	22.2	
	40	9.41	7.87	22.9	
d	70	13.20	7.95	23.2	
	90	15.71	8.00	24.0	

z = 23.6 km: $\bar{u}$ = 6.30 km/s, $\bar{w}$ = 6.44 km/s.

TABLE 47.—*Velocity-depth function of the profile from San Luis Obispo(3) to NTS(19)*

Curve	Distance, Δ (km)	Traveltime, T (s)	Velocity, V (km/s)	Depth, z (km)	Gradient, dV/dz (km/s/km)
a	0	0	3.57	0	
	30	6.01	5.89	5.1	
	60	10.99	6.13	7.7	
	90	15.78	6.39	12.0	
	110	18.90	6.41	12.6	
c	60	13.12	7.70	24.6	5.00
	70	14.43	7.28	24.5	5.00
	80	15.80	7.04	24.2	2.00
	100	18.71	6.75	24.0	.20
	120	21.72	6.60	22.8	.05
	140	24.78	6.52	19.2	.01
	160	27.85	6.50	17.0	.005
d	100	18.18	7.96	25.7	.04
	120	20.70	8.00	27.1	.027
	210	30.56	8.10	34.8	.015

z = 24.6 km: $\bar{u}$ = 5.90 km/s, $\bar{w}$ = 5.92 km/s.

Hanksville and 358 km from Chinle. The line crosses the eastward extension of the profile from NTS to Navajo Lake about 80 km south of Hanksville and 195 km east of Navajo Lake. The shotpoints of Hanksville and Chinle were both located in structural basins. The recording line crosses the east flank of the intrusive Henry Mountains, the Monument uplift, and the Comb monocline south of the Colorado River. A detailed description and interpretation of this survey was published by Roller (1965). In addition to the line, an extensive survey between Hanksville and Chinle was carried out in 1964 in central Arizona. Two profiles in the 1964 survey were located in the southern part of the Colorado Plateau (position of shotpoints is shown in fig. 82). These seismic-refraction measurements were analyzed in detail by Warren (1969). In this report, only the 1963 survey is discussed in detail.

The record sections of the two profiles to 100 km (figs. 74 and 75, pl. 2; tables 102, 103) permit correlation only of curve *a*. The delays of the first arrivals on the profile from Hanksville to Chinle between 10 and 50 km were caused by low-velocity sedimentary rocks in the basin in which the stations were located.

Increasing depth of the top of the Chinle Formation (Triassic) to about 1 km below the surface in the area south of Hanksville is indicated by the Tectonic Map of the United States (Cohee, 1962). The Basement Rock Map of the United States (Bailey and Muehlberger, 1968) shows a depth to Precambrian basement in this area of as much as 3 km. The first arrivals forming curve *a* on the reverse profile from Chinle to Hanksville confirm that the basement is shallower near Chinle, as indicated by the cited maps. Early first arrivals on this profile at distances of 100–160 km can be combined to form a cusp with the first arrivals at shorter distances and some fairly strong later arrivals, yielding a rapid velocity increase from 6.1 to 6.3 km/s at a depth of 6–7 km. Such first arrivals beyond 100 km were not found on the profile extending south from Hanksville. On this profile, first arrivals at distances of 110–170 km were delayed with respect to curve *a*, probably because the stations were located in large structural basins (Roller, 1965). Phase *a–b* can be identified on the profiles from both Chinle and Hanksville up to 180 km. This phase can be correlated with well-defined arrivals at distances of 280–300 km on the profile from Hanksville to Chinle. Curve *b* can be correlated on both profiles at distances beyond 110 km. Some arrivals at smaller distances suggest that curve *b* may be traced backward toward the shotpoints to distances of less than 110 km. Curve *c* is defined by clear secondary arrivals beyond 110 km. The fact that the curve *d* is tangent to curve *c* at a distance of 140–150 km indicates that the part of curve *c* nearest the shotpoint has to be interpreted as a reflected phase. This reflected phase seems to be recognizable beyond a distance of 60–70 km. Curve *d* is well determined by first arrivals at distances beyond 220 km. The apparent velocity of the P_n phase defined by this curve is 7.6 km/s up to a distance of 300 km and increases to 7.8 km/s north of Hanksville.

Curve *d* crosses the distance axis at a distance of 210 km. This is a large distance compared with the corresponding crossover distances on the profiles in the Basin and Range province and is in agreement with the position of the P_n curve on a profile recorded southeast from Sunrise, Ariz., 45 km south of Chinle (Warren, 1969). Several phases can be recognized at distances beyond 210 km. These arrivals, however, are scattered, which complicates the correlation of the different phases. This is especially true for the profile from Chinle to Hanksville. Some of the secondary arrivals may belong to a traveltime curve that is parallel to

curve *d* (see for example Prodehl, 1965). Curve *c* seems to be the most reliable correlation, whereas the extension of curves *b* and *a-b* on the profile from Hanksville beyond the intersection with curve *c* is not clear.

Tables 48 and 49 show the calculated velocity-depth relations, and figure 76 (pl. 3) shows the velocity-depth functions and the resulting crustal cross section for the Hanksville-Chinle profile. The velocity gradient at 25-29 km depth derived from curve *b* is large. The velocity increases from 6.4-6.5 km/s to 6.65-6.75 km/s within a small depth range that corresponds to the intermediate boundary found by Roller (1965) at a slightly greater depth. This zone dips downward from south to north, also in agreement with Roller's result. However, the velocity increase is not very large, and the velocity difference of 0.2 km/s between neighboring lines of equal velocity does not permit recognition of this zone in the crustal cross section of figure 76. At depths greater than 31-35 km, the velocity increases gradually from about 6.8 to about 7.6 km/s at the base of the crust at a depth of 42-43 km. As shown by Roller, the transition zone between crust and mantle (indicated by merging velocity lines in fig. 76) dips downward from north to south, revealing that the thickness of the crust as a whole as well as the lower part of the crust increases toward the south. A similar crustal model was proposed by Warren (1969) for the southern part of the Colorado Plateau on the basis of his interpretation of the profile between Sunrise and the Tonto Forest Seismological Observatory near Payson, Ariz.

TABLE 48.—*Velocity-depth function of the profile from Hanksville(30) to Chinle(31)*

Curve	Distance, Δ (km)	Traveltime, *T* (s)	Velocity, *V* (km/s)	Depth, *z* (km)	Gradient, *dV/dz* (km/s/km)
a	0	0	4.90	0	
	20	3.70	5.82	2.4	
	40	7.06	6.03	4.0	
	60	10.35	6.08	4.9	
	80	13.63	6.11	5.9	
a-b	140	24.29	6.48	23.1	0.15
	160	27.39	6.41	22.4	.07
	200	33.60	6.30	20.5	.04
	240	39.94	6.22	17.1	.04
	280	46.45	6.17	15.7	.01
b	130	23.34	6.75	29.1	.50
	140	24.82	6.71	28.9	.20
	160	27.84	6.60	28.2	.10
	200	33.90	6.53	27.0	.028
	240	40.05	6.50	25.2	.01
c	140	25.81	7.60	42.0	.50
	160	28.50	7.35	41.5	.25
	180	31.18	7.17	40.5	.15
	200	33.98	7.03	39.2	.075
	220	36.84	6.93	37.4	.04
	260	42.66	6.82	34.3	.02
	300	48.56	6.76	30.4	.01

z = 42.0 km: $\bar{u}$ = 6.31 km/s, $\bar{w}$ = 6.33 km/s.

TABLE 49.—*Velocity-depth function of the profile from Chinle(31) to Hanksville(30)*

Curve	Distance, Δ (km)	Traveltime, *T* (s)	Velocity, *V* (km/s)	Depth, *z* (km)	Gradient, *dV/dz* (km/s/km)
a	0	0	4.39	0	
	20	3.75	6.00	3.2	
	50	8.71	6.06	4.0	
	70	12.01	6.07	4.6	
	90	15.30	6.09	5.3	
	110	18.58	6.10	6.2	
	30	5.57	6.24	6.5	
	70	11.93	6.29	7.1	
	110	18.28	6.30	7.7	
	150	24.63	6.305	8.3	
a-b	160	26.73	6.33	14.4	0.01
b	130	23.08	6.64	27.4	>5.00
	150	26.13	6.57	27.2	.15
	180	30.71	6.50	26.6	.075
	220	36.81	6.44	25.5	.03
	280	46.11	6.40	21.6	.005
c	160	28.24	7.60	43.3	.24
	170	29.55	7.41	42.5	.22
	180	30.93	7.27	41.8	.19
	200	33.74	7.08	40.8	.15
	220	36.59	6.97	39.7	.09
	240	39.47	6.89	38.4	.05
	280	45.31	6.80	35.2	.02

z = 43.3 km: $\bar{u}$ = 6.37 km/s, $\bar{w}$ = 6.44 km/s.

MIDDLE ROCKY MOUNTAINS

The Rocky Mountains face the Great Plains to the east and are divided into three major parts (King, 1959): the Northern Rocky Mountains extending from Idaho and western Montana into Canada, the Middle Rocky Mountains in Wyoming and adjacent states, and the Southern Rocky Mountains in Colorado and adjacent states (fig. 1). Only a few seismic-refraction lines have been recorded in the Rocky Mountains. The University of Wisconsin, in cooperation with other institutions, completed a detailed seismic-refraction survey in Montana in 1962 (Steinhart and Meyer, 1961; Pakiser and Steinhart, 1964). In 1963, a seismic-refraction line was recorded in the Middle Rocky Mountains between American Falls Reservoir (27) in Idaho and Flaming Gorge Reservoir (29) in Utah. Some seismic refraction surveys were carried out in the Southern Rocky Mountains and the adjacent Great Plains of Colorado in 1961, 1964, and 1965 (Jackson and others, 1963; Jackson and Pakiser, 1965; Healy and Warren, 1969; Prodehl and Pakiser, 1979). Furthermore, in 1972 a seismic refraction profile was recorded from Bingham, Utah, to the northeast, crossing the Basin and Range province and the Middle Rocky Mountains (Braile and others, 1974).

This report presents only the seismic-refraction line recorded in 1963 in the Middle Rocky Mountains between American Falls Reservoir in Idaho and Flaming Gorge Reservoir in Utah. The Middle Rocky Mountains in this area "consist of ranges of miogeosynclinal Paleozoic and Mesozoic sediments which have been thrown down into closely packed folds and thrust slices without exposing any Precambrian basement.

Their structures trend *** northeastward into Idaho and Montana and southward into the Wasatch and other ranges of Utah***" (King, 1959).

The recording line extends from the southeast edge of the Snake River Plain southeastward across the southeastern Idaho-western Wyoming overthrust belt (Rubey and Hubbert, 1959) and acrosss the southwestern part of the Green River Basin to the north flank of the Uinta Mountains (Willden, 1965). It is 336.6 km long, with an intermediate shotpoint at Bear Lake (28), 176.2 km northwest of Flaming Gorge Reservoir and 160.3 km southeast of American Falls Reservoir. Shots from the shotpoints at the ends of the line were recorded along the entire line (figs. 77 and 78, pl. 2; tables 104, 105), whereas the profiles from Bear Lake were recorded only to a distance of 150 km toward the northwest (fig. 79, pl. 2; table 106) and to a distance of 115 km toward the southeast (fig. 80, pl. 2; table 107). The recording length of not more than 150 km was too short to obtain any reliable information about the base of the crust and the upper mantle. Willden (1965) first interpreted these profiles.

The shotpoint at Flaming Gorge Reservoir and the two stations nearest to it were located on the northeast slope of the Uinta Mountains over Permian rocks (Hansen, 1965). Seismic stations were located in the Green River Basin at distances up to 100 km from Flaming Gorge Reservoir. The Precambrian surface there is more than 8,000 m below the surface (Bradley, 1964; Bailey and Muehlberger, 1968). The thick section of sedimentary rocks in the Green River Basin accounts for the delays of curve *a* on the profile from Flaming Gorge (fig. 78) and of curve *d* at distances greater than 220 km on the reverse profile from American Falls (fig. 77).

In addition to the first arrivals, secondary arrivals on all four profiles can be correlated by curves *a–b* and *b*. These curves are interpreted as retrograde curves similar to those on other profiles. On the profile from Flaming Gorge to American Falls (fig. 78), curve *a–b* forms a cusp with curve *a*, and this relation may also be true for the reverse profile from American Falls (fig. 77). The cusping does not seem to be the case for the profiles from Bear Lake, however (fig. 79–80). Curves *c* and *d* can only be identified on the profiles from American Falls and Flaming Gorge at distances beyond 115 km. Phase *c* is prominent between 110 and 220 km, but the correlation on this phase becomes questionable at greater distances. Curve *d* is well defined on recordings from both American Falls and Flaming Gorge. On the profile from American Falls (fig. 77), there is evidence for a traveltime curve that is parallel to curve *d*. This phase is similar to a phase found on the profiles in the Colorado Plateau. The average velocity measured on curve *d* is about 8.05 km/s from American Falls and 7.95 km/s from Flaming Gorge, indicating that the upper mantle velocity is 8.0 km/s.

The corresponding velocity-depth functions (tables 50–53) and the resulting crustal cross section (fig. 81, pl. 3) show that the basement under the Green River Basin is more than 8 km below the surface. The top of the Chinle Formation (Triassic) is approximately 4 km below the surface, according to the Tectonic Map of the United States (Cohee, 1962). The basement dips northwest near the American Falls shotpoint, in accord with the northwest dip of the Tertiary rocks that

TABLE 50.—*Velocity-depth function of the profile from American Falls Reservoir(27) to Flaming Gorge Reservoir(29)*

Curve	Distance, Δ (km)	Traveltime, T (s)	Velocity, V (km/s)	Depth, z (km)	Gradient, dV/dz (km/s/km)
a	0	0	5.00	0	
	30	5.61	5.57	2.5	
	60	10.86	5.85	6.1	
	90	15.90	6.01	9.1	
	120	20.87	6.05	10.5	
a–b	80	15.15	6.48	18.4	1.00
	110	19.82	6.33	17.6	.04
	140	24.59	6.27	15.8	.01
b	100	18.78	6.80	25.2	.35
	120	21.75	6.66	24.2	.06
	140	24.77	6.56	19.5	.01
c	140	25.66	8.00	45.2	.40
	150	26.91	7.81	44.7	.40
	170	29.53	7.56	43.8	.20
	190	32.21	7.33	42.4	.125
	210	34.97	7.12	40.6	.09
	230	37.83	6.97	38.4	.05
	250	40.74	6.89	36.5	.03
	270	43.65	6.85	34.3	.02
	300	48.02	6.83	33.0	.01

z = 45.2 km: $\bar{u}$ = 6.41 km/s, $\bar{w}$ = 6.49 km/s; z = 25.2 km: $\bar{u}$ = 5.98 km/s, $\bar{w}$ = 5.96 km/s, V = 5.8 km/s for z = 18.5–19.4 km.

TABLE 51.—*Velocity-depth function of the profile from Flaming Gorge Reservoir(29) to American Falls Reservoir(27)*

Curve	Distance, Δ (km)	Traveltime, T (s)	Velocity, V (km/s)	Depth, z (km)	Gradient, dV/dz (km/s/km)
a	0	0	4.16	0	
	30	6.49	5.45	5.2	
	60	11.54	6.12	9.8	
	90	16.38	6.21	11.5	
a–b	130	22.82	6.25	13.2	
	50	10.23	6.49	14.2	
	90	16.38	6.52	14.7	
	130	22.52	6.57	17.1	
	150	25.54	6.62	18.9	
b	110	20.46	6.80	24.6	0.075
	130	23.45	6.64	19.7	.01
c	130	23.96	7.94	41.0	.30
	150	26.52	7.48	39.3	.20
	170	29.26	7.16	37.6	.15
	190	32.14	6.97	36.3	.10
	210	35.03	6.90	35.2	.045
	240	39.40	6.85	33.4	.024
	280	45.27	6.82	31.4	.01

z = 41.0 km: $\bar{u}$ = 6.30 km/s, $\bar{w}$ = 6.41 km/s; z = 24.6 km: $\bar{u}$ = 5.85 km/s, $\bar{w}$ = 5.89 km/s.

TABLE 52.—*Velocity-depth function of the profile from Bear Lake(28) to American Falls Reservoir(27)*

Curve	Distance, Δ (km)	Traveltime, T (s)	Velocity, V (km/s)	Depth, z (km)	Gradient, dV/dz (km/s/km)
a	0	0	4.25	0	
	10	2.17	5.05	1.2	
	30	5.64	5.98	4.4	
	50	8.96	6.05	5.4	
a-b	70	13.23	6.40	15.8	1.00
	90	16.37	6.34	15.3	.05
	110	19.54	6.26	13.1	.01
b	90	16.95	6.62	21.4	.30
	110	19.99	6.51	20.9	.075
	120	21.53	6.43	19.3	.03

z = 21.4 km: $\bar{u}$ = 5.97 km/s, $\bar{w}$ = 5.88 km/s, V = 5.8 km/s for z = 15.9-19.2 km.

TABLE 53.—*Velocity-depth function of the profile from Bear Lake(28) to Flaming Gorge Reservoir(29)*

Curve	Distance, Δ (km)	Traveltime, T (s)	Velocity, V (km/s)	Depth, z (km)	Gradient, dV/dz (km/s/km)
a	0	0	4.41	0	
	20	3.90	5.73	2.9	
	30	5.60	5.96	4.0	
a-b	70	12.93	6.34	14.2	1.00
	80	14.51	6.28	14.0	.20
	100	17.71	6.23	13.1	.025
	110	19.31	6.22	12.6	.015
b	60	12.47	6.86	18.8	1.00
	80	15.42	6.71	18.3	.05
	110	19.92	6.64	16.8	.01

z = 18.8 km: $\bar{u}$ = 5.96 km/s, $\bar{w}$ = 5.88 km/s, V = 5.8 km/s for z = 14.3-16.7 km.

are exposed southeast of the reservoir (Carr and Trimble, 1963).

The base of the crust in this area is at a depth of more than 40 km, dipping from about 41 km under the Green River Basin to about 45 km under the Middle Rocky Mountains and a wedge of the Basin and Range province northwest of Bear Lake. According to traveltime curves a-b and b, there are two depth ranges within the crust where the velocity gradient is relatively large, increasing downward by about 0.2 km/s/km. The zone corresponding to phase a-b dips from 13 km near Flaming Gorge to 18 km near American Falls, whereas the zone corresponding to phase b is located at about 25 km depth at both ends of the line, rising to 14-16 km under the Middle Rocky Mountains near Bear Lake. A zone with a velocity inversion must be assumed between zones a-b and b to satisfy the comparison of the average velocities $\bar{u}$ and $\bar{W}$ (tables 50, 52, 53). This zone of velocity inversion, in which the velocity decreases from 6.3-6.5 km/s to 5.8 km/s (average value), is evident on the profiles from Bear Lake, but it is probably not present near Flaming Gorge. It is thin in the vicinity of American Falls. The velocity inversion on the profile from American Falls is based only on curve b; the velocity comparison based on curve c indicates that no inversion is present. The assumed velocity of 5.8 km/s in the velocity-inversion zone is an average value. The details of the velocity-depth function within this zone cannot be determined.

The profile from Bingham, Utah, to the northeast crosses the line from American Falls Reservoir to Flaming Gorge Reservoir close to Bear Lake. The crustal structure obtained by Braile, Smith, Keller, Welch, and Meyer (1974) for the profile from Bingham at the intersection of both lines is in good agreement with the structure beneath Bear Lake as shown in figure 81.

RESULTS AND DISCUSSION

BASIC DATA

The record sections of the profiles recorded by the U.S. Geological Survey from 1961 to 1963 and of a profile published by Diment, Stewart, and Roller (1961) (fig. 38) in the area of investigation show that the traveltime curves fit into a basic traveltime diagram (fig. 5). In addition to curves a and d, which are based on first arrivals, a strong phase c is the most evident feature in nearly all record sections.

Because phases corresponding to curves a, c, and d exist on all profiles within the area of investigation, we should look for parameters that use these curves to give objective information on the general features of crustal structure before determining detailed velocity-depth relations. In the Alps and western Germany, Choudhury, Giese, and de Visintini (1971), Giese (1970), and Giese and Stein (1971) successfully mapped typical parameters from the basic traveltime diagrams (see also Giese and others, 1976).

The distance Δ_d at which the traveltime curve d (P_n) crosses the distance axis is one parameter that does not contain subjective elements of interpretation. Other objective parameters are the so-called "critical" distance Δ_c at which curve d is tangent to curve c, and the corresponding reduced traveltime $\overline{T}_c = T_c - \Delta_c/6$. These parameters were mapped for the area of investigation. Δ_d and Δ_c were plotted at half their values (figs. 82, 83). To a first approximation, both maps represent the variation of total crustal thickness. Under the Basin and Range province, the crust is thinner than under the surrounding provinces to the west, north, and east, and it is evident that crustal thickness decreases south of the line from China Lake to Lake Mead. The inclusion of the P_n data from a 1964 crustal study in Arizona (Warren, 1969) in the contour map of the crossover distance Δ_d confirms that the crust thickens from the Basin and Range province eastward into the Colorado Plateau. The P_n traveltime curve for

the eastern Basin and Range province (Berg and others, 1960) was also included in the map of Δ_d, providing evidence that the crustal thickness minimum under central Nevada extends into northwestern Utah. Both Δ_c and Δ_d maps indicate a thick crust under the Middle Rocky Mountains, the Colorado Plateau, and the Sierra Nevada, whereas the thickening of the crust under the Snake River Plain is shown by the map of the "critical" distance Δ_c only, because no P_n arrivals were found here. The thick crust under the Sierra Nevada is not restricted to the Sierra Nevada but also extends eastward into the ranges east of Owens Valley and southward into the Transverse Ranges north of Los Angeles. Additional data for the Coast Ranges of central California were made available by S.W. Stewart (1968a; written commun., 1969) for inclusion in the map of the crossover distance Δ_d. In the Coast Ranges a thin crust that thins from east to west is indicated.

The reduced traveltime $\overline{T}_c$ at the critical distance was corrected by using the reduced P_g traveltime to eliminate the traveltime delays caused by sedimentary layers. The resulting time difference, $\overline{T}_c - \overline{T}_{a,c}$, was plotted at the distance $\Delta_c/2$ (fig. 84). Large values indicate that the crust contains material of relatively low P-wave velocities, that the crust is relatively thick, or both. The map shows two maximums, one in central Nevada near Eureka and the other extending across southern Nevada into the southern Sierra Nevada and toward the Transverse Ranges of California. Small values of $\overline{T}_c - \overline{T}_{a,c}$ were found on the profiles in the Middle Rocky Mountains, the Colorado Plateau, and the Coast Ranges of central California. Comparison of this map with the results of the analysis of the seismic-refraction profiles leads to the conclusion that large values of $\overline{T}_c - \overline{T}_{a,c}$ are characteristic of areas of relatively low crustal P-wave velocities and relatively thin crust. The low-velocity zone found under the Middle Rocky Mountains (fig. 81), however, is not indicated in the contour map of $\overline{T}_c - \overline{T}_{a,c}$. This is probably because values $\overline{T}_c - \overline{T}_{a,c}$ were available in this area only for the profiles from the shotpoints of American Falls and Flaming Gorge, where evidence for a velocity inversion was weak or lacking. Because of the lack of data, no conclusions can be drawn concerning the low-velocity zone under the southern Cascade Mountains.

The contour map of average P_n velocity (fig. 85; table 54) is based on curve d. The velocity gradient in the upper mantle is very small because curve d is a nearly straight line on most traveltime curves. The resulting velocity values are strongly influenced by horizontal velocity gradients and also by dip on the M-discontinuity. To obtain approximately true velocities, therefore, an average value of the velocity from curve d was used for reversed profiles and plotted at the middle of the corresponding two shotpoints. However, in unreversed profiles, and in profiles for which the subsurface refracted path along the M-discontinuity was not reversed, some effects of variations in dip of the M-discontinuity probably remain.

The P_n velocities found for the Western United States are generally less than 8.0 km/s, ranging between 7.6 and 7.9 km/s. Only beneath the Coast Ranges of California, in southern California, and in the Middle Rocky Mountains were P_n velocities of 8 km/s and higher obtained. The lowest P_n velocity (7.6 km/s) was found in Utah. The 7.6 km/s contour extends across the eastern part of the Great Basin into the Colorado Plateau. The low velocity found on the unreversed profile from Delta to SHOAL (table 54) is supported to some extend by the profile from SHOAL to Delta (fig. 86), for which Eaton, Healy, Jackson, and Pakiser (1964) reported apparent velocities for first arrivals of 8.1 km/s between 240 and 410 km and 7.6 km/s between 410 and 547 km, suggesting that the true velocity west of Delta (16) may not exceed 7.6 km/s. The variations of apparent velocity along this profile, however, clearly indicate variations in dip of the M-discontinuity. Berg, Cook, Narans, and Dolan (1960) reported a velocity of 7.6 km/s from unreversed traveltime data in the eastern part of the Basin and Range province. No subcrustal velocity can be given for the Snake River Plain because of the lack of P_n arrivals on the corresponding profiles. Recordings in the Snake River Plain from nuclear explosions at NTS, however, suggest that the P_n velocity in the Snake River Plain is about 7.9 km/s (Hill and Pakiser, 1966, 1967).

CRUSTAL STRUCTURE

The results of the velocity-depth determinations along 15 lines were compiled in a fence diagram (fig. 87, pl. 1). For a clearer presentation, the cross section based on the profile extending northwest from China Lake (fig. 61) was omitted. The fence diagram was constructed to be viewed from the southwest, approximately parallel to a line from Los Angeles to Salt Lake City. The diagram shows lines of equal velocity with a contour interval of 0.2 km/s. The equal-velocity contours are dashed in areas where velocity data were estimated because of lack of observations, for example in the Great Valley of California, the western flank of the Sierra Nevada, and the line from NTS through Navajo Lake to Colorado (see figs. 12, 45, 63).

A distinct lower crustal layer or zone is present under the northern part of the Basin and Range province (see also figs. 12, 25); velocity increases from 6.4-6.6 to 7.0 km/s in a narrow depth range between

the upper and lower crustal zones. This transition zone from upper to lower crust was not found under the southern part of the Basin and Range province (see also figs. 25, 36–40, 45). In the southern part of the province, low *P*-wave velocities are found in the upper 20 km of the crust. Near Lake Mead and NTS, material with *P*-wave velocities of 6.0–6.1 km/s seems to exist at even greater depths.

Under the Sierra Nevada (central part of the line between Shasta Lake and China Lake) and east of Mono Lake (see also figs. 12, 36, 50, 61–63), the velocity increases steadily with increasing depth between 10 and 35 km from 6.2 to 6.6 km/s. Near China Lake, however, the velocity distribution is different; low-velocity material (6.1 km/s) extends to depths of 20 km, and the base of the crust rises from 42 km at Mono Lake to 33 km depth at China Lake. Toward Shasta Lake in the southern Cascade Mountains, the 6.4-km/s velocity contour rises to about a depth of 7 km, and it is underlain by a velocity inversion in which the velocity decreases to 6.0 km/s (see also fig. 50).

Under the Coast Ranges west of the San Andreas fault system in central California, the crust is only 24–25 km thick and has uniform velocity increase with depth from 6.2 to 6.8 km/s between depths of 10 and 25 km. The velocity increases at the base of the crust from 6.8 to 8.0 km/s within a depth range of only 2–3 km (see also fig. 68).

A fairly uniform velocity increase with depth was also found under the Colorado Plateau. The velocity increases smoothly from 6.1–6.2 to 6.7–6.8 km/s between depths of 7 and 33 km, and the base of the crust is at a depth of 42–43 km (see also fig. 76).

Under the western Snake River Plain, a distinct lower crust with velocities of 6.8–7.0 km/s extends from 11–17 km to a depth of about 35 km (see also fig. 25). Under the Middle Rockly Mountains, velocities of 6.8–7.0 km/s were also found between depths of 20 and 40 km, indicating a distinct and rather homogeneous lower crust that in its lower part joins the transition zone between crust and mantle. In the upper crust of the Middle Rocky Mountains, a narrow velocity inversion zone in which velocity decreases with depth from 6.4 to 5.8 km/s was found at a depth of about 17 km (see also fig. 81).

The base of the crust as interpreted by the conventions discussed above is generally not a sharp discontinuity but rather a transition zone, the thickness of which varies between 2 and 10 km and in which the velocity increases gradually from 6.6–7.0 km/s to about 7.8 km/s. This transition zone is about 10 km thick under the Sierra Nevada, the Middle Rocky Mountains, and the Colorado Plateau and is relatively

TABLE 54.—*Average* Pn velocities, based on curve d, and velocities v (Δ_c) at the depth z (Δ_c)

Profile	Average P_n velocity (Curve *d*) (km/s)	Velocity v (Δ_c) (km/s)
Delta(16) to SHOAL(10)	7.3–7.8	7.24
Eureka(15) to Fallon(9)	7.9	7.86
Fallon(9) to Eureka(15)	7.7	7.68
Boise(11) to Elko(14)		7.55
Strike(12) to Elko(14)		7.77
Mountain City(13) to Boise(11)		7.91
Mountain City(13) to Eureka(15)	7.6–8.0	7.48
Elko(14) to Boise(11)	(7.9)	7.75
Elko(14) to Eureka(15)		7.74
Eureka(15) to Mountain City(13)	7.9	7.90
Eureka(15) to Lake Mead(22)	7.9–8.0	7.80
Lake Mead(22) to Eureka(15)	7.6–8.1	7.50
Lake Mead(22) to Mono Lake(6)	7.7–7.9	7.61
Lake Mead(22) to Santa Monica Bay(4)	8.0–8.1	7.90
NTS(19) to Kingman(26)	8.0	7.57
Kingman(26) to NTS(19)	7.6–7.9	7.34
NTS(19) to Ludlow(25)	8.2	7.80
Ludlow(25) to NTS(19)	7.9	7.85
NTS(19) to Navajo Lake(21)	7.7	7.70
Navajo Lake(21) to NTS(19)	7.9	7.80
NTS(19) to Elko(14)	7.6 ($\Delta < 290$ km)	7.60
	8.0 ($\Delta > 290$ km)	
NTS(19) to San Luis Obispo(3)	8.0 ($\Delta > 260$ km)	7.65
Ludlow(25) to Mojave(23)	8.1–8.25	7.80
Barstow(24) to Ludlow(25)	8.25	8.00
Barstow(24) to Mojave(23)	(7.9)	7.80
Mojave(23) to Ludlow(25)	8.0	7.80
Shasta Lake(5) to Mono Lake(6)	7.9 ($\Delta > 210$ km)	7.54
Mono Lake(6) to Shasta Lake(5)	(7.9)	7.65
Mono Lake(6) to China Lake(8)		7.86
China Lake(8) to Mono Lake(6)	(7.8)	7.60
China Lake(8) to northwest		7.35
China Lake(8) to Santa Monica Bay(4)	7.9	7.84
Mono Lake(6) to Santa Monica Bay(4)		(6.98)
Fallon(9) to San Francisco(1)	7.7–7.8	7.90
Fallon(9) to Mono Lake(6)	7.5–7.6 ($\Delta > 290$ km)	7.60
Mono Lake(6) to Fallon(9)	8.5	7.90
Fallon(9) to China Lake(8)	7.6–7.8	7.90
Mono Lake(6) to Lake Mead(22)	8.0	7.70
San Francisco(1) to Camp Roberts(2)	8.0 ($\Delta > 190$ km)	7.78
Camp Roberts(2) to San Francisco(1)	7.9–8.1	7.80
Camp Roberts(2) to Santa Monica Bay(4)	7.9	7.70
Santa Monica Bay(4) to Camp Roberts(2)	8.3	8.00
Santa Monica Bay(4) to Mono Lake(6) / Santa Monica Bay(4) to China Lake(8)	8.0	8.00
Santa Monica Bay(4) to Lake Mead(22)	7.9–8.1	7.84
San Francisco(1) to Fallon(9)	(8.0) ($\Delta < 120$ km)	7.87
San Luis Obispo(3) to NTS(19)	7.8–8.2 ($\Delta < 220$ km)	7.70
Hanksville(30) to Chinle(31)	7.6	7.60
Chinle(31) to Hanksville(30)	7.6–7.8	7.60
American Falls Res(27) to Flaming Gorge Res(29)	8.05	8.00
Flaming Gorge Res(29) to American Falls Res(27)	7.95	7.94

Velocity increases with increasing distance.

FIGURES 82–84.—FIGURE 82, Crossover distance Δ_d for California and Nevada and adjacent areas between $d(P_n)$ and $v = 6$ *km/s* (Δ-axis, see fig. 5). Contour interval is 20 km. Values shown by crosses are plotted at half the distance Δ_d from the corresponding shotpoint. Full circles, shotpoints according to figure 1 and table 1. Open squares, shotpoints of other seismic-refraction surveys, the P_n traveltime curves of which are included. To a first approximation the map represents the variation of total crustal thickness.

FIGURE 83, "Critical" distance Δ_c for California and Nevada and adjacent areas. Contour interval is 20 km. Values shown by crosses are plotted at half the distance Δ_c from the shotpoint. To a first approximation the map represents the variation of total crustal thickness.

FIGURE 84, Reduced traveltime $\overline{T}_c - \overline{T}_{a,c}$ in California and Nevada and adjacent areas. The reduced traveltime $\overline{T}_c$ of the wave group *c* at the "critical" distance Δ_c is corrected by the corresponding traveltime $\overline{T}_{a,c}$ of the wave group $a(P_g)$ at the same distance. The contour interval is 1 second. The values shown by crosses are plotted at half the critical distance Δ_c from the corresponding shotpoint. High values indicate that the medium of wave propagation contains material with relatively low *P*-wave velocities.

thin under the Basin and Range province, the western Snake River Plain, and the Coast Ranges of California (fig. 87). Most previous authors (for example, Pakiser, 1963) have interpreted the base of the crust (M-discontinuity) as a relatively sharp discontinuity.

The transition zone between crust and mantle is

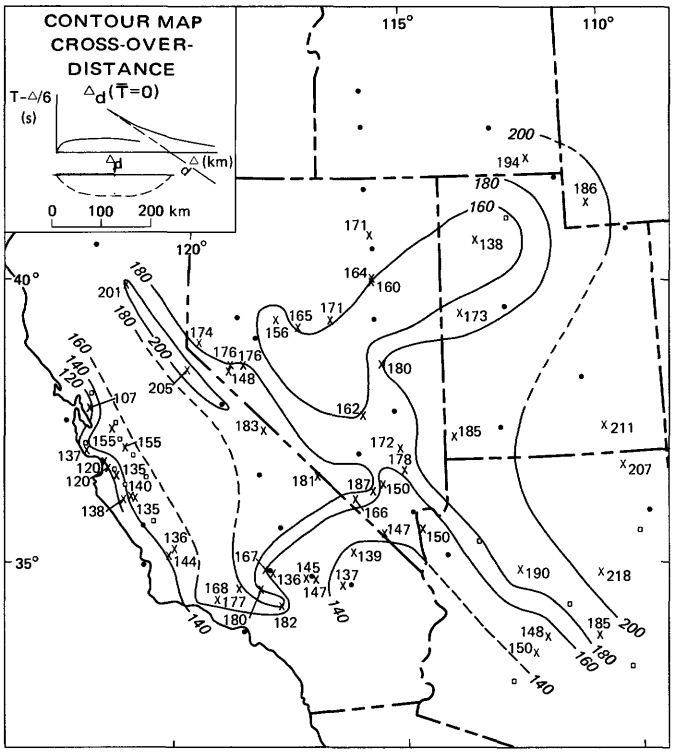

FIGURE 82

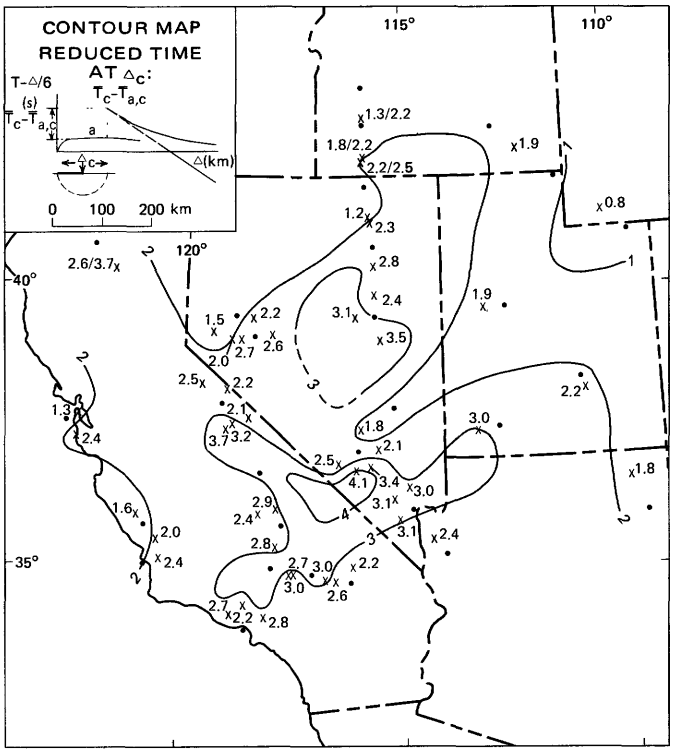

FIGURE 84

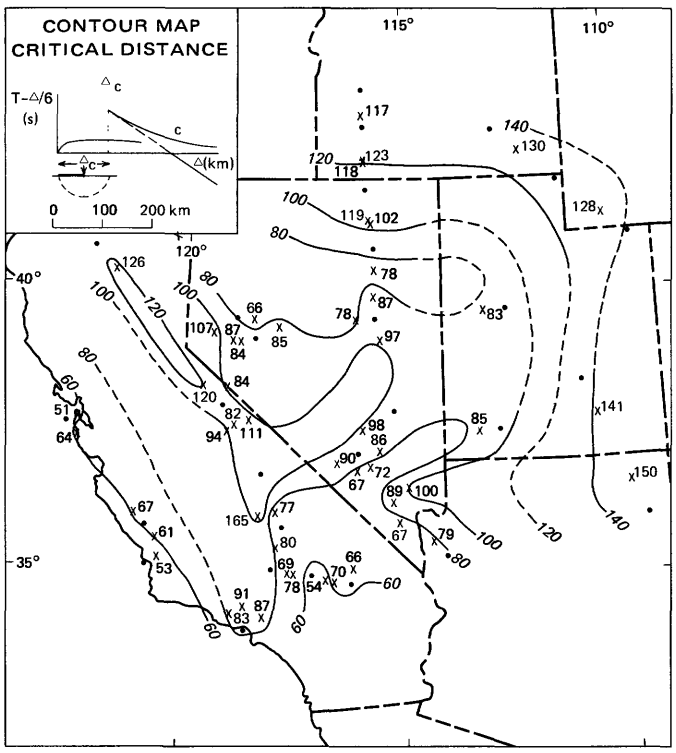

FIGURE 83

characterized by increasing velocities and increasing velocity gradients. The depth to the strongest velocity gradient is defined in this report as the base of the crust in drawing a contour map of crustal thickness. The uncertainty of the depth of the maximum velocity gradient in the crust-mantle transition zone is small (about 3-5 percent). Figure 88 shows the map of the depth of the strongest velocity gradient, $z(\Delta_c)$, for the area of investigation. It represents a contour map of the total crustal thickness. The dashed contour lines in the Great Valley and the western flank of the Sierra Nevada in California and the eastern Basin and Range province in Utah were based on very few data points and were extrapolated into areas not traversed by profiles.

The crust is generally thinner under the Basin and Range province than under the surrounding provinces, as is also suggested by the contour maps of the parameters Δ_d and Δ_c. The average thickness in the Basin and Range province is 32-34 km, with minimum thickness of 29-30 km near Fallon, Nev., and Delta, Utah. South of Eureka, Nev., the crust thickens to 37-38 km between Eureka and Navajo Lake. Farther south, the crust thins to 31-32 km near Hiko and in the area north and east of NTS, reaching a minimum thickness of 28 km between Kingman, Ariz., and Ludlow, Calif. As suggested by the contour maps of Δ_c and Δ_d, the crust is relatively thick east of the Sierra Nevada between Mono Lake and China Lake and thins southward to 29-31 km under the Mojave Desert.

Under the Sierra Nevada, the total crustal thickness is 42-43 km between Shasta Lake and Mono Lake, thinning toward the south to 33 km northwest of China Lake. Under the Transverse Ranges north of Los Angeles, a crustal thickness of 36-37 km was inferred, whereas the crust under the Coast Ranges of central California between San Luis Obispo and San Francisco is only 24-26 km thick.

From the Basin and Range province, the base of the crust dips downward to the east under the Colorado Plateau, where it reaches a depth of 42-43 km between Hanksville, Utah, and Chinle, Ariz. The crust is thick under the Middle Rockly Mountains, reaching a maximum thickness of 45 km between American Falls Reservoir and Bear Lake. The nature of the transition from the Basin and Range province to the Middle Rocky Mountains can only be suggested. According to an interpretation of Berg, Cook, Narans, and Dolan (1960), the top of a layer with a velocity of 7.59 km/s was found at a depth of 25 km in northwestern Utah. This layer is probably the same as that bounded by the base of the crust at a depth of 29 km west of Delta, Utah (figs. 12, 87, and 88). These results suggest that the crust is very thin under northwestern Utah and thickens abruptly toward the northeast under the Middle Rocky Mountains and adjacent provinces in Idaho and Wyoming. The interpretation of the profile from Bingham, Utah, to the northeast (Braile and others, 1974) confirms this suggestion.

The crust is 40-44 km thick under the Snake River Plain between Boise and Mountain City, with a probable maximum thickness south of Strike Reservoir. In addition to the depth at which the velocity gradient reaches its maximum value (fig. 88), the velocity $v(\Delta_c)$ corresponding to this depth was mapped (fig. 89 and right column of table 54). As the comparison of this map with the map of the P_n velocity (fig. 85) shows, the velocity $v(\Delta_c)$ cannot be identified with the velocity within the uppermost mantle. For some areas, significantly lower velocity values were compiled in figure 89 than in the contour map of the P_n velocity (fig. 85). These differences may be explained by a decreasing velocity gradient below the depth of strongest velocity gradient.

DISCUSSION

From published interpretations available a few years ago, Hamilton and Pakiser (1965) published a crustal cross section across the United States along the 37th parallel. Pakiser and Zietz (1965) published a cross section along a transcontinental aeromagnetic profile. As part of the Transcontinental Geophysical Survey of the U.S. Upper Mantle Project, Warren (1968a, b, c, d) reviewed and compiled more recent interpretations of seismic profiles in the United States between lats 35° and 39° N. in the form of a fence diagram. A two-layer crust convention with constant velocities within the layers was used for most of the profiles (see also Healy and Warren, 1969, figs. 1-4). The crustal thicknesses shown by Warren, with few exceptions, do not differ

FIGURES 85, and 88-90.—Average P_n velocity for California and Nevada and adjacent areas, based on curve *d* (see table 54). For the construction of the contour lines, for reversed profiles an average value was used, for profiles where the P_n velocity increases with increasing distance the lowest well-defined value was used.

FIGURE 88.—Total crustal thickness under California and Nevada and adjacent areas. The contour lines show the depth of strongest velocity gradient, $z(\Delta_c)$, in the transition zone between crust and mantle in the western United States. Contour interval is 2 km. Dashed contour lines indicate uncertain results. Values shown by crosses are plotted at half the critical distance from the corresponding shotpoint.

FIGURE 89.—Velocity $v(\Delta_c)$ at the depth of strongest velocity gradient $z(\Delta_c)$ in the crust-mantle transition zone. Values are plotted at half the critical distance from the corresponding shotpoint (see table 54).

FIGURE 90.—Bouguer gravity anomaly map of the area of investigation. Contour interval is 50 mgal. From the Bouguer gravity anomaly map of the United States (Am. Geophys. Union, 1964).

significantly from the results shown in figures 87 and 88.

The fact that no distinct lower crust was found under the southern Basin and Range province is compatible with the map of Pakiser and Zietz (1965, fig. 2) showing the variations in crustal thickness, mean crustal velocity, and upper mantle velocity. According to these authors, the mean crustal velocity is less than

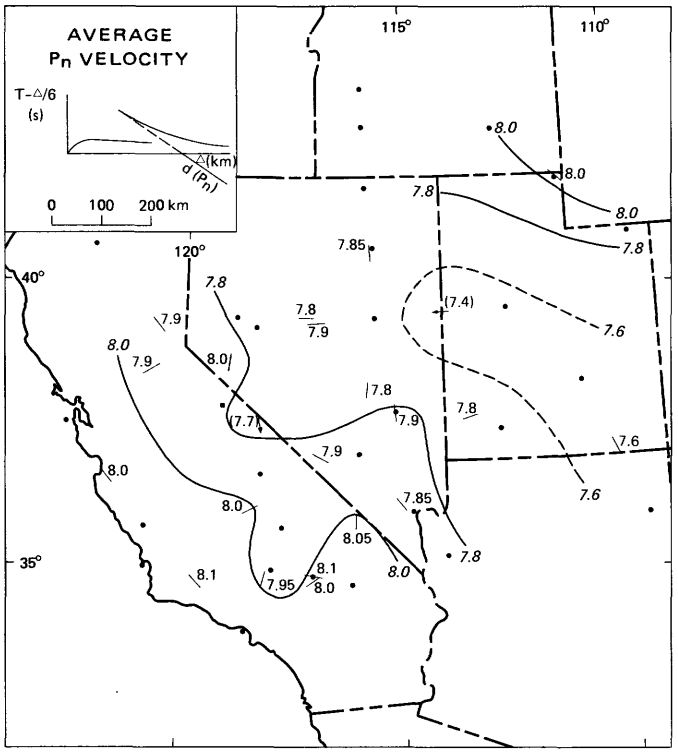

FIGURE 85

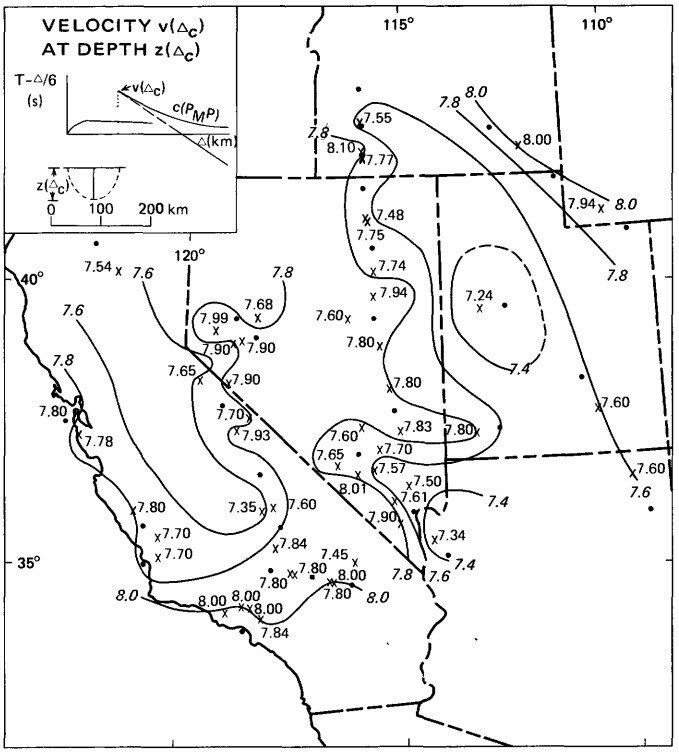

FIGURE 89

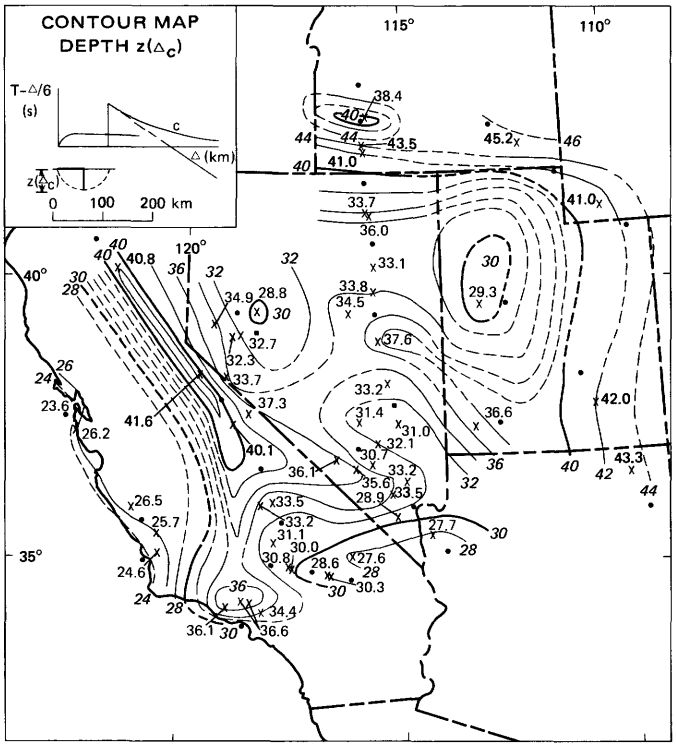

FIGURE 88

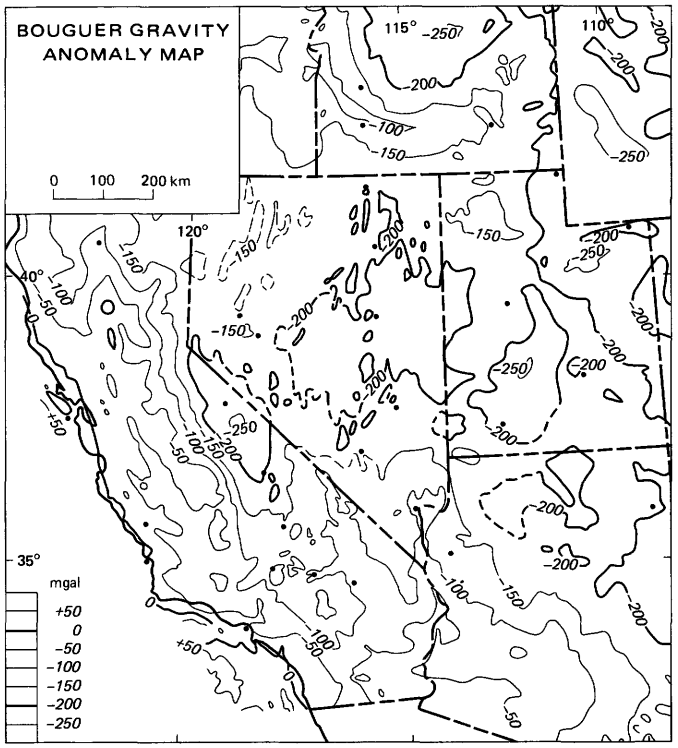

FIGURE 90

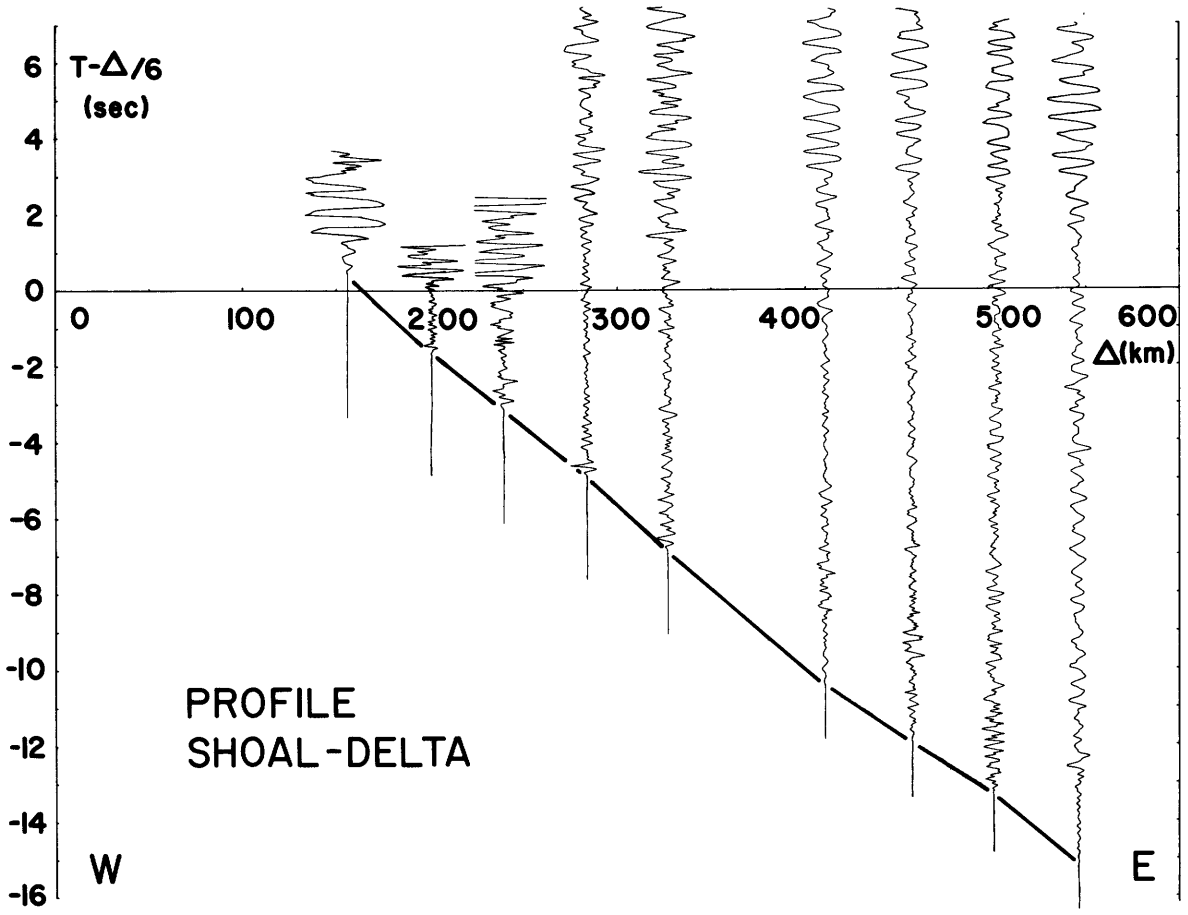

FIGURE 86.—Record section of the profile from SHOAL (10) to Delta (16).

6.2 km/s in the main part of the Basin and Range province, and this is consistent with the present interpretation. The increase in mean crustal velocity to 6.2-6.5 km/s shown by Pakiser and Zietz toward the north, east, and west of the central Basin and Range province is compatible with the presence of a distinct lower crust of higher average velocity under the northern part of the Basin and Range province and the nearly uniform velocity increase with depth under the Colorado Plateau and the Sierra Nevada. Under the Snake River Plain, the mean crustal velocity is greater than 6.5 km/s because of the shallow depth to the top of the lower crust.

Whereas the P_n velocity in most parts of the world is usually equal to or greater than 8.0 km/s (see for example Closs, 1969; Healy and Warren, 1969; Kosminskaya and others, 1969; Sollogub, 1969), the P_n velocity in the Western United States is less than 8.0 km/s in most areas, ranging between 7.6 and 7.9 km/s. Similar values have been reported for profiles in Japan and the Kuril Islands (Kosminskaya and Riznichenko, 1964; James and Steinhart, 1966; Research Group for Explosion Seismology, 1966). The P_n-velocity values reported here are in general agreement with those of previous investigations (Pakiser, 1963; Pakiser and Steinhart, 1964; Stuart and others, 1964; Pakiser and Zietz, 1965; James and Steinhart, 1966; Herrin, 1969), except for the higher velocity for the Mojave Desert in southern California reported here. The velocity of 8.0-8.1 km/s shown by Herrin (1969) for southern Utah was not confirmed by the results of interpretation of the lines from the NTS to Navajo Lake and Hanksville to Chinle, where apparent velocities of 7.7-7.9 and 7.6-7.8 km/s were found (table 54).

Some previous authors (for example, Berg and others, 1960) have suggested that the discontinuity at a depth of 24-25 km at which the velocity changes from less than 6.5 to about 7.6 km/s overlies a deeper discontinuity at which the velocity increases to more than 8 km/s. James and Steinhart (1966) noted that no such discontinuity has ever been reported for profiles wholly within the Basin and Range province. In comparing the record sections of all profiles investigated by the author, it can be seen that the traveltime curves *c* and *d* (fig. 5) are similar on all profiles throughout the Western United States; the distance to the point of cri-

tical reflection, Δ_c, (fig. 83) and the crossover distance, Δ_d, (fig. 82) increase or decrease as crustal thicknesss increases or decreases (fig. 88). The boundary zone derived from these curves and identified with the M-discontinuity seems to be well defined throughout the area of investigation (fig. 87).

Comparison of crustal structure with the Bouguer gravity map of the study area (fig. 90) shows a general agreement between crustal structure (fig. 87, 88) and Bouguer gravity for areas outside the Basin and Range province. The gravity high of the Coast Ranges of California corresponds to a thin crust. Gravity lows of the Colorado Plateau, the Middle Rocky Mountains, and the Sierra Nevada, including the area east of Owens Valley, correspond to a thick crust. The gravity highs under the Snake River Plain and the southern Cascade Mountains in the vicinity of Shasta Lake correspond to a thin upper and a thick lower crust with high *P*-wave velocities. The local gravity low in the Lassen Peak area of California interpreted by Pakiser (1964) is in agreement with the seismic low-velocity zone. The thinning of the crust in the southern Basin and Range province from north to south is expressed by increasing gravity. However, there does not generally seem to be a correlation between gravity and the thinning of the crust from the Sierra Nevada toward the Basin and Range province. The generally low gravity in the Basin and Range province is probably caused by lower density of the upper mantle in this area of P_n velocity less than 8 km/s and heat flow of 2 μcal/cm^2/s or more (Lee and Uyeda, 1965).

Johnson (1976) derived a velocity structure for *P* waves in the upper mantle under the Basin and Range province from $dT/d\Delta$ measurements from the array at the Tonto Forest Seismological Observatory in Arizona. Johnson's structure includes a low-velocity zone at a depth of 60–160 km in which the velocity decreases from 7.8–7.9 km/s to 7.6–7.7 km/s. Similar conclusions were reached by Green and Hales (1968) and Archambeau, Flinn, and Lambert (1969). The main part of the gravity low in the Basin and Range province obviously has its origin in a low-density upper mantle, although some of the anomalies can be explained as differences in crustal structure. Relative gravity highs near Fallon and in northwestern Utah can be associated with the fact that the crust is thinner in these places than it is along the line from Mountain City to Lake Mead. The fact that a dense lower crust is well defined north of Eureka and decreases in thickness and distinctness toward the south corresponds with a slight decrease in gravity from Eureka toward the south. The thick crust between Eureka and Navajo Lake and the decrease in crustal thickness toward the south is roughly in agreement with the gravity minimum in central Nevada and southwestern Utah and the general gravity increase toward the south. That some form of regional isostatic compensation exists within the Basin and Range province was suggested by Mabey (1960), who noted the correlation between low Bouguer anomaly values and high regional topography. These areas also coincide fairly well with the areas where a relatively thick crust is found.

From gravity data, Thompson and Talwani (1964) computed models of crustal structure from the Pacific Basin to central Nevada. The depth (about 22 km) that they find for the upper mantle under the Coast Ranges of California corresponds approximately to the results reported by Eaton (1963) and Healy (1963) and in this report. The depth of the upper mantle under the Sierra Nevada reported by Thompson and Talwani (maximum depth of 34 km), however, differs significantly from the depth determinations by seismic-refraction data (Eaton, 1963, 1966; Prodehl, 1970a, b; this report). Thompson and Talwani's depth to the upper mantle of 27–28 km east of the Sierra Nevada near Fallon, Nev., and the increasing crustal thickness east of Fallon correspond to the results in this report.

As the seismic-refraction results show, the thick crust under the Sierra Nevada is not restricted to the area of the Sierra Nevada but extends eastward from Owens Valley to the western part of the Basin and Range province. This fact underlines the statement (Bateman and others, 1963, p. D6) that "the eastern limit of the synclinorium" that is occupied by the Sierra Nevada batholith "is probably marked by a belt of Precambrian and Cambrian rocks that extends from the White Mountains (southeast of Mono Lake) southeastward into the Death Valley region***." Hunt and Mabey (1966) and Hall (1971) suggest that the Sierra Nevada batholith extends to the Panamint Range at the western edge of Death Valley. East of the southern part of the Owens Valley, however, the batholith "is broken into numerous large and small basin-and-range blocks***" (Hamilton and Myers, 1967, p. C25).

The present result for the Sierra Nevada obtained from the recording line from Shasta Lake to China Lake agrees with Eaton's (1966) result from the upper crust down to about 20 km. According to Hamilton and Myers (1967), the Sierra Nevada batholith extends no deeper than 10 km. They interpreted the underlying high-velocity (6.4 km/s) rocks as metasomatized schist and gneiss. Bateman and Eaton (1967, p. 1413) correlated the downward increase in *P*-wave velocity in the upper crust from 6.0 km/s to 6.4 km/s to a "downward increase in the proportion of diorite, quartz-diorite, and

calcic granodiorite or their gneiss equivalents relative to quartz monzonite and granite***." The thick layer of Bateman and Eaton with a velocity of 6.9 km/s below 25 km was not confirmed by our investigation, which indicates that the velocity does not exceed 6.6 km/s down to a depth of about 35 km. This result appears to agree with Hamilton and Myers (1967, p. C20), who stated that "the eastern part of the Sierra Nevada batholith consists largely of light-colored quartz monzonite and granodiorite***" and that "Mesozoic metavolcanic rocks are mostly dacite and quartz latite***." They concluded, "the lower crust is richer in potassium and is less mafic***" than the upper crust. Unfortunately, the available seismic data are inadequate to determine the crustal structure beneath the western part of the Sierra Nevada where, according to Hamilton and Myers, the lower crust is expected to be more mafic.

Under the southern Cascade Mountains of northern California, upper crustal silicic material is probably thin or absent, as is indicated by volcanic surface material consisting mainly of pyroxene andesites and basaltic andesites and also by higher seismic velocities of 6.5-6.6 km/s at a depth of only 7 km. Hamilton and Myers (1966, p. 540) assumed that "the southern Cascades consist of a surface pile of relatively light volcanic and plutonic rocks, 6-10 km thick, resting on a dense basaltic crust***." On the basis of seismic data, Hamilton (1969, p. 2421) suggested that "the metamorphic terrane of the northwestern Sierra Nevada is truncated against new volcanic crust at the north end of the range***."

The velocity inversion from 6.6 to about 6.0 km/s observed between depths of 8 and 17 km occurs in the area of a gravity low (Pakiser, 1964) and may be restricted to the area of Lassen Volcanic National Park. The gravity low and the velocity inversion might also be explained as a buried silicic batholith, a thick sedimentary sequence, a low-density thermally expanded body of rock, or "a volcano-tectonic depression filled with volcanic material of low-average density***" (Pakiser, 1964, p. 617).

The average composition of the crust in the Basin and Range province is fairly silicic, as has been suggested by Pakiser and Robinson (1966a, b). The velocity-depth functions obtained for the province may suggest a petrographic interpretation for the upper crust similar to that proposed of Giese (1966, 1968) for the Bohemian massif in southern Germany. The travel-time curve *a* represents mainly Precambrian plutonic rocks (Hamilton and Pakiser, 1965), the velocity of which may increase with increasing depth according to increasing metamorphism.

Birch (1958) and Hughes and Maurette (1956, 1957) suggested that the increase of pressure with depth is the most important influence on velocity within the upper 5 km of the crust. This was demonstrated by Giese, who interpreted several seismic-refraction lines that were located entirely on basement rocks (Giese, 1963, 1966). At depths below 5 km, however, temperature also has a significant influence on velocity, as experiments in laboratories have shown. Temperature effects may partly explain the decrease of velocity with depth in the upper part of the crust that has been observed on many profiles in the Basin and Range province.

Another possible explanation of the origin of a velocity inversion with increasing depth is given by Giese (1966), following Bederke (1962), who observed that, with increasing metamorphism, the density of schists (demonstrated by experiments on rocks of the Bündner Schiefer, fig. 91) increases to 3-3.2 g/cm^3. But at higher grades of metamorphism, the density may decrease to 2.8 g/cm^3. Consequently, by applying the velocity-density relation of Woollard (1959), for example, the velocity decreases with depth also. Finally, with granitization, the density decreases still more and may be as low as 2.60-2.65 g/cm^3. Figure 91 shows the results of Bederke (1962, figs. 3, 4) and Giese (1966, fig. H3; 1). According to Winkler (1967), melting begins in terranes of high-grade metamorphism if quartz-feldspar-mica gneisses and water are present at the surprisingly low temperature of 650°-700°C, independently of the amount of water available. Giese (1968) infers that anatexis has the greatest influence on velocity inversion. In the part of the Western United States covered by this report, however, velocity inversions due to anatexis probably can be excluded because the inversions are not very strong. The low-velocity zone in the crust of the Middle Rocky Mountains may be correlated with decreasing density because of increasing temperature and (or) increasing metamorphism (Bederke, 1962). The narrow depth range in which the velocity inversion is evident suggests that anatexis is not involved.

Hamilton and Myers (1966, 1968) suggested that the northern part of the Basin and Range province has undergone a total crustal extension of between 50 and 300 km, accompanied by rebuilding of the crust by surface volcanism and intrusion at depth. Pakiser and Zietz (1965) suggested a similar process of crustal thickening. According to Hamilton and Myers (1968, p. 343), "both the width of the province and the proportion of Cenozoic volcanic and sedimentary rocks within it increase northward in the province***." These interpretations are in good agreement with the geophysical definition of a distinct lower crust beneath the northern Basin and Range province, whereas the transition

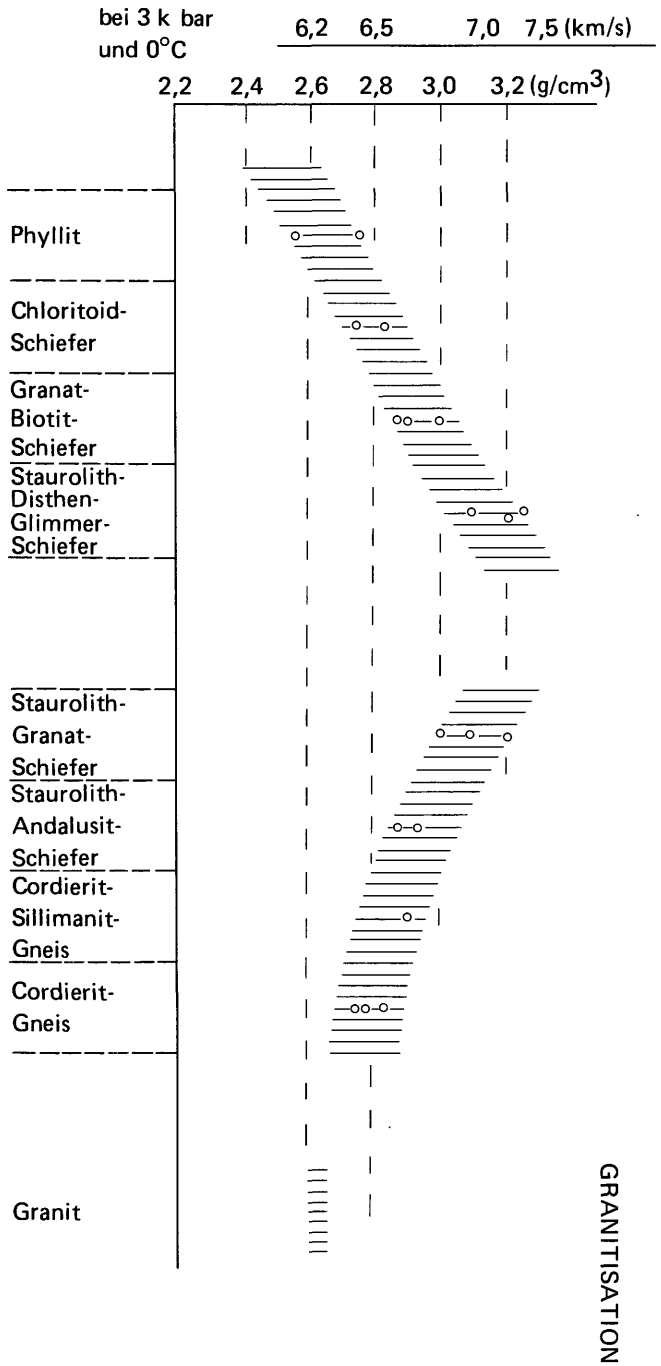

FIGURE 91.—Relation between grade of metamorphism and density of the Bündner Schiefer (after Bederke, 1962, figs. 3, 4, with supplements by Giese, 1966, fig. H3; 1). The velocity scale, drawn by aid of the density-velocity curve by Woollard (1959), is plotted without marks to demonstrate that the correlation is not precise.

zone between upper and lower crust disappears toward the south. Material with low *P*-wave velocities extends to greater depths beneath the southern part of the Great Basin. The average velocity for the lower part of the crust increases from 6.4 to 6.8 km/s along the line from Eureka to Delta and from Eureka to Mountain City, which may indicate an increasing proportion of new mantle material within the lower crust under the northern Basin and Range province toward the east and north.

This interpretation of the lower crust under the northern Basin and Range province is particularly appropriate for the western Snake River Plain. Hill and Pakiser (1966, 1967) pointed out that high-velocity material is found at shallow depths beneath the Snake River Plain. They concluded that the Snake River Plain is a rift through the continental crust filled with basaltic material from the mantle, produced, according to Hamilton and Myers (1966), by the northwestward shift of the Idaho batholith. The mafic material has a velocity of 6.8 km/s or more. The transition zone at a depth of about 40 km may mark a phase boundary rather than a chemical change in material. A similar relation may hold for the southern Cascade Mountains, which were traversed by only a small part of the profile from Shasta Lake to Mono Lake. The composition of the low-velocity anomalous upper mantle in the Basin and Range province remains unknown. During recent years, it has been thought that pressure-temperature conditions at the M-discontinuity are incompatible with those for the basalt-eclogite transition and that the petrologic considerations are also unfavorable to the hypothesis that the M-discontinuity represents the basalt-eclogite transition. However, Ito and Kennedy (1969) have shown recently that the basalt-eclogite transition seems to occur in two fairly sharp steps, from basalt to garnet granulite and from garnet granulite to eclogite, at pressures that are equivalent to depths in the lower crust and uppermost mantle and that the "two-step transitions are expected to produce sharp seismic discontinuities in the lower crust and upper mantle***." These results, therefore, restore the basalt-eclogite hypothesis for the M-discontinuity as a tenable. one. Alternatively, the anomalous upper mantle may be "grossly heterogeneous, consisting primarily of peridotite, but with large lenses or blocks of basaltic to intermediate and perhaps even silicic material distributed through it***" (L.C. Pakiser, written commun., 1970).

COMPARISON WITH SEISMIC-REFRACTION STUDIES IN CENTRAL EUROPE

At the same time as the intensive seismic investigation of the Western United States was made, a systematic seismic investigation of the crust and upper mantle was made in the Alps and adjacent areas. The

measurements were coordinated by the Sub-Commission for Explosions in Southern and Western Europe of the European Seismological Commission, and they were carried out by many geophysical institutions from several European countries. About 40 profiles from 12 shotpoints covered the Alps (fig. 92). The total number of recording points was approximately 1,500. Explosions in small lakes, boreholes, and tunnels, and commercial quarry blasts were used as energy sources for the seismic experiments. A detailed list of publications resulting from these studies was published by Morelli, Bellemo, Finetti, and de Visintini (1967). In order to collect the most important data and to elaborate the general features of the alpine crustal structure, a working group was elected, the synthesis of which was first published in 1967 (Choudhury and others, 1971; Giese and others, 1976).

In the following sections, the main results of this investigation are summarized to provide background for a comparison of the crustal structure of the Western United States and central Europe. Figure 92 shows an index map of the seismic-refraction profiles recorded in the Alps and vicinity.

THE TRAVELTIME DIAGRAM

Record sections were prepared for most profiles shown in figure 92 in the same manner as those described in this paper. Figure 93 shows three typical record sections: the profile from Eschenlohe to Böhmischbruck in the Bavarian Molasse Basin outside the Alps, the profile from Eschenlohe to Lago Lagorai extending across the eastern Alps from north to south, and the profile from Lago Lagorai toward the east in the southern Alps. In a detailed investigation of several profiles in central Europe, Giese (1966) pointed out that a basic traveltime diagram of the type shown in figure 5 can be used to represent all seismic-refraction profiles in central Europe. These traveltime curves are designated *a*, *a–b*, *b*, *c*, and *d*, as in this report.

Giese (1966) noted a difference in the shape of curve *a* depending on the type of basement rocks. On profiles

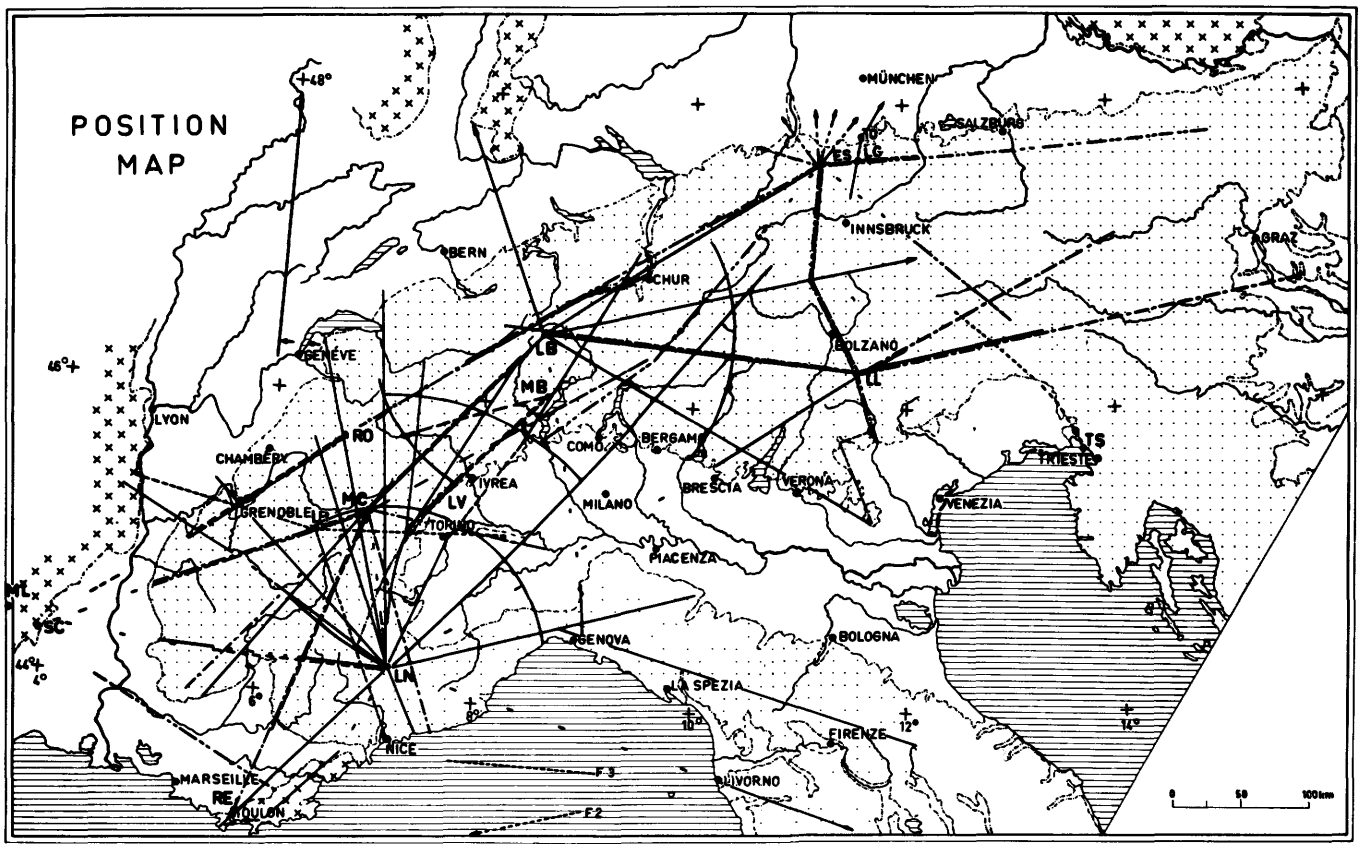

FIGURE 92.—Index map of seismic-refraction profiles in the Alps and their vicinity. Shotpoints: ES, Eschenlohe; LB, Lago Bianco; LG, Lenggries; LL, Lago Lagorai; LN, Lac Nègre; LR, Lac Rond; LV, Levone; MB, Monte Bavarione; MC, Mont Cenis; ML, Mont Lozere; RE, Le Revest; RO, Roselend; SC, Ste. Cécile d'Andorge; TÖ, Tölz. Double lines, reverse profiles. Single lines, recorded in one direction only. Dotted region: Alps, Apennines, and Dinarides (Tertiary age). Area marked with ×: Crystalline areas of Variscan age.

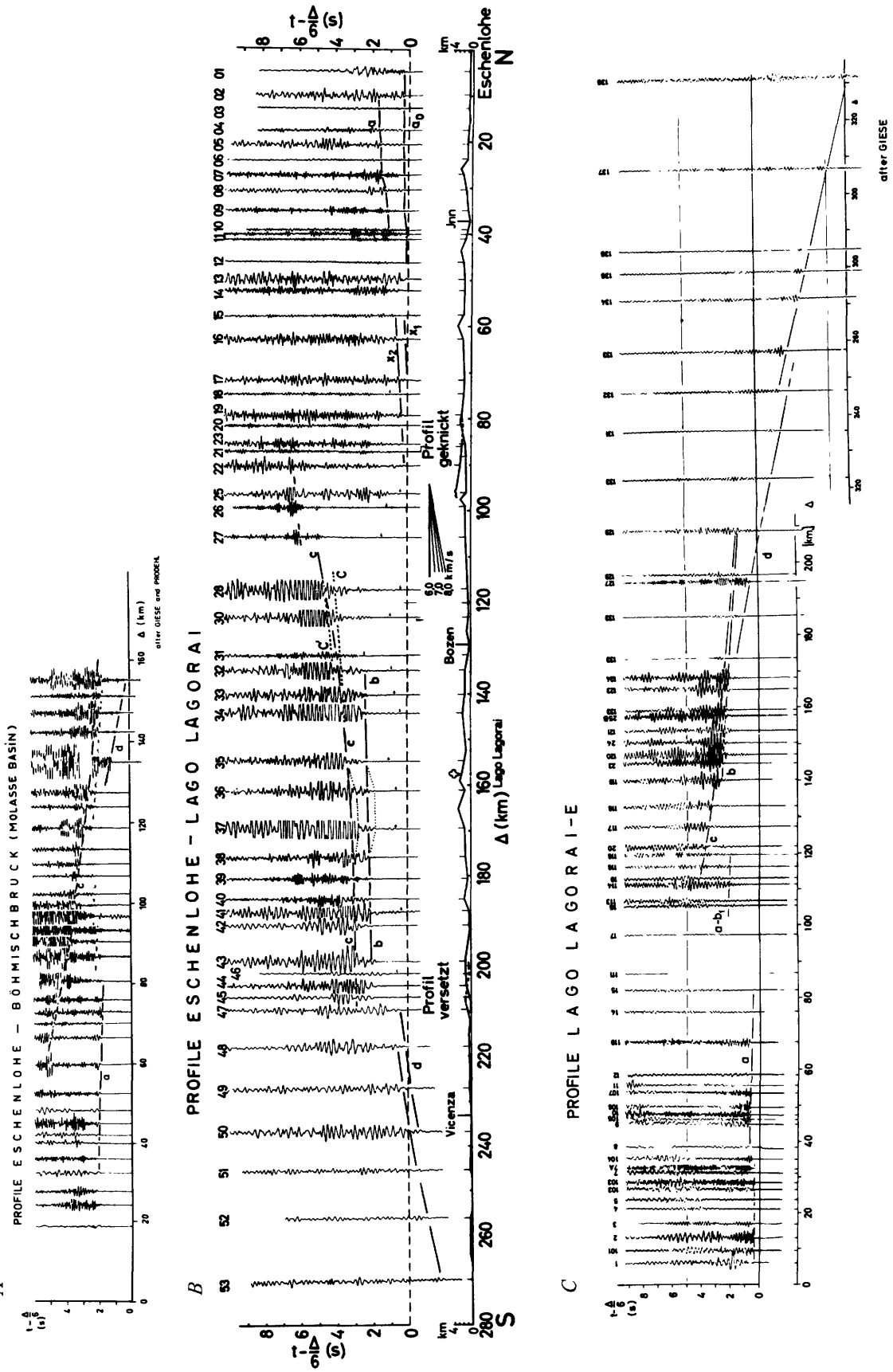

FIGURE 93.—Record section of profiles in central Europe. *A*, Eschenlohe—Böhmischbruck. The profile crosses the Bavarian Molasse Basin toward the Bohemian crystalline massif (Giese, 1966, fig. G22, 3a). *B*, Eschenlohe—Lago Logarai. The profile crosses the eastern Alps in north-south direction (Prodehl, 1965, fig. 11; Giese, 1966, fig. G32.1). *C*, Lago Lagorai—east. The profile was recorded in the southern Alps (Giese, 1966, fig. G5.1).

on Variscan basement in southern Germany (Voggendorf toward the southeast, Böhmischbruck to Eschenlohe) the first arrivals on traveltime curve *a* are formed by the same phase, whereas, on a profile on Pennine rocks (gneisses) in the central Alps (Lago Bianco toward the southeast), phase correlation results in several short en-echelon traveltime branches, and so average curve *a* does not connect arrivals of the same phase. Because recording stations usually are not located consistently on basement rocks and because the spacing of the stations is generally not close enough, phase differences of that kind cannot be detected on most profiles.

The same features are generally evident in the traveltime diagrams for profiles in central Europe as in the Western United States. In spite of the wide spacing of recording stations on the profiles in the Western United States, curve *a* can be correlated by a single phase comparable to that for the Variscan basement of central Europe. This correlation is especially certain for the profiles recorded in 1967 in the Coast Ranges of central California (S.W. Stewart, written commun., 1969).

In addition to traveltime curves *a* and *d*, which are based on first arrivals, a strong phase *c* characterized by well-determined secondary arrivals with large amplitudes on nearly all record sections is the most evident similarity between the American and Alpine data. This phase seems to be strongest on profiles at the margin or just outside the Alps (Eschenlohe toward the east, Lago Lagorai toward the east, Eschenlohe to Böhmischbruck, and Massif Central of France) and not as well expressed on profiles within the central Alps (for example, Lago Lagorai to Lago Bianco and its reverse; Choudhury and others, 1971). A similarly weak phase *c* can be seen on the profiles in the Sierra Nevada and the Middle Rocky Mountains, in contrast to the prominent phase *c* on the profiles in the Basin and Range province. However, published record sections of profiles in the Great Plains (Jackson and others, 1963; Stewart, 1968b) and the Southern Rocky Mountains (Jackson and Pakiser, 1965; Prodehl and Pakiser, 1979) indicate that this conclusion probably cannot be generalized.

On the profiles in the Sierra Nevada, the Middle Rocky Mountains, and the Colorado Plateau and on the profiles in the central Alps, curve *d* crosses the distance axis at greater distances than on profiles in other areas, indicating a thicker crust (figs. 82, 88, 94, 95). At distances greater than 150 km on some profiles in the Western United States, a traveltime curve parallel to curve *d* can be traced through distinct secondary arrivals that follow the first arrivals by about 0.5 s. Similar arrivals were found by Prodehl (1965) and Giese (1970) on profiles from Eschenlohe to

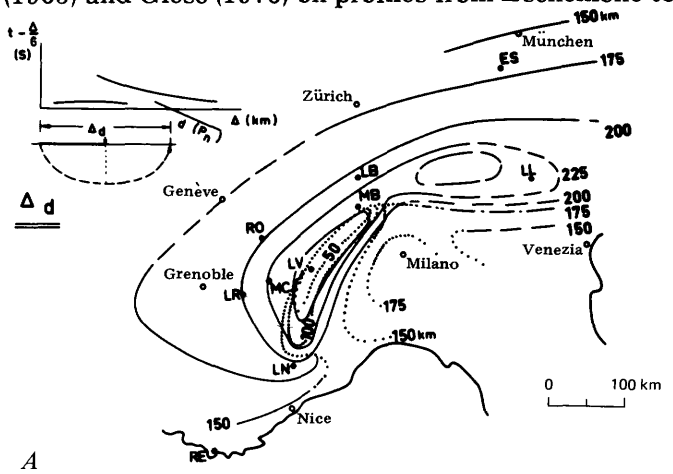

A

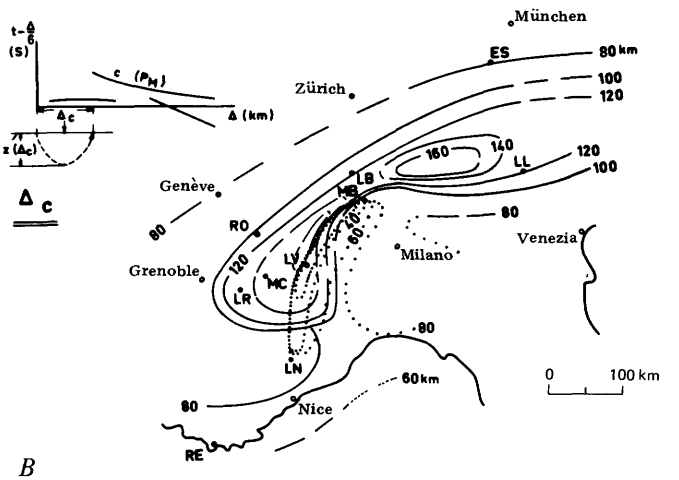

B

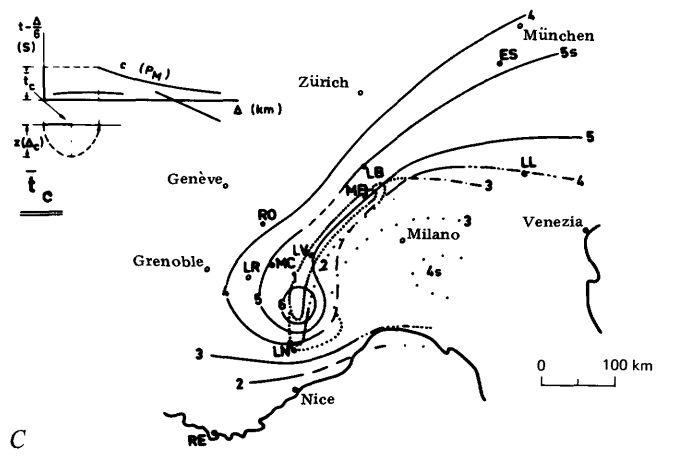

C

the Bohemian crystalline massif and by Meissner and Berckhemer (1967) on profiles across the northern Rhinegraben. Meissner and Berckhemer explained the occurrence of the two parallel traveltime curves, the first of which was recorded only to a distance of 210 km, as a layer with a velocity of 7.2-7.4 km/s at a depth of 30 km at the base of the crust that pinches out east and west of the Rhinegraben (Mueller and others, 1967). According to Meissner and Berckhemer, the first arrivals represent a wave P_3 propagating in this layer, whereas the wave P_5 representing the secondary arrivals propagates in the upper mantle. Explosion seismology experiments carried out in France (for example, Hirn and others, 1973) have shown that the first arrivals recorded at distances beyond 300 km cannot be correlated by a single P_n phase but have to be correlated by additional phases that are clearly separated from the P_n phase as well as from each other and which can be partly correlated in secondary arrivals. These phases are interpreted as having originated at discontinuities within the upper mantle beneath the M-discontinuity, and a velocity-depth model is presented for the lower lithosphere between 30 and 100 km depth (Hirn and others, 1973).

The fairly well correlated phases scattered between phases *a* and *c* at distances to 160-200 km on most profiles in the Western United States correspond to weak phases on profiles in central Europe. However, in the Western United States phase *b* can be very well correlated in some areas, indicating a definite boundary zone within the crust. In some areas curve *d*(*b*) also was found tangent to the retrograde curve *b* at the point of critical reflection. Those areas are the Snake River Plain, the Middle Rocky Mountains, and the northern part of the Basin and Range province in Nevada and Utah. In central Europe, on some of the profiles crossing the zone of Ivrea, phases designated *c*(*i*) and *d*(*i*) (Giese, 1966; Giese and others, 1967a, 1971) may be comparable with phases *b* and *d*(*b*) in the Western United States.

BASIC DATA

Contour maps of the parameters Δ_d, Δ_c, and $\overline{T}_c$ (fig. 82-84) were drawn by Choudhury, Giese, and de Visintini (1971) for the Alps. These maps were revised and extended by Giese (1970) and Giese and Stein (1971) into western Germany. The maps for the Alps are reproduced here (fig. 94) from Choudhury, Giese, and de Visintini (1971, figs. 12-14). Δ_d represents the crossover distance of curve d ($\overline{T} = 0$), Δ_c the critical distance, and $\overline{T}_c$ the reduced traveltime of the critical reflection. The contour map of $\overline{T}_c$ for the Alps reproduced here was not corrected for the reduced P_g traveltime $\overline{T}_a$ at Δ_c, however. All three contour maps represent approximately the general configuration of the crust of the Alps. Δ_d, Δ_c, and $\overline{T}_c$ increase toward the axis of the Alpine crustal root. According to Choudhury, Giese, and de Visintini (1971), to a first approximation the contour maps of the parameters Δ_d and Δ_c reflect the total crustal thickness. A maximum thickness of the crust under the Alps is indicated in the region of Gran Paradiso and Bernina.

Comparison of the contour maps of the basic data of the Alps (fig. 94) and western Germany (Giese and Stein, 1971, figs. 4-8) with those of figures 82-84 shows that the maximum values of Δ_d ($\geqslant$ 200 km) and Δ_c (120-140 km) in the Western United States are comparable with those for the Alps, whereas the minimum values of Δ_d (120-140 km) and Δ_c (60-80 km) in the Western United States are comparable with those for areas in western Germany outside the Alps. Values of $\overline{T}_c - \overline{T}_{a,c}$ of 3-4 seconds, found in central Nevada, southern Nevada, and adjacent parts of California, can be found also on the corresponding map for western Germany in southeastern Bavaria and adjacent parts of Tyrol. Times of 1-2 seconds in other areas of the Western United States are comparable with values found in the main part of the western Germany. According to Choudhury, Giese, and de Visintini (1971), the values of $\overline{T}_c$ represent approximately the intensity of a velocity inversion.

The P_n velocity (based on curve *d*) of the Alps (including their foreland) differs significantly from that of the Western United States. For the profiles in the Alps and southern Germany, P_n velocities are generally greater than 8.0 km/s (Fuchs and others, 1963; German Research Group for Explosion Seismology, 1964; Prodehl, 1965; Closs, 1966, 1969; Fuchs and Landisman, 1966; Giese, 1966, 1970; Meissner, 1967; Ansorge, 1968; Giese and Stein, 1971; Bamford, 1973; Rhinegraben Research Group for Explosion Seismology, 1974; Edel and others, 1975). A maximum P_n velocity seems to be present under the Bavarian Molasse Basin ($\geqslant$ 8.4 km/s). Under the Western United States, on the other hand, the P_n velocity is generally less than 8.0 km/s. Only under the Middle Rocky Mountains, the Mojave

FIGURE 94.—Contour maps of the parameters Δ_d, Δ_c, and $\overline{T}_c$ for the Alps (Choudhury and others, 1971). Shotpoints: ES, Eschenlohe; LB, Lago Bianco; LL, Lago Lagorai; LN, Lac Nègre; LR, Lac Rond; LV, Levone; MB, Monte Bavarione; MC, Mont Cenis; RE, Le Revest; RO, Roselend. *A*, Contour map of the crossover distance Δ_d (see fig. 82). Contour interval is 25 km. *B*, Contour map of the "critical" distance Δ_c (see fig. 83). Contour interval is 20 km. *C*, Contour map of the reduced traveltime $\overline{t}_c$ at the "critical" point at Δ_c. Contour interval is 1 sec. The time $\overline{t}_c$ corresponds to the uncorrected time $\overline{T}_c$ (see fig. 84).

Desert, and the Coast Ranges of California does the P_n velocity equal or exceed 8.0 km/s.

CRUSTAL STRUCTURE

The determination of the velocity-depth relation for

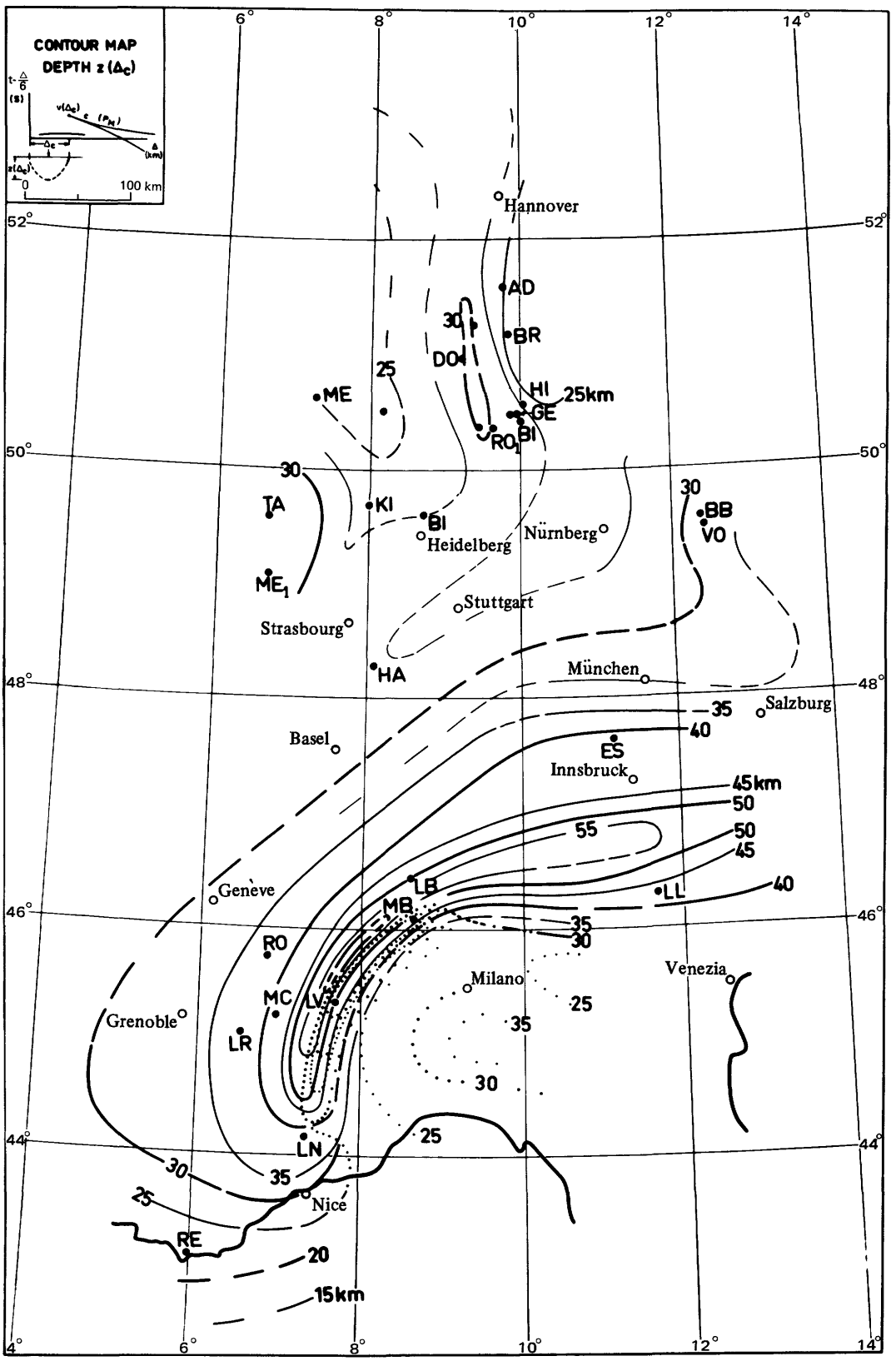

each profile was made by the approximation method of Giese previously described. For the fence diagram (fig. 96), Choudhury, Giese, and de Visintini (1971) compiled velocity-depth cross sections along lines across the Alps. These lines include many reversed and intersecting profiles. The fence diagram (fig. 96) was revised by Giese (written commun., 1969). From the axis of the Alps toward the west and north, total crustal thickness and thickness of the crust-mantle transition zone decrease. Crustal thickness also decreases toward the Mediterranean coast. Figure 95 shows the contour map of total crustal thickness. The contour lines represent the depth to strongest velocity gradient ($z(\Delta_c)$) for central Europe as drawn by Peter Giese (written commun., 1969). The comparable map for the Western United States is presented in figure 88. Although the tectonic relations of the Western United States are not directly comparable with those of the Alps, some significant differences and similarities in crustal structure can be identified. Total crustal thickness, that is, the depth to the strongest velocity gradient, is the parameter that can be most readily compared. The Alps, the Sierra Nevada, and the Middle Rocky Mountains are underlain by a thicker crust than that of surrounding areas. However, the crust under the Colorado Plateau is just as thick as it is under the adjacent Middle Rocky Mountains. The total crustal thickness is about the same under the Southern Rocky Mountains and the adjacent Great Plains of eastern Colorado (Pakiser, 1965).

The crustal structure of the Colorado Plateau may be similar to that of the Great Plains of eastern Colorado (Jackson and others, 1963) and southern Missouri (Stewart, 1968b). However, the crustal thickness of more than 40 km under the Colorado Plateau and the Great Plains is sigmificantly greater than that found for the "normal" crust in central Europe, which is 30 km thick.

The Great Valley and Coast Ranges of California may be similar to the Po Plain and Apennines in northern Italy. According to Giese (1968), the top of the upper mantle lies at about 35 km depth under the Po Plain near Milan and at a depth of 20–25 km under the Apennines between Genoa and Florence (Giese and others, 1967b, 1968). The crustal thickness under the Apennines is comparable with that under the Coast Range of central California. Future surveys and interpretations may reveal whether or not the details of the crustal and upper mantle structure of the northern Apennines and the adjacent Po Plain in northern Italy are like the crustal and upper mantle structure of the Coast Ranges and the adjacent Great Valley of central California.

The transition zone between crust and mantle in which the velocity increases rapidly from 6.6–7.0 to 7.8–8.0 km/s extends under the central Alps over a depth range of more than 10 km and becomes thinner at the northern and western margins. A thickness of 10 km was also found for this transition zone under the Middle Rocky Mountains. The thickness of the transition zone is also greater under the Sierra Nevada than under the surrounding areas. The well-defined low-velocity zone under the Alps, however, is generally not present under the Western United States. Under the Alps, a low-velocity zone was found between depths of 10 and 25 km in which the velocity decreases from 6.0–6.2 to 5.5–5.6 km/s. This zone of velocity inversion is accentuated under the axis of the Alps and smaller under adjacent areas outside the Alps. Under western Germany, Giese and Stein (1971) reported a velocity decrease of 0.1–0.45 km/s at a depth of about 10–15 km.

The special problem concerning the body of Ivrea and its transition into the upper mantle under the Po Plain and the northern Apennines, the depth of which is indicated by dotted lines in figure 95, was discussed in detail by Giese (1968), Giese, Günther, and Reutter (1968), and Giese, Morelli, Prodehl, and Vecchia (1971). Giese postulated the existence of a very intense low-velocity zone under the basic material of the Ivrea body (velocity 6.8–7.4 km/s) in which the velocity may decrease to 4 km/s.

The narrow low-velocity zone found under the Middle Rocky Mountains (fig. 81) may be comparable with that under the Alps, but this low-velocity zone is confined to a small area and depth range. As shown by Prodehl and Pakiser (1979), this zone is more distinct under the Southern Rocky Mountains. A low-velocity zone was not found under the Sierra Nevada, indicating that the Sierran crustal structure differs significantly from that under the central Alps. A velocity inversion was found under the southern Cascade Range (fig. 50), but it is not evident from the existing seismic data whether this zone is confined to the Lassen Peak area or if it is a general feature of the Cascade Mountains.

FIGURE 95.—Contour map of total crustal thickness under central Europe. Contour lines show depth of strongest velocity gradient $z(\Delta_c)$ in the transition zone between crust and mantle of central Europe. The contour interval is 5 km within, 2.5 km outside the Alps. Dashed lines indicate uncertain results. Dotted contour lines indicate the top of the body of Ivrea and its transition into the upper mantle under the Po Plain and the northern Apennines. Map compiled by Peter Giese (written commun., 1969). Shotpoints in addition to those on figure 94: AD, Adelesbsen; BB, Böhmischbruck; BI Bischofsheim; BI_1, Birkenau; BR, Bransrode; DO, Dorheim; GE, Gersfeld; HA, Haslach; HI, Hilders; KI, Kirchheimbolanden; ME, Mehrberg, ME_1, Merlebach; RO_1, Romsthal; TA, Taben-Rodt; VO, Voggendorf.

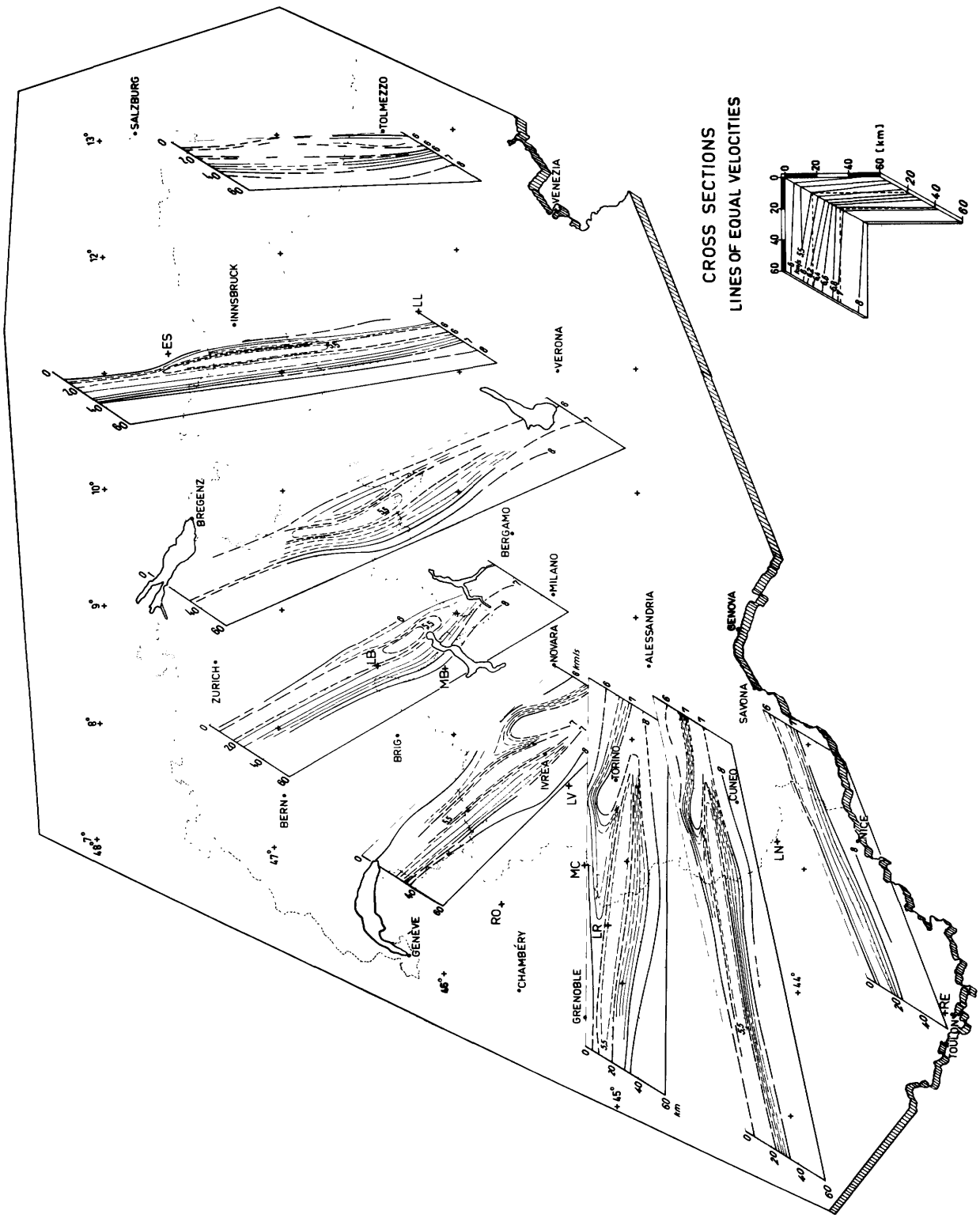

FIGURE 96.—Fence diagram showing the crustal structure under the Alps (Choudhury and others, 1971). Cross sections cross the Alps perpendicular to the general tectonic features and contain a maximum number of reverse and cross profiles. No vertical exaggeration. Names of shotpoints, see figure 91. No intermediate line of equal velocity is shown between the 7.0 and 8.0 km/s lines; the contour interval between the 6.0 and 7.0 km/s lines is 0.2 km/s, except within the zone of low velocity where only the 5.5-km/s contour is drawn. Dashed lines indicate uncertain results. Near-surface velocities of less than 6 km/s are not shown.

REFERENCES CITED

American Geophysical Union, 1964, Bouguer gravity anomaly map of the United States, exclusive of Alaska and Hawaii; prepared by a special committee for the geophysical and geological study of the continents, G. P. Woollard, chm., and the U.S. Geological Survey, H. R. Joesting, coordinator: U.S. Geol. Survey Spec. Map, 2 sheets, scale 1:2,500,000.

Ansorge, J., 1968, Die Struktur der Erdkruste an der Westflanke der Zone von Ivrea [The structure of the earth's crust at the western flank of the zone of Ivrea]: Schweizer. Mineralog. u. Petrog. Mitt., v. 48, p. 247-254.

Archambeau, C. B., Flinn, E. A., and Lambert, D. G., 1969, Fine structure of the upper mantle: Jour. Geophys. Research, v. 74, p. 5825-5865.

Bailey, E. H., Irwin, W. P., and Jones, D. L., 1964, Franciscan and related rocks, and their significance in the geology of western California: California Div. Mines Bull. 183, 177 p.

Bailey, R. W., and Muehlberger, W. R., 1968, Basement rock map of the United States, exclusive of Alaska and Hawaii: U.S. Geol. Survey Spec. Map, 2 sheets, scale 1:2,500,000.

Bamford, D., 1973, Refraction data in western Germany—A time-term interpretation: Zeitschr. Geophysik, v. 39, p. 907-927.

Bateman, P. C., 1968, Geologic structure and history of Sierra Nevada: UMR (Univ. Missouri, Rolla) Jour., v. 1, p. 121-131.

Bateman, P. C., Clark, L. D., Huber, N. K., Moore, J. G., and Rinehart, C. D., 1963, The Sierra Nevada batholith—A synthesis of recent work across the central part: U.S. Geol. Survey Prof. Paper 414-D, 46 p.

Bateman, P. C., and Eaton, J. P., 1967, Sierra Nevada batholith: Science, v. 158, p. 1407-1416.

Bateman, P. C., and Wahrhaftig, Clyde, 1966, Geology of the Sierra Nevada, *in* Bailey, E. H., ed., Geology of northern California: California Div. Mines Bull. 190, p. 107-172.

Bederke, E., 1962, Altersgliederung und Dichteverteilung im kristallinen Grundgebirge [Age classification and density distribution within the crystalline basement]: Geol. Rundschau, v. 52, p. 1-12.

Berg, J. W., Cook, K. L., Narans, H. D., and Dolan, W. M., 1960, Seismic investigation of crustal structure in the eastern part of the Basin and Range province: Seismol. Soc. America Bull., v. 50, p. 511-535.

Birch, F., 1958, Interpretation of the seismic structure of the crust in the light of experimental studies of wave velocities in rocks, *in* Benioff, H., Ewing, Maurice, Howell, B. F., and Press, F., eds., Contributions in geophysics in honor of B. Gutenberg: London—New York, Pergamon Press, p. 158-170.

Bradley, W. H., 1964, Geology of Green River formation and associated Eocene rocks in southwestern Wyoming and adjacent parts of Colorado and Utah: U.S. Geol. Survey Prof. Paper 496-A, 86 p.

Braile, L. W., Smith, R. B., Keller, G. R., Welch, R. M., and Meyer, R. P., 1974, Crustal structure across the Wasatch Front from detailed seismic refraction studies: Jour. Geophys. Research, v. 79, p. 2669-2677.

Bram, K., and Giese, Peter, 1968, Die Geschwindigkeitsverteilung der P-Welle in der Erdkruste im Raum Augsburg (Süd-Deutschland)—Ergebnisse und Vergleich zweier seismischer Messungen [The velocity distribution of the P-wave within the Earth's crust in the area of Augsburg (southern Germany)—Results and comparison of two seismic measurements]: Zeitschr. Geophysik, v. 34, p. 611-626.

Bullen, K. E., 1963, An introduction to the theory of seismology [3d ed.]: Cambridge, Cambridge Univ. Press, 381 p.

Carr, W. J., and Trimble, D. E., 1963, Geology of the American Falls quadrangle, Idaho: U.S. Geol. Survey Bull. 1121-G, 44 p.

Choudhury, M., Giese, Peter, and de Visintini, G., 1971, Crustal structure of the Alps: Some general features from explosion seismology: Boll. Geofisica Teor. ed Appl., v. 13, p. 211-240.

Closs, H., 1966, Der Untergrund der Alpen im Lichte neuerer geophysikalischer Untersuchungen [The deep structure of the Alps in light of recent geophysical investigation]: Erdöl u. Kohle, v. 19, p. 81-88.

_____ 1969, Explosion seismic studies in western Europe, *in* Hart, P. J., ed., The earth's crust and upper mantle: Am. Geophys. Union Mon. 13, p. 178-188.

Cohee, G. V., chm., 1962, Tectonic map of the United States, exclusive of Alaska and Hawaii; prepared by a joint committee of the U.S. Geological Survey and the American Association of Petroleum Geologists: U.S. Geol. Survey Spec. Map, 2 sheets, scale 1:2,500,000.

Compton, R. R., 1966, Granitic and metamorphic rocks of the Salinian block, California Coast Range, *in* Bailey, E. H., ed., Geology of northern California: California Div. Mines Bull. 190, p. 277-288.

Cooper, J. F., Strozier, O. A., and Martina, B. A., 1962, Field operations and shotpoint refraction survey of 1962 crustal studies program, western United States: United Electrodynamics, Inc., United Geophysical Corp., rept., 56 p.

Crowell, J. C., 1968, The California Coast Ranges: UMR (Univ. Missouri, Rolla) Jour., v. 1, p. 133-156.

Dibblee, T. W., 1967, Areal geology of the western Mojave Desert, California: U.S. Geol. Survey Prof. Paper 522, 153 p.

Diment, W. H., Stewart, S. W., and Roller, J. C., 1961, Crustal structure from the Nevada Test Site to Kingman, Arizona, from seismic and gravity observations: Jour. Geophys. Research, v. 66, p. 201-214.

Dix, C. H., 1955, Seismic velocities from surface measurements: Geophysics, v. 20, p. 17-26.

Eardley, A. J., 1962, Structural geology of North America [2d ed.]: New York, Harper and Bros., 624 p.

Eaton, J. P., 1963, Crustal structure from San Francisco, California, to Eureka, Nevada, from seismic-refraction measurements: Jour. Geophys. Research, v. 68, p. 5789-5806.

_____ 1966, Crustal structure in northern and central California from seismic evidence, *in* Bailey, E. H., ed., Geology of northern California: California Div. Mines Bull. 190, p. 419-426.

_____ 1967, Instrumental seismic studies, *in* Brown, R. D., and others, The Parkfield-Cholame, California, earthquakes of June-August 1966: U.S. Geol. Survey Prof. Paper 579, p. 57-65.

_____ 1968, Spatial distribution of aftershocks of the June 27, 1966, Parkfield-Cholame earthquake in the San Andreas fault zone, *in* Dickinson, W. R., and Grantz, A., eds., Proceedings of Conference on Geologic Problems of San Andreas fault system: Stanford, Calif., Stanford Univ. School of Earth Sciences, p. 84.

Eaton, J. P., Healy, J. H., Jackson, W. H., and Pakiser, L. C., 1964, Upper mantle velocity and crustal structure in the eastern Basin and Range province, determined from SHOAL and chemical explosions near Delta, Utah [abs.]: Seismol. Soc. America, 1964 Ann. Mtg., Prog., p. 30-31.

Edel, J. B., Fuchs, K., Gelbke, C., and Prodehl, Claus, 1975, Deep structure of the southern Rhinegraben area from seismic-refraction investigations: Zeitschr. Geophysik, v. 41, p. 333-356.

Fenneman, N. M., and Johnson, D. W., 1946, Physical divisions of the United States: U.S. Geol. Survey Map, scale 1:7,000,000.

Frankovitch, C. J., Cooper, J. F., and Forbes, C. B., 1962, Seismic studies of the crustal structure, California-Nevada region (1961): United Electrodynamics, Inc., United Geophysical Corp., rept., 72 p.

Fuchs, K., and Landisman, M., 1966, Detailed crustal investigation along a north-south section through the central part of western Germany, *in* Steinhart, J. S., and Smith, T. J., eds., The earth beneath the continents: Am. Geophys. Union Mon. 10, p. 433-452.

Fuchs, K., Mueller, S., Peterschmitt, E., Rothé, J. P., Stein, A., and Strobach, K., 1963, Krustenstruktur der Westalpen nach refraktionsseimischen Messungen [Crustal structure of the Western Alps from seismic-refraction measurements]: Gerlands Beitr. Geophysik, v. 72, p. 149-169.

German Research Group for Explosion Seismology, 1964, Crustal structure in western Germany: Zeitschr. Geophysik, v. 30, p. 209-234.

Gibbs, J. F., and Roller, J. C., 1966, Crustal structure determined by seismic-refraction measurements between the Nevada Test Site and Ludlow, California, *in* Geological Survey research 1966: U.S. Geol. Survey Prof. Paper 550-D, p. D125-D131.

Giese, Peter, 1963, Die Geschwindigkeitsverteilung im obersten Bereich des Kristallins, abgeleitet aus Refraktionsbeobachtungen auf dem Profil Böhmischbruck-Eschenlohe [The velocity distribution in the uppermost part of the basement, derived from refraction measurements on the profile Böhmischbruck-Eschenlohe]: Zeitschr. Geophysik, v. 29, p. 197-214.

_____ 1966, Versuch einer Gliederung der Erdkruste im nördlichen Alpenvorland, in den Ostalpen und in Teilen der Westalpen mit Hilfe charakteristischer Refraktions-Laufzeitkurven, sowie eine geologische Deutung [Towards a classification of the Earth's crust in the northern Alpine foreland, in the Eastern Alps, and in parts of the Western Alps, using characteristic refraction-traveltime curves, as well as a geological interpretation]: Habil. Schrift, Math. Naturwiss. Fak. Freie Univ. Berlin, 143 p. (republished 1968: Inst. Meteorol. und Geophysik FU Berlin, Geophys. Abh., 1/2, 214 p.)

_____ 1968, Die Struktur der Erdkruste im Bereich der Ivrea-Zone [The structure of the Earth's crust in the area of the Ivrea zone]: Schweizer. Mineralog. u. Petrog. Mitt., v. 48, p. 261-284.

_____ 1970, The structure of the Earth's crust in central Europe: European Seismol. Comm., 10th General Assembly (Leningrad 1968), Proc. Acad. Sci. USSR, Moscow, p. 387-403.

Giese, Peter, Günther, K., and Reutter, K. J., 1968 (1970) Vergleichende geologische und geophysikalische Betrachtungen der Westalpen und des Nordapennins [Comparing geological and geophysical considerations of the Western Alps and the Northern Appenine]: Zeitschr. Deutsch. geol. Gesell., v. 120, p. 152-196.

Giese, Peter, Morelli, C., Prodehl, Claus, and Vecchia, O., 1971, Crust and upper mantle beneath the southern part of the zone of Ivrea: European Seismol. Comm., 12th General Assembly (Luxembourg 1970), Proc., Obs. Royal de Belgique, Comm. Sér. A. no. 13, Sér. Géophys. no. 101, p. 182-183.

Giese, Peter, Prodehl, Claus, and Behnke, C., 1967a, Ergebnisse refraktionsseismischer Messungen 1965 zwischen Französischem Zentralmassiv und den Westalpen [Results of seismic-refraction measurements 1965 between the French Massif Central and the Western Alps]: Zeitschr. Geophysik, v. 33, p. 215-261.

Giese, Peter, Prodehl, Claus, and de Visintini, G., 1967b, Ergebnisse refraktionsseismischer Messungen im Grenzbereich Alpen/Apennin und im Nordapennin [abs.] [Results of seismic-refraction measurements in the border area Alps/Apennines and in the Northern Apennines]: Zeitschr. Deutsch. geol. Gesell., v. 119, Hauptversammlung.

Giese, Peter, Prodehl, Claus, and Stein, A., eds., 1976, Explosion seismology in central Europe—Data and results: Berlin-Heidelberg-New York, Springer-Verlag, 429 p.

Giese, Peter, and Stein, A., 1971, Versuch einer einheitlichen Auswertung tiefenseismischer Messungen aus dem Bereich zwischen der Nordsee und den Alpen [Toward a unified interpretation of deep-seismic sounding measurements of the area between the North Sea and the Alps]: Zeitschr. Geophysik, v. 37, p. 237-272.

Gilluly, J., 1963, The tectonic evolution of the western United States: Quart. Jour. [London] Geol. Soc., v. 119, p. 133-174.

Green, R. W. E., and Hales, A. L., 1968, The traveltimes of P-waves to 30° in the central United States and upper mantle structure: Seismol. Soc. America Bull., v. 58, p. 267-289.

Hackel, O., 1966, Summary of the geology of the Great Valley, *in* Bailey, E. H., ed., Geology of northern California: California Div. Mines Bull. 190, p. 217-252.

Hall, W. E., 1971, Geology of the Panamint Butte quadrangle, Inyo County, California: U.S. Geol. Survey Bull. 1299, 67 p.

Hamilton, W., 1969, Mesozoic California and the underflow of Pacific mantle: Geol. Soc. America Bull., v. 80, p. 2409-2430.

Hamilton, W., and Myers, W. B., 1966, Cenozoic tectonics of the western United States: Rev. Geophysics, v. 4, p. 509-549.

_____ 1967, The nature of batholiths: U.S. Geol. Survey Prof. Paper 554-C, 30 p.

_____ 1968, Cenozoic tectonic relationships between the western United States and the Pacific Basin, *in* Dickinson, W. R., and Grantz, A., eds., Proceedings of Conference on Geologic Problems of San Andreas fault system: Stanford, Calif., School of Earth Sciences, p. 342-357.

Hamilton, W., and Pakiser, L. C., 1965, Geologic and crustal cross section of the United States along the 37th parallel: U.S. Geol. Survey Misc. Geol. Inv. Map I-448.

Hansen, W. R., 1965, Geology of the Flaming Gorge area, Utah-Colorado-Wyoming: U.S. Geol. Survey Prof. Paper 490, 196 p.

Healy, J. H., 1963, Crustal structure along the coast of California from seismic-refraction measurements: Jour. Geophys. Research, v. 68, p. 5777-5787.

Healy, J. H., Cooper, J. F., Eaton, J. P., Forbes, C. B., Frankovitch, C. J., Roller, J. C., and Stewart, S. W., 1962, Crustal studies in western United States, part IV: Study of seismic propagation paths and regional traveltimes in the California-Nevada region: U.S. Geol. Survey Report, Denver, Colo., 103 p.

Healy, J. H., and Warren, D. H., 1969, Explosion seismic studies in North America, *in* Hart, P. J., ed., The earth's crust and upper mantle: Am. Geophys. Union Mon. 13, p. 208-220.

Herrin, E., 1969, Regional variations of P-wave velocity in the upper mantle beneath North America, *in* Hart, P. J., ed., The earth's crust and upper mantle: Am. Geophys. Union Mon. 13, p. 242-246.

Hill, D. P., 1963, Gravity and crustal structure in the western Snake River Plain, Idaho: Jour. Geophys. Research, v. 68, p. 5807-5819.

Hill, D. P., and Pakiser, L. C., 1966, Crustal structure between the Nevada Test Site and Boise, Idaho, from seismic refraction measurements, *in* Steinhart, J. S., and Smith, T. J., eds., The earth beneath the continents: Am. Geophys. Union Mon. 10, p. 391-419.

_____ 1967, Seismic-refraction study of crustal structure between the Nevada Test Site and Boise, Idaho: Geol. Soc. America Bull., v. 78, p. 685-704.

Hirn, A., Steinmetz, L., Kind, R., and Fuchs, K., 1973, Long range profiles in western Europe: II. Fine structure of the lower lithosphere in France (southern Bretagne): Zeitschr. Geophysik, v. 39, p. 363-384.

Hughes, D. S., and Maurette, C., 1956, Variation of elastic wave velocities in granites with pressure and temperature: Geophysics, v. 21, p. 277-284.

_____ 1957, Variation of elastic wave velocities in basic igneous rocks with pressure and temperature: Geophysics, v. 22, p. 23-31.

Hunt, C. B., and Mabey, D. R., 1966, Stratigraphy and structure, Death Valley, California: U.S. Geol. Survey Prof. Paper 494-A, 62 p.

Ito, K., and Kennedy, G. C., 1969, The fine structure of the basalt-eclogite transition [abs.]: Geol. Soc. America and associated societies, Annual Meeting, Atlantic City, N.J., 1969, part 7, Abs. with Program, p. 113.

Jackson, W. H., and Pakiser, L. C., 1965, Seismic study of crustal structure in the southern Rocky Mountains, *in* Geological Survey research: U.S. Geol. Survey Prof. Paper 525-D, p. D85-D92.

Jackson, W. H., Stewart, S. W., and Pakiser, L. C., 1963, Crustal structure in eastern Colorado from seismic-refraction measurements: Jour. Geophys. Research, v. 68, p. 5767-5776.

James, D. E., and Steinhart, S. W., 1966, Structure beneath continents: A critical review of explosion studies 1960-1965, *in* Steinhart, J. S., and Smith, T. J., eds., The earth beneath the continents: Am Geophys. Union Mon. 10, p. 293-333.

Jobert, G., and Perrier, G., 1974, Demonstration de $z(V) \leqslant z_{max}$, *in* Coulomb, J., and Jobert, G., eds., Traité de Géophysique interne, Compléments et erratum de Tome I in Tome II: Paris, Masson et Cie.

Johnson, L. R., 1965, Crustal structure between Lake Mead, Neada, and Mono Lake, California: Jour. Geophys. Research, v. 70, p. 2863-2872.

_____ 1967, Array measurements of P velocities in the upper mantle: Jour. Geophys. Research, v. 72, p. 6309-6325.

King, P. B., 1959, The evolution of North America: Princeton, N.J., Princeton Univ. Press, 189 p.

_____ 1967, Tectonic features: National Atlas, Sheet no. 70, U.S. Geol. Survey, scale 1:7,500,000.

Kistler, R. W., and Bateman, P. C., 1966, Stratigraphy and structure of the Dinkey Creek roof pendant in the central Sierra Nevada, California: U.S. Geol. Survey Prof. Paper 524-B, 14 p.

Kosminskaya, I. P., and Riznichenko, Y. V., 1964, Seismic studies of the earth's crust in Eurasia, *in* Odishaw, H., ed., Research in Geophysics, v. 2, Solid earth and interface phenomena, chap. 4: Cambridge, Mass., Massachusetts Inst. Technology Press, p. 81-122.

Kosminskaya, I. P., Belyaevsky, N. A., and Volvovsky, I. S., 1969, Explosion seismology in the USSR, *in* Hart, P. J., ed., The earth's crust and upper mantle: Am. Geophys. Union Mon. 13, p. 195-208.

Lee, W. H. K., and Uyeda, S., 1965, Review of heat flow data, *in* Lee, W. H. K., ed., Terrestrial heat flow: Am. Geophys. Union Mon. 8, p. 87-190.

Mabey, D. R., 1960, Regional gravity survey of part of the Basin and Range province, *in* Short papers in the geological sciences 1960: U.S. Geol. Survey Prof. Paper 400-B, p. B283-B285.

Macdonald, G. A., 1966, Geology of the Cascade Range and Modoc Plateau, *in* Bailey, E. H., ed., Geology of northern California: California Div. Mines Bull. 190, p. 65-96.

Macdonald, G. A., and Gay, T. E., 1968, Geology of the Cascade Range: California Div. Mines Mineral Inf. Ser., v. 21, p. 108-111.

Meissner, R., 1967, Zum Aufbau der Erdkruste. Ergebnisse der Weitwinkelmessungen im bayerischen Molassebecken [Structure of the Earth's crust. Results of wide-angle measurements in the Bavarian Molasse Basin]: Gerlands Beitr. Geophysik, v. 76, p. 211-254, 295-314.

Meissner, R., and Berckhemer, H., 1967, Seismic-refraction measurements in the northern Rhinegraben, *in* Rothé, J. P., and Sauer, K., eds., The Rhinegraben progress report 1967: Abh. geol. Landesamt Baden-Württemberg, Freiburg, Heft 6—Mém. Serv. Carte Géol. Alsace et Lorraine, Strasbourg, no. 26, p. 105-107.

Mikumo, T., 1965, Crustal structure in central California in relation to the Sierra Nevada: Seismol. Soc. America Bull., v. 55, p. 65-84.

Morelli, C., Bellemo, S., Finetti, I., and de Visintini, G., 1967, Preliminary depth contour maps of the Conrad and Moho discontinuities in Europe: Boll. Geofisica Teor. ed Appl., v. 9, p. 142-157.

Mueller, S., and Landisman, M., 1966, Seismic studies of the earth's crust in continents. I: Evidence for a low-velocity zone in the upper part of the lithosphere: Geophys. Jour., v. 10, p. 525-538.

Mueller, S., Peterschmitt, E., Fuchs, K., and Ansorge, J., 1967, The rift structure of the crust and upper mantle beneath the Rhinegraben, *in* Rothé, J. P., and Sauer, K., eds., The Rhinegraben Progress Report 1967: Abh. Geol. Landesamt Baden-Württemberg, Freiburg, Heft 6—Mém Serv. Carte Géol. Alsace et Lorraine, Strasbourg, no. 26, p. 108-112.

Nolan, T. B., 1943, The Basin and Range province in Utah, Nevada, and California: U.S. Geol. Survey Prof. Paper 197-D, p. D141-D196.

Officer, C. B., 1958, Introduction to the theory of sound transmission: McGraw-Hill, New York, 284 p.

Osmond, J. C., 1960, Tectonic history of the Basin and Range province in Utah and Nevada: Mining Engineering, v. 217, p. 251-265.

Page, B. M., 1966, Geology of the Coast Ranges of California, *in* Bailey, E. H., ed., Geology of northern California: California Div. Mines Bull. 190, p. 255-275.

Pakiser, L. C., 1963, Structure of the crust and upper mantle in the western United States: Jour. Geophys. Research, v. 68, p. 5747-5756.

_____ 1964, Gravity, volcanism, and crustal structure in the southern Cascade Range, California: Geol. Soc. America Bull., v. 75, p. 611-620.

_____ 1965, The basalt-eclogite transformation and crustal structure in the Western United States, *in* Geological Survey research 1965: U.S. Geol. Survey Prof. Paper 525-B, 8 p.

_____ 1970, Structure of Mono Basin, California: Jour. Geophys. Research, v. 75, p. 4077-4080.

Pakiser, L. C., and Hill, D. P., 1963, Crustal structure in Nevada and southern Idaho from nuclear explosions: Jour. Geophys. Research, v. 68, p. 5757-5766.

Pakiser, L. C., Kane, M. F., and Jackson, W. H., 1964, Structural geology and volcanism of Owens Valley region, California—A geophysical study: U.S. Geol. Survey Prof. Paper 438, 68 p.

Pakiser, L. C., and Robinson, R., 1966a, Composition and evolution of the continental crust as suggested by seismic observations: Tectonophysics, v. 3, p. 547-557.

——— 1966b, Composition of the continental crust as estimated from seismic observations, *in* Steinhart, J. S., and Smith, T. J., eds., The earth beneath the continents: Am. Geophys. Union Mon. 10, p. 620-626.

Pakiser, L. C., and Steinhart, J. S., 1964, Explosion seismology in the western hemisphere, *in* Odishaw, H., ed., Research in Geophysics, v. 2, Solid earth and interface phenomena, chap. 5: Cambridge, Mass., Massachusetts Inst. Technology Press, p. 123-147.

Pakiser, L. C., and Zietz, Isidore, 1965, Transcontinental crustal and upper mantle structure: Rev. Geophysics, v. 3, p. 505-520.

Payne, M. P., 1967, San Andreas fault cross sections: Am. Assoc. Petroleum Geologists, Pacific Sec.

Perrier, G., 1973, La croute terrestre, *in* Coulomb, J., and Jobert, G., eds., Traité de géophysique interne, v. I: Sismologie et pesanteur: Paris, Masson et Cie., p. 229-281.

Prodehl, Claus, 1965, Struktur der tieferen Erdkruste in Südbayern und längs eines Querprofiles durch die Ostalpen, abgeleitet aus refraktionsseismischen Messungen bis 1964 [Structure of the deep crust in Southern Bavaria and along a traversing profile through the Eastern Alps, derived from seismic-refraction measurements to 1964]: Boll. Geofisica Teor. ed Appl., v. 7, p. 35-88.

——— 1970a, Seismic refraction study of crustal structure in the western United States: Geol. Soc. America Bull., v. 81, p. 2629-2646.

——— 1970b, Crustal structure of the western United States from seismic-refraction measurements in comparison with central European results: Zeitschr. Geophysik, v. 36, 477-500.

Prodehl, Claus, and Pakiser, L. C., 1979, Crustal structure of the Southern Rocky Mountains from seismic measurements: Geol. Soc. America Bull., v. 89 [in press].

Research Group for Explosion Seismology, 1966, Explosion seismological research in Japan, *in* Steinhart, J. S., and Smith, T. J., eds., The earth beneath the continents: Am. Geophys. Union Mon. 10, p. 334-348.

Rhinegraben Research Group for Explosion Seismology, 1974, The 1972 seismic refraction experiment in the Rhinegraben—First results, *in* Illies, H., and Fuchs, K., eds., Approaches to taphrogenesis: Stuttgart, Schweizerbart, p. 122-137.

Rinehart, C. D., and Ross, D. C., 1964, Geology and mineral deposits of the Mount Morrison quadrangle, Sierra Nevada, California: U.S. Geol. Survey Prof. Paper 385, 106 p.

Roberts, R. J., 1968, Tectonic framework of the Great Basin: UMR (Univ. Missouri, Rolla) Jour., v. 1, p. 101-119.

Roller, J. C., 1964, Crustal structure in the vicinity of Las Vegas, Nevada, from seismic and gravity observations, *in* Geological Survey research 1964: U.S. Geol. Survey Prof. Paper 475-D, p. D108-D111.

——— 1965, Crustal structure in the eastern Colorado Plateaus province from seismic-refraction measurements: Seismol. Soc. America Bull., v. 55, p. 107-119.

Roller, J. C., and Gibbs, J. F., 1964, Chemical explosions detonated by the U.S. Geological Survey from July 1961 to July 1964: U.S. Geol. Survey CS [Crustal Studies] Tech. Letter No. 24, Denver, Colo., 13 p.

Roller, J. C., and Healy, J. H., 1963, Seismic-refraction measurements of crustal structure between Santa Monica Bay and Lake Mead: Jour. Geophys. Research, v. 68, p. 5837-5849.

Roller, J. C., Jackson, W. H., Cooper, J. F., and Martina, B. A., 1963, Crustal structure in the western United States; Study of seismic propagation paths and regional traveltimes in the California-Nevada region: U.S. Geol. Survey CS [Crustal Studies] Tech. Letter No. 9, Denver, Colo., 57 p.

Roller, J. C., Strozier, O. P., Jackson, W. H., and Healy, J. H., 1963, Preliminary report on seismic-refraction studies of crustal structure in the western, central, and southern United States: U.S. Geol. Survey CS [Crustal Studies] Tech. Letter No. 14, Denver, Colo., 55 p.

Rubey, W. W., and Hubbert, M. K., 1959, Overthrust belt in geosynclinal area of western Wyoming in light of fluid-pressure hypothesis: Geol. Soc. America Bull., v. 70, p. 167-206.

Ryall, A., and Stuart, D. J., 1963, Traveltimes and amplitudes from nuclear explosions, Nevada Test Site to Ordway, Colorado: Jour. Geophys. Research, v. 68, p. 5821-5835.

Sollogub, V. B., 1969, Seismic crustal studies in southeastern Europe, *in* Hart, P. J., ed., The earth's crust and upper mantle: Am. Geophys. Union Mon. 13, p. 189-195.

Steinhart, J. S., and Meyer, R. P., 1961, Explosion studies of continental structure: Carnegie Inst. Washington Pub. 622, 409 p.

Stewart, S. W., 1968a, Preliminary comparison of seismic traveltimes and inferred crustal structure adjacent to the San Andreas fault in the Diablo and Gabilan Ranges of central California, *in* Dickinson, W. R., and Grantz, A., eds., Proceedings of Conference on Geologic Problems of San Andreas Fault System: Stanford Univ., Stanford, Calif., School of Earth Sciences, p. 218-230.

——— 1968b, Crustal structure in Missouri by seismic-refraction methods: Seismol. Soc. America Bull., v. 58, p. 291-323.

Stuart, D. J., Roller, J. C., Jackson, W. H., and Mangan, G. B., 1964, Seismic propagation paths, regional traveltimes, and crustal structure in the western United States: Geophysics, v. 29, p. 178-187.

Thompson, G. A., 1959, Gravity measurements between Hazen and Austin, Nevada, a study of Basin-Range structure: Jour. Geophys. Research, v. 64, p. 217-230.

Thompson, G. A., and Talwani, M., 1964, Crustal structure from Pacific basin to central Nevada: Jour. Geophys. Research, v. 69, p. 4813-4837.

Warren, D. H., 1968a, Transcontinental geophysical survey (35°-39° N.) seismic refraction profiles of the crust and upper mantle from 112° W. longitude to the coast of California: U.S. Geol. Survey Misc. Geol. Inv. Map I-532-D, scale 1:1,000,000.

——— 1968b, Transcontinental geophysical survey (35° - 39°N.) seismic refraction profiles of the crust and upper mantle from 100° to 112° W. longitude: U.S. Geol. Survey Misc. Geol. Inv. Map I-533-D, scale 1:1,000,000.

——— 1968c, Transcontinental geophysical survey (35° - 39°N.) seismic refraction profiles of the crust and upper mantle from 87° to 100° W. longitude: U.S. Geol. Survey Misc. Geol. Inv. Map -534-D, scale 1:1,000,000.

——— 1968d, Transcontinental geophysical survey (35° - 39° N.) seismic refraction profiles of the crust and upper mantle from 74° to 87° W. longitude: U.S. Geol. Survey Misc. Geol. Inv. Map I-535-D, scale 1:1,000,000.

——— 1969, A seismic-refraction survey of crustal structure in central Arizona: Geol. Soc. America Bull. v. 80, p. 257-282.

Warrick, R. E., Hoover, D. B., Jackson, W. H., Pakiser, L. C., and Roller, J. C., 1961, The specification and testing of a seismic-refraction system for crustal studies: Geophysics, v. 26, p. 820-824.

Willden, Ronald, 1965, Seismic-refraction measurements of crustal structure between American Falls Reservoir, Idaho, and Flaming Gorge Reservoir, Utah: U.S. Geol. Survey Prof. Paper 525-C, p. C44-C50.

Winkler, H. G. F., 1967, Petrogenesis of metamorphic rocks [2d ed]: Berlin-New York, Springer-Verlag, 237 p.

Woollard, G. P., 1959, Crustal structure from gravity and seismic measurements: Jour. Geophys. Research, v. 64, p. 1521-1544.

Yerkes, R. F., McCulloh, T. H., Schoellhamer, J. E., and Vedder, J. G., 1965, Geology of the Los Angeles basin, California—An introduction: U.S. Geol. Survey Prof. Paper 420-A, 57 p.

TABLES 55–108

Tables 55–107 show the data for the corresponding record sections. The first column identifies the recording station. The second column shows the distance from the shotpoint referring to the location of the closest and most distant seismometer of the corresponding spread, that is, traces 1, 6, 9, and 14 (fig. 3). The coordinates and the elevation in columns 4–6 are given for the seismometer, the trace number of which is shown in column 3. Column 7 shows the traces according to figure 3 that are included in the corresponding record section, the first number referring to the seismometer of the corresponding spread closest to the shotpoint, the last number to the seismometer most distant from the shotpoint. Table 108 lists the corrections applied to some profiles.

TABLE 55.—*Data for the record-section of the profile from Eureka(15) to Fallon(9) (fig. 10)*

Station	Distance (km) (traces 1, 6)	Trace No. of coordinates and elevation	Coordinates Lat	Coordinates Long	Elevation (feet)	Traces included in section
S-4	1.2 - 3.7	1	39°36.00′	115°37.70′	6,050	3
J-3	18.6 - 21.1	6	39°31.39′	115°53.90′	6,800	4
Q-1	26.4 - 28.9	1	39°34.54′	115°59.90′	5,970	1
T-12	38.7 - 41.2	1	39°36.12′	116°08.87′	6,050	1,6
I-4	42.4 - 44.9	1	39°36.41′	116°09.94′	6,020	5
P-3	56.6 - 58.9	6	39°31.42′	116°21.46′		3,6
Q-8	61.5 - 63.9	6	39°30.90′	116°24.40′	6,200	2,5
P-8	77.8 - 80.3	6	39°26.20′	116°35.10′	6,500	1,6
J-12	83.5 - 85.5	1	39°33.65′	116°38.50′	6,450	1
I-10A	84.1 - 86.1	1	39°33.65′	116°38.50′	6,450	4
J-8	98.6 -101.1	6	39°23.84′	116°49.00′	5,820	1,11,6
K-2	106.4 -108.9	6	39°23.84′	116°54.08′	5,740	1
K-8	108.9 -111.2	1	39°24.44′	116°55.3′	6,000	1,11,6
J-9	117.7 -119.6	1	39°28.71′	117°01.75′	7,200	1,11,6
H-9	125.1 -127.6	3	39°36.02′	117°09.28′	5,775	2,6
I-8	130.6 -133.0	1	39°25.95′	117°10.50′	5,760	1,11,6
H-8	139.7 -142.2	3	39°28.41′	117°18.16′	6,050	2,6
J-1	153.4 -155.9	3	39°31.51′	117°27.58′	6,250	9
I-9	153.0 -155.2	3	39°21.20′	117°25.46′	6,100	6
K-9	157.0 -158.0	3	39°33.24′	117°30.0′	6,000	1
I-11	159.6 -162.1	3	39°22.47′	117°31.10′	6,100	2,6
S-9	164.0 -166.1	3	39°22.08′	117°34.02′	6,300	1,6
L-12	179.6 -182.0	3	39°29.7′	117° 46.3′	5,300	1,5
K-11	182.5 -185.0	3	39°31.79′	117°48.70′	5,300	4
H-11	185.0 -186.5	3	39°32.20′	117°50.1′	5,400	1,5
S-11	207.1 -209.5	3	39°32.46′	118°05.78′	4,000	9,13
S-10A	215.9 -216.8	1	39°13.77′	118°07.71′	6,000	9,14
Q-11	236.0 -238.4	1	39°16.38′	118°24.45′	4,300	9,13,14
K-10	240.4 -242.4	3	39°32.02′	118°29.22′	3,900	10,14
H-10A	246.7 -248.9	1	39°03.78′	118°28.53′		9,13
P-11	264.3 -266.8	1	39°40.90′	118°46.51′	3,900	9,13
P-10	274.1 -276.5	1	39°31.97′	118°50.64′	4,020	10,13
K-10A	278.2 -280.7	1	39°03.24′	118°50.91′	4,400	9,14
T-10A	312.4 -314.9	1	39°09.15′	119°16.50′	4,600	9,11,12,14
R-11	315.5 -318.0	6	39°39.02′	119°20.31′	4,400	10,13

TABLE 56.—*Data for the record-section of the profile Fallon(9) to Eureka(15) (fig. 11)*

Station	Distance (km) (traces 1, 6)	Trace No. of coordinates and elevation	Coordinates Lat	Coordinates Long	Elevation (feet)	Traces included in section
P-7	1.4	6	39°31.97′	118°50.64′	4,020	6
H-18	10.1 - 12.2	6	39°30.70′	118°44.14′	3,940	1,5
I-7	24.2 - 25.8	6	39°32.03′	118°34.44′	3,900	2,6
J-7	26.2 - 28.7	1	39°32.92′	118°34.89′	3,900	2,6
K-7	32.3 - 34.3	4	39°32.02′	118°29.22′	3,900	1,5
H-1	32.7 - 34.9	1	39°23.29′	118°32.42′	4,050	1,6
Q-8	48.9 - 51.2	1	39°16.38′	118°24.45′	4,500	1,6
I-18	59.7 - 61.9	1	39°32.15′	118°10.80′	4,150	2,6
S-8	65.7 - 68.1	4	39°32.46′	118°05.78′	4,000	6,2
K-18	67.7 - 69.2	1	39°33.00′	118°05.20′	4,150	1
H-8	89.8 - 91.3	4	39°32.20′	117°50.10′	5,400	5
K-8	90.0 - 92.5	4	39°31.79′	117°48.70′	5,300	1,5
L-18	93.8 - 96.0	4	39°29.70′	117°46.30′	5,300	2,5
K-6	118.4 -119.4	4	39°33.24′	117°30.00′	6,000	2,6
I-6	120.0 -122.5	4	39°31.51′	117°27.58′	6,250	2,6
J-8	143.4 -145.9	4	39°36.57′	117°12.50′	5,750	1,11,6
H-6	146.6 -149.1	4	39°36.02′	117°09.28′	5,775	2,6
J-6	156.7 -158.7	6	39°28.71′	117°01.75′	7,200	1,11,6
K-5	166.3 -168.6	6	39°24.44′	116°55.30′	6,000	14,9
J-5	117.6 -179.9	1	39°23.84′	116°49.00′	5,820	1,11,6
S-18	190.0 -191.9	6	39°33.64′	116°38.49′	6,440	10,6
P-5	197.1 -199.6	1	39°26.20′	116°35.10′	6,500	1,11,6
P-4	212.5 -214.9	6	39°31.26′	116°22.28′	6,120	1,6
T-18	234.4 -236.6	1	39°36.12	116°08.84′	6,040	9,13
J-3	256.7 -259.2	1	39°31.39′	115°53.90′	6,800	9,12
K-3	272.8 -275.1	6	39°35.80′	115°40.40′	5,860	9,14
H-3	282.2 -284.4	1	39°36.36′	115°34.75′	6,300	10,14
I-3	294.5 -297.0	4	39°36.41′	115°26.22′	6,100	10,14
K-4	301.3 -303.8	4	39°34.84′	115°21.14′	6,100	11
Q-4	318.4 -320.9	4	39°37.23′	115°09.22′	6,400	11
J-4	328.8 -331.1	4	39°37.57′	115°02.06′	6,300	11

TABLE 57.—*Data for the record-section of the profile from Boise(11) to Elko(14) (fig. 13)*

Station	Distance (km) (traces 1, 6)	Trace No. of coordinates and elevation	Coordinates Lat	Coordinates Long	Elevation (feet)	Traces included in section
J-1	7.03- 7.84	1	43°32.25′	115°54.96′		2,6
R-1	13.41- 15.37	1	43°27.58′	115°57.14′		2,5
L-1	28.82- 31.11	1	43°20.52′	115°50.15′		1,5
S-1	33.55- 36.02	1	43°16.62′	115°57.35′		2,6
Q-1	42.77- 45.19	1	43°11.72′	115°55.77′		3,4
H-1	54.83- 57.34	1	43°05.10′	115°57.96′		3,5
I-1	70.39- 72.87	1	42°57.24′	115°50.10′		2,5
K-1	75.76- 76.76	1	42°53.92′	115°54.42′		1,6
T-1	87.60- 89.89	1	42°47.44′	115°55.97′		1,5
P-1	103.59-105.92	1	42°39.40′	115°47.35′		2,6
J-2	107.42-109.51	1	42°37.26′	115°47.81′	3,950	2,6
R-2	115.13-117.56	1	42°32.52′	115°58.61′	4,830	1,6
L-2	125.68-128.02	1	42°26.82′	115°58.78′	5,310	1,5
S-2	139.41-141.83	1	42°19.50′	115°53.79′	5,400	1,11,6
H-2	143.19-145.74	1	42°17.46′	115°53.73′	5,200	1,12,6
I-2	157.64-160.12	1	42°09.75′	115°51.18′	5,800	1,11,6
K-2	169.38-170.59	1	42°03.42′	115°50.67′	5,700	1,11,5
T-2	176.91-178.94	1	41°59.33′	115°50.95′	6,650	9,12,6
Q-2	182.99-184.34	1	41°56.00′	115°51.94′	6,500	12
P-2	184.41-186.57	1	41°55.20′	115°52.87′	64,50	2,12,6
R-3	196.28-197.80	1	41°48.77′	115°53.25′	6,250	1,12,6
S-3	200.88-203.21	1	41°46,52′	115°47.69′	6,500	1,12
J-3	203.73-205.99	1	41°44.96′	115°47.98′	6,540	1,11,6
L-3	208.91-211.07	1	41°42.19′	115°47.35′	6,370	1,11,5
H-3	221.29-223.47	1	41°35.42′	115°48.60′	6,380	1,11,6
I-3	233.64-236.12	1	41°28.73′	115°48.75′		1,12,6
K-3	244.87-247.35	1	41°22.94′	115°43.39′		1,12,6
T-3	254.44-256.72	1	41°17.55′	115°46.98′		1,12,6
P-3	260.15-262.02	1	41°14.52′	115°45.75′	5,800	1,12,6
Q-3	311.87-313.99	1	40°46.80′	115°40.42′	5,320	10,12,14

TABLE 58.—*Data for the record-section of the profile from Strike Reservoir(12) to Boise(11) (fig. 14)*

Station	Distance (km) (traces 1, 6)	Trace No. of coordinates and elevation	Coordinates Lat	Coordinates Long	Elevation (feet)	Traces included in section
I-1	5.13- 6.08	6	42°57.24′	115°50.10′		1,5
H-1	16.68- 19.06	6	43°05.10′	115°57.96′		1,3,6
Q-1	28.13- 30.55	6	43°11.72′	115°55.77′		2.12.14
S-1	37.34- 39.80	6	43°16.62′	115°57.35′		1,3,5
L-1	44.48- 46.96	6	43°20.52′	115°50.15′		2,4,6
R-1	58.27- 59.97	6	43°27.58′	115°57.14′		1,4,6
J-1	66.49- 68.46	6	43°32.25′	114°54.96′		1,3,6

TABLE 59.—*Data for the record-section of the profile from Strike Reservoir(12) to Elko(14) (fig. 15)*

Station	Distance (km) (traces 1, 6)	Trace No. of coordinates and elevation	Coordinates Lat	Coordinates Long	Elevation (feet)	Traces included in section
K-1	2.72- 4.80	1	42°53.92′	115°54.42′		1,3,6
T-1	14.86- 17.12	1	42°47.44′	115°55.97′		1,6
P-1	30.67- 32.88	1	42°39.40′	115°47.35′		1,5
J-2	34.34- 36.32	1	42°37.26′	115°47.81′	3,950	1,5
R-2	42.69- 45.13	1	42°32.52′	115°58.61′	4,830	1,5
L-2	53.17- 55.39	1	42°26.82′	115°58.78′	5,310	1,5
S-2	66.26- 68.65	1	42°19.50′	115°53.79′	5,400	1,6
H-2	70.04- 72.59	1	42°17.46′	115°53.73′	5,200	3,6
I-2	84.38- 86.87	1	42°09.75′	115°51.18′	5,800	1,11,6
K-2	96.12- 97.29	1	42°03.42′	115°50.67′	5,700	1,5
T-2	103.67-105.72	1	41°59.33′	115°50.95′	6,650	9,6
Q-2	109.79-111.18	1	41°56.00′	115°51.94′	6,500	11
P-2	111.25-113.42	1	41°55.20′	115°52.87′	6,450	11
R-3	123.15-124.63	1	41°48.77′	115°53.25′	6,250	1,6
S-3	127.58-129.93	1	41°46.52′	115°47.69′	6,500	1,6
J-3	130.44-132.71	1	41°44.96′	115°47.98′	6,540	2,6
L-3	135.61-137.77	1	41°42.19′	115°47.35′	6,370	1,5
H-3	148.03-150.23	1	41°35.42′	115°48.60′	6,380	1,11,6
I-3	160.39-162.86	1	41°28.73′	115°48.75′		2,12,6
K-3	171.55-174.04	1	41°22.94′	115°43.39′		1,11,6
T-3	181.18-183.45	1	41°17.55′	115°46.98′		1,12,6
P-3	186.87-188.75	1	41°14.52′	115°45.75′	5,800	1,12,6
Q-3	238.57-240.69	1	40°46.80′	115°40.42′	5,320	10,12,14

TABLE 60.—*Data for the record-section of the profile from Mountain City(13) to Boise(11) (fig. 16)*

Station	Distance (km) (traces 1, 6)	Trace No. of coordinates and elevation	Coordinates Lat	Coordinates Long	Elevation (feet)	Traces included in section
Q-3	7.24- 9.46	6	41°55.23′	115°52.81′	6,550	2,6
T-5	15.23- 17.40	6	41°59.33′	115°50.95′	6,650	1,5
K-5	24.35- 24.91	6	42°03.42′	115°50.67′	5,700	1,6
I-5	33.93- 36.43	6	42°09.75′	115°51.18′	5,800	1,6
H-5	47.98- 50.54	6	42°17.46′	115°53.73′	5,200	1,6
S-5	51.93- 54.32	6	42°19.50′	115°53.79′	5,400	1,6
L-5	65.82- 68.22	6	42°26.82′	115°58.78′	5,310	2,6
R-5	76.32- 78.71	6	42°32.52′	115°58.61′	4,830	1,6
J-5	85.28- 87.57	6	42°37.26′	115°47.81′	3,950	2,6
P-4	89.12- 91.58	6	42°39.40′	115°47.35′		1,6
T-4	103.79-106.09	6	42°47.44′	115°55.97′		2,12,6
K-4	116.93-118.05	6	42°53.92′	115°54.42′		2,11,6
I-4	121.79-124.29	6	42°57.24′	115°50.10′		2,12,5
H-4	136.35-138.86	6	43°05.10′	115°57.96′		2,11,6
Q-4	148.61-151.02	6	43°11.72′	115°55.77′		9,11,14
S-4	157.67-160.15	6	43°16.62′	115°57.35′		9,11,13
L-4	164.87-167.36	6	43°20.52′	115°50.15′		2,12,6
R-4	178.80-180.43	6	43°27.58′	115°57.14′		1,12,6
J-4	187.03-189.02	6	43°32.25′	115°54.96′		1,11,6

TABLE 61.—*Data for the record-section of the profile from Mountain City(13) to Eureka(15) (fig. 17)*

Station	Distance (km) (traces 1, 6)	Trace No. of coordinates and elevation	Coordinates Lat	Coordinates Long	Elevation (feet)	Traces included in section
R-3	2.65- 4.52	6	41°48.77′	115°53.25′	6,250	5,2
S-6	10.73- 12.12	1	41°46.52′	115°47.69′	6,500	3,6
J-3	12.49- 14.40	1	41°44.96′	115°47.98′	6,540	3,6
L-6	17.19- 19.51	1	41°42.19′	115°47.35′	6,370	10,13
H-6	28.19- 30.18	1	41°35.42′	115°48.60′	6,380	9,14
I-6	40.26- 42.82	1	41°28.73′	115°48.75′		9,6
K-6	52.39- 54.71	1	41°22.94′	115°43.39′		9,13
T-6	61.09- 63.43	1	41°17.55′	115°46.98′		9,14
P-6	66.90- 68.65	1	41°14.52′	115°45.75′	5,800	1,14
R-2	81.45- 83.22	1	41°06.63′	115°45.18′	6,500	2,5
L-2	87.35- 89.70	1	41°03.00′	115°51.17′	6,100	1,5
S-2	97.70-100.16	1	40°57.78′	115°45.10′		2,6
Q-2	107.69-110.00	1	40°52.29′	115°45.78′	5,440	2,13
Q-6	118.74-120.75	1	40°46.80′	115°40.42′	5,320	2,12,6
I-2	130.96-133.40	1	40°39.77′	115°44.23′		1,11,6
K-2	141.62-144.18	1	40°34.35′	115°40.05′	5,700	1,11,6
T-2	145.76-148.16	1	40°31.77′	115°43.80′	5,400	3,5
P-2	148.99-151.30	1	40°30.05′	115°43.30′	5,400	2,5
T-1	157.61-157.89	1	40°25.25′	115°41.41′	5,440	6
R-1	158.20-160.55	1	40°25.14′	115°42.16′	5,420	1,11,6
J-1	169.64-172.11	1	40°19.09′	115°40.10′	5,860	1,12,6
L-1	178.38-180.76	1	40°14.15′	115°41.25′	5,910	1,11,6
S-1	188.72-191.22	1	40°08.60′	115°41.80′	6,100	2,12,6
Q-1	197.05-199.53	1	40°04.10′	115°41.54′	6,100	2,13
H-1	207.74-210.12	1	39°58.35′	115°40.80′	6,150	1,11,6
I-1	216.78-219.17	1	39°53.56′	115°39.11′	6,140	2,12,6
K-1	229.78-232.26	1	39°46.44′	115°40.13′	5,920	1,11,6
P-1	247.47-249.84	1	38°36.85′	115°40.11′	5,920	9,12,14

TABLE 62.—*Data for the record-section of the profile from Elko(14) to Boise(11) (fig. 18)*

Station	Distance (km) (traces 1, 6)	Trace No. of coordinates and elevation	Coordinates Lat	Coordinates Long	Elevation (feet)	Traces included in section
Q-2	10.61- 13.10	1	40°52.29′	115°45.78′	5,440	6,2
S-2	19.63- 22.15	6	40°57.78′	115°45.10′		2,6
L-2	32.09- 34.42	1	41°03.00′	115°51.57′	6,100	5,1
R-2	36.45- 38.22	1	41°06.63′	115°45.18′	6,500	5,1
P-3	51.01- 52.79	6	41°14.52′	115°45.75′	5,800	2,6
T-3	56.25- 58.58	6	41°17.55′	115°46.98′		1,6
K-3	65.53- 68.03	6	41°22.94′	115°43.39′		1,11,6
I-3	76.88- 79.41	6	41°28.73′	115°48.75′		2,5
H-3	89.55- 91.67	6	41°35.42′	115°48.60′	6,380	1,3,5
L-3	101.79-103.96	6	41°42.19′	115°47.35′	6,370	2,12,6
J-3	106.88-109.15	6	41°44.96′	115°47.98′	6,540	1,6
S-3	109.66-111.99	6	41°46.52′	115°47.69′	6,500	11,6
R-3	115.38-117.02	6	41°48.77′	115°53.25′	6,250	2,6
Q-3	126.54-128.79	6	41°55.23′	115°52.81′	6,550	9,12
Q-4	128.80-130.05	6	41°56.00′	115°51.94′	6,500	3,14
T-4	134.04-136.02	6	41°59.33′	115°50.95′	6,650	2,12,6
K-4	142.27-143.52	6	42°03.42′	115°50.67′	5,700	1,11,6
I-4	152.78-155.25	6	42°09.75′	115°51.18′	5,800	1,12,6
P-4	160.08-162.80	6	42°13.74′	115°52.68′		1,11,6
H-4	167.26-169.80	6	42°17.46′	115°53.73′	5,200	2,5
S-4	171.13-173.57	6	42°19.50′	115°53.79′	5,400	2,12,6
L-4	185.42-187.84	6	42°26.82′	115°58.78′	5,310	2,13
R-4	195.91-198.27	6	42°32.52′	115°58.61′	4,830	2,14
J-4	203.57-205.75	6	42°37.26′	115°47.81′	3,950	2,4
P-5	207.28-209.68	6	42°39.40′	115°47.35′		2,6
T-5	223.06-225.34	6	42°47.44′	115°55.97′		2,5
K-5	236.14-237.11	6	42°53.92′	115°54.42′		9,14
I-5	240.35-242.85	6	42°57.24′	115°50.10′		10,13
H-5	255.64-258.15	6	43°05.10′	115°57.96′		9,13
S-5	276.85-279.32	6	43°16.62′	115°57.35′		9,12,14
L-5	283.41-285.91	6	43°20.52′	115°50.15′		1,11,5
R-5	297.81-299.53	6	43°27.58′	115°57.14′		9, 12,14
J-5	306.02-307.95	6	43°32.25′	115°54.96′		9,11,6

TABLE 63.—*Data for the record-section of the profile from Elko(14) to Eureka(15) (fig. 19)*

Station	Distance (km) (traces 1, 6)	Trace No. of coordinates and elevation	Coordinates Lat	Coordinates Long	Elevation (feet)	Traces included in section
I-2	12.81- 14.76	1	40°39.77′	115°44.23′		1,5
K-2	22.03- 24.56	1	40°34.35′	115°40.05′	5,700	1,6
T-2	27.06- 29.52	1	40°31.77′	115°43.80′	5,400	1,6
P-2	30.13- 32.35	1	40°30.05′	115°43.30′	5,400	2,5
T-1	38.33- 38.93	6	40°25.25′	115°41.41′	5,440	6,1
R-1	39.07- 41.52	1	40°25.14′	115°42.16′	5,420	3,6
J-1	50.24- 52.71	1	40°19.09′	115°40.10′	5,860	1,6
L-1	59.19- 61.60	1	40°14.25′	115°41.25′	5,910	1,11,6
S-1	69.65- 72.17	1	40°08.60′	115°41.80′	6,100	2,6
Q-1	77.97- 80.45	6	40°04.10′	115°41.54′	6,100	5,12,2
H-1	88.61- 91.02	1	39°58.35′	115°40.80′	6,150	2,12,6
I-1	97.51- 99.85	1	39°53.56′	115°39.11′	6,140	1,11,6
K-1	110.66-113.17	1	39°46.44′	115°40.13′	5,920	1,12,6
P-1	128.40-130.72	1	39°36.85′	115°40.11′	5,920	1,12,6

TABLE 64.—*Data for the record-section of the profile from Eureka(15) to Mountain City(13) (fig. 20)*

Station	Distance (km) (traces 1, 6)	Trace No. of coordinates and elevation	Coordinates Lat	Coordinates Long	Elevation (feet)	Traces included in section
P-5	8.89- 11.27	6	39°36.85′	115°40.11′	5,920	1,6
K-5	26.46- 28.95	6	39°46.44′	115°40.13′	5,920	1,6
I-5	39.77- 42.08	6	39°53.56′	115°39.11′	6,140	2,6
H-5	48.61- 51.01	6	39°58.35′	115°40.80′	6,150	1,6
Q-5	59.21- 61.69	6	40°04.10′	115°41.54′	6,100	9,5
S-5	67.51- 70.03	6	40°08.60′	115°41.80′	6,100	9,5
L-5	78.04- 80.43	1	40°14.25′	115°41.25′	5,910	6,12,1
J-5	86.87- 89.34	6	40°19.09′	115°40.10′	5,860	1,12,6
R-5	98.23-100.62	1	40°25.14′	115°42.16′	5,420	6,13,2
P-6	107.49-109.78	6	40°30.05′	115°43.30′	5,400	1,11,5
T-6	110.58-113.00	6	40°31.77′	115°43.80′	5,400	2,12,6
K-6	115.07-117.58	6	40°34.35′	115°40.05′	5,700	2,6
I-6	125.41-127.81	6	40°39.77′	115°44.23′		2,6
H-6	138.52-140.80	6	40°46.83′	115°43.40′	5,900	1,12,6
Q-6	148.81-151.08	6	40°52.29′	115°45.78′	5,440	10,12,14
S-6	158.75-161.16	6	40°57.78′	115°45.10′		9,11,5
L-6	169.14-171.52	6	41°03.00′	115°51.57′	6,100	1,4,6
R-6	175.75-177.53	6	41°06.63′	115°45.18′	6,500	1,4,14
P-7	190.27-192.15	6	41°14.52′	115°45.75′	5,800	2,12,6
T-7	195.58-197.85	6	41°17.55′	115°46.98′		1,12,6
K-7	205.08-207.59	6	41°22.94′	115°43.39′		1,11,6
I-7	216.17-218.65	6	41°28.73′	115°48.75′		9,10,11
H-7	228.82-231.00	6	41°35.42′	115°48.60′	6,380	9,12,14
L-7	241.28-243.42	6	41°42.19′	115°47.35′	6,370	1,11,5
J-7	246.32-248.58	6	41°44.96′	115°47.98′	6,540	9,13
S-7	249.10-251.45	6	41°46.52′	115°47.69′	6,500	11,14
R-7	254.54-256.10	6	41°48.77′	115°53.25′	6,250	10,5
Q-7	265.73-267.98	6	41°55.23′	115°52.81′	6,550	9,14

TABLE 65.—*Data for the record-section of the profile from Eureka(15) to Lake Mead(22) (fig. 21)*

Station	Distance (km) (traces 1, 6)	Trace No. of coordinates and elevation	Coordinates Lat	Coordinates Long	Elevation (feet)	Traces included in section
H-4	6.97- 9.46	1	39°27.06′	115°38.75′		9,5
L-4	12.96- 15.47	1	39°23.82′	115°38.78′		10,14
I-4	19.32- 21.76	1	39°20.38′	115°38.86′		10,14
K-4	28.27- 30.54	1	39°15.66′	115°36.58′		9,14
T-4	38.48- 41.04	1	39°10.20′	115°35.53′		9,14
P-4	47.97- 50.33	1	39°05.03′	115°35.62′		9,13
J-10	76.13- 78.79	1	38°49.68′	115°38.10′		9,13
H-3	89.97- 91.74	1	38°43.17′	115°26.55′		9,11,14
Q-10	96.20- 98.52	1	38°39.36′	115°29.49′		1,12,6
L-10	108.34-110.51	1	38°32.53′	115°31.88′		2,12,6
R-10	120.45-122.20	1	38°25.83′	115°34.20′		1,11,6
P-3	128.19-130.59	1	38°23.26′	115°19.33′		9,12
P-10	133.11-135.31	1	38°18.88′	115°39.78′		1,12,6
Q-2	138.80-141.05					1,11,6
S-2	148.86-150.40	1	38°11.82′	115°19.50′		1,11,6
L-2	158.40-161.03	1	38°06.99′	115°16.77′		1,11,6
H-2	171.08-173.65	1	38°00.67′	115°12.72′		1,11,6
I-2	176.93-179.45	1	37°56.74′	115°17.11′		9,14
K-2	188.31-190.65	1	37°51.15′	115°12.69′		1,11,5
T-2	198.67-200.85	1	37°46.13′	115°08.55′		1,11,5
P-2	206.28-207.63	1	37°41.55′	115°10.75′		1,11,5
Q-1	219.77-222.75	1	37°33.69′	115°13.81′		10,12
S-1	224.63-226.67	1	37°31.82′	115°08.32′		10,12
L-1	238.43-240.97	1	37°24.85′	115°04.40′		10,12,14
H-1	248.01-249.97	1	37°19.77′	115°03.12′		9,12,14
I-1	258.58-260.76	6	37°12.65′	115°12.23′		12,10,9
K-1	266.53-268.14	1	37°08.81′	115°08.21′		9,14
T-1	277.83-279.86	1	37°01.93′	115°14.10′		10,13
P-1	285.75-287.30	1	36°59.98′	114°56.85′		9,14

TABLE 66.—*Data for the record-section of the profile from Hiko(20) to Eureka(15) (fig. 22)*

Station	Distance (km) (traces 1, 6)	Trace No. of coordinates and elevation	Coordinates Lat	Coordinates Long	Elevation (feet)	Traces included in section
I-2	4.34- 6.65	6	37°56.74′	115°17.11′		9,14
H-2	9.51- 12.09	6	38°00.67′	115°12.72′		1,14
L-2	21.40- 24.03	6	38°06.99′	115°16.77′		9,10,14
S-2	32.23- 33.61	6	38°11.82′	115°19.50′		9,12,14
P-3	51.91- 54.34	6	38°23.26′	115°19.33′		9,11,14
T-3	62.16- 63.68	6	38°28.62′	115°14.25′		9,13
K-3	73.83- 75.61	6	38°32.53′	115°31.88′		9,14
I-3	84.15- 86.44	6	38°39.30′	115°29.40′		9,12,14
H-3	90.71- 92.45	1	38°43.17′	115°26.55′		6,11,1

TABLE 67.—*Data for the record-section of the profile from Hiko(20) to Lake Mead(22) (fig. 23)*

Station	Distance (km) (traces 1, 6)	Trace No. of coordinates and elevation	Coordinates Lat	Coordinates Long	Elevation (feet)	Traces included in section
K-2	5.19- 8.23	1	37°51.15′	115°12.69′		10,5
T-2	16.87- 19.22	1	37°46.13′	115°08.55′		9,14
P-2	23.85- 25.27	1	37°41.55′	115°10.75′		9,12
Q-1	38.22- 40.66	1	37°33.69′	115°13.81′		11,14
S-1	42.20- 44.25	1	37°31.82′	115°08.32′		9,12
L-1	56.06- 58.60	1	37°24.85′	115°04.40′		9,11,14
H-1	65.63- 67.55	1	37°19.77′	115°03.12′		9,12,14
I-1	76.90- 78.99	6	37°12.65′	115°12.23′		14,11,9
K-1	84.38- 86.12	1	37°08.81′	115°08.21′		2,11,6
T-1	96.69- 98.86	1	37°01.93′	115°14.10′		2,5
P-1	103.40-104.90	1	36°59.98′	114°56.85′		9,13

TABLE 68.—*Data for the record-section of the profile from Lake Mead(22) to Eureka(15) (fig. 24)*

Station	Distance (km) (traces 1, 6)	Trace No. of coordinates and elevation	Coordinates Lat	Coordinates Long	Elevation (feet)	Traces included in section
P-7	19.50- 21.85	6	36°16.17′	114°53.61′		1,6
K-7	40.13- 40.62	1	36°26.89′	114°52.81′		6,1
I-7	53.90- 54.73	6	36°34.78′	114°45.05′		1,14
H-7	58.82- 60.03	6	36°37.63′	114°51.68′		1,6
L-7	74.92- 76.44	6	36°46.61′	114°48.09′		1,5
S-7	78.14- 80.09	6	36°48.49′	114°51.49′		1,6
Q-7	88.90- 91.20	6	36°54.37′	114°53.72′		3,6
P-8	100.35-102.03	6	36°59.98′	114°56.85′		1,6
T-8	110.10-111.80	6	37°01.93′	115°14.10′		2,5
K-8	119.89-121.31	6	37°08.81′	115°08.21′		2,6
I-8	127.50-129.74	6	37°12.65′	115°12.23′		1,5
H-8	137.59-139.61	6	37°19.77′	115°03.12′		1,11,6
L-8	146.64-149.19	6	37°24.85′	115°04.40′		1,12,6
S-8	160.88-162.90	6	37°31.82′	115°08.32′		3,13,6
Q-8	165.06-167.98	1	37°33.69′	115°13.81′		5,11,1
P-9	179.90-181.25	6	37°41.55′	115°10.75′		1,12,6
T-9	186.90-189.02	6	37°46.13′	115°08.55′		1,12,6
K-9	196.88-199.23	6	37°51.15′	115°12.69′		1,6
I-9	280.11-210.64	6	37°56.74′	115°17.11′		1,11,6
H-9	213.97-216.56	6	38°00.67′	115°12.72′		1,12,6
L-9	226.50-229.13	6	38°06.99′	115°16.77′		1,12,6
S-9	237.17-238.67	6	38°11.82′	115°19.50′		3,12,5
Q-9	246.49-248.72					1,11,5
P-10	256.99-259.40	6	38°23.26′	115°19.33′		1,11,6
T-10	266.69-267.97	6	38°28.62′	115°14.25′		1,11,5
K-10	278.01-279.99	6	38°32.53′	115°31.88′		1,12,6
I-10	289.04-291.39	6	38°39.30′	115°29.40′		1,12,6
H-10	295.81-297.55	6	38°43.17′	115°26.55′		1,12,6

TABLE 69.—*Data for the record-section of the profile from Lake Mead(22) to Mono Lake(6) (fig. 26)*

Station	Distance (km) (traces 1, 6)	Trace No. of coordinates and elevation	Coordinates Lat	Coordinates Long	Elevation (feet)	Traces included in section
T-6	24.01- 26.35	1	36°12.59′	115°01.19′	1,860	9,13
S-6	29.79- 32.26	1	36°13.56′	115°05.00′	1,900	1,6
Q-6	37.78- 40.19	1	36°13.46′	115°11.04′	2,200	1,5
P-6	50.45- 52.62	1	36°19.17′	115°16.93′	2,600	1,6
L-6	60.88- 63.33	1	36°23.57′	115°21.75′	2,840	2,6
I-6	68.02- 70.44	1	36°29.53′	115°22.12′	3,350	3,6
K-6	69.75- 71.09	1	36°21.86′	115°29.77′	2,880	1,6
H-6	77.70- 79.92	1	36°30.12′	115°29.82′	3,200	9,13
T-5	88.62- 90.58	6	36°27.41′	115°40.45′	5,150	13,9
S-5	103.34-105.74	1	36°34.65′	115°46.71′	3,900	9,14
Q-5	109.02-111.49	5	36°32.76′	115°52.40′	3,960	14,1
P-5	115.92-116.19	6	36°33.12′	115°57.35′	4,000	14
L-5	131.28-133.23	1	36°33.14′	116°08.64′	2,600	9,6
K-5	139.71-142.16	6	36°32.57′	116°15.00′	2,500	14,10
I-5	149.99-152.49	1	36°34.20′	116°21.60′	2,500	1,6
T-4	160.30-162.50	1	36°36.69′	116°29.40′	2,500	1,12,14
S-4	169.07-171.27	1	36°39.44′	116°32.81′	2,520	1,11,6
Q-4	180.76-182.63	1	36°48.80′	116°36.28′	3,300	1,11,6
P-4	189.78-191.82	1	36°52.99′	116°40.46′	4,400	9,3,6
L-4	200.22-202.34	1	36°55.81′	116°46.56′		1,11,6
K-4	209.92-212.40	1	36°57.12′	116°53.06′	4,380	1,12,6
I-4	224.17-226.21	1	37°03.81′	116°59.55′	4,300	11,14
T-3	233.13-235.18	1	37°08.80′	117°03.02′	4,100	1,11,6
S-3	240.77-243.37	1	37°12.80′	117°06.09′	4,000	1,14
P-3	252.68-255.36	1	37°15.15′	117°13.70′	6,000	9,14
L-10	263.40-263.70	1	37°18.77′	117°19.69′	6,400	10
K-3	275.62-278.06	6	37°19.44′	117°28.49′	5,600	6,12,2
I-3	278.14-279.71	1	37°17.55′	117°31.72′	4,510	12
S-2	282.28-284.35	1	37°19.66′	117°33.48′	5,500	9,12
T-2	288.33-290.60	1	37°22.43′	117°36.26′	7,100	9,14
Q-3	299.97-302.40	1	37°26.99′	117°42.10′	6,000	9,13
P-2	307.56-310.17	1	37°27.07′	117°47.93′	5,300	9,14
L-2	311.93-314.46	1	37°28.24′	117°50.50′	5,140	10,14
K-2	325.99-328.03	1	37°33.04′	117°58.08′	5,120	10,14

TABLE 70.—*Data for the record-section of the profile from Lake Mead(22) to Santa Monica Bay(4) (fig. 27)*

Station	Distance (km) (traces 1, 6)	Trace No. of coordinates and elevation	Coordinates Lat	Coordinates Long	Elevation (feet)	Traces included in section
T-1	2.0 - 4.4	1	36°04.66'	114°49.68'	1,470	2,6
S-1	17.7 - 20.2	6	35°58.93'	114°59.04'	2,330	1,6
R-1	22.8 - 25.2	1	36°01.82'	115°02.86'	2,000	1,6
Q-1	35.4	1	35°58.23'	115°11.09'	2,500	1
P-1	50.0 - 52.2	6	35°50.24'	115°15.71'	3,030	6,3
L-1	60.2 - 62.7	1	35°46.32'	115°20.60'	2,930	1,5
K-1	65.2 - 67.7	1	35°44.70'	115°23.24'	2,930	4,6
J-1	75.9 - 78.3	1	35°41.94'	115°29.58'	3,170	1,6
I-1	88.9 - 91.1	1	35°38.30'	115°36.68'	3,470	1,6
H-1	98.8 -101.3	1	35°33.25'	115°40.75'	3,600	2,5
T-2	106.7 -109.2	6	35°31.85'	115°48.10'	3,500	2,4
S-2	118.9 -121.3	6	35°24.94'	115°53.18'	3,470	2,6
Q-2	140.0 -142.5	6	35°23.47'	116°07.44'	930	1,5
P-2	149.9 -151.9	6	35°22.98'	116°14.43'	1,400	2,14
L-2	163.1 -165.6	6	35°15.70'	116°19.44'	1,970	10,13
J-2	174.3 -176.7	6	35°05.46'	116°19.16'	1,330	10,14
I-2	183.3 -185.8	6	35°05.36'	116°26.80'	1,900	1,11,6
T-3	209.0 -211.3	6	35°02.22'	116°45.80'	1,730	1,4
H-2	211.5 -213.4	6	35°01.58'	116°45.80'	1,770	2,12,6
S-3	226.8 -229.2	6	34°59.86'	116°56.85'	2,670	1,6
R-3	223.2 -235.7	6	34°55.33'	116°58.38'	2,330	9,14
Q-3	247.3 -249.8	6	34°49.02'	117°04.32'	2,600	9,14
P-3	259.1 -261.5	6	34°49.72'	117°13.44'	2,630	9,14
L-3	268.8 -271.2	1	34°45.68'	117°18.00'	2,630	14,9
K-3	277.5 -279.7	6	34°42.02'	117°22.28'	2,730	9,13
J-3	283.9 -286.4	6	34°39.21'	117°25.26'	2,770	11,14
I-3	293.3 -295.8	1	34°37.06'	117°29.60'	2,830	9,14
H-3	303.7 -306.1	6	34°37.73'	117°39.60'	2,900	10,14

TABLE 71.—*Data for the record-section of the profile from Kingman(26) to NTS(19) (fig. 29)*

Station	Distance (km) (traces 1, 6)	Trace No. of coordinates and elevation	Coordinates Lat	Coordinates Long	Elevation (feet)	Traces included in section
S-2	7.13- 8.71	6	35°22.28'	114°06.99'		1,6
Q-2	14.27- 15.31	6	35°24.44'	114°11.90'		1,5
P-2	29.23- 31.13	6	35°32.75'	114°16.39'		9,14
H-2	35.47- 37.29	6	35°33.65'	114°21.31'		11,14
K-2	45.89- 48.35	6	35°39.23'	114°24.70'		9,14
I-2	56.52- 58.88	6	35°44.60'	114°27.67'		9,13
S-1	78.80- 81.30	6	35°54.16'	114°36.82'		1,5
Q-1	87.59- 90.00	6	35°57.95'	114°40.25'		1,5
H-1	95.92- 97.59	6	36°01.74'	114°42.46'		9,14
K-4	101.94-103.83	6	36°02.14'	114°48.49'		9,14
P-4	106.16-108.19	6	36°04.65'	114°49.33'		1,11,6
T-1	120.76-121.69	6	36°08.82'	114°57.16'		1,12,6
K-1	125.59-127.99	6	36°14.57'	114°55.14'		1,11,5
I-1	135.18-137.29	6	36°18.25'	114°59.42'		9,11
Q-4	141.05-143.48	6	36°13.91'	115°11.63'		1,11,14
S-4	151.44-153.80	6	36°18.60'	115°15.59'		9,13
T-3	163.55-165.80	6	36°26.39'	115°17.08'		9
S-3	164.34-166.24	6	36°31.50'	115°09.86'		10,14
L-4	171.26-173.70	6	36°28.22'	115°22.43'		9,14
Q-3	186.18-187.81	6	36°39.56'	115°20.58'		10,13
P-3	196.75-198.92	6	36°48.73'	115°17.65'		9,14
L-3	205.15-207.63	6	36°54.37'	115°17.64'		9,14
K-3	223.57-226.37	6	37°09'	115°12.0'		1,14
J-4	249.66-251.17					9,13
I-4	256.76-258.60	6	37°03.00'	115°59.72'		9,14
H-3	262.54-264.48	6	36°54.4'	115°17.7'		9,11,14
R-4	265.52-267.80	6	37°08.65'	116°01.18'		9,13
T-4	277.20-279.41	6	37°11.45'	116°09.00'		10,13

TABLE 72.—*Data for the record-section of the profile from NTS(19) to Ludlow(25) (fig. 30)*

Station	Distance (km) (traces 1, 6)	Trace No. of coordinates and elevation	Coordinates Lat	Coordinates Long	Elevation (feet)	Traces included in section
R-55	66.29- 68.75	1	36°31.80'	116°08.50'	2,590	11
K-55	84.17- 86.74	1	36°23.50'	116°18.08'	2,240	2,6
Q-55	103.23-105.36	6	36°10.50'	116°07.17'	2,590	6
P-55	129.72-132.05	1	35°58.03'	116°16.13'	1,520	1,5
J-52	140.25-142.28	1	35°47.53'	116°05.70'	2,290	2,6
J-55	147.40-149.70	1	35°47.70'	116°05.82'	2,290	2,6
K-52	154.85-157.25	1	35°40.60'	116°17.93'	510	2,6
P-52	169.85-172.29	1	35°31.75'	116°10.78'	760	2,6
J-51	186.71-188.50	1	35°21.75'	116°06.30'	910	2,4
I-52	207.89-209.96	1	35°10.97'	116°07.05'	970	1,4
I-51	208.25-210.65	6	35°08.80'	116°06.38'	970	6
S-52	214.87-217.18	6	35°07.20'	116°07.28'	1,120	5,1
T-52	232.51-235.00	1	34°57.80'	116°11.10'	1,370	1,5
L-51	246.89-249.02	1	34°49.36'	116°11.02'	1,320	10,6
P-51	264.29-266.42	1	34°39.85'	116°09.00'	1,930	9,4
S-56	315.17-317.36	1	34°11.96'	115°57.60'	1,730	10,6

TABLE 73.—*Data for the record-section of the profile from Ludlow(25) to NTS(19) (fig. 31)*

Station	Distance (km) (traces 1, 6)	Trace No. of coordinates and elevation	Coordinates Lat	Coordinates Long	Elevation (feet)	Traces included in section
P-4	3.00- 5.48	6	34°52.29'	116°11.56'	1,370	1,6
L-4	13.48- 15.98	6	34°58.00'	116°11.09'	1,370	1,6
K-4	32.48- 34.78	6	35°07.78'	116°06.38'	970	1,6
T-4	36.80- 39.11	6	35°10.17'	116°06.40'	970	1,6
Q-4	39.51- 41.08	6	35°11.40'	116°07.61'	970	6
R-4	51.70- 53.98	6	35°18.12'	116°04.91'	910	1,6
J-4	58.82- 60.30	6	35°21.74'	116°06.29'	910	1,6
S-4	66.40- 68.47	6	35°26.36'	116°09.19'	760	1,5
H-4	75.91- 78.31	6	35°31.71'	116°10.72'	760	1,6
I-4	85.11- 87.07	6	35°36.35'	116°14.75'	760	1,6
P-5	93.73- 96.20	6	35°41.10'	116°17.64'	510	3,14
L-5	105.87-108.13	6	35°47.68'	116°05.77'	2,290	1,5
K-5	110.24-112.46	6	35°50.14'	116°08.39'	2,030	2,6
T-5	120.85-123.24	6	35°55.89'	116°15.87'	1,520	1,5
Q-5	132.12-134.60	6	36°02.15'	116°11.40'	3,150	1,5
R-5	140.90-143.38	6	36°06.90'	116°10.90'	2,740	1,12,6
J-5	150.15-152.25	6	36°11.66'	116°08.02'	2,590	2,6
S-5	157.38-159.75	6	36°15.75'	116°10.08'	2,590	2,12,6
H-5	166.96-169.28	6	36°20.67'	116°02.97'	3,050	1,12,14
I-5	176.05-178.51	6	36°25.74'	116°04.26'	3,400	2,12,6
P-6	184.32-186.70	6	36°30.30'	116°08.34'	2,540	1,11,14
L-6	197.80-199.93	6	36°37.26'	116°02.64'	3,300	1,13
K-6	201.15-202.54	6	36°38.80'	116°05.70'	3,860	11,6
R-6	211.89-213.81	6	36°44.70'	116°01.11'	3,450	10,14
T-6	228.59-230.99	6	36°54.27'	116°10.37'	4,780	10,13
J-6	241.70-244.16	6	37°01.30'	116°04.97'	4,170	9,14
I-6	249.59-252.09	6	37°05.64'	116°07.12'	4,470	9,13
H-6	257.64-259.74	1	37°08.59'	116°04.93'	4,520	9,12

TABLE 74.—*Data for the record-section of the profile from Mojave(23) to Ludlow(25) (fig. 35)*

Station	Distance (km) (traces 1, 6)	Trace No. of coordinates and elevation	Coordinates Lat	Coordinates Long	Elevation (feet)	Traces included in section
L-1	9.77- 12.13	6	35°05.24'	117°52.82'	5,900	2,6
P-1	19.68- 22.16	6	35°04.33'	117°45.84'	6,000	1,6
I-2	30.15- 32.52	6	35°03.45'	117°38.95'	2,540	2,6
S-2	48.74- 51.21	6	35°01.61'	117°26.70'	2,430	2,6
J-2	58.49- 61.11	6	34°58.86'	117°20.48'	2,200	1,6
R-2	69.34- 71.36	6	34°57.49'	117°13.91'	2,170	1,6
Q-2	77.14- 79.59	6	34°57.95'	117°08.38'	2,170	9,13
T-2	87.95- 89.88	6	34°55.85'	117°01.91'	2,400	1,11,6
K-2	98.41-100.80	6	34°55.51'	116°54.72'	2,100	1,4
L-2	109.50-111.79	6	34°57.25'	116°47.19'	2,400	2,6
P-2	124.21-126.74	6	34°59.53'	116°37.17'	1,770	9,14
I-3	128.29-130.75	6	34°53.65'	116°35.18'	1,800	9,12
H-3	140.21-142.14	6	34°53.75'	116°27.62'	2,300	9,14
S-3	150.04-152.17	6	34°47.94'	116°22.10'	2,200	9,14
J-3	163.25-165.32	6	34°50.49'	116°12.82'	1,540	9,14
R-3	170.50-171.79	6	34°48.48'	116°08.91'	1,340	9,13
Q-3	184.75-186.83	6	34°37.80'	116°01.65'	1,280	9,14
T-3	190.85-193.40	6	34°36.25'	115°57.71'	1,100	9,12
K-3	207.25-209.49	6	34°40.91'	115°45.51'	2,600	9,13
L-3	214.12-216.59	6	34°39.58'	115°41.10'	2,100	9,14
P-3	227.10-229.64	6	34°41.09'	115°32.01'	2,300	9,14

TABLE 75.—*Data for the record-section of the profile from NTS(19) to Navajo Lake(21) (fig. 41)*

Station	Distance (km) (traces 1, 6)	Trace No. of coordinates and elevation	Coordinates Lat	Coordinates Long	Elevation (feet)	Traces included in section
I-28	52.6 - 54.7	1	37°22.70'	115°31.95'	4,400	1,6
J-26	86.0 - 88.5	1	37°16.55'	115°06.35'	3,400	9,12
J-28	103.6 -106.1	1	37°19.75'	114°53.75'	4,600	9,14
Q-28	123.1 -124.8	1	37°14.65'	114°39.25'	3,900	1,6
L-28	132.1 -134.2	1	37°18.20'	114°34.45'	4,000	2,5
Q-26	171.6 -174.1	1	37°32.40'	114°11.85'	5,400	1,6
P-28	187.1 -189.0	1	37°37.55'	114°01.00'	6,000	1,5
I-23	204.60-204.64	1	37°49.80'	113°56.35'	5,700	9
S-26	222.6 -224.8	1	37°25.10'	113°34.10'	6,000	9,13
I-24	255.0 -257.5	1	37°36.10'	113°14.03'	5,500	10,13
J-24	298.8 -300.9	6	37°52.90'	112°46.95'	5,780	9,14
S-28	319.6 -322.1	1	37°37.65'	112°28.85'	7,000	1,6
L-24	356.3 -358.8	1	37°37.45'	112°04.50'	6,400	9,12
T-28	387.9 -389.9	1	37°45.70'	111°43.45'	6,500	10,14
Q-24	409.1 -411.6	1	37°44.88'	111°29.48'	6,000	9,13

TABLE 76.—*Data for the record-section of the profile from Navajo Lake(21) to NTS(19) (fig. 42)*

Station	Distance (km) (traces 1, 6)	Trace No. of coordinates and elevation	Coordinates Lat	Coordinates Long	Elevation (feet)	Traces included in section
P-2	2.48- 3.38	6	37°31.66'	112°49.57'		2,4,6
H-2	15.08- 16.39	6	37°30.97'	112°58.50'		1,6
R-2	23.57- 25.80	6	37°32.16'	113°05.06'		1,6
J-2	34.86- 37.46	6	37°33.45'	113°12.96'		1,14
T-2	40.35- 42.79	6	37°28.94'	113°16.24'		14
S-2	55.94- 58.26	6	37°33.51'	113°27.09'		9,14
K-1	67.01- 69.42	6	37°31.35'	113°34.65'		10,14
Q-1	71.52- 74.04	6	37°24.96'	113°36.87'		9,11,14
I-2	85.00- 86.73	6	37°31.00'	113°46.39'		10,14
L-1	94.77- 96.70	6	37°29.80'	113°53.09'		9,13
P-1	104.15-105.91	6	37°37.20'	113°59.25'		9,14
H-1	116.39-118.65	6	37°32.70'	114°08.10'		10,13
R-1	125.68-127.37	6	37°29.22'	114°13.89'		9,12,14
J-1	143.76-144.80	6	37°28.34'	114°25.87'		9,13
T-1	155.13-156.97	6	37°19.80'	114°32.76'		10,14
K-3	167.56-169.35	6	37°26.88'	114°42.23'		9,12
Q-3	176.47-178.71	1	37°26.97'	114°48.60'		13,10
I-3	186.15-188.63	6	37°25.93'	114°55.25'		9,12
L-3	195.04-197.34	6	37°22.95'	115°00.84'		9,11,14
P-3	203.45-205.79	6	37°20.76'	115°06.30'		9,11,13
H-3	214.27-216.77	6	37°21.28'	115°13.85'		9,11,13
R-3	230.18-230.31	6	37°25.35'	115°23.53'		11
J-3	236.85-239.32	6	37°23.25'	115°29.44'		9,12,14
T-3	248.16-250.54	6	37°20.90'	115°36.80'		10,12,14

TABLE 77.—*Data for the record-section of the profile from NTS(19) to Elko(14) (fig. 43)*

Station	Distance (km) (traces 1, 6)	Trace No. of coordinates and elevation	Coordinates Lat	Coordinates Long	Elevation (feet)	Traces included in section
P-33	68.03- 70.30	1	37°43.17'	115°53.22'	5,300	1,5
J-33	97.74-100.27	1	37°59.90'	115°59.50'	4,700	1,11,6
T-33	116.32-118.61	1	38°09.78'	115°55.83'	5,100	1,4,13
R-38	138.84-141.25	1	38°22.05'	115°51.83'	4,850	3,6
Q-33	157.62-160.19	1	38°31.55'	115°46.66'	4,800	1,11,6
S-33	186.45-189.04	1	38°46.24'	115°38.87'	5,200	9,14
P-31	205.95-208.46	1	39°02.93'	115°45.00'	5,900	9,13
L-33	215.80-218.29	1	39°02.93'	115°46.00'	5,900	1,11,5
Q-38	235.02-237.31	1	39°14.4'	115°41.0'	6,500	2,12,5
I-33	248.45-250.88	1	39°20.90'	115°47.52'	6,000	1,11,5
Q-43	256.94-259.42	1	39°20.90'	115°47.52'	6,000	10,14
Q-44	262.09-264.58	1	39°20.90'	115°47.52'	6,000	2,14
P-38	276.56-278.75	1	39°36.25'	115°45.44'	5,870	1,6
J-31	301.89-304.37	1	39°55.24'	115°44.31'	6,100	9,13
J-38	327.72-330.25	1	40°04.1'	115°47.0'	6,000	1,11,6
P-45	367.81-370.05	6	40°30.05'	115°43.30'	5,400	9,12
T-45	370.71-373.17	6	40°31.77'	115°43.80'	5,400	9,14
K-45	375.93-378.36	6	40°34.35'	115°40.05'	5,700	1,6
T-31	381.08-383.34	1	40°38.30'	115°43.51'	5,200	9,13
I-45	385.62-387.89	6	40°39.77'	115°44.23'		9,13
P-45+X	394.20-396.64	6	40°38.30'	115°43.51'	5,300	1,6
H-45	398.66-401.01	6	40°46.83'	115°43.40'	5,900	9,14
Q-45	408.75-410.87	6	40°52.29'	115°45.78'	5,440	2,6
S-45	418.77-421.07	6	40°57.78'	115°45.10'		9,5
L-45	427.95-430.27	6	41°03.00'	115°51.57'	6,100	1,6
R-45	435.65-437.42	6	41°06.63'	115°45.18'	6,500	1,6

TABLE 78.—*Data for the record-section of the profile from NTS(19) to San Luis Obispo(3) (fig. 44))*

Station	Distance (km) (traces 1, 6)	Trace No. of coordinates and elevation	Coordinates Lat	Coordinates Long	Elevation (feet)	Traces included in section
L-3	2.70- 5.15	6	37°16.93'	115°57.52'	4,000	1,4
L-2	24.60- 26.83	6	37°06.36'	116°05.77'	4,300	9,11,14
K-3	36.00- 38.49	6	37°02.46'	116°12.12'	5,000	1,4,14
S-3	77.40- 79.93	6	36°57.36'	116°41.87'	3,800	1,4
R-3	78.50- 80.97	6	36°56.30'	116°41.95'	3,500	5
T-3	89.95- 92.50	1	36°54.98'	116°47.94'	4,000	1,11,6
P-3	106.52-109.00	1	36°50.30'	116°57.47'	4,400	1,5
T-2	125.40-127.42	1	36°47.36'	117°11.40'	400	6,12,2
I-5	132.96-134.50	1	36°23.80'	117°16.80'	4,800	9
J-3	134.48-136.50	1	36°41.46'	117°12.85'	80	2,12,6
S-2	157.57-159.60	1	36°36.84'	117°27.40'	5,000	1,14
I-3	158.04-159.60	1	36°23.76'	117°16.79'	4,700	3
Q-29	172.74-174.90	1	36°27.15'	117°48.75'	4,000	9,11
Q-30	174.21-176.58	1	36°28.65'	117°49.58'	4,300	11,14
R-2	183.83-185.80	6	36°29.02'	117°42.14'	6,200	14,10
K-5	189.13-191.10	1	36°12.15'	117°52.00'	4,600	10,13
J-2	194.06-196.10	1	36°27.24'	117°48.76'	4,000	10,12
L-4	195.90-198.41	6	36°19.24'	117°46.71'	4,700	12,9
Q-2	199.50-201.97	6	36°23.34'	117°52.10'	3,700	10,13
I-2	208.50-211.01	6	36°19.66'	117°56.42'	3,660	9,14
P-2	212.65-214.65	6	36°22.60'	118°01.33'	3,600	9
K-4	213.04-215.00	1	36°12.15'	117°52.00'	4,600	10,14
J-29	219.62-221.86	1	36°00.35'	118°06.65'	6,000	9,12,14
Q-3	221.58-223.60	1	36°16.24'	118°02.12'	4,400	13
L-29	255.27-257.50	1	36°11.25'	118°40.30'	3,500	9,11,14
J-5	272.15-274.65	1	36°01.70'	118°47.70'	900	9,13
I-4	275.00-276.46	6	36°11.30'	118°40.64'	3,600	10,14
L-30	281.38-283.69	1	36°01.90'	118°53.09'	1,000	9,11,13
P-5	290.29-292.50	1	35°56.15'	118°57.80'	600	10,13
P-29	302.26-304.63	1	35°52.60'	119°04.20'	500	10,12
Q-5	320.81-323.10	1	35°51.75'	119°17.70'	260	9,13
Q-37	335.42-337.43	1	35°42.70'	119°22.40'	250	9,13
J-30	351.67-354.20	1	35°34.40'	119°27.90'	250	9,14
P-30	365.95-367.15	1	35°38.70'	119°41.60'	300	9,14
I-30	378.29-380.30	1	35°41.70'	119°52.60'	575	9,14
T-5	387.34-389.80	1	35°35.55'	119°57.10'	1,000	11
S-30	404.51-407.00	1	35°28.70'	120°04.00'	2,250	9,14
H-5	437.14-439.14	1	35°20.15'	120°24.50'	1,350	9,12
R-37	455.34-457.85	1	35°14.00'	120°33.50'	1,000	1,6
T-37	475.46- 477.01	1	35°18.65'	120°51.20'	100	9

TABLE 79.—*Data for the record-section of the profile from Shasta Lake(5) to Mono Lake(6) (fig. 46)*

Station	Distance (km) (traces 1, 6)	Trace No. of coordinates and elevation	Coordinates Lat	Coordinates Long	Elevation (feet)	Traces included in section
I-4	10.80- 13.05	1	40°43.34'	122°07.21'	1,400	1
H-4	20.28- 22.61	6	40°33.97'	122°13.11'	500	6
S-4	33.14- 35.11	1	40°30.85'	122°01.75'	1,600	1,6
J-4	39.99- 42.22	6	40°29.20'	121°53.91'	3,400	1
R-4	50.57- 52.69	1	40°25.69'	121°50.19'	2,900	1,6
Q-4	58.83- 60.81	1	40°22.10'	121°46.69'	3,000	10,14
T-4	70.60- 72.78	1	40°16.19'	121°43.01'	4,200	1,6
K-4	80.48- 82.20	1	40°10.61'	121°41.15'	3,600	1,5
L-4	92.02- 94.35	1	40°09.03'	121°30.64'	5,200	1,6
P-4	100.49-102.70	1	40°06.36'	121°25.60'	5,900	1,6
I-3	107.71-110.00	1	40°01.75'	121°24.73'	6,700	2,6
S-3	126.31-127.89	1	39°53.91'	121°16.56'	4,800	9,14
J-3	137.06-139.25	1	39°50.51'	121°10.11'	5,600	1,6
R-3	150.32-152.17	1	39°43.62'	121°06.30'	5,300	1,6
T-3	169.33-170.33	1	39°36.30'	120°56.89'	4,600	1,6
K-3	174.83-176.57	1	39°35.90'	120°51.60'	5,000	1,6
L-3	184.09-185.99	1	39°30.64'	120°49.57'	5,700	2,6
P-3	197.89-199.33	1	39°25.99'	120°41.79'	6,000	9,14
I-2	208.48-209.64	1	39°20.24'	120°39.12'	4,800	9,14
H-2	214.47-216.10	1	39°18.95'	120°34.63'	6,000	9,14
S-2	228.96-230.69	1	39°10.61'	120°31.78'	6,400	9,14
J-2	235.77-237.24	1	39°10.76'	120°24.18'	5,800	9,14
R-2	249.43-250.72	1	39°02.23'	120°22.50'	6,200	9,14
Q-2	255.87-258.06	1	38°56.84'	120°24.08'	5,400	9,14
K-2	279.05-281.15	1	38°54.41'	120°02.60'	6,700	9,14
L-2	287.20-289.29	1	38°49.46'	120°01.30'	6,400	9,14
H-1	316.96-318.56	1	38°41.12'	119°42.32'	6,800	9,13
S-1	322.86-325.04	1	38°36.91'	119°42.22'	6,400	10,13
J-1	336.99-338.67	1	38°33.36'	119°32.70'	7,500	9,14
R-1	346.56-348.20	1	38°28.80'	119°29.30'	6,400	9,14
K-1	376.60-378.28	1	38°14.04'	119°19.40'	6,800	9,14
L-1	385.82-387.74	1	38°11.74'	119°13.12'	6,800	10,14
P-1	403.10-405.52	1	38°06.19'	119°03.22'	6,640	9,13

TABLE 80.—*Data for the record-section of the profile from Mono Lake(6) to Shasta Lake(5) (fig. 47)*

Station	Distance (km) (traces 1, 6)	Trace No. of coordinates and elevation	Coordinates Lat	Coordinates Long	Elevation (feet)	Traces included in section
P-8	13.46- 14.76	6	38°06.19'	119°03.22'	6,640	1,6
L-8	22.54- 24.91	6	38°11.74'	119°13.12'	6,800	1,6
K-8	30.93- 32.74	6	38°14.04'	119°19.40'	6,800	1,6
T-8	45.03- 46.76	1	38°19.40'	119°26.50'	7,600	1,6
R-8	61.63- 63.58	6	38°26.60'	119°29.30'	6,400	1,6
J-8	71.38- 73.35	1	38°32.10'	119°32.74'	7,500	1
T-1A	76.01- 77.76	1	38°37.60'	119°24.76'		1,6
S-8	84.20- 86.41	6	38°36.91'	119°42.22'	6,400	2,6
H-8	91.24- 92.91	8	38°41.12'	119°42.32'	6,800	6
L-1A	98.10- 97.99	1	38°39.97'	119°48.14'	6,000	1,6
I-8	101.26-103.06	1	38°39.09'	119°54.90'	7,800	2,6
P-9	108.21-110.68	1	38°44.38'	119°54.50'	7,800	1,6
L-9	119.67-121.76	6	38°49.46'	120°01.30'	6,400	1,6
P-1A	128.03-130.03	1	38°53.55'	120°01.74'	6,600	1,6
T-9	150.46-151.45	1	38°54.23'	120°23.50'	5,600	1,6
R-9	158.86-159.81	6	39°02.23'	120°22.50'	6,200	1,6
J-9	171.71-173.19	6	39°10.76'	120°24.18'	5,800	9,6
S-9	176.45-180.27	6	39°10.61'	120°31.78'	6,400	2,6
H-2	192.85-194.48	6	39°18.95'	120°34.63'	6,000	9,6
I-9	199.45-200.54	1	39°19.23'	120°39.43'	4,800	2
P-10	209.63-211.06	6	39°25.99'	120°41.79'	6,000	1,6
L-10	222.97-224.89	6	39°30.64'	120°49.57'	5,700	1,5
K-10	232.39-234.14	6	39°35.90'	120°51.80'	5,000	1,6
T-10	236.76-239.69	6	39°36.30'	120°56.89'	4,600	2,5
Q-10	248.57-250.44	1	39°40.58'	121°00.01'	5,500	1,4
R-10	256.88-258.76	6	39°43.62'	121°06.30'	5,300	1,6
J-10	269.71-271.90	6	39°50.51'	121°10.11'	5,600	1,14
S-10	281.11-282.71	6	39°53.91'	121°16.58'	4,800	2,6
I-10	298.99-301.28	6	40°01.75'	121°24.73'	6,700	1,6
P-11	306.31-308.50	6	40°06.36'	121°25.60'	5,900	9,14
L-11	314.61-316.94	8	40°09.03'	121°30.64'	5,200	9,14
K-11	327.30-329.14	6	40°10.61'	121°41.15'	3,600	1,6
Q-11	348.15-350.14	8	40°22.10'	121°46.89'	3,000	1,13
R-11	356.28-358.40	6	40°25.69'	121°50.19'	2,900	9,14
I-11	396.61-398.79	6	40°43.34'	122°07.21'	1,400	1,6

TABLE 81.—*Data for the record-section of the profile from Mono Lake(6) to China Lake(8) (fig. 48)*

Station	Distance (km) (traces 1, 6)	Trace No. of coordinates and elevation	Coordinates Lat	Coordinates Long	Elevation (feet)	Traces included in section
I-12	10.78- 12.90	1	37°54.71'	119°02.62'	7,000	2,6
H-12	20.12- 22.29	1	37°52.12'	118°56.97'	7,700	1,6
S-12	28.32- 30.58	1	37°46.34'	118°56.74'	7,400	1,6
J-12	37.10- 38.62	6	37°39.58'	118°57.94'	7,900	3,6
R-12	42.57- 44.96	1	37°43.12'	118°48.60'	6,840	9,14
Q-12	67.01- 69.27	1	37°31.41'	118°38.04'	6,300	9,13
T-12	68.33- 70.62	6	37°30.10'	118°36.19'	6,400	5
K-12	81.93- 83.44	1	37°23.32'	118°34.58'	5,200	9,13
L-12	87.83- 89.84	1	37°18.46'	118°36.51'	7,700	1,6
S-7	104.84-107.20	1	37°12.00'	118°27.80'	9,900	9,4
P-12	109.18-111.48	1	37°12.99'	118°21.14'	4,050	10,14
Q-7	116.74-118.18	1	37°09.22'	118°18.87'	4,200	1,4
R-7	128.32-130.77	6	37°01.92'	118°15.25'	4,300	5
I-7	137.45-139.57	1	36°58.15'	118°14.09'	3,840	9,14
H-7	152.27-154.13	1	36°47.00'	118°17.39'	5,800	9,14
K-7	159.68-161.90	1	36°46.37'	118°05.39'	3,840	1,6
L-7	162.93-163.45	6	36°43.12'	118°11.57'	4,200	5
J-7	170.30-170.76	1	36°40.58'	118°07.20'	4,200	9,14
P-7	178.38-180.68	1	36°35.67'	118°06.87'	4,650	2,13
S-6	188.93-191.23	1	36°29.76'	118°05.45'	6,000	1,6
Q-6	199.90-202.33	1	36°29.33'	117°52.15'	3,620	11
R-6	211.41-211.66	1	36°20.39'	117°55.40'	3,660	1,6
I-6	217.24-219.68	1	36°15.15'	117°59.09'	3,710	11,14
T-6	226.41-228.66	1	36°11.89'	117°53.84'	4,400	1,6
S-13	227.99-230.25	6	36°09.67'	117°53.31'	4,600	14
L-6	240.46-242.17	1	36°05.19'	117°49.22'	5,000	2
H-6	247.08-247.78	1	35°59.24'	117°53.82'	3,360	11
K-6	259.29-261.58	1	35°51.66'	117°54.72'	3,400	9,6
J-6	269.77-272.21	1	35°47.95'	117°47.81'	2,270	9,14
P-6	279.16-281.49	1	35°44.10'	117°43.36'	2,190	10,13
H-13	294.11-296.35	1	35°36.38'	117°40.15'	2,360	9,12,14
I-13	308.45-310.74	1	35°24.63'	117°49.23'	2,500	2,5

TABLE 82.—*Data for the record-section of the profile from China Lake(8) to Mono Lake(6) (fig. 49)*

Station	Distance (km) (traces 1, 6)	Trace No. of coordinates and elevation	Coordinates Lat	Coordinates Long	Elevation (feet)	Traces included in section
J-1	3.63- 4.66	6	35°47.98'	117°47.81'	2,270	1,6
P-1	5.88- 8.23	1	35°44.10'	117°43.36'	2,190	1,5
K-1	15.55- 16.99	6	35°51.61'	117°54.72'	3,400	1,5
H-1	25.89- 28.27	6	35°59.24'	117°53.82'	3,360	2,5
L-1	32.45- 34.24	6	36°05.19'	117°49.22'	5,000	1,2,3,5,6
T-1	45.43- 47.84	6	36°11.89'	117°53.84'	4,400	4
I-1	53.82- 56.22	6	36°15.15'	117°59.09'	3,710	1,3,6
R-1	62.87- 63.71	6	36°20.39'	117°55.40'	3,660	1,3,6
Q-1	76.91- 79.02	6	36°29.33'	117°52.15'	3,620	2,6
S-1	82.54- 84.84	6	36°29.76'	118°05.45'	6,000	1,6
P-2	93.41- 95.81	6	36°35.67'	118°06.87'	4,650	9,14
J-2	103.65-104.54	6	36°40.58'	118°07.20'	4,200	1,8
L-2	111.07-111.15	6	36°43.52'	118°10.04'	4,200	4
K-2	115.12-117.55	6	36°48.37'	118°05.39'	3,840	1,5
H-2	119.51-121.24	6	36°47.00'	118°17.39'	5,800	1,6
T-2	123.88-125.99	1	36°51.94'	118°05.25'	5,600	3
I-2	136.21-138.61	6	36°58.15'	118°14.09'	3,840	9,6
R-2	145.77-148.23	6	37°03.12'	118°16.00'	4,300	1,5
Q-2	158.31-160.26	6	37°09.22'	118°18.87'	4,200	9,14
P-3	165.49-167.96	6	37°12.99'	118°21.14'	4,050	1,5
S-2	167.49-169.72	6	37°12.00'	118°27.80'	9,900	6
L-3	183.72-185.63	6	37°18.48'	118°36.51'	7,700	1,14
K-3	191.01-192.90	6	37°23.32'	118°34.58'	5,200	1,6
T-3	205.40-207.33	6	37°30.78'	118°37.61'	8,400	1,5
Q-3	206.56-208.68	6	37°31.41'	118°38.04'	6,300	6
R-3	231.10-233.54	6	37°43.12'	118°48.60'	6,840	11,14
J-3	234.87-236.21	6	37°40.76'	118°57.08'	7,900	1,5
S-3	242.86-245.20	6	37°46.34'	118°56.74'	7,400	9,13
H-3	252.58-254.99	6	37°52.12'	118°56.97'	7,700	10,13
I-3	260.53-262.91	1	37°53.34'	119°02.46'	7,000	1,4

TABLE 83.—*Data for the record-section of the profile from China Lake(8) to northwest (fig. 51)*

Station	Distance (km) (traces 1, 6)	Trace No. of coordinates and elevation	Coordinates Lat	Coordinates Long	Elevation (feet)	Traces included in section
S-6	16.3- 18.4	1	35°50.51'	117°54.33'	3,500	1,6
J-5	27.1- 29.5	1	35°52.58'	118°01.17'	6,700	1,6
J-2	86.7- 88.0	1	35°58.76'	118°28.56'	3,800	14,10
I-6	104.8-107.2	1	36°11.30'	118°47.78'	1,450	2,6
P-6	114.1-116.4	6	36°19.92'	118°50.45'	3,600	1,6
I-7	131.1-132.1	1	36°29.48'	118°54.69'	1,200	1
I-8	132.0-133.8	1	36°36.55'	118°48.35'	7,200	1,5
P-8	172.5-174.7	1	36°54.14'	119°07.30'	1,200	9,14

TABLE 84.—*Data for the record-section of the profile from China Lake(8) to west (fig. 52)*

Station	Distance (km) (traces 1, 6)	Trace No. of coordinates and elevation	Coordinates Lat	Coordinates Long	Elevation (feet)	Traces included in section
K-3	137.8-140.3	1	35°25.20'	119°12.17'	350	11,14
P-3	164.4-166.9	1	35°21.36'	119°29.11'	360	9,14
S-3	205.4-207.9	1	35°17.56'	119°55.39'	1,925	1,12,6
R-3	242.6-243.4	8	35°03.76'	120°17.19'	750	11,14

TABLE 85.—*Data for the record-section of the profile from China Lake (8) to Santa Monica Bay(4) (fig. 53)*

Station	Distance (km) (traces 1, 6)	Trace No. of coordinates and elevation	Coordinates Lat	Coordinates Long	Elevation (feet)	Traces included in section
S-1	12.3- 14.7	1	35°40.98'	117°45.47'	2,350	1,6
T-6	21.4- 23.8	1	35°36.45'	117°50.15'	2,700	1,6
Q-2	48.6- 50.8	1	35°32.99'	118°12.32'	3,850	9,14
Q-1	60.8- 63.0	6	35°21.82'	118°13.00'	4,000	9,14
I-1	76.1- 78.4	1	35°09.11'	118°03.37'	2,350	9,12
S-5	99.1-101.2	6	35°01.06'	118°20.90'	4,050	1,6
R-2	132.2-134.5	6	34°49.01'	118°36.50'	3,000	10,14
R-5	151.6-154.2	1	34°36.54'	118°29.24'	1,730	2,6
K-2	156.1-158.5	1	34°33.59'	118°34.36'	1,400	12,14
K-5	166.2-169.9	6	34°26.90'	118°39.15'	1,400	9,14
I-2	179.3-181.2	6	34°18.81'	118°36.45'	1,750	9,14
I-5	207.3-209.3	6	34°02.82'	118°36.30'	400	9,12

TABLE 86.—*Data for the record-section of the profile from Mono Lake(6) to Santa Monica Bay(4) (fig. 54)*

Station	Distance (km) (traces 1, 6)	Trace No. of coordinates and elevation	Coordinates Lat	Coordinates Long	Elevation (feet)	Traces included in section
I-3	3.2- 5.2	1	37°58.03′	119°05.99′	6,480	1,3,6
K-3	10.9- 13.4	1	37°53.22′	119°06.01′	7,120	9,11,14
L-3	20.5- 22.7	1	37°48.44′	119°03.37′	7,740	10,14
J-3	40.4- 41.8	1	37°38.08′	118°59.71′	8,400	3,6
S-3	94.0- 96.3	6	37°13.40′	118°36.05′	8,400	2,5
Q-3	138.8-141.1	1	36°44.38′	118°57.80′	6,500	2,4
P-3	187.8-189.8	6	36°17.66′	118°47.20′	3,600	1,6
H-1	198.2-200.5	6	36°12.60′	118°41.00′	6,200	2,6
I-1	218.4-220.0	6	36°03.47′	118°32.45′	6,800	2,5
J-1	224.6-226.2	1	36°00.86′	118°32.40′	4,800	2,6
K-1	240.5-242.3	6	35°52.16′	118°26.90′	3,200	9,14
L-1	259.4-261.6	1	35°42.96′	118°25.05′	2,760	1,5
P-1	271.1-273.3	1	35°38.38′	118°15.95′	2,920	9,14
Q-1	288.3-290.0	1	35°27.58′	118°20.78′	6,500	1,6
R-1	300.0-302.2	6	35°19.54′	118°23.45′	3,100	1,6
S-1	318.8-321.2	6	35°08.42′	118°27.20′	4,000	9,5
T-1	366.9-368.9	6	34°40.42′	118°43.80′	3,600	9,14

TABLE 87.—*Data for the record-section of the profile from Fallon(9) to San Francisco(1) (fig. 55)*

Station	Distance (km) (traces 1, 6)	Trace No. of coordinates and elevation	Coordinates Lat	Coordinates Long	Elevation (feet)	Traces included in section
K-15	6.6- 8.7	6	39°29.56′	118°58.00′	4,030	1,6
L-15	17.6- 19.9	1	39°26.14′	119°02.65′	4,200	1,6
H-15	33.4- 34.8	1	39°20.72′	119°12.45′	4,200	3,1
I-15	48.9- 51.2	1	39°18.10′	119°21.90′	4,250	1,5
J-15	62.2- 64.5	1	39°15.80′	119°30,85′	4,360	1,6
P-15	65.1- 67.6	6	39°14.50′	119°34.20′	4,350	10,13
Q-15	81.0- 83.1	6	39°08.56′	119°42.05′	4,700	1,14
P-17	94.2- 96.6	1	39°05.44′	119°48.85′	5,000	1,11,5
R-15	94.6- 97.0	1	39°03.82′	119°47.10′	4,700	14
S-15	106.3-108.1	6	38°58.38′	119°54.50′	7,200	12
K-17	114.8-116.5	6	38°54.10′	119°57.60′	6,500	1,12,6
I-17	120.0-120.9	1	38°46.46′	119°55.35′	7,300	1,11,6
T-15	120.9-122.1	1	38°55.62′	120°02.75′	6,400	5
L-17	122.9-125.0	6	38°52.48′	120°03.60′	7,200	2,5
K-16	140.0-141.5				6,640	11,14
L-16	152.1-154.2	6	38°48.18′	120°24.00′	5,400	9,6
H-16	157.5-159.9	6	38°48.22′	120°28.44′	4,920	9,12
I-16	172.0-174.2	6	38°42.64′	120°35.60′	3,450	1,11,6
J-16	185.6-188.0	1	38°38.06′	120°42.60′	2,100	2,13
P-16	197.3-199.3	6	38°35.32′	120°50.45′	1,200	1,11,6
Q-16	212.1-214.3	1	38°33.30′	120°59.20′	600	9,14
R-16	226.0-227.5	1	38°28.51′	121°07.47′	170	9,13
S-16	235.2-237.3	1	38°25.40′	121°11.62′	100	2,6
J-18	246.8-249.3	1	38°22.10′	121°18.15′	50	9,6
Q-17	269.9-272.1	1	38°16.24′	121°32.45′	0	1,4
T-17	291.7-293.7	6	38°09.52′	121°41.35′	220	1,11,6
P-18	293.8-296.1	1	38°12.28′	121°48.20′	100	11,14

TABLE 88.—*Data for the record-section of the profile from Fallon(9) to Mono Lake(6) (fig. 56)*

Station	Distance (km) (traces 1, 6)	Trace No. of coordinates and elevation	Coordinates Lat	Coordinates Long	Elevation (feet)	Traces included in section
J-19	4.0- 6.2	6	39°34.46′	118°50.47′	3,960	1,6
R-9	10.6- 13.0	6	39°25.30′	118°48.00′	3,960	2,6
R-10	18.7- 20.9	1	39°22.00′	118°47.70′	3,930	1,6
T-19	28.5	1	39°16.06′	118°50.90′		1
H-10	38.2- 40.5	6	39°09.66′	118°49.35′	4,800	1,6
Q-19	45.7	1	39°06.70′	118°53.20′		1
P-19	58.4- 60.5	6	38°58.80′	118°50.50′	4,500	1,6
J-9	71.6					11
L-19	87.1- 89.0	6	38°43.52′	118°58.50′	4,720	1,6
Q-10	146.1-148.5	1	38°12.70′	119°00.70′	8,400	2,6
H-11	150.6-153.0	6	38°11.64′	119°13.15′	6,800	5,1
Q-9	158.5-160.5	6	38°04.94′	119°02.38′	6,640	1,5
I-20	173.6-175.6	1	37°58.03′	119°05.99′	6,480	1,6
Q-13	181.2-183.6	1	37°55.32′	119°15.24′	9,840	2
K-20	183.1-185.6	1	37°53.22′	119°06.01′	7,040	9,13
L-20	191.2-193.4	1	37°48.44′	119°03.37′	7,760	1,11,14
J-20	209.9-212.2	1	37°38.08′	118°59.77′	8,400	9,12,14
S-20	254.1-256.6	6	37°13.45′	118°36.08′	8,500	10,13
P-13	291.8-294.3	1	36°54.14′	119°07.30′	1,200	9,11,14
P-12	307.7-309.7	6	36°44.00′	118°53.85′	6,200	10,12
I-13	321.0-323.5	1	36°36.55′	118°48.35′	7,200	14,10
T-20	345.4-347.6	6	36°23.48′	118°52.65′	1,120	9,12
P-20	356.7-358.5	6	36°17.66′	118°47.20′	3,600	9,12,14

TABLE 89.—*Data for the record-section of the profile from Mono Lake(6) to Fallon(9) (fig. 57)*

Station	Distance (km) (traces 1, 6)	Trace No. of coordinates and elevation	Coordinates Lat	Coordinates Long	Elevation (feet)	Traces included in section
I-2	47.3- 49.8	1	38°22.22′	118°54.10′	6,000	1,5
K-2	54.4- 56.9	6	38°28.00′	118°54.75′	6,400	1,6
L-2	83.4- 85.3	1	38°43.52′	118°58.50′	4,730	11,14
P-2	113.4-115.4	1	38°58.80′	118°50.50′	4,200	10,13
Q-2	124.6-127.0	6	39°06.70′	118°53.20′	4,300	1,5
T-2	143.2-144.6	6	39°10.06′	118°50.90′	4,050	1,6
S-2	173.0-175.5	1	39°31.65′	118°51.35′	4,000	12,14
J-2	178.3-180.6	1	39°34.46′	118°50.47′	3,960	1,6

TABLE 90.—*Data for the record-section of the profile from Fallon(9) to China Lake(8) (fig. 58)*

Station	Distance (km) (traces 1, 6)	Trace No. of coordinates and elevation	Coordinates Lat	Coordinates Long	Elevation (feet)	Traces included in section
J-19	4.0- 6.2	6	39°34.46′	118°50.47′	3,960	1,6
R-9	10.6- 13.0	6	39°25.30′	118°48.00′	3,960	2
R-10	18.7- 20.9	1	39°22.00′	118°47.70′	3,930	1,6
T-19	28.5	1	39°16.06′	118°50.90′		1
H-10	38.2- 40.5	6	39°09.66′	118°49.35′	4,800	1,6
Q-19	45.7	1	39°06.70′	118°53.20′		1
P-19	58.4- 60.5	6	38°58.80′	118°50.50′	4,500	1,6
I-9	67.7- 70.2	1	38°55.32′	118°45.88′	4,100	9,12
I-10	82.0- 84.2	6	38°48.23′	118°41.03′	4,250	2,6
S-10	97.0- 99.4	6	38°38.76′	118°38.65′	4,200	1,5
S-9	100.9-103.2	1	38°38.04′	118°38.00′	4,130	2,6
P-9	109.7-112.2	6	38°34.00′	118°27.40′	4,450	2,6
P-10	133.9-136.3	6	38°19.28′	118°33.20′	5,700	1,6
I-14	159.0-161.0	6	38°04.10′	118°46.46′	6,900	2,6
Q-14	165.1-167.4	1	38°02.32′	118°45.50′	7,120	2,6
K-14	176.1-178.6	1	37°56.66′	118°56.66′	6,540	9,14
J-14	186.1-188.6	1	37°51.80′	118°34.80′	6,440	2,6
T-14	210.9-211.9	1	37°37.90′	118°39.35′	7,520	9
K-13	210.1-212.3	1	37°39.25′	118°34.90′	6,750	4,14
P-14	213.1-215.5	6	37°37.04′	118°24.09′	4,540	2,6
Q-12	218.2-220.6	1	37°34.38′	118°33.90′	6,700	1,11,5
T-13	219.9-222.1	1	37°33.28′	118°39.30′	6,560	11
R-13	254.1-256.4	6	37°13.45′	118°36.08′	8,500	9,12,14
T-12	261.3-263.0	1	37°12.34′	118°21.00′	4,050	10,13
S-11	271.1-273.5	6	37°05.94′	118°19.10′	5,400	9,14
K-12	305.6-308.0	6	36°49.13′	118°05.38′	4,400	9,13
J-13	327.3-329.7	1	36°37.22′	118°04.85′	3,760	13,10
K-11	331.5-333.9	6	36°37.00′	118°00.50′	3,680	11
J-12	334.5-337.0	1	36°34.36′	118°05.85′	4,620	9,12,14
S-13	390.2-392.6	1	36°11.05′	117°53.55′	4,600	9,14
J-11	391.7-394.1	6	36°03.68′	117°52.90′	4,200	9
S-12	397.2-399.7	1	36°01.68′	117°54.45′	3,340	10,12
Q-11	441.9-444.4	1	35°38.44′	117°49.32′	2,500	10,13

TABLE 91.—*Data for the record-section of the profile from Mono Lake(6) to Lake Mead(22) (fig. 59)*

Station	Distance (km) (traces 1, 6)	Trace No. of coordinates and elevation	Coordinates Lat	Coordinates Long	Elevation (feet)	Traces included in section
S-1A	7.76- 10.37	6	37°56.20′	119°01.47′		3,6
K-1	39.31- 41.80	6	37°56.34′	118°39.26′	6,530	2,5
P-1	51.03- 52.49	6	37°48.00′	118°34.60′	6,500	1,6
Q-2	60.21- 62.05	6	37°44.10′	118°29.70′		2,5
T-1	68.49- 71.21	6	37°41.36′	118°24.46′		2,5
S-1	78.89- 81.19	6	37°35.53′	118°20.87′	5,000	2,5
K-2	110.87-112.82	6	37°33.04′	117°58.08′	5,120	2,6
L-2	124.24-126.77	6	37°28.24′	117°50.50′	5,140	1,6
P-2	128.51-131.13	6	37°27.07′	117°47.93′	5,300	1,6
T-2	148.09-150.37	6	37°22.43′	117°36.26′	7,100	2,6
S-2	154.32-156.39	6	37°19.66′	117°33.48′	5,500	2,6
I-3	158.95-160.54	6	37°17.55′	117°31.72′	4,510	1,5
K-3	160.67-163.10	6	37°19.44′	117°28.49′	5,600	5
P-3	183.53-186.20	6	37°15.15′	117°13.70′	5,600	1,11,5
T-3	203.64-205.61	6	37°08.80′	117°03.02′	4,100	11,5
I-4	212.45-214.51	6	37°03.81′	116°59.55′	4,300	9,12,14
K-4	226.53-229.02	6	36°57.12′	116°53.06′	4,380	2,12,6
L-4	236.43-238.57	6	36°55.81′	116°46.56′		9,13
P-4	246.95-249.03	6	36°52.99′	116°40.46′	4,400	9,13
Q-4	256.33-258.32	6	36°48.80′	116°36.28′	3,300	9,13
S-4	269.53-271.93	6	36°39.44′	116°32.81′	2,520	9,12,14
T-4	278.98-281.40	6	36°36.69′	116°29.40′	2,500	9,12
I-5	288.97-291.22	6	36°34.20′	116°21.60′	2,500	1,11,5
K-5	298.60-301.11	6	36°32.57′	116°15.00′	2,500	10,13
L-5	306.90-308.56	6	36°33.14′	116°08.64′	2,600	10,12
P-5	322.58-323.00	1	36°34.32′	115°56.81′	4,000	14,9
Q-5	327.26-329.72	6	36°32.76′	115°52.40′	3,960	9,11,13
S-5	332.99-335.42	6	36°34.65′	115°46.71′	3,900	9,11,13
T-5	348.25-350.13	6	36°27.41′	115°40.45′	5,150	9,12
H-5	361.26-363.82	6	36°30.45′	115°27.90′		1,14

TABLE 92.—*Data for the record section of fan observations from Mono Lake(6) at 230 km distance (fig. 60)*

Station	Azimuth (epicenter to station)	Distance (km) (traces 1, 6)	Trace No. of coordinates and elevation	Coordinates Lat	Coordinates Long	Elevation (feet)	Trace included in section
L-4	119.3	236.43-238.57	6	36°55.81′	116°55.81′		13
P-13	124.6	236.16-237.30	1	36°45.23′	116°56.10′	3,800	3
L-13	131.7	233.83-235.61	6	36°34.26′	117°08.59′	400	14
K-13	133.9	248.70-250.53	1	36°25.71′	117°06.55′	5,600	9
T-13	137.0	240.40-241.92	1	36°22.69′	117°17.01′	4,800	3
Q-13	140.3	237.58-240.03	1	36°20.15′	117°25.13′	1,550	1
R-13	143.1	221.36-223.62	1	36°23.26′	117°37.85′	4,900	9
J-13	146.4	219.62-222.09	1	36°20.14′	117°45.45′	4,700	9
S-13	151.4	227.99-230.25	6	36°09.67′	117°53.31′	4,600	14
J-1	166.5	224.71-226.20	1	36°00.86′	118°32.40′	4,800	6

TABLE 93.—*Data for the record-section of the profile from San Francisco(1) to Camp Roberts(2) (fig. 64)*

Station	Distance (km) (traces 1, 6)	Trace No. of coordinates and elevation	Coordinates Lat	Coordinates Long	Elevation (feet)	Traces included in section
H-6	25.4- 27.9	1	37°34.54′	122°24.40′	350	1,6
I-4	33.1- 35.6	1	37°24.18′	122°24.22′	200	9,14
J-6	45.7- 47.7	6	37°19.52′	122°16.75′	750	1,6
K-4	64.2- 66.2	6	37°14.00′	122°06.18′		2,14
L-4	70.7- 72.7	6	37°06.64′	122°08.75′		2,6
P-6	82.9- 84.9	1	37°01.52′	122°05.73′	1,150	1,6
Q-6	96.9- 98.8	6	36°59.30′	121°53.00′	200	2,6
R-6	108.5-111.0	6	36°53.76′	121°48.95′		10,11
S-6	111.7-114.1	1	36°52.46′	121°49.30′	25	9,12,14
T-6	126.8-129.3	6	36°43.18′	121°44.43′	20	10,14
H-5	137.7-140.0	6	36°38.36′	121°40.37′	40	10,12,14
J-5	161.4-163.9	6	36°29.04′	121°29.20′	150	2,4,6
K-6	176.8-179.2	6	36°23.50′	121°21.95′	150	9,12,14
L-6	194.1-196.4	1	36°15.58′	121°17.65′	550	1,12,6
P-5	208.3-210.2	6	36°09.56′	121°09.90′	900	9,13
Q-5	217.0-219.3	1	36°05.78′	121°08.85′	1,000	10,14
R-5	227.4-229.5	1	36°01.42′	121°04.05′	1,500	9,6
S-5	240.5-243.0	1	35°56.66′	120°57.30′	1,100	9,14
I-5	275.1-277.4	1	35°40.80′	120°44.89′	900	10,13
K-5	303.5-305.5	1	35°31.40′	120°29.34′		9,12,14
L-5	319.2-321.6	6	35°26.30′	120°18.11′	1,760	11,14

TABLE 94.—*Data for the record-section of the profile from Camp Roberts(2) to San Francisco(1) (fig. 65)*

Station	Distance (km) (traces 1, 6)	Trace No. of coordinates and elevation	Coordinates Lat	Coordinates Long	Elevation (feet)	Traces included in section
T-2	6.5- 8.7	1	35°50.90′	120°50.85′	500	1,6
S-2	17.6- 20.1	6	35°56.66′	120°57.30′	1,100	1,6
R-2	31.2- 33.3	6	36°01.42′	121°04.05′	1,500	2,6
Q-2	41.9- 44.2	6	36°05.78′	121°08.85′	1,000	1,6
P-2	51.5- 53.8	1	36°09.22′	121°11.36′	800	1,6
L-1	66.5- 68.8	1	36°15.58′	121°17.65′	550	5,1
K-1	82.1- 84.6	1	36°23.50′	121°21.95′	150	9,11,14
J-2	93.6- 95.1	1	36°22.98′	121°34.45′	1,550	1,6
I-2	99.2-101.5	1	36°23.72′	121°38.70′	800	1,6
I-1	104.6-106.8	1	36°32.42′	121°32.35′	90	9,14
H-2	120.6-123.0	1	36°38.36′	121°40.37′		9,11,13
T-1	131.4-133.9	1	36°43.18′	121°44.43′	20	9,13
S-1	149.4-151.8	6	36°52.46′	121°49.30′	25	14,9
Q-1	163.5-165.4	1	36°59.30′	121°53.00′	200	1,5
P-1	175.7-177.7	6	37°01.52′	122°05.78′	1,150	9,14
L-2	187.9-189.9	1	37°06.64′	122°08.82′		10,13
K-2	196.4-198.4	1	37°14.00′	122°06.18′		10,13
J-1	214.9-217.1	1	37°19.52′	122°16.75′	750	9,14
H-1	240.4-242.9	6	37°34.54′	122°24.40′	350	10,12,14

TABLE 95.—*Data for the record-section of the profile from Camp Roberts(2) to Santa Monica Bay(4) (fig. 66)*

Station	Distance (km) (traces 1, 6)	Trace No. of coordinates and elevation	Coordinates Lat	Coordinates Long	Elevation (feet)	Traces included in section
H-3	4.4- 6.8	1	35°46.81′	120°47.10′	700	1,3,14
I-3	15.4- 17.6	6	35°40.05′	120°43.50′	900	1,6
K-3	42.9- 45.4	1	35°31.40′	120°29.34′		1,6
L-3	59.3- 61.8	6	35°26.31′	120°18.15′	1,550	1,4,6
P-3	72.5- 75.0	1	35°21.08′	120°14.38′	2,250	1,6
Q-3	94.2- 96.7	6	35°13.51′	120°01.25′	2,000	1,4,6
R-3	102.9-105.4	6	35°09.34′	119°58.06′	2,750	4
S-3	121.9-124.4	1	35°01.69′	119°51.86′	1,500	10,13
T-3	132.8-135.2	1	34°57.38′	119°46.98′	2,200	1,4
H-4	149.5-152.0	1	34°50.35′	119°40.15′		10,14
I-4	159.9-162.4	1	34°47.21′	119°34.17′		9,12
J-4	175.8-178.3	6	34°42.26′	119°23.37′	3,500	9,13
K-4	194.3-196.5	1	34°34.22′	119°16.67′	3,700	10,14
L-4	202.1-204.6	1	34°32.20′	119°13.39′	3,400	9,14
P-4	215.5-218.0	1	34°26.88′	119°07.05′		9,14
Q-4	232.9-235.0	6	34°19.36′	118°58.50′	700	10,13
R-4	249.7-251.3	6	34°13.51′	118°50.55′	1,000	10,14
S-4	264.3-266.4	1	34°08.17′	118°43.55′	750	10,14
T-4	267.1-269.1	6	34°04.40′	118°45.18′	2,000	11,14

TABLE 96.—*Data for the record-section of the profile from Santa Monica(4) to Camp Roberts(2) (fig. 67)*

Station	Distance (km) (traces 1, 6)	Trace No. of coordinates and elevation	Coordinates Lat	Coordinates Long	Elevation (feet)	Traces included in section
T-10	19.1- 21.1	1	34°04.40′	118°45.18′	2,000	1,5
S-10	19.5- 21.6	6	34°08.17′	118°43.45′	750	2,6
R-10	36.3- 37.9	6	34°13.51′	118°50.55′	1,000	6,1
Q-10	52.6- 54.7	1	34°19.36′	118°58.50′	700	2,6
P-10	69.2- 71.7	6	34°26.88′	119°07.05′		1,6
L-10	83.0- 85.5	1	34°32.20′	119°13.39′	3,400	6,12,1
K-10	90.5- 92.7	6	34°35.22′	119°16.67′	3,700	3,14
J-10	109.6-112.1	1	34°42.26′	119°23.37′	3,500	2,5
I-10	125.1-127.6	6	34°47.21′	119°34.17′		1,5
H-10	135.8-138.3	6	34°50.35′	119°40.15′		9,13
T-9	152.3-154.7	6	34°57.38′	119°46.98′	2,200	1,6
S-9	163.1-165.6	6	35°01.69′	119°51.86′	1,500	2,14
R-9	182.2-184.7	1	35°09.34′	119°58.06′	2,750	11,14
Q-9	190.0-192.5	1	35°13.51′	120°01.25′	2,000	9,14
P-9	212.6-215.1	6	35°21.08′	120°14.38′	2,250	9,14
L-9	225.9-228.4	6	35°26.31′	120°18.15′	1,550	13,9
K-9	242.1-244.6	6	35°31.40′	120°29.34′		9,14
J-9	260.4-262.6	6	35°36.94′	120°37.30′	900	13,9
I-9	271.2-273.4	1	35°40.05′	120°43.50′	900	9,13
H-9	281.3-283.7	6	35°46.81′	120°47.10′	700	9,14

TABLE 97.—*Data for the record-section of the profile from Santa Monica Bay(4) to Mono Lake(6) (fig. 69)*

Station	Distance (km) (traces 1, 6)	Trace No. of coordinates and elevation	Coordinates Lat	Coordinates Long	Elevation (feet)	Traces included in section
I-3	35.0- 36.3	1	34°18.82′	118°36.45′	1,750	2,6
K-5	50.4- 51.4	6	34°26.90′	118°39.15′	1,000	13,10
K-3	60.0- 62.0	6	34°33.59′	118°34.36′	1,400	1
R-5	60.7- 62.2	1	34°33.54′	118°29.24′	1,750	6,1
T-11	76.3- 78.2	1	34°40.42′	118°43.80′	3,600	1,12,6
R-3	90.8- 93.3	1	34°49.01′	118°38.50′	3,000	1,6
R-2	94.0- 96.5	1	34°50.32′	118°23.70′	2,650	9,14
S-5	111.8-114.3	6	35°01.06′	118°20.90′	4,050	1,11,6
S-11	126.7-129.1	1	35°08.42′	118°27.25′	4,000	10,12,14
R-11	147.7-149.9	1	35°19.54′	118°23.45′	3,100	9,14
Q-2	154.3-156.8	1	35°21.82′	118°13.00′	3,950	10,14
Q-11	161.1-162.9	6	35°27.58′	118°20.78′	6,500	9,12,14
S-3	168.6-171.1	1	35°32.62′	118°30.50′	3,360	5,2
Q-3	172.2-174.7	6	35°32.99′	118°12.32′	3,700	9,14
P-11	181.4-183.7	6	35°38.38′	118°15.95′	2,900	9,14
J-4	185.5-185.9	1	35°40.25′	118°22.70′	2,500	13
L-11	188.3-190.6	6	35°42.96′	118°25.05′	2,600	9,12
J-2	203.0-205.2	6	35°50.94′	118°27.00′	3,050	10,12,14
J-3	215.8-217.7	1	35°56.76′	118°28.58′	3,600	9,12
J-11	221.7-223.3	6	36°00.86′	118°32.40′	4,800	11,14
I-11	228.2-229.7	1	36°03.46′	118°32.45′	6,800	10,14
I-6	243.6-245.9	1	36°11.30′	118°47.76′	1,500	10,14
H-11	245.3-247.6	1	36°12.60′	118°41.00′	6,400	12
P-6	255.3-257.8	6	36°18.96′	118°50.37′	3,600	9,14
I-7	278.2-279.9	1	36°29.48′	118°54.89′	1,200	9,14
I-8	290.3-292.8	1	36°36.55′	118°48.35′	7,200	10,12
P-8	323.4-325.9	6	36°54.14′	119°07.30′	1,150	9,11
T-7	353.7-356.0	6	37°12.33′	118°21.00′	4,020	9,11,13
R-8	357.5-359.8	1	37°13.45′	118°36.08′	8,600	9,12
T-8	392.2-394.4	6	37°33.30′	118°39.32′	6,560	10
Q-7	394.0-396.4	6	37°34.38′	118°33.90′	6,700	9,14
Q-8	439.6-442.1	1	37°55.31′	119°15.24′	9,950	10

TABLE 98.—*Data for the record-section of the profile from Santa Monica Bay(4) to China Lake(8) (fig. 70)*

Station	Distance (km) (traces 1, 6)	Trace No. of coordinates and elevation	Coordinates Lat	Coordinates Long	Elevation (feet)	Traces included in section
I-3	35.0- 36.3	1	34°18.82'	118°36.45'	1,750	2,6
K-5	50.4- 51.4	6	34°26.90'	118°39.15'	1,000	13,10
K-3	60.0- 62.0	6	34°33.59'	118°34.36'	1,400	1
R-5	60.7- 62.2	1	34°33.54'	118°29.24'	1,750	6,1
K-2	80.8- 83.2	1	34°42.22'	118°19.40'	2,500	9,14
R-2	94.0- 96.5	1	34°50.32'	118°23.70'	2,650	9,14
S-5	111.8-114.3	6	35°01.06'	118°20.90'	4,050	1,11,6
I-2	133.0-135.4	6	35°09.11'	118°03.37'	2,600	9,14
P-1	153.2-155.7	1	35°18.75'	118°01.71'	2,520	9,13
Q-2	154.3-156.8	1	35°21.82'	118°13.00'	3,950	14
Q-3	172.2-174.7	6	35°32.99'	118°12.32'	3,700	9,14
T-6	187.5-189.9	6	35°36.42'	117°50.17'	2,750	1,11,6
Q-1	191.3-193.8	6	35°38.43'	117°49.31'	2,500	9,11
Q-5	195.2-197.4	6	35°44.54'	118°06.75'	3,400	9,12
S-2	197.9-200.2	6	35°40.98'	117°45.47'	2,350	9,12,14
J-5	213.7-215.4	1	35°52.58'	118°01.17'	6,600	9,14
S-7	230.0-232.3	6	36°01.68'	117°54.45'		3,6
J-1	236.6-239.0	1	36°03.68'	117°52.19'	4,100	9,11,14
J-6	281.1-283.5	6	36°31.74'	118°05.60'	5,200	9,11,14
J-7	285.9-288.3	6	36°34.36'	118°05.85'	4,630	9,12
J-8	293.7-295.9	1	36°37.22'	118°04.85'	3,770	9,14
K-6	305.2-307.1	1	36°44.04'	118°09.95'	3,920	10,13
K-7	315.4-317.8	1	36°49.13'	118°05.38'	4,400	10,13

TABLE 99.—*Data for the record-section of the profile from Santa Monica Bay(4) to Lake Mead(22) (fig. 71)*

Station	Distance (km) (traces 1, 6)	Trace No. of coordinates and elevation	Coordinates Lat	Coordinates Long	Elevation (feet)	Traces included in section
H-14	7.0- 8.7	1	34°02.68'	118°29.95'	300	1,6
I-14	13.7- 15.3	1	34°06.16'	118°28.38'	1,270	1,6
J-14	26.1- 28.4	1	34°08.83'	118°19.89'	570	2,14
K-14	36.2- 38.4	1	34°09.64'	118°12.68'	770	1,6
L-14	41.7- 43.1	1	34°13.40'	118°11.36'	2,000	9,14
P-14	50.5- 52.6	1	34°15.54'	118°06.15'	4,670	1,6
Q-14	64.9- 67.3	6	34°20.60'	117°58.90'	6,000	6,1
R-14	75.1- 76.9	6	34°25.58'	117°55.17'	4,970	5,1
S-14	86.7- 88.6	1	34°28.54'	117°48.40'	3,700	2,6
T-14	90.8- 93.3	6	34°31.50'	117°43.65'	3,230	1,12,6
H-13	108.3-110.7	1	34°37.73'	117°39.60'	2,900	2,12,6
I-13	116.7-119.2	6	34°37.06'	117°29.60'	2,830	1,11,6
J-13	127.2-129.7	1	34°39.21'	117°25.26'	2,770	1,12,6
L-13	142.2-144.6	1	34°45.68'	117°18.00'	2,630	9,14
P-13	151.9-154.3	1	34°49.72'	117°13.44'	2,630	9,13
Q-13	163.3-165.8	1	34°49.02'	117°04.32'	2,600	9,14
R-13	177.7-180.2	1	34°55.33'	116°58.38'	2,330	10,14
S-13	184.4-186.8	1	34°59.86'	116°56.85'	2,670	10,13
H-12	199.9-201.8	6	35°01.58'	116°45.80'	1,770	14,12
T-13	202.0-204.3	1	35°02.22'	116°45.80'	1,730	9,14
J-12	228.0-230.5	1	35°05.36'	116°26.80'	1,900	1,11,6
I-12	239.8-242.2	1	35°05.46'	116°19.16'	1,330	11,13
L-12	247.7-250.2	1	35°15.70'	116°19.44'	1,970	10,13
P-12	261.6-263.6	1	35°22.98'	116°14.43'	1,400	9,11,14
Q-12	270.9-273.4	1	35°23.47'	116°07.44'	930	9,14
R-12	274.3-276.8	1	35°23.77'	116°04.92'	1,470	11,14
S-12	290.5-292.9	1	35°24.94'	115°53.18'	3,470	10,14
T-12	303.9-306.4	1	35°31.85'	115°48.10'	3,500	11

TABLE 100.—*Data for the record-section of the profile from San Francisco(1) to Fallon(9) (fig. 72)*

Station	Distance (km) (traces 1, 6)	Trace No. of coordinates and elevation	Coordinates Lat	Coordinates Long	Elevation (feet)	Traces included in section
S-4	23.6- 26.1	6	37°46.06'	122°28.90'	150	11,14
Q-4	50.7- 52.7	1	37°55.97'	122°17.80'	550	2,6
T-4	58.9- 60.5	1	37°55.44'	122°09.70'	900	2,6
J-4	66.2- 68.2	1	37°59.00'	122°06.90'	250	10,13
H-4	92.2- 94.3	1	38°06.62'	121°51.80'	0	9,12
T-3	107.7-109.7	1	38°09.52'	121°41.35'	220	1,11,5
J-3	119.1-121.5	6	38°11.80'	121°32.00'	0	9,11,14
Q-3	122.5-124.7	6	38°16.24'	121°32.45'	0	2
S-3	125.9-128.4	1	38°18.06'	121°33.90'	0	1,6
T-2	147.1-149.4	6	38°21.42'	121°27.15'	10	1,5
S-2	158.0-160.1	6	38°25.40'	121°11.62'	100	10,14
R-2	167.8-169.4	6	38°28.51'	121°07.47'	170	9,14
Q-2	181.1-183.3	6	38°33.30'	120°59.20'	600	10,13
P-2	194.7-196.7	1	38°35.32'	120°50.45'	1,200	9,13
J-2	205.8-208.2	6	38°38.06'	120°42.60'	2,100	9,14
I-2	221.3-223.5	1	38°42.64'	120°35.60'	3,450	9,12,13
H-2	232.2-234.6	1	38°46.22'	120°28.44'	4,920	12,14
L-2	241.0-243.0	1	38°48.18'	120°24.00'	5,400	10,13
K-2	251.8-253.3				6,640	9,13
L-3	270.3-272.4	1	38°52.48'	120°03.60'	7,200	9,14
I-3	276.3-277.2	6	38°46.46'	119°55.35'	7,300	9,13
K-3	279.2-280.8	6	38°54.10'	119°57.60'	6,500	14,9
P-3	298.6-301.0	6	39°05.44'	119°48.85'	5,000	9,11,14

TABLE 101.—*Data for the record-section of the profile from San Luis Obispo(3) to NTS(19) (fig. 73)*

Station	Distance (km) (traces 1, 6)	Trace No. of coordinates and elevation	Coordinates Lat	Coordinates Long	Elevation (feet)	Traces included in section
R-3	20.53- 22.90	1	35°13.62'	120°35.74'	500	1,6
S-3	36.78- 38.79	1	35°21.29'	120°29.51'	2,000	1,5
Q-3	41.85- 44.24	1	35°20.30'	120°24.27'	2,000	9,2,6
H-3	48.62- 50.56	1	35°21.92'	120°20.22'	1,400	1,5
K-3	52.47- 54.24	1	35°21.07'	120°16.66'	2,000	2,6
L-3	73.81- 76.30	1	35°27.83'	120°05.13'	2,000	1,11,5
T-3	84.6- 86.6	1			1,500	1,6
P-3	88.70- 91.29	1	35°34.63'	119°58.73'	1,000	1,6
I-3	99.98-102.41	1	35°38.55'	119°52.96'	600	1,5
R-4	103.48-105.85	1	35°37.31'	119°49.20'	500	1,6
T-2	112.44-114.62	1	35°38.65'	119°43.26'	300	1,3,5
L-4	126.15-128.57	1	35°41.13'	119°34.53'	235	1,4,6
J-3	131.44-133.89	1	35°39.29'	119°29.40'	240	1,4,6
H-4	141.48-143.74	1	35°42.65'	119°24.02'	250	3
R-2	141.95-144.08	1	35°46.18'	119°26.00'	230	1,14
Q-2	154.57-156.82	1	35°48.73'	119°18.15'	250	1,5
S-2	164.10-166.20	1	35°54.36'	119°14.85'	270	1,6
T-4	174.53-176.73	1	35°52.61'	119°05.65'	500	1,6
S-4	191.46-193.78	1	35°54.63'	118°54.28'	1,000	2,6
P-2	197.08-199.33	1	36°01.53'	118°54.58'	1,000	1,11,6
J-4	201.29-203.64	1	36°05.95'	118°54.57'	1,300	1,5
Q-4	220.58-222.65	1	36°09.82'	118°42.42'	3,000	2,4,6
I-2	224.26-224.59	6	36°11.28'	118°40.38'	3,000	6
P-4	233.06-234.61	1	36°07.45'	118°31.25'	7,500	1,6
K-4	255.28-255.37	1	36°02.42'	118°12.00'	7,500	1,3
K-2	287.81-290.06	1	36°12.14'	117°53.55'	4,500	1,12,5
I-1	289.83-292.26	6	36°20.57'	117°55.16'	3,600	3,6
Q-1	298.67-301.06	1	36°23.36'	117°52.10'	3,600	1,4
L-2	303.10-303.36	1	36°19.91'	117°46.70'	4,700	2,5
J-1	304.29-306.35	6	36°27.15'	117°48.75'	4,000	5
R-1	314.73-316.70	1	36°29.24'	117°43.77'	5,000	2,5
S-1	341.15-342.90	6	36°36.84'	117°27.40'	5,000	4,5

TABLE 102.—*Data for the record-section of the profile from Hanksville(30) to Chinle(31) (fig. 74)*

Station	Distance (km) (traces 1, 6)	Trace No. of coordinates and elevation	Coordinates Lat	Coordinates Long	Elevation (feet)	Traces included in section
K-2	0.15- 2.44	1	38°21.97'	110°55.54'	4,930	1,6
L-2	9.95- 12.38	1	38°17.28'	110°52.34'	5,230	1,6
P-2	24.08- 26.37	1	38°12.18'	110°44.79'	5,670	1,14
Q-2	32.09- 34.09	1	38°11.77'	110°37.86'	5,300	10,14
S-2	39.80- 42.02	1	38°04.58'	110°39.62'	5,970	9,14
T-3	48.62- 50.62	6	37°59.00'	110°36.85'	5,470	6,12,1
R-3	63.24- 65.33	1	37°54.60'	110°27.82'	4,400	1,14
J-3	71.14- 73.43	1	37°49.82'	110°28.98'	3,900	9,13
I-3	79.65- 81.53	1	37°48.79'	110°20.95'	5,130	1,14
H-3	92.34- 94.56	1	37°43.80'	110°15.00'	5,270	1,14
K-3	101.27-103.69	1	37°39.90'	110°11.40'	5,070	10,14
L-3	113.77-115.75	6	37°30.00'	110°14.16'	6,000	14,12,9
P-3	117.87-119.72	1	37°27.66'	110°11.25'	5,330	9,14
S-3	141.20-143.06	6	37°20.34'	109°57.00'	7,200	14,12,9
T-4	149.32-151.73	1	37°16.26'	109°56.58'	5,670	1,6
R-4	161.26-162.63	1	37°07.47'	109°58.68'	5,670	1,12,6
J-4	169.96-171.29	1	37°03.08'	109°54.65'	5,030	1,12,6
I-4	180.10-182.37	1	36°58.68'	109°52.25'	5,070	2,12,6
K-4	197.69-199.71	1	36°47.43'	109°53.07'	5,530	2,11,6
S-4	237.64-239.84	1	36°30.15'	109°36.36'	5,670	1,12,6
H-4	257.05-259.59	6	36°18.24'	109°36.45'	5,800	6,12,1
L-4	276.84-279.26	1	36°07.00'	109°34.78'	5,670	1,3,6
P-4	293.41-295.58	1	35°57.25'	109°34.54'	6,330	9,11,14

TABLE 103.—*Data for the record-section of the profile from Chinle(31) to Hanksville(30) (fig. 75)*

Station	Distance (km) (traces 1, 6)	Trace No. of coordinates and elevation	Coordinates Lat	Coordinates Long	Elevation (feet)	Traces included in section
P-3	0.65- 2.98	6	35°57.25'	109°34.54'	6,370	1,6
P-4	3.22- 5.62	6	35°58.67'	109°34.71'	6,200	4
H-4	6.73- 8.72	6	36°00.15'	109°36.13'	6,070	1,6
R-4	12.14- 14.60	6	36°03.37'	109°36.43'	6,000	1,6
L-3	18.51- 21.01	6	36°07.00'	109°34.78'	5,670	1,6
H-3	39.37- 41.90	6	36°18.24'	109°36.45'	5,800	1,6
T-4	48.35- 50.71	6	36°22.77'	109°39.33'	5,600	1,6
S-3	61.65- 63.89	6	36°30.15'	109°36.36'	5,670	1,6
S-4	68.07- 69.82	6	36°32.85'	109°42.33'	5,700	9,14
Q-3	80.42- 82.58	6	36°37.20'	109°50.25'	5,370	1,6
K-4	86.36- 88.97	6	36°41.88'	109°50.85'	5,270	1,6
K-3	97.57- 99.75	6	36°47.43'	109°53.07'	5,530	1,13
I-4	113.18-114.52	6	36°56.79'	109°37.52'	4,970	9,6
I-3	117.33-119.59	1	36°58.68'	109°52.25'	5,070	14,9
J-3	128.33-130.19	6	37°03.08'	109°54.65'	5,030	1,12,6
R-3	136.93-137.69	6	37°07.47'	109°58.68'	5,670	1,12,6
T-3	150.65-152.72	6	37°16.26'	109°56.58'	5,670	1,11,6
S-2	160.15-162.23	6	37°20.34'	109°57.00'	7,200	1,12,6
P-2	178.80-180.99	6	37°27.66'	110°11.25'	5,330	1,11,6
L-2	182.57-184.27	6	37°30.00'	110°14.16'	6,000	1,11,6
K-2	198.53-200.52	6	37°39.90'	110°11.40'	5,070	2,12,6
H-2	206.55-208.94	6	37°43.80'	110°15.00'	5,270	1,4,6
I-2	219.13-220.40	6	37°48.79'	110°20.95'	5,130	1,12,6
J-2	224.14-226.20	6	37°49.82'	110°28.98'	3,900	2,6
R-2	233.67-235.96	6	37°54.60'	110°27.82'	4,400	1,12,6
T-2	246.26-248.49	6	37°59.00'	110°36.85'	5,470	1,6
Q-1	266.29-268.77	6	38°11.77'	110°37.86'	5,300	1,11,6
P-1	270.65-273.23	6	38°12.18'	110°44.79'	5,670	1,11,6
L-1	283.87-286.27	6	38°17.28'	110°52.34'	5,230	1,11,6
K-1	296.15-298.08	6	38°21.97'	110°55.54'	4,930	10,6
H-1	302.15-304.59	6	38°27.72'	110°53.38'	4,670	1,12,6
I-1	310.51-311.30	6	38°30.59'	110°55.20'	5,170	9,6
J-1	323.22-324.96	6	38°38.26'	110°54.48'	6,250	10,14
R-1	328.33-330.11	6	38°41.47'	110°52.15'	6,900	9,14
T-1	336.64-338.59	6	38°47.78'	110°48.45'	7,100	1,11,6

TABLE 104—*Data for the record section of the profile from American Falls Reservoir(27) to Flaming Gorge Reservoir(29) (fig. 77)*

Station	Distance (km) (traces 1, 6)	Trace No. of coordinates and elevation	Coordinates Lat	Coordinates Long	Elevation (feet)	Traces included in section
T-1	12.30- 12.94	1	42°48.40'	112°39.95'	4,570	9,14
J-1	30.90- 32.58	1	42°45.09'	112°27.06'	6,700	2,6
I-1	34.97- 36.55	1	42°42.48'	112°25.23'	5,700	1,6
H-1	48.61- 50.67	1	42°39.18'	112°16.29'	5,380	1,6
K-1	58.99- 60.39	1	42°35.88'	112°10.02'	4,980	1,6
L-1	67.50- 68.75	1	42°31.74'	112°06.00'	5,800	1,6
T-2	80.81- 82.75	1	42°23.61'	112°01.74'	5,280	2,6
J-2	101.23-102.83	1	42°22.74'	111°44.61'	5,180	2,6
I-4	111.23-113.49	1	42°18.84'	111°39.36'	6,100	2,6
H-2	116.50-118.71	1	42°07.77'	111°45.81'	5,180	9,14
K-2	130.13-132.22	1	42°11.52'	111°29.28'	6,600	1,6
L-2	137.06-138.33	1	42°05.19'	111°29.22'	7,520	2,6
P-2	151.14-152.94	1	42°06.21'	111°15.72'	6,100	10,14
Q-2	158.54-159.36	1	41°58.05'	111°16.20'	6,100	9,13
T-3	178.58-180.65	1	41°50.28'	111°07.08'	6,400	1,6
R-3	188.61-190.98	1	41°46.32'	111°02.07'	6,500	1,6
I-3	210.02-211.50	1	41°47.36'	110°41.50'	7,020	9,14
H-3	220.66-222.88	1	41°43.26'	110°35.97'	6,700	1,14
L-3	238.66-239.31	1	41°34.14'	110°28.86'	6,600	9,14
P-3	247.34-249.79	1	41°28.02'	110°27.36'	6,700	9,14
Q-3	258.11-260.58	1	41°24.00'	110°21.75'	6,870	9,14
S-3	272.80-275.13	1	41°22.26'	110°10.08'	6,650	9,14
P-4	279.26-281.75	1	41°20.04'	110°06.51'	7,020	9,14
R-4	289.06-291.42	1	41°08.10'	110°10.71'	7,450	1,11,6
J-4	298.69-301.03(?)	1	41°15.75'(?)	109°53.31'(?)	6,800	1,12,6
Q-4	308.08-310.33	1	41°10.14'	109°50.58'	7,170	1,11,6
H-4	318.35-320.80	1	41°01.65'	109°52.56'	7,120	9,14
K-4	325.42-328.08	1	41°03.54'	109°41.70'	6,970	2,6
S-4	335.34-336.11	6	40°55.14'	109°41.76'	6,200	14
L-4	336.17-336.57	1	40°55.95'	109°40.06'	6,150	5

TABLE 105.—*Data for the record-section of the profile from Flaming Gorge Reservoir(29) to American Falls Reservoir(27) (fig. 78)*

Station	Distance (km) (traces 1, 6)	Trace No. of coordinates and elevation	Coordinates Lat	Coordinates Long	Elevation (feet)	Traces included in section
L-4	0.39- 2.75	6	40°55.95'	109°40.06'	6,150	1,6
S-4	3.30- 5.56	6	40°55.14'	109°41.76'	6,200	1,5
K-4	10.98- 13.04	6	41°03.54'	109°41.70'	6,970	1,6
H-4	19.38- 21.78	6	41°01.65'	109°52.46'	7,120	2,6
Q-4	28.25- 30.04	6	41°10.14'	109°50.58'	7,170	1,6
J-4	39.04- 40.84(?)	6	41°15.75'(?)	109°53.31'(?)	6,800	1,6
R-4	47.77- 49.86	6	41°08.10'	110°10.71'	7,450	1,6
P-4	55.96- 58.30	6	41°20.04'	110°06.51'	7,020	1,6
S-3	62.37- 64.70	6	41°22.26'	110°10.08'	6,650	1,6
Q-3	76.33- 78.81	6	41°24.00'	110°21.75'	6,870	1,6
P-3	87.12- 89.58	6	41°28.02'	110°27.36'	6,700	1,6
L-3	98.39- 98.72	6	41°34.14'	110°28.86'	6,600	1,13
K-3	109.36-111.59	6	41°37.38'	110°37.50'	6,970	1,5
H-3	115.69-117.69	6	41°43.26'	110°35.97'	6,700	1,12,6
I-3	126.65-128.47	6	41°47.36'	110°41.50'	7,020	1,11,6
P-1	135.30-137.42					1,6
J-3	139.57-140.89	6	41°46.44'	110°53.73'	6,700	1,11,6
R-3	146.05-148.39	6	41°46.32'	111°02.07'	6,500	1,6
T-3	156.27-158.37	6	41°50.28'	111°07.08'	6,400	2,6
S-2	166.29-168.12	6	41°55.47'	111°10.53'	7,020	1,11,6
P-2	184.62-186.65	6	42°06.21'	111°15.72'	6,100	1,11,6
L-2	198.29-199.50	6	42°05.19'	111°29.22'	7,520	1,4
K-2	205.20-207.10	6	42°11.52'	111°29.28'	6,600	1,6
H-2	218.40-220.59	6	42°07.77'	111°45.81'	5,180	9,4
I-2	224.28-226.46	6	42°18.84'	111°39.36'	6,100	10,13
J-2	234.72-236.65	6	42°22.74'	111°44.61'	5,180	10,12
R-2	247.56-249.27	6	42°23.81'	111°55.47'	6,100	2,14
T-2	253.81-255.74	6	42°23.61'	112°01.74'	5,280	1,6
L-1	268.23-269.76	6	42°31.74'	112°06.00'	5,800	1,12,6
K-1	277.11-278.90	6	42°35.88'	112°10.02'	4,980	1,6
H-1	287.67-289.40	6	42°39.18'	112°16.29'	5,380	9,14
I-1	300.71-302.70	6	42°42.48'	112°25.23'	5,700	9,14
T-1	325.22-325.85	6	42°48.40'	112°39.95'	4,570	9,14

TABLE 106.—*Data for the record-section of the profile from Bear Lake(28) to American Falls Reservoir(27) (fig. 79)*

Station	Distance (km) (traces 1, 6)	Trace No. of coordinates and elevation	Coordinates Lat	Coordinates Long	Elevation (feet)	Traces included in section
P-2	16.18- 18.35	6	42°06.21′	111°15.72′	6,100	9,14
L-2	22.49- 23.40	6	42°05.19′	111°29.22′	7,520	1,5
K-2	31.41- 32.73	6	42°11.52′	111°29.28′	6,600	1,6
H-2	42.81- 44.91	6	42°07.77′	111°45.81′	5,180	1,6
I-2	49.76- 51.72	6	42°18.84′	111°39.36′	6,100	2,12,6
T-2	77.62- 79.54	6	42°23.61′	112°01.74′	5,280	1,5
L-1	92.27- 93.91	6	42°31.74′	112°06.00′	5,800	2,6
K-1	101.29-103.20	6	42°35.88′	112°10.02′	4,980	9,14
H-1	111.99-113.60	6	42°39.18′	112°16.29′	5,380	1,6
I-1	124.66-126.71	6	42°42.48′	112°25.23′	5,700	1,6
J-1	129.68-131.81	6	42°45.09′	112°27.06′	6,700	9,14
T-1	149.07-149.77	6	42°48.40′	112°39.95′	4,570	9,6

TABLE 107.—*Data for the record-section of the profile from Bear Lake(28) to Flaming Gorge Reservoir(29) (fig. 80)*

Station	Distance (km) (traces 1, 6)	Trace No. of coordinates and elevation	Coordinates Lat	Coordinates Long	Elevation (feet)	Traces included in section
S-2	9.23- 10.33	6	41°55.47′	111°10.53′	7,020	6,1
T-3	17.84- 19.96	1	41°50.28′	111°07.08′	6,400	1,6
R-3	27.88- 30.27	6	41°46.32′	111°02.07′	6,500	6,3,1
J-3	36.35- 37.18	1	41°46.44′	110°53.73′	6,700	2,6
I-3	52.00- 52.92	1	41°47.36′	110°41.50′	7,020	1,6
H-3	61.89- 64.25	6	41°43.26′	110°35.97′	6,700	6,1
K-3	65.15- 67.43	1	41°37.38′	110°37.50′	6,970	1,5
L-3	78.50- 79.40	1	41°34.14′	110°28.86′	6,600	1,11,5
P-3	86.67- 89.11	1	41°28.02′	110°27.36′	6,700	9,6
Q-3	97.41- 99.88	1	41°24.00′	110°21.75′	6,870	1,12,6
S-3	112.43-114.74	1	41°22.26′	110°10.08′	6,650	1,12,6

TABLE 108.—*Corrections applied to record sections*

Figure	Distance (km)	Thickness of sediments, assumed (m)	Time delay applied (s)
52	137.8-140.3	3,000	1.0
	164.4-166.9	6,000	1.5
	205.4-207.9	>2,000	1.0
72	92.2- 94.3	4,000	1.20
	107.7-109.7?	5,000?	---
	119.1-121.5	4,500	1.30
	122.5-124.7	4,000	1.20
	125.9-128.4	3,800	1.20
	147.1-149.4	1,400	.60
	158.0-160.1	800	.35
	167.8-169.4	500	.20
73	89.0- 91.5	1,000	.40
	99.6-102.1	2,500	.90
	103.5-105.9	3,500	1.10
	112.1-114.4	4,500	1.30
	125.6-127.9	5,500	1.45
	131.0-133.5	5,000	1.40
	141.0-143.2	4,000	1.20
	153.5-155.7	3,000	1.00
	163.3-165.4	1,500	.60
	173.5-175.9	500	.20

GPO 689-035